Author:
Bourahla, Nouredine

Title:
Knee bracing system for earthquake resisting steel frames.

KNEE BRACING SYSTEM
FOR
EARTHQUAKE RESISTING STEEL FRAMES

by

Nouredine Bourahla

A thesis submitted for the Degree

of Doctor of Philosophy in Engineering

at the University of Bristol

April 1990

ABSTRACT

The different approaches to minimise the response of structures subjected to earthquakes are reviewed. A particular emphasis is directed towards the development of steel frames buildings in resisting earthquakes by enhancement of their energy dissipation capacity. A newly proposed system called knee bracing system (KBS) showed sufficient promise to be worth investigating in detail.

The main improvement in the seismic behaviour of this technique is gained by shifting the earthquake damage from the structural members to specially designed and strategically placed knee elements which can be replaced after damage in an earthquake. The knee elements provide a major source of energy dissipation capacity by plastically deforming in flexure.

A comprehensive analytic study intended to provide a qualitative assessment of the dynamic behaviour of the KBS, investigated the effect of the geometric characteristics and the end-fixity conditions of the knee elements parametrically. On the basis of these analyses a set of guidelines on the general design of good knee bracing arrangement are determined. Several simple expressions for hand calculations of the elastic and post-elastic lateral stiffness, and ductility demand of a knee bracing frame are developed to serve as simple procedures for the practical design of KBFs. The effectiveness of the dissipative system is measured by an energy audit which calculate the energy distribution and dissipation within the frame. The effectiveness of the system at protecting the main structure is determined by a damage survey in which the yield of elements is listed against increasing ground acceleration. Under several measures of structural performance the KBF is shown to produce markedly better behaviour than the moment resisting frame and the concentrically braced frame.

In order to corroborate the analytical findings, a small scale model of a ten storey building is tested experimentally on the six axis shaking table of the Earthquake Engineering Laboratory of the Civil Engineering department of Bristol University. Three extensive series of tests covered the energy dissipation capacity aspect of the frames, the performance of different bracing arrangements in medium-rise buildings under wide range of earthquake types, and the torsional coupling behaviour of space KBFs. The experimental results are used to develop simple and sophisticated mathematical models which are critically compared in terms of simplicity and accuracy.

This work shows that the knee element acts effectively as energy dissipator, and more importantly as a force distributor that enforces a predetermined yield sequence in the frame according to the requirements of the philosophy of seismic design.

In the name of God, Most Gracious, Most Merciful

When the Earth is Shaken to her (utmost) earthquake
And the earth throws up Her burdens (from within),
And man cries (distressed): 'What is the matter with her?'
On that Day will she Declare her tidings:
For that thy Lord will Have given her inspiration.
On that Day will men Proceed in companies sorted out,
To be shown the Deeds that they (had done).
Then shall anyone Who Has done an atom's weight of good, see it!
And anyone who Has done an atom's weight of evil, shall see it.

Qur'an 'Chapter : 99'

Dedicated to my parents
to my sisters and my brothers
in love, gratitude, and respect

ACKNOWLEDGEMENTS

The author is pleased to thank Dr. A. Blakeborough for his valuable supervision, advice, and encouragement during this research. He is grateful to Prof. R. T. Severn and Prof. D. I. Blockley for the opportunity of working in the department. Gratitude is also extended to Dr. A. Dumanoglu for his constructive criticisms. The author would also like to thank the staff of the Earthquake Engineering Research Centre of Bristol University, especially Dr. C. A. Taylor, Dr. J. M. W. Brownjohn, and Dr. D. E. Key for their technical help and stimulating discussions. Also the essential help of all technicians in the earthquake laboratory and workshop is acknowledged.

The author thanks sincerely his friends for providing an agreeable family atmosphere through these years.

Finally the deep gratitude of the author is owed to the Algerian Ministry of Higher Education for their financial support for this study.

MEMORANDUM

The accompanying dissertation entitled " Knee Bracing System for Earthquake Resisting Steel Frames", is submitted for the degree of Doctor of Philosophy in the Faculty of Engineering at the University of Bristol.

The dissertation is based entirely on the independent work carried out by the author between October 1986 and April 1990 under the supervision of Dr. A. Blakeborough.

The work and ideas recorded are original except where acknowledged in the text or by references.

The contents of this dissertation have not previously been submitted for a degree or diploma of this, or any other, University or Examining Board.

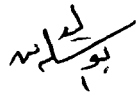

N. Bourahla

April 1990

TABLE OF CONTENTS

LIST OF FIGURES

LIST OF TABLES

SYMBOLS, AND ABBREVIATIONS

A	Cross sectional area
ACU	Analogue control unit
ADC	Analogue to digital conveter
a_i, b_i	Fourier coefficients
C	Damping matrix
CBF	Concentrically braced frame
C_i	End-fixity coefficient
CM, CR	Centre of mass, centre of stiffness
DAC	Digital to analogue converter
D_b, D_c	Ratio of the maximum bending moment of the beam or the column to the plastic moment
d_d, d_k	Longitudinal elongation of the brace, midspan deformation of the knee element
dF_i	Force increment
DFT, IDFT, FFT	Discrete, inverse, and fast Fourier transform
d_{y1}, d_{y2}	First and second yield deformation at midspan and the end of the knee element
e	Static eccentricity
E	Young's modulus
EBF	Eccentrically braced frame
E_D	Viscous damping energy
E_H	Hysteretic energy
E_I	Input energy
E_K	Kinetic energy
E_S	Recoverable elastic energy
F_b,F_m	Lateral load carried by the KBS, and the MRF
f_c	Cutoff frequency
F_d	Axial brace force

F_{el}	Elastic limit of the shear force storey
f_i	i^{th} natural frequency
f_L	Uncoupled lateral frequency
f_m	Lowest frequency that can be resolved from a sampled signal of length T
f_N	Nyquist frequency
f_T	Uncoupled torsional frequency
g	Acceleration due to gravity
G(i)	Discrete Fourier transform of g(n)
g(n)	Periodic, sampled time history
g(n),x(t)	Functions of time
h	Sampling period
H	Storey height
I_b,I_c,I_k	Moment of inertia of the beam, column, and the knee element
j	$(-1)^{\frac{1}{2}}$
K	Stiffness matrix
K_1,K_2	First and second slope of a bilinear loop
K_b,K_m	Equivalent lateral stiffness of a KBS and the MRF
KBF	Knee braced frame
KBS	Knee bracing system
K_θ	Joint rotational spring stiffness
L	Bay width
l_k	Knee element length
M	Mass matrix
M, M_p	Maximum and plastic bending moment of a cross-section
MDOF	Multi-degree of freedom
MRF	Moment resisting frame
n	Number of degrees of freedom
N	Number of time increment
{P(t)}	Vector of an arbitrary time varying loads

P_c	Collapse load
P_{y1}, P_{y2}	First and second yield load of the knee element
r	Radius of gyration
r	Ratio of the maximum ductility in a partially fixed knee element to that of ended fixed knee element
RT_{xy}	Maximum response in the direction of the input motion to the orthogonal induced response
R[u(t)]	Restoring force for the structure
S, S_o	Shear and yield shear force of the knee element
SDOF	Single degree of freedom
S_l,S_t,S_f,S_E	Scaling factor for length, time, frequency and modulus of elasticity
T	Period of vibration, record of length (seconds)
t	Time
TK	Torsional stiffness
u_g	Ground acceleration
$\{\ddot{u}_g\}$	Ground acceleration vector
$\{u_r\}$,$\{\dot{u}_r\}$,$\{\ddot{u}_r\}$	Relative displacement, velocity and acceleration vector
$\{u\}$,$\{\dot{u}\}$,$\{\ddot{u}\}$	Absolute displacement, velocity and acceleration vector
x	Distance between the beam-column connection and the knee element-beam connection
y	Distance between the beam-column connection and the knee element-column connection
Δ	Increment
ξ	Damping ratio
ω	Angular frequency
ω_n	Angular frequency of the n^{th} vector component, natural frequency of the n^{th} mode
α	Angle that the knee element makes with the beam
π_i	Dimensionless products of Buckingham theorem
σ_y	Yield stress
μ	Maximum ductility
τ	Duration of time

Φ	Mode shape matrix
θ	Angle that the knee element makes with the brace
δ, δ_{el}	Storey drift, elastic limit of the storey drift
ϕ	Angle between the brace element and the beam
ϕ_n	n^{th} mode shape

Chapter 1

INTRODUCTION

INTRODUCTION

1.1 INTRODUCTION

Thousands of earthquakes occur each year, and they are widely distributed over the earth's surface. Those that are of interest to the structural engineer are those that can cause structural damage; these are called strong-motion earthquakes. According to statistics there were more than two and half million lives lost due to earthquakes over the world since the beginning of this century, regardless of the social and economic consequences, which means that major earthquakes rank in the top few of all natural disasters [45]. This has lead to the present improvement in earthquake engineering design which leads to constructions better able to resist the extreme loads and reduce the terrible loss of life.

Frames are a common type of design for public building where many people and much investment are at risk in seismically active areas. The purpose of this work is to participate to the advancement of the earthquake resisting frames to reduce the hazard to life and improve the capability of essential facilities to function during and after an earthquake.

From an energetic point of view, an earthquake can be stated as a process of energy exchange between the ground and the structure. A structure designed to resist earthquake motion should have the capacity to store and dissipate the energy imparted by the earthquake safely. Thus one objective of a good structural design is to govern the manner in which the structure transforms the input energy by designing a succession of nonstructural and structural damage that avoids collapse.

Based on this principle, this thesis describes investigations into a new type of bracing system for seismic frames which in addition to the stiffness and strength play dominant role in the energy dissipation capacity and yield sequence in the frame. In this chapter the adoption of energy dissipation mechanisms in building in general and steel

frames in particular is reviewed, paying attention to the torsional coupling aspect of such structures. The last section goes on to summarise the scope and objectives of this research.

1.2 DESIGN PHILOSOPHY OF BUILDINGS WITH ENERGY DISSIPATION MECHANISMS

A general conclusion drawn from the Learning From Earthquakes Program [32] is that in areas where buildings are designed according to good codes, where construction is closely supervised, and where the earthquake is commensurate with the expected seismicity, the damage is a small fraction of that observed in areas where these conditions do not apply. This conclusion shows that earthquake damage can be reduced, through improvements in knowledge and conscientious work during design and construction. Although earthquakes still provide many surprises, steady progress has been made towards the ultimate goal of preventing earthquakes from becoming disasters.

One way of minimizing the response of a structure under earthquake motions is to include energy absorbing elements, both within the structure and connected to points of support outside the structure. The concept is an attempt to separate the load carrying function of the structure from the energy dissipation function, at least when the structure is at a rest. However, the magnitude of damping required and the position of the dampers is not always easily determined [60]. Another way to improve the structural damping capacity is to rely on the inelastic deformations of nonstructural or structural elements especially designed and strategically placed in the structure to absorb energy.
An important feature that damping mechanisms should possess is a large energy absorption capacity, so they can be effective during a sequence of earthquakes. This characteristic is mostly needed in seismically active areas where minor and moderate earthquakes are frequent, and those where earthquakes are characterised by several distinct strong motions. From the author's observations, the El-Affroun and Tipaza region of Algeria is a case where several moderate earthquakes happened recently which left many buildings in a vulnerable state, even though the engineers confirmed that no

structural damage had occurred. Similarly ten years ago, the after shock of the El-Asnam earthquake of October 1980 in Algeria [30] resulted in the partial or total collapse of several buildings which survived the principal shock with little damage. Most of these buildings consumed all their energy dissipation capacity, mainly provided by cracking in the nonstructural masonry walls during the first shock.

Different approaches to protect structures from earthquakes using energy absorbing elements will be briefly discussed, and the performance of steel structure buildings however will be reviewed in greater detail.

1.2.1 TUNED MASS DAMPERS

If an appendage to a structure vibrates out of phase it will apply a restoring force to oppose the vibration of the structure, so that it acts effectively as vibration reducing device, commonly known as a tuned mass damper or vibration absorber. The appendage usually consisting of a spring supported mass with a damping element, requires the ability to withstand large amplitude vibrations (Fig. 1.1). The historical, theoretical and practical aspects of tuned mass dampers were investigated [60] and conclusion was drawn that the vibration absorber is not a practicable method for earthquake resisting building, although they are used widely in reducing the aerodynamic motion of cable stayed bridges and towers.

1.2.2 SOFT FIRST STOREY

The essential characteristic of a soft storey is the discontinuity - of strength and stiffness - which occurs at the second floor column connection of a building. The soft first storey is used to reduce the forces on the upper part of the building. However large displacements at the first storey occur producing unacceptable secondary damage. The soft storey concept is commonly regarded as a building configuration with a known poor performance, nevertheless for architectural reasons and because of advances in research in material behaviour and energy dissipation concepts, all of which improve the

reliability of the soft storey notion, its continued existence is certain in the foreseeable future [4].

1.2.3 BASE ISOLATION SYSTEMS

The idea that a building can be uncoupled from the damaging effects of the ground movement produced by a strong earthquake has appealed to inventors and engineers for more than a century [59]. Many ingenious devices have been proposed to achieve this [26,98,101], some are illustrated in Fig. 1.2. Very few have been tried in practice. The concept, now generally referred to as base isolation, or seismic isolation has yet to become acceptable to the engineering profession as a whole. In recent years a few practical systems have emerged and been implemented. Shaking table tests and related static testing of full-scale components, such as isolation bearings has led to a degree of acceptance by the profession, and the number of practical implementations will undoubtedly increase.

1.2.4 DISCRETELY DAMPED STRUCTURES

The dynamic response of building structures can be greatly improved by an intelligent introduction of discrete dampers, either within the structure or connected to supports outside the structure. Studies of the location and size of viscous dampers on a multi-storey frame and cable stayed pedestrian bridge showed that the optimum size and location of such dampers are not easily determined in a multi-degree of freedom system [107]. However, an investigation into the seismic performance of energy absorbing dampers in building structures [60] concluded that substantial benefits in reducing shears and displacements can be achieved by distributed damping systems.

The various types of damping mechanisms can be classified into three main classes, namely, steel energy absorbers, viscous and sliding friction devices, and lead rubber shear dampers. The steel dampers like those developed in Ref. [99], utilise solid beams deformed plastically in various combinations of torsional, flexural and shear deformation. Some are shown in Fig. 1.3 with examples of their use.

The friction type dampers, however, dissipate energy mechanically in friction rather than by plastic deformation. Some are shown in Fig. 1.4 and are suitable for use with diagonal steel bracing, joint for precast concrete large-panel, and concrete shearwalls [1,78].

The lead and rubber shear dampers have found their main application in base isolation systems. Other types of dampers have been suggested (such as visco-elastic dampers and spring-dashpots [46,96,105]) but their use in practice is very limited.

1.2.5 ACTIVE DAMPERS

Active dampers are powered control systems which motivate mechanisms to reduce the response of structures during earthquakes.

In recent years, the idea of applying such devices to reduce damage in structures has become an area of interest, and control algorithms and control systems have been proposed and investigated. While the analytical and simulation results have been encouraging, an extensive experimental study is necessary before any application could be adopted [22,95]. An example of a model with an active control system [22] is shown in Fig. 1.5. The model structure was controlled using prestressing tendons connected to a servo-hydraulic actuator. An optimal closed-loop control scheme was used to reduce the response of the structure under base motion generated by a seismic simulator.

1.2.6 STRUCTURAL HYSTERETIC DAMPERS

One of the most important features of steel structures is that integral parts of the structure such as beams, columns, or other components can be designed to contribute to the process of energy absorption by plastic deformation. During an earthquake, these parts play a similar role to the energy absorbers considered so far in addition to their load carrying function. The development of the seismic design of steel structures leading to the use of structural hysteretic dampers will be discussed in the next section.

1.3 REVIEW OF RESEARCH IN THE IMPROVEMENT OF THE EARTHQUAKE PERFORMANCE OF STEEL FRAMES

In recent years important developments in design have taken place, nurtured by research and the intensive updating of seismic codes have taken place [7,87]. Part of the research trend in this field and the evolution of the structural steel fabrication are directed by the approach adopted in seismic codes based on the following philosophy :

1. A building must resist a minor shake without damage;
2. In moderate earthquakes some nonstructural damage is permissible;
3. During a major earthquake, the building must not collapse, but some structural and nonstructural damage may occur.

In order to accomplish these ends, a structure must possess sufficient strength, stiffness, and capacity for energy dissipation to withstand major earthquakes. The objective of good member design is to design a hierarchy of failure modes into each member ensuring that the member reaches its strength in a preselected mode (e.g in flexure in the beams of a moment resisting frame, and plastic shear in the links of an eccentrically braced frame). Similarly, the objective of good system design is to design a hierarchy of member strengths into the structural system enforcing a sequence of yielding with good energy dissipation, and stiffness characteristics [71]. In this manner the concept of code procedures which concentrated almost solely on the member level (elastic member force distribution), is moving towards an inelastic aseismic design procedure which takes account of the effect of the sequence of yielding [58,71].

1.3.1 MOMENT RESISTING FRAMES

In the design of steel buildings, moment resisting structural frames (MRF) are more widely used than any other type. This kind of framing results in no obstructions between the columns, allowing maximum freedom for interior planning and fenestration [87]. MRFs are capable of undergoing large plastic deformations during earthquakes and thus they have the potential for excellent energy dissipation [37,50,82,103]. However, the large deformations that arise may threaten the

stability of the structure and lead to excessive nonstructural damage. The lateral integrity of such a frame depends on having beam-column joints not only of sufficient strength but also possessing good ductility. Moment connections are basic to the whole field of steel fabrication, and in practice continuous changes take place to improve their characteristics [62,81].

1.3.2 CONCENTRICALLY BRACED FRAMES

As mentioned earlier moment resisting frames tend to be quite flexible and the seismic requirements for the lateral drift can make their adoption uneconomical for tall buildings. Braced frames, on the other hand, are very efficient in providing side way resistance. However, the dilemma of using this kind of bracing system is that slender braces are characterised by a poor energy dissipation capacity, and relatively strong braces cause an excessive degree of plasticity in frame members when subjected to severe earthquake motion [48]. In seismic applications a brace may be subjected to severe cyclic load reversals, and experimental evidence shows the poor behaviour of such braces [38,47,52,84]. An example illustrating the significant degradation of the hysteretic behaviour of a strut during cyclic loading is shown in Fig. 1.6. Analytical models for determining such hysteretic behaviour were developed to predict the dynamic response of concentrically braced frames (CBF) [5,31,40,68,90,97]. As a result of the deterioration of the braces strict limits were recommended on the use of CBFs in regions of high seismicity [87].

1.3.3 DAMPED BRACED FRAMES

Since it was recognized that the brace-carrying capacity in CBFs is reduced during cyclic loading, different schemes have been advanced to overcome this problem. In all these schemes the braces are designed not to buckle, and various ingenious devices are becoming available to achieve this. By incorporating sliding friction devices (Fig. 1.4) in the bracing system of the framed buildings, the energy dissipation capacity can be enhanced, and the brace element can be prevented from buckling by allowing a low slip

load in compression [1,6,33,78]. In a similar way, as an alternative to the inelastic buckling, the braces of a concentrically braced frame can be connected by means of long slotted bolt holes (Fig. 1.7) where slip displacement can occur at a designated friction resistance [34]. In another method the viscoelastic dampers [96] of Fig. 1.4 produce a spring force proportional to displacement, and a damping force proportional to velocity when they are deformed. Buildings which posses some frames designed as CBFs with other designed as MRFs (dual systems) show a better behaviour than a fully CBF design, but still suffer from severe local buckling of the braces [13].

1.3.4 ECCENTRICALLY BRACED FRAMES

As an alternative to a CBF, one can employ an eccentric braced frame (EBF) to accomplish the same end.

The main characteristic of the EBF is that the axial forces induced in the braces are transmitted, either to a column or another brace, through shear and bending in a beam segment called a link. A few types of eccentrically braced frames are shown in Fig. 1.8. At service loads an EBF provides a good laterally stiff structural system, whereas during severe earthquake the links yield and dissipate energy effectively. The links are designed to yield in shear rather than flexure, as shown in Fig. 1.9, and the maximum length of the link is determined accordingly [66]. Experimental and analytical studies have demonstrated that shear links provide a larger dissipation of energy than links which form only end plastic moments [54,55,64,65,91]. Since publication of a research paper on EBFs for seismic bracing in 1978 [93], this concept has become a subject of considerable interest [8,43,57,70,85,110], and it has been rapidly adopted in practice. Several major buildings in California have been constructed using this approach, and others are under construction or are being designed employing this system of bracing [56]. Recently series of full and reduced scale models were tested and analysed in order to study the behaviour of a combined eccentrically braced and moment resisting frame [108].

The eccentric bracing shear link, however, possesses some drawbacks. For example, the energy dissipation capacity is provided by shear links that are integral parts of the

frame. Their repair and/or replacement after severe earthquake requires 'major surgery', which can be both time-consuming and expensive. In addition heavy eccentric bracing elements are required to activate the energy dissipation of the shear links that only become effective when the structure is subjected to severe or destructive lateral loads. A new and practical technique for lateral bracing of steel framed buildings, called Disposable Knee Bracing, has been recently proposed [3]. This system possesses the favourable characteristics of the eccentric bracing shear link technique and eliminates the draw-backs mentioned above.

1.3.5 KNEE BRACED FRAMES

Knee braced frames (KBFs) are steel framed buildings incorporating disposable knee bracing. The principle behind the system seeks to concentrate earthquake damage in specially designed and strategically placed knee elements which may be replaced if necessary after damage in an earthquake. The methods works by the knee elements absorbing plastic work and thereby reducing the energy available to do other damage. Frames with different arrangements of knee elements are shown in Fig. 1.10. Criteria have been proposed [71] to identify elements that are suited as primary energy dissipating elements which are as follows:

- Their yielding must be restricted by other still elastic elements.
- They should not be primary gravity load bearing elements except for low-rise structures.
- They must be ductile and exhibit full and stable hysteresis loops.
- They should provide a significant portion of the overall stiffness and yet be relatively flexible.

These seemingly contradictory criteria can be met by the knee bracing system. The system should be designed with three cases in mind. Loads due to frequent wind and minor earthquakes should be resisted elastically. In a moderate earthquake the system should provide a first line of defence by yielding and absorbing energy. The knee elements themselves may suffer significant damage but they should protect the main load

bearing structure from any damage. In a severe earthquake the system should still help by absorbing energy but some structural damage may be expected. It is important however in this extreme case that the system should not induce a collapse failure of the main structure.

1.4 TORSIONAL COUPLING OF BUILDING WITH ENERGY DISSIPATION MECHANISMS

As seen in the previous sections large number of studies have investigated the reduction of the lateral response of buildings with energy absorbing dampers by optimisation of their location through the height of the building. However little research has been carried out into the torsional aspect of these buildings. Although several studies concentrated on the torsional behaviour of simple nonlinear asymmetric model [41, 44, 76, 102], most of the attention has focused on the effect of dynamic and geometric characteristics on the conventional structural response parameters and the ductility demand.

Analysis of earthquake behaviour of torsionally coupled buildings with nonlinear resisting elements using finite resonance response analysis method (FRRA) [109] revealed that the energy absorption was constant despite an increasing eccentricity ratio.

An other important aspect related to the 3-D behaviour of buildings concerns the response to multicomponent earthquake motions, and the effect of yield interaction. Some results [76], showed that the energy input in each of the 2 horizontal directions was not necessarily dissipated or stored in that direction; in other words, there was a redistribution of energy due to the inelastic interaction of the behaviour in separate directions.

Recognizing the importance of the torsional coupling effect, the enhancement of the torsional resistance of building frames by the knee bracing system as an energy dissipator will also be investigated experimentally.

1.5 OBJECTIVES AND SCOPE OF THE PRESENT RESEARCH WORK

The journey to the object of the research in this thesis started from the author's inquiry about an efficient way of reducing the response of structures subjected to earthquakes. A particular attention is paid to practical improvements of structural steel buildings. After examination of the different possibilities to enhance the damping capacity of these types of structures, the newly proposed knee bracing system seemed to have a high potential to dissipate energy within the requirements of the seismic design philosophy. The major part of the present work is to study analytically and experimentally the overall behaviour of KBFs, and to establish experimentally the several merits of this system.

The aim of Chapter 2 is to provide a qualitative assessment of the behaviour of the knee bracing system by a parametric study of a simple structure which represents the essence of any framing system employing this bracing arrangement. The post-elastic behaviour of the KBFs, and the effect of the partial end-fixity of the knee element on the fundamental characteristics of the KBFs is investigated.

In Chapter 3, the energy concept is introduced as a structural parameter to evaluate the capacity of the KBS to dissipate energy. The amount of damage the knee elements may suffer after an earthquake and the sequence of yielding of the KBF are included in this presentation. Before presenting and interpreting the results, some analytical modeling techniques and theoretical aspects related to structural dynamics are described.

In Chapter 4 the design details of a one twelfth scale model of a ten storey building are presented with a series of cyclic tests performed on knee bracing systems in order to determine their hysteretic loop characteristics. A detailed analysis of the implications of imperfect similitude is presented, and a mass adjustment technique is adopted to compensate for the modeling distortion.

A description of the various pieces of apparatus and instruments employed in seismic tests and the operation of the data acquisition system constitutes the core of Chapter 5.

Chapter 6 then presents the results of three test series that simulated the structural behaviour of KBFs under earthquakes. The first series of tests deal with the energetic aspect of the frames and their capacity to dissipate the imparted energy, the second investigates the performance of different bracing arrangements in medium-rise buildings under a wide range of earthquake types, and the third series focuses on the torsional coupling behaviour of space KBFs.

The primary objective of Chapter 7 is to use the results of the experimental work as basis for developing numerical models which reflect the observed dynamic properties of several frame structures. In this respect simple and refined models are discussed in terms of their accuracy by comparing the predicted results with the experimental data.

The main conclusions are summarised in Chapter 8, including requirements for further research needed to complement the findings presented and to make new advances in knee braced frames.

Chapter 2

PARAMETRIC STUDY OF THE KNEE BRACING SYSTEM

PARAMETRIC STUDY OF THE KNEE BRACING SYSTEM

2.1 INTRODUCTION

At this stage little, if any information is available about the dynamic characteristics of the knee bracing frames (KBFs), and so general recommendations for the seismic design of these frames are required. The aim of this chapter is to provide a qualitative assessment of the behaviour of the knee bracing system. The strength, stiffness, and ductility of properly designed knee bracing frames are directly related to the knee element characteristics, to this end some of the main properties of the elastic behaviour of the KBFs are examined parametrically by a simple structure which represents the essence of any framing system employing this bracing arrangement.

As pointed out in Chapter 1, the KBFs should be designed to resist minor earthquakes elastically, and during a rare, intense seismic event, a structure must be safe from collapse. Therefore a quasi-static analysis is used to investigate the post-elastic behaviour of the KBF, focusing on the assessment of the ductility demand and the energy dissipation capacity of the frame.

Difficulties are encountered in realising perfect rigid connections in practice, so the effect of partial end-fixity of the knee element on the fundamental characteristics of the behaviour of the knee braced frames also is investigated.

2.2 INFLUENCE OF THE GEOMETRIC CHARACTERISTICS OF THE KNEE ELEMENT

Considering a family of knee braced frames shown in Fig. 2.1(a) parameterised by the knee element length ratio l_k/H (l_k is the knee element length, and H is the storey height), the knee element stiffness ratio I_k/I_c (I_k and I_c are the inertia moments of the knee element and the column respectively) and the geometric configuration factor x/l_k (x is the distance between the knee element-beam connection and the column-beam node).

2.2.1 EFFECT OF THE KNEE ELEMENT STIFFNESS

In order to determine the effect of the knee element moment of inertia on the lateral stiffness of the frame, and the local distribution of forces in the beam, the column, the brace, and the knee element itself the ratio I_k/I_c was varied from 0 (MRF) to 1 (moment of inertia of the knee element equal to that of the column)

2.2.1.1 Lateral stiffness of the frame

The elastic stiffness of a structure is a measure of its ability to meet drift control requirements. Since the effective lateral load from earthquake excitation depends upon the stiffness (natural frequency), the relationship between stiffness and maximum storey drift is not linear. In general however, higher stiffness indicates better drift control [43]. For the simple configuration, the relative lateral stiffness is expressed in terms of the ratio of the storey drift in the MRF to the corresponding KBF (Fig. 2.1) The effectiveness of the bracing system can be seen by considering how the frame stiffness changes with the relative stiffness of the knee element I_k/I_c. For $I_k/I_c < 0.30$ a great benefit is gained from the knee bracing system regardless of the ratio I_b/I_c (which characterises the relative stiffness of the beam to the column).

2.2.1.2 Local distribution of forces in the beams and columns

To enforce yielding in knee elements without damaging the main structure, and to limit the inelastic deformation of the knee element at the same time, the size of the knee element should be carefully chosen. It is useful to consider the variation of a parameter D which represents the ratio of the maximum bending moment of the column or the beam to the corresponding plastic moment at the knee element yield

$$D_c = (M_c/M_{cp}) \times (M/M_p) \text{ for columns} \qquad (2\text{-}1)$$

$$D_b = (M_b/M_{bp}) \times (M/M_p) \text{ for beams} \qquad (2\text{-}2)$$

where :

M_c, M_{cp} : are the maximum and the plastic bending moment of the column

M_b, M_{bp} : are the maximum and the plastic bending moment of the beam

M, M_p : are the maximum and the plastic bending moment of the knee element

Fig. 2.2(a) shows the knee element is always the first element to reach the yield point even for very strong elements. However for practical sizes say $I_k/I_c<0.3$ an early yield in the knee element can be achieved leading to sufficient ductility before the main frame members yield.

An other important feature of the knee element effect on the local force distribution can be visualised by Fig. 2.2(b) where the ratio of the beam to the column bending moment is plotted. The yield hierarchy which is of primary importance in the seismic design can be controlled by the knee element size. The yield of beams before columns - generally preferred in seismic design - can be effectively obtained by a good selection of the knee element size even for strong beam design.

2.2.1.3 Axial and shear force in the knee and the brace element

The study of the variation of the axial and shear forces developed in the knee element with the ratio I_k/I_c is intended to investigate the extent to which these forces may reduce the plastic moment of resistance of the knee element. Fig. 2.3(a) shows the variation of the axial force ratio N/N_0 (where N is the axial force, and $N_0=A\sigma_0$ is the squash force of the knee element) at the yielding point with I_k/I_c ratio. The three curves corresponding to the different values I_b/I_c present a minimum in the interval [0.01, 0.1]. However the knee element shear force ratio S/S_0 (where S is the max knee element shear force, and S_0 is the knee element shear capacity) is characterised by steady increase in the interval of [0.01, 0.2] for the different values of I_b/I_c as shown in Fig. 2.3(b)

The shear force ratio is higher than the axial ratio and may reach 20% at $I_k/I_c = 0.2$, but both effects can be considered to be minor according to the curves characterising the moment-axial-shear force interaction which means that the full plastic bending capacity of the knee element can be used conservatively in the design process for values of $I_k/I_c<0.2$.

To guarantee that the knee elements yield first and the diagonal braces remain elastic at all times, the yield (or critical) force capacity of the diagonal brace should be greater than

$$F_d = 8M_p/l_k \sin\theta \qquad (2\text{-}3)$$

where

M_p: plastic moment capacity of the knee element

θ : angle that the brace element makes with the knee element

The estimated brace force using Eq. (2-3) constitutes the upper bound, as shown in Fig. 2.3(c). The normalised axial forces developed in the brace elements are slightly lower than those estimated by the expression (2-3) which is mainly due to the knee element and brace flexible supports, and the brace elongation, which were not considered in the above equation. However in general stiff knee elements lead to heavy diagonal braces.

2.2.2 EFFECT OF THE KNEE ELEMENT CONFIGURATION

This investigation was undertaken in an effort to understand the manner in which the knee element geometric configuration affects the elastic behaviour of KBFs. For this purpose the variation of the initial lateral stiffness and certain member forces of the simple KBF, as a function of the angle α, have been considered for different values of the ratio H/L. The relative frame stiffness decreases at a very slow rate with α, and tends to be less sensitive for wide bays as shown in Fig. 2.4(a).

An important aspect of the knee element configuration is that the bending moment can be optimised for $\alpha=\phi$ as shown in Fig. 2.4(b) (where α, ϕ are the angles that the knee element makes with the column, and the beam respectively). It corresponds to a position where the brace element centre line crosses the beam/column connection, however the minimum of the diagonal axial force is also close to these values, in the region where neither the beam bending moment nor the column shear force reaches its maximum value.

The general elastic behaviour is not very sensitive to the knee element positions, however the geometric configuration satisfying $\alpha = \phi$ leading to :

$$x = l_k/\sqrt{1+(2H/L)^2} \tag{2-4}$$

$$y = l_k/\sqrt{1+(L/2H)^2} \tag{2-5}$$

where :

H : Column height.

L : Beam length.

x : distance between the beam-column connection and knee element-beam connection Fig. 2.1(a).

y : distance between the beam-column connection and knee element-column connection Fig. 2.1(a), seems to be the best position.

2.2.3 EFFECT OF THE KNEE ELEMENT LENGTH

The effect of knee element length is felt mostly in the initial lateral stiffness, and in the parameter D_c (defined in Section 2.2.1.2). As shown in Fig. 2.5(a) the elastic stiffness is inversely proportional to the knee element length for values of l_k/H between 0.10 and 0.30. The other important aspect of the knee element length can be explained with the aid of Fig. 2.5(b), which shows that the elastic regime of the knee braced frame elastic measured by the ratio D_c can be controlled by the knee element length. For a fixed size an earlier yield can be obtained in the range 0.2 to 0.3 of l_k/H. However shortening the length of the knee elements is another way to extend the KBFs elastic regime and to limit the inelastic deformations in the knee element.

2.3 POST-ELASTIC BEHAVIOUR OF KNEE BRACED FRAMES

The quasi-static inelastic method was used to investigate the post-elastic behaviour of two knee braced configurations namely X and K knee bracing system (Fig. 2.6). The study compares the lateral stiffness and strength, the ductility demand and the energy dissipation capacity of the frames.

2.3.1 GEOMETRY OF PLASTIC DEFORMATION EXCURSION MECHANISM

For design purposes, the inelastic (plastic) deformation of the knee element must be quantified. This can be most easily done by constructing energy dissipation mechanisms, in plastic analysis commonly known as the collapse mechanism [85]. The basic geometry of the plastic deformation mechanisms is shown in Fig. 2.6(c). A good estimation of the knee element ductility can be found by geometric compatibility, in which the inelastic rotations at midspan and the end of the knee element depend entirely on the ultimate storey drift and the geometry of the frame. The maximum ductility can be derived as follow. In Fig 2.6(c):

$$d = \delta \cos \phi \tag{2-6}$$

$$\mu = d/d_{el} \tag{2-7}$$

From Eqs.(2-6) and (2-7)

$$\mu = (\delta / d_{el}) \cos \phi \tag{2-8}$$

for a perfectly rigid knee element ends the elastic deformation limit is given by

$$d_{el} = M_p l_k^2/24EI_k \tag{2-9}$$

and for a pinned knee element the Eq. (2-9) becomes

$$d_{el} = M_p l_k^2/12EI_k$$

where:

μ : maximum ductility

δ : maximum storey drift

d : maximum plastic deflection of the knee element at midspan.

d_{el} : elastic deflection limit of the knee element at midspan

ϕ : the angle between the beam and the diagonal brace

I_k : Inertia moment of the knee element

Because the knee element is neither perfectly fixed nor perfectly pinned, the effect of a partial end-fixity due to elastic supports or to semi-rigid connections will be discussed in Section 2.4.2. However expression (2-8) can be used in the design of knee braced frames to predict the maximum knee element ductility for a given maximum storey drift. As shown in Fig. 2.7 the estimated and actual ductility are within 5% for a reasonably high ductility. It should be noted that Eq. (2-8) is applicable only to frames having $\alpha + \phi \approx 90°$, that is where the knee element and the diagonal brace are almost perpendicular.

2.3.2 LATERAL STABILITY OF THE KNEE BRACED FRAMES

The global lateral resistance in the knee braced frame is assured by an interaction of the knee bracing system and the MRF in two distinct phases namely the pre-yield and post-yield regimes.

During the first stage the lateral forces are mainly resisted by the knee bracing system, however in the second phase the greater part is carried by the MRF and consequently a rearrangement of the force distribution in the different parts of the structure occurs immediately after the knee elements yield.

It is apparent from the curves of Fig. 2.8(a) that the X-bracing is stiffer than the K-bracing. The former shows greater strength as well, and both configurations suffer a considerable reduction in the lateral stiffness due to the knee elements yielding which reflects the significant contribution of the KBS to the lateral stiffness of the frame compared to the MRF.

The maximum axial force developed in the brace element depends on the plastic moment of the knee element, and during the post-elastic phase produces only a small increase in the brace force with a substantial increase in the storey drift as shown in Fig. 2.8(b).

The redistribution of the bending moment in the column and the beam where the knee element is connected to is shown in Fig. 2.9. Here the ratios of the bending moment at the locations indicated are plotted against the lateral displacement ratio of the frame.

Most are characterised by a change of more or less significance in the slope on yield. The redistribution can be beneficial in delaying the yield in the main members.

2.3.3 ENERGY DISSIPATION CAPACITY

The primary feature of the KBF is its ability to dissipate energy through the sacrificial elements (knee element) with a good reserve of elastic restoring force which prevents a total collapse. The area enclosed by each of the lateral force-deflection hysteresis loops is the energy dissipated by the frame in that cycle. The X-knee bracing system (XKBS) has the ratio of the energy dissipated during one cycle to the maximum storey drift greater than that corresponding to the K-knee bracing system (KKBS), this is however with a penalty of an increase in the global shear force. However the amount of energy dissipated in one cycle under the same cyclic loading is larger in the KKBS configuration. From the energetic point of view the XKBS seems to be more suitable for structures where storey drift has to be controlled, the case for tall buildings, whereas the KKBS is more beneficial for structure where shear force constitutes a major problem.

2.4 PARTIAL END-FIXITY OF THE KNEE ELEMENT

In practice the knee element connections to the beams and columns cannot be perfectly rigid Fig. 2.10(a). The effect of partial end-fixity on the dynamic behaviour of knee braced frames is investigated in this section

2.4.1 END-FIXITY COEFFICIENTS

The knee element and its support are simulated by a uniform beam resting on four supports as shown in Fig. 2.10(b). The central span is of fixed length l_k and carries a central concentrated load P, and two outer spans are of variable length $C_1 l_k$, $C_2 l_k$, the nondimensional parameters C_1, C_2 specifies the degree of rotational constraint at the ends of the central span. With $C_1=C_2=0$ the central span becomes fixed-ended, while if C_1 and C_2 are infinite this span is effectively simply supported at its ends [72].

The bending moments M_1 and M_2 at the intermediate supports of the beam shown in Fig. 2.10(b) can be found using the three moment equation

$$M_1 = [3(1+2C_2) / 8(3+4C_1+4C_2+4C_1C_2)]\, Pl_k \qquad (2\text{-}10)$$

$$M_2 = [3(1+2C_1) / 8(3+4C_1+4C_2+4C_1C_2)]\, Pl_k \qquad (2\text{-}11)$$

The bending moment diagram at the first yield is shown in Fig. 2.10(b), the corresponding yield load P_{y1} can be obtained by statics

$$P_{y1} = (8M_p/l_k)\, [(3+4C_1+4C_2+4C_1C_2)/(3+5C_1+5C_2+8C_1C_2)] \qquad (2\text{-}12)$$

Above P_{y1} rotation occurs at the central plastic hinge. The bending moment at the support 1 corresponding to the smallest coefficient C_1 reaches the value M_p when P attains the value P_{y2}, where P_{y2} is the load at which a plastic hinge is formed at node 1, the second yield point can be found as

$$P_{y2} = (16M_p/l_k)\, [(3+4C_1+4C_2+4C_1C_2)/(6+5C_1+11C_2+8C_1C_2)] \qquad (2\text{-}13)$$

The bending moments at support 2 reaches the value M_p when

$$P = P_c = 8M_p/l_k \qquad (2\text{-}14)$$

which is the collapse load. Eq. (2-14) shows that the collapse load is independent of the degree of end-fixity as specified by C_1 and C_2.

Estimation of deflections at the yield points and the collapse point is simplified by neglecting strain-hardening effect and the spread of plastic zones. Using the equations of equilibrium and compatibility, the deflection at midspan d_{y1} corresponding to the first yielding point can found as

$$d_{y1} = (M_p l_k^2/24EI)\, [(3+10C_1+4C_2+16C_1C_2)/(3+5C_1+5C_2+8C_1C_2)] \qquad (2\text{-}15)$$

and in terms of the maximum elastic deflection for a fixed-ended beam d_{el} the above equation becomes

$$d_{y1} = d_{el}\,[(3+10C_1+4C_2+16C_1C_2)/(3+5C_1+5C_2+8C_1C_2)] \tag{2-16}$$

For $C_1 = C_2 = C$, the yield and collapse point and their corresponding deflections are

$$P_{y1} = (8M_p/l_k)\,[(3+2C)/(3+4C)] \tag{2-17}$$

$$d_{y1} = (M_p l_k^2/24EI)\,[(3+8C)/(3+4C)] \tag{2-18}$$

$$P_c = 8M_p/l_k \tag{2-19}$$

$$d_c = (M_p l_k^2/24EI)\,(1+4C) \tag{2-20}$$

where

P_c : collapse load

d_c : deformation corresponding to the collapse point.

Load-deformation relations derived from these results are shown in Fig. 2.10(c). When C=0 (the fixed-ended condition), the yield load P_{y1} coincides with the collapse load P_c, showing that in this special case all three plastic hinges form simultaneously. As C increases both P_{y1} and the slope of the load-deflection relation between P_{y1} and P_c are progressively reduced, so that the deflection d_c at the point of collapse becomes larger. For the values of C in excess of, say, 3, unacceptably large deflection would develop before the plastic collapse load was reached, in such cases the ultimate collapse load would be of little interest to the designer since the normal purpose of calculating the collapse load is to determine the load at which large deflections are imminent.

In the extreme case when C is infinite, the deflection at the point of collapse is $4M_p/l_k$ which is the collapse load for simply supported beam of span l_k [72].

The coefficient C represents the degree of the end-fixity of the knee element includes the specific joint flexibility (semi-rigidity of the connections) and the effect of beam and column flexibility. The yield occurs simultaneously or distinctly at the ends and the midspan of the knee element depending on the degree of rigidity of the connections and the relative flexibility of the beams and the columns with respect to the knee element, the yielding sequence can be estimated using Eqs.(2-17) to (2-20).

2.4.2 EFFECT ON THE INITIAL ELASTIC STIFFNESS :

Applying this analysis to the particular case here. The stiffness of the KBS increases with the degree of fixity of the knee element connections. KBSs with perfectly fixed ended knee elements are twice as stiff as those with pinned knee elements. Between these two extremes the stiffness varies according to the values of C. As shown in Fig. 2.11 when C=0 the yield occurs simultaneously at the midspan and the ends of the knee element and results in a bilinear relationship of the overall load-deformation of a single cell frame, however for small values of C the yield occurs first at midspan and then at the ends which results in multilinear load-deformation relationships.

2.4.3 EFFECT ON THE KNEE ELEMENT DUCTILITY

Based on the yield mechanism of a fixed-ended beam, the knee element ductility can be estimated by the expression (2-8) developed in Section 2.3.1. However for a partially fixed knee element characterised by the coefficients C_1 and C_2, the maximum ductility, μ_c, corresponding to the maximum storey drift, δ, is given by

$$\mu_c = (\delta/d_{y1}) \cos\phi \tag{2-21}$$

the ratio, r, of the maximum ductility in a partially fixed knee element, μ_c Eq. (2-21), to that of a perfectly rigid knee element, μ Eq. (2-8), can be written as

$$r = \mu_c/\mu = d_{el}/d_{y1} = (3+5C_1+5C_2+8C_1C_2)/(3+10C_1+4C_2+16C_1C_2) \tag{2-22}$$

This implies that for a given storey drift the maximum ductility in a partially fixed knee element characterised by a coefficient $C_1=C_2=C$ is reduced by the factor

$$r = (3+4C)/(3+8C) \tag{2-23}$$

2.4.4 EFFECT ON THE ENERGY DISSIPATION CAPACITY

As seen in Section 2.4.2 the end-fixity coefficients may affect the load-deformation relationship, consequently the energy absorption capacity for a given storey drift is also altered. Fig. 2.12 shows the hysteresis loops for rigid, semi-rigid, and pinned

connections. The loops are bilinear for fixed-ended and pinned knee elements. In these cases, the total energy dissipated in a complete symmetrical hysteresis loop is proportional to the collapse load P_c [36] and is given by the following expression

$$E_H = 4P_c(1-k_2/k_1)\delta_0 \qquad (2\text{-}24)$$

where k_1 and k_2 are the first and the second slope of the bilinear loop, and d_0 is the displacement incurred during yielding (Fig. 2.12). Eq. (2-24) implies that the energy dissipated by a fixed-ended knee element is almost twice the corresponding energy dissipated by a pinned knee element. These two values constitute the upper and lower bounds of the energy dissipated by a partially fixed knee element ($C \neq 0$) having a multilinear hysteresis loop.

2.5 CONCLUSION

The introduction of the design parameters I_k/I_c, l_k/H, and α characterising the knee element stiffness, length, and geometric configuration play dominant roles on the elastic behaviour of the knee braced frames. Knowing the influence of these parameters is very useful in the design process to control the initial elastic stiffness, the strength, and the energy dissipation capacity of the frame. It has been shown that a high elastic stiffness can be achieved by reducing the length of the knee element or by increasing its stiffness, and more importantly is the ability of the knee element to affect the force distribution in the different structural members and consequently to enforce a certain yielding sequence in the frame. On the basis of the previous analysis, general guidelines for the design of the knee element can be summarised as

I_k/I_c : [0.01, 0.30]

l_k/H : [0.20, 0.35]

$\alpha \approx \phi$ or $x = l_k/\sqrt{1+(2H/L)^2}$ $y = l_k/\sqrt{1+(L/2H)^2}$

Although the results presented herein are subject to the limitation of the assumptions made in the analysis, initial values can be selected within these boundaries and then refined with regard to each parameter to meet the requirements of specific cases.

An expression to estimate the ductility demand in a knee braced frame has been developed and compared with the results of quasi-static analysis. A comparison between two different knee bracing system showed that the X-knee bracing system is more efficient in meeting drift control requirements than the K-knee bracing system, but with the penalty of an increase in the global shear force.

The effect of partial end-fixity in the knee element on the frame characteristics was investigated. Generally rigid knee element connections result in stiff knee braced frames and lead to large plastic deformations and a high energy dissipation capacity for a given storey drift.

Chapter 3

DYNAMIC BEHAVIOUR OF KNEE BRACED FRAMES

DYNAMIC BEHAVIOUR OF KNEE BRACED FRAMES

3.1 INTRODUCTION

This chapter is intended to investigate the performance of knee braced frames under earthquake motions. The capacity of the KBS to dissipate energy is evaluated using the energy concept which will be briefly described. The amount of damage the knee elements may suffer after an earthquake will be measured by the conventional maximum ductility and the number of yield and reversal excursions. The sequence of yielding of the KBF and the range of contained yielding will be examined. However, before the presentation and interpretation of the results it is worth looking at some analytical modeling techniques and theoretical aspects related to structural dynamics, and the way they were implemented in the computer programs used in this study.

3.2 ANALYSIS PROCEDURE

A brief description of the dynamic theory of structures is given in the following section. The purpose of the presentation is to explain the basis of the methods of analysing the forces and deflections developed in a structure when it is subjected to an arbitrary dynamic loading. Details of the structural dynamics may be found in several books [23,27,75,106]

3.2.1 BASICS OF STRUCTURAL DYNAMICS

The equation of motion of a multi-degree of freedom (MDOF) system can be written as:

$$M\{\ddot{u}\} + C\{\dot{u}\} + K\{u\} = \{P(t)\} \qquad (3\text{-}1)$$

where {P(t)} is a vector of arbitrary time varying loads or of effective loads which result from ground motion, in this case equation (3-1) can be expressed as

$$M\{\ddot{u}_r\} + C\{\dot{u}_r\} + K\{u_r\} = -M\{\ddot{u}_g\} \qquad (3\text{-}2)$$

where

M : mass matrix

C : damping matrix

K : stiffness matrix

{u} : absolute displacement vector, the dots represent differentiation with respect to time

$\{u_r\}$: relative displacement vector with respect to the ground

$\{\ddot{u}_g\}$: ground acceleration vector

For a seismic analysis the solution of the above equation (3-2) is sought. The most commonly used methods for the analysis of the seismic response of structure are :

i) mode superposition method

ii) direct integration methods

iii) response spectrum method.

The mode-superposition procedure is based on the normal-coordinate transformation, which serves to change the set of *n* coupled equations of motion of a MDOF system into a set of *n* uncoupled equations, each of which is then solved 'exactly' using the Duhamel integral, or by numerical integration techniques. The solution for each mode is summed to give the structure's total response. This method can be used to evaluate the dynamic response of any linear structure for which the displacements have been expressed in terms of a set of *n* discrete coordinates and where the damping can be expressed by modal damping ratios [23]. The mode-superposition procedure is described in detail in Ref. [88] and briefly in appendix A. The most time consuming phase of the analysis is the solution of the eigenvalue problem. If the order of the matrices is large, the computer time required to solve all eigenvalues and vectors can be enormous. However, it is usually sufficiently accurate to include only the lowest eigenvalues and associated vectors in the analysis because the participation of higher modes in the response is insignificant [9].

An alternative procedure to obtain the solution to Eq. (3-2) is by direct integration. In this case the step-by-step integration is performed directly on equation (3-2). The

advantages of this method is its general applicability for the analysis of linear and nonlinear systems, and the damping matrix need not be selected to satisfy modal orthogonality conditions. Many procedures are available for the numerical integration of the incremental equation of motion, namely, the Newmark generalized acceleration scheme, the Houbolt method and the Wilson θ-method [9,10,11]. The Newmark method (also called the constant average acceleration method) implemented in DRAIN2D and ANSYS program is discussed in detail in appendix A [14,25].

As with any numerical integration process the accuracy of the step-by-step methods depends on the size of the time increment, Δt. Three factors must be considered in the selection of this interval: (1) the rate of variation of the applied loading, (2) the complexity of the nonlinear damping and stiffness properties, (3) the highest frequency of interest. In general, an increment-period ratio $\Delta t:T = 1:10$ is a good rule of thumb for obtaining reliable results. If there is any doubt about the accuracy of the given solution, a second analysis can be made halving the time increment; if the response is not changed appreciably in the second analysis, it may be assumed that the errors introduced by the numerical integration are negligible [23]. An assessment of the stability and accuracy of the different integration schemes in terms of period elongation and amplitude decay is presented in Ref. [9,42].

As mentioned earlier the mode-superposition methods requires the evaluation of the mode shapes and frequencies, which is a very large computational task in systems with many degrees of freedoms. In these cases it may be advantageous to use the direct integration approach for the analysis of linear systems. In general, direct step-by-step integration tends to be more useful in evaluating the response of large, complex structures to short-duration impulsive loads which tend to excite many modes but which require that only a short response history be evaluated [23].

In some cases for initial building design it is sufficient to determine only the maximum of the response quantities. To this end the concept of response spectrum was introduced which can be briefly stated as a plot of the maximum response (maximum displacement, velocity, acceleration, or any other quantity of interest) to a specified load function for

all possible single degree of freedom systems. The abscissa of the spectrum is the natural frequency (or sometimes the period) of the system and the ordinate is the maximum response [79]. The maximum response of any mode of a MDOF system with a frequency f and damping ratio ξ can be obtained from a given earthquake response spectra as a SDOF. In general the modal response maxima do not occur simultaneously, and thus they cannot be superposed directly to obtain the total maximum. Therefore several methods are actually used to combine the response of all modes of interest in efficient manner these being the *root mean square method*, the *complete quadratic combination method*, and the *double sum method* [17].

3.2.2 FINITE ELEMENT PROGRAMS USED FOR DYNAMIC ANALYSIS

Two finite element programs were used in this project to carry out modal, linear, and nonlinear dynamic analyses of a variety of planar and space frames subjected to earthquake loading. A number of aspects of the two packages will be briefly described below.

The DRAIN2D finite element package [53] is designed for the determination of the inelastic dynamic response of a planar assemblage of discrete elements to earthquake type ground motions. The program uses step-by-step integration with a constant average acceleration assumption to calculate the dynamic response. Within each time step, the structure is assumed linear and has a stiffness equal to the tangent value at the beginning of the step. Any unbalanced loads resulting from errors in the assumed linear behaviour within the time step are corrected by substraction the unbalanced loads from the external dynamic load in the next time step. To prevent overshoots and to ensure the accuracy of the calculation a small time step is required throughout the computation. At times during the analysis for the work here slight numerical overshoots have occurred but these had only negligible effect on the accuracy of the results.

The program package ANSYS is a general purpose finite element program. It offers a wide range of elements and analysis types, and with a powerful pre- and post-processing capabilities. The use here was to extract the mode shapes and the natural frequencies of

the structures and to carry out linear and nonlinear dynamic analyses of two and three dimensional frames.

ANSYS uses three mode extraction procedures [29,61], (1) complete extraction from reduced matrices, (2) partial extraction from reduced matrices, and (3) partial extraction from full matrices. These procedures are referred to as (1) Householder, (2) reduced subspace, and (3) full subspace, respectively. The first two procedures include a Householder extraction step; the full subspace scheme uses Jacobi iterative eigenvalue extraction [10]. Which procedure is best depends upon the nature of the problem. The reduced subspace procedure was used in most of the analyses because the selection of the master degrees of freedom was easy and only the lowest modes were needed.

A powerful feature of the ANSYS program is the capability to solve the response of a large structural system by the Guyan reduction. The reduced stiffness matrix is exact, whereas the reduced mass and damping are approximate. Ideally the master degrees of freedom should have a large participation in the lowest modes and frequencies of the structure, while those eliminated should be associated with higher modes and frequencies.

The ANSYS program uses the same integration scheme as DRAIN2D (appendix A) but it has a convergence algorithm which corrects the response whenever an element exceeds its elastic limit within a time step. This process, however was ruled out by the large amount of run time and storage capacity needed. In addition to the power of the software and hardware, the modeling techniques of structures play dominant role in the efficiency of the calculations and the reliability of the results.

3.2.3 PRACTICAL MODELING OF KNEE BRACED FRAMES

The overall approach used in this section is aimed at developing practical analytical techniques for seismic prediction of knee braced frames, and investigating the degree to which simple practical mathematical models can accurately reflect the linear and nonlinear dynamic properties of this type of frame. The effects considered will be the flexibility of the joints, the effect of the floor rigidity on the overall stiffness, and

the various way mass can be modelled as well as the effect of level of detail of the modeling which will be considered again in Chapter 7 when the analytical and experimental results are compared.

Although the use of more advanced analysis techniques and more representative descriptions of earthquake excitations generally lead to improved accuracy in predicting structural response, several difficulties arise in the implementation of these procedures in practical design of the KBS. In order to assist the design engineer in overcoming these difficulties a simple one-dimensional model is developed here which may be used for preliminary design of knee braced frames by dynamic or equivalent static analysis procedures.

The total initial stiffness of a KBF is the sum of the lateral stiffness of the MRF and the knee bracing system (KBS) as illustrated in Fig. 3.1(a)

3.2.3.1 *Lateral stiffness of the moment resisting frame*

Most of the manual procedures for estimating storey deflections of unbraced steel frames are based on the following assumptions:

(1) The beams and columns are inextensible and the effect of shear stress is disregarded.

(2) Beams and columns have points of contraflexure at midspan or midstorey.

(3) The centre-to-centre spacing of columns is constant across the frame, and the storey height is constant.

Since the deflections will be the same for any column line of a frame, a typical interior column line as shown in Fig. 3.1(b) can be selected as the basis for calculating the storey equivalent stiffness [21].

For upper storeys

$$K_m = \frac{12\ EI_c}{H^3[1+I_cL/I_bH]} \qquad (3\text{-}3)$$

For the bottom storey

$$K_m = \frac{24\ EI_c}{H^3[2+I_cL/I_bH]} \tag{3-4}$$

An equivalent equation to (3-3) is given in Ref.14 where the beam depth was taken into account

$$K_m = \frac{12\ EI_c}{[(H^2L/I_b) + (H-d)^3/I_c]} \tag{3-4}$$

The effect of beam-to-column joint flexibility was accounted for by reducing the beam rigidity using the formula

$$\frac{I_b}{L}_{red} = \frac{I_b/L}{[1 + 6EI_b/K_\theta L]} \tag{3-5}$$

where

K_m : equivalent lateral stiffness of the MRF

I_b : moment of inertia of a beam

I_c : moment of inertia of a column

E : Young's modulus of elasticity

L : bay width

H : storey height

d : beam depth

K_θ : joint rotational spring stiffness.

3.2.3.2 Lateral stiffness of the knee bracing system

Assuming that the lateral load F_b carried by the KBS, as shown in Fig. 3.1(c), is transmitted to the knee elements through the diagonal braces as

$$P = F_b/(2\cos\phi) \tag{3-6}$$

which causes a longitudinal elongation of brace element

$$d_d = \frac{P\, l_d}{EA_d} \tag{3-7}$$

where l_d, and A_d are the length and cross sectional area of the brace, respectively.

The deflection caused by the same force at midspan of a fixed-ended knee element can be calculated using

$$d_k = \frac{P \sin(\phi+\alpha)\, l_k^2}{192\, EI_k} \tag{3-8}$$

Using the geometric compatibility of Fig. 3.1(c) an expression relating the maximum storey drift δ to the brace and knee element deflection can expressed as

$$\delta \cos\phi = d_k + d_d \tag{3-9}$$

Using Eqs.(3-6) to (3-9), the equivalent lateral stiffness of the KBS, K_b can be derived from

$$F_b = K_b\, \delta \tag{3-10}$$

which yields

$$K_b = \frac{384\, EI_k\, A_d \sin(\alpha+\phi) \cos^2\phi}{192\, I_k l_d + A_d l_k^3} \tag{3-11}$$

where α and ϕ as shown in Fig. 3.1(c) represent the angles between the knee element and the beam, and the brace element and the beam, respectively.

3.2.3.3 **Effect of the knee element flexible supports**

For a pinned knee element Eq. (3-11) becomes

$$K_b = \frac{96\, EI_k\, A_d \sin(\alpha+\phi) \cos^2\phi}{48\, I_k l_d + A_d l_k^3} \tag{3-12}$$

In the actual case, however, the knee elements are neither pinned nor perfectly rigid, because of the beams and columns flexibility, and the imperfection of connections. To take account of these effects, the end-fixity coefficient C defined in Section 2.4 can be incorporated in expression (3-11)

$$K_b = \frac{384\ EI_k\ A_d \sin(\alpha+\phi) \cos^2\phi}{192\ I_k l_d + A_d l_k^3[(3+8C/3+2C)]} \tag{3-13}$$

3.2.3.4 Elastic and post-elastic characteristics of the one dimensional model

In the elastic phase the lateral stiffness of the KBF, K_1 is given by

$$K_1 = K_m + K_b \tag{3-14}$$

The post-elastic stiffness K_2 of a KBF with either a pinned or fixed-ended knee element is idealised by an elasto-plastic model which gives a value for K_2 equal to the lateral stiffness of the MRF, K_m. In this case the overall shear storey-drift relationship is bilinear (Section 2.4). The yield deflection δ_{el} and the corresponding shear force storey F_{el} in terms of the plastic bending moment of the knee element M_p can be written as

$$\delta_{el} = \frac{8\ M_p\ \cos\phi}{K_b\ l_k\ \sin(\phi+\alpha)} \quad \text{for pinned knee element} \tag{3-15}$$

$$\delta_{el} = \frac{16\ M_p\ \cos\phi}{K_b\ l_k \sin(\phi+\alpha)} \quad \text{for encastre knee element} \tag{3-16}$$

and the shear yield force

$$F_{el} = K_1\ \delta_{el} \tag{3-17}$$

The first yield point of a KBF with partially fixed knee elements can be approximated from the yield displacement

$$\delta_{el} = \frac{16\ M_p\ (3 + 2C)\ \cos\phi}{K_b\ l_k\ (3 + 4C)\ \sin(\phi+\alpha)} \qquad (3\text{-}18)$$

3.2.3.4 Assessment of the one dimensional model

A comparative study is performed on a two dimensional and a one dimensional model of a 10-storey prototype structure given in Ref. [21] and described in Section 4.2. The purpose of this analysis is to test the accuracy of the results predicted by the one dimensional model. This model consists of a shear type beam with masses lumped at floor levels as shown in Fig. 3.2. The elastic and post-elastic characteristics of the beam were determined using the equations (3-4), (3-11), (3-14), (3-16), and (3-17). As shown in Fig. 3.3(a) the mode shapes and the natural frequencies predicted by the one dimensional model are in good agreement with those of the two dimensional (less than 8%). The differences between the 1-D model and the 2-D model result from the fact that some cantilever type deformation (in addition to shear type) is caused by axial extension or compression of the columns in the 2-D model, whereas the 1-D model behaves as shear beam with little or no cantilever type response. Both models were subjected to El-Centro earthquake which caused plastic deformations in the knee elements of the 2-D model and the 1-D beam model nearly at the same time. The shear type phenomenon in 1-D model can be clearly seen in Fig. 3.3(b) where the maximum lateral displacements of the simplified 1-D model constituted an envelope to those predicted by the 2-D model. The envelope margin varies from 60% at the bottom storey to 0% near the top of the frame. The time histories of the displacement of the top floor plotted in Fig. 3.3(c) show an excellent correlation between the two models in the elastic phase, but some discrepancies in terms of amplitude and phase characterise the inelastic phase, nevertheless the overall pattern was in fairly good agreement.

3.3 ENERGY CONCEPT

In addition to the usual parameters employed for evaluating the performance of structures under earthquake excitation the energy concept will be used throughout this study as a key element for the assessment of the energy dissipation capacity of the

KBFs. A number of aspects of the energy concept need to be elaborated in order to be used efficiently and accurately.

The equation of motion for a single degree of freedom (SDOF) shown in Fig. 3.4 subjected to an earthquake excitation can be written as follows:

$$m\ddot{u}_r(t) + c\dot{u}_r(t) + R[u_r(t)] = -m\ddot{u}_g \tag{3-19}$$

or in terms of the total displacement u

$$m\ddot{u}(t) + c\dot{u}_r(t) + R[u_r(t)] = 0 \tag{3-20}$$

where

m : mass of the structure

c : damping coefficient

u(t) : absolute displacement of the mass

$u_r(t)$: relative displacement of the mass

$\ddot{u}_g(t)$: ground acceleration

$R[u_r(t)]$: restoring force for the structure.

Integration of the differential equation of motion (3-20) with respect to the displacement u_r yields :

$$\int_0^u m\ddot{u}(t)du_r + \int_0^u c\dot{u}_r(t)du_r + \int_0^u R[u_r(t)]du_r = 0 \tag{3-21}$$

Replacing du_r by $(du-du_g)$ in the first term of Eq. (3-21)

$$\int_0^u m\ddot{u}(t)du + \int_0^u c\dot{u}_r(t)du_r + \int_0^u R[u_r(t)]du_r = \int_0^u m\ddot{u}(t)du_g \tag{3-22}$$

The first term on the left-hand side of Eq. (3-22) represents the absolute kinetic energy (E_K) of the structure considered. The second term represents the energy dissipated by viscous damping (E_D), and the third term represents the sum of the irrecoverable hysteretic energy (E_H) plus the recoverable elastic strain energy (E_S). The right-hand

side is conventionally defined as the total input energy (E_I) to the structure which represents the work done by the total base shear at the foundation displacement. The energy equation given by Eq. (3-22) can be written as follows:

$$E_I = E_K + E_D + E_a$$

or

$$E_I = E_K + E_D + E_H + E_S \qquad (3\text{-}23)$$

During the seismic response of an inelastic system, part of the imparted energy is dissipated by damping and inelastic deformation of the components of the structure, and the reminder is stored temporarily in the system in the form of kinetic and strain energy. By the end of the response all the imparted energy is dissipated [6].

3.3.1 ENERGY TIME HISTORY CHARACTERISTICS

The properties of the energy time histories will be investigated through a nonlinear response of a typical single storey knee braced frame subjected to two types of earthquake motion as shown in Fig. 3.4(b). This section deals with the manner in which the input energy to the structure is transformed into the different forms of energies. The results obtained from the analysis showed that a large proportion of the total energy imparted to the elastic frame (or system with poor energy dissipation capacity) is temporarily stored in form of kinetic and strain energy and is therefore characterised by the high spikes shown in Fig. 3.5. The same phenomenon has been observed before [111] for a very low frequency structure. However in the inelastic response, the hysteretic energy (in this case dissipated by the knee elements) constitutes a major part of the total input energy. From Fig. 3.5 it is apparent that the stored energy represents only a small proportion of the energy imparted to the structure, the latter is dissipated almost immediately by yielding. Most of the inelastic deformation in the knee elements, when subjected to Parkfield earthquake (impulsive type), took place at the same ıme the peak ground acceleration resulting in large hysteretic loops with few yield excursions whereas the yield excursions under San Fernando earthquake were more numerous and more

uniformly distributed in time. This is shown in Fig. 3.6. The energy time history of damped systems are characterised by a minimum difference between the input and absorbed energy, however, large fluctuations generally reflect an inefficiency of the damping mechanism.

3.4 SEISMIC RESPONSE OF KNEE BRACED FRAMES

The purpose of this part of analysis is to investigate the dynamic nonlinear response of a prototype KBF in terms of the energy dissipated by inelastic deformations of the knee elements, the ductility distribution through the height, and the order of yielding in the frame members. The response of the analysis when compared with the computed response for a similar moment resisting frame (MRF) and a concentrically braced frame (CBF), show the superior performance of the KBF.

3.4.1 DESCRIPTION OF THE STRUCTURES

The structure used for analysis is a typical 10 storey frame of those used in commercial office buildings. The dimensions, member sizes, and other properties of the moment resisting frame are similar to those given in Ref. [21] (the structure is used as a prototype for a small scale model -see Chapter 4 for details). The cross sectional area of the braces was determined to retain 80% of their original buckling capacity [77]. The family of three 10 storey frames are shown in Fig. 3.7.

DRAIN 2D was used for this analysis [53]. The mass is assumed to be lumped at the nodes, and the moment-rotation relationships at the plastic hinges are represented by a bilinear model taking into account the effect of the axial forces by selecting appropriate axial-bending moment interaction surfaces. The three frames were subjected to El-Centro earthquake scaled by factors increasing from 0.1 to 2.0 to give peak accelerations from 0.035g to 0.70g respectively.

3.4.2 KNEE ELEMENT DAMAGE CAPACITY

The displacement ductility does not account for the cumulative damage that may occur as a result of reversed inelastic deformation, so both the maximum knee element ductility and the accumulated plastic rotations are considered. In addition the number of yield excursions (number of times the knee element is in a yield state) and the number of yield reversals (number of times the knee elements yield consecutively in opposite directions) as defined in Ref. [111] are introduced for a better assessment of the damage a knee element may suffer during an earthquake. A greater number of yield excursions and yield reversals are associated with more damage. Although the knee elements are designed to be replaced after an earthquake they should not lose their hysteretic characteristics because of excessive damage during the earthquake. Fig. 3.8 shows the yield sequence time history, the number of yield excursions, the number of reversals, and the maximum ductility at mid-span of the knee elements at 1.5 times El-Centro excitation. The yield reversals of the knee element show a better distribution through the lower storeys of the building compared to the corresponding numbers of excursions. To withstand such a severe earthquake the knee element of a lower storey should have stable hysteretic loops for a dozen cycles with a maximum ductility of 8. Considering the knee element characteristics (shape, material, and mode of yielding) a balance between the above mentioned parameters is very important to prevent any one of them degrading the hysteretic behaviour of the loops. In general such requirements can be easily met in structural steel members [39,83,86].

3.4.3 DUCTILITY AND HYSTERETIC ENERGY DISTRIBUTION

One important feature of the KBF is that the ductility and the hysteretic energy are not concentrated in only one or two storeys as shown Fig. 3.9. A good design should allow a uniform distribution of ductility through the height. Therefore an attempt was made to predict the distribution by considering mode shapes of the knee element deformations plotted in Fig. 3.10. The maximum elastic and moderate plastic deformations of the knee elements followed more or less closely the shape of the knee

element deformation determined by the first mode, whereas the plastic deformations of the knee elements of the lower storeys during severe intensities tend to be amplified because of the lateral stiffness reduction. The yield concentration depends on the ratio of the equivalent lateral stiffness of the KBS to the total stiffness of the frame, generally strong post-elastic restoring force (provided by the still elastic main structural members) prevents excessive local yielding. The yield concentration is more pronounced in the MRF and the CBF because of the significant reduction of their stiffness caused by the yield of the main structural members (beams and columns) as shown in Fig. 3.9.

3.4.4 STRUCTURAL RESPONSE PARAMETERS

The effectiveness of the KBS in improving the seismic response is seen in comparisons of the results with the MRF and the CBF. The maximum lateral deflection, shear envelopes, and the column maximum bending moment of the three frames are plotted in Fig. 3.11. The deflection at the top of the KBF is about 45% of MRF and about 60% of CBF. The maximum shear at the base of the KBF is 83% and 60% of the MRF and CBF respectively. The maximum column bending moment of the bottom storey of the KBF was less than half of the MRF and the CBF.

The energy dissipated by the knee elements alone through plastic deformations is a major part of the total energy imparted to the KBF as shown in Fig. 3.12. The input energy is almost immediately absorbed by the knee elements which helped to minimise at all times the free energy. However the hysteretic energy of the MRF is characterised by discrete major jumps which resulted in larger peaks of the free energy (the difference between the input and the dissipated energy). As can be seen from Fig. 3.12 the growth of the free energy and consequently the maximum top floor displacement of the frames occurred nearly at the same time, similarly at the end of the time history the stored energy in the MRF was very small and the top floor displacement was reduced.

3.4.5 YIELDING ORDER IN KBFs

As mentioned earlier (Chapter 1) the prediction and control of the sequence of yielding in ductile systems is very important. The parametric study (Chapter 2) demonstrated that it is possible to enforce a certain sequence of yield in the KBFs. In this section an attempt to investigate this feature was made by observing the propagation of yielding in the three frames when subjected to increasing earthquake intensities. The damage experienced by different frames after being subjected to increasing intensity levels is shown in Fig. 3.13. A diagram which illustrates the elastic and post-elastic regimes as well as the percentage of damaged (yielded) elements is sketched in Fig. 3.14. In this particular case an early yielding of the knee element started at very low intensity, sometimes it is advantageous to increase the elastic region so that the frame can resist wind load and minor earthquakes elastically. This can be achieved easily by increasing the knee element strength. One advantage of the KBF is that it has a wide range of contained yielding before any damage reaches the main framing. An early yield of the knee elements occurred at an acceleration lower than 0.1g, at the same time the braces of the CBF started to buckle meanwhile the MRF was still in the elastic range. At 1.8 times El-Centro excitation (0.63g) 55% of the beams yielded in the MRF, 50% beams, 5% columns and 80% of braces yielded in the CBF, while none of the members yielded in the KBF. Of course, most of the knee elements (90%) yielded and participated to the process of energy dissipation.

3.5 CONCLUSIONS

The following remarks can be picked out from the results of this study

(1) Under certain assumptions the elastic and post-elastic equivalent lateral stiffness of KBFs can be estimated by hand calculations for preliminary design using simple analytical expressions.

(2) Energy time histories may be used for the assessment of the performance of a structure.

(3) Requirements for the maximum ductility, number of yield and reversal excursions of knee elements of a KBF under severe earthquake could be easily met by a well designed steel members.

(4) Energy is dissipated by the knee elements throughout the height of the building rather than by localised plastic deformations of the main structural members.

(5) The KBS is efficient in reducing the response of the frame.

(6) The yield of the knee elements provide the frame with a wide range of contained yielding.

(7) The knee element acts as safety valve to limit the loads exerted on the braces and hence buckling and yielding of the these are prevented.

Chapter 4

DIMENSIONAL ANALYSIS AND MODEL DESIGN

DIMENSIONAL ANALYSIS AND MODEL DESIGN

4.1 INTRODUCTION

The purpose of producing models of dynamic structural behaviour is to allow the assessment in the laboratory of the probable response of a structure to a prescribed loading. It is obviously of paramount importance to construct these models to reflect reality as accurately as possible. The problem with this is that the similitude requirements are sometimes impractical, whereas the difficulties in the mathematical modeling is that the real dynamic behaviour of structures is imperfectly known [49], and in both cases there are always differences between models and reality.

In this chapter a brief introduction to dimensional analysis is given emphasising the practical techniques used in small scale modeling of steel structures. Design details of a 1:12 scale model of a ten storey building are presented with a sequence of cyclic testing of the knee bracing system in order to determine the stiffness, strength and the hysteretic loop characteristics of the knee elements. The strain-displacement curves will be used later to convert the strain time-histories into displacement time-histories. The implications of imperfect similitude are investigated, and a mass adjustment technique is proposed to compensate for the modeling distortion. Finally the merits and limitations of using this technique in small scale modeling are discussed.

4.2 SIMILITUDE REQUIREMENTS

Any structural model should be designed, loaded, and interpreted according to a set of similitude requirements that relate the model to the real structure. These similitude requirements are based upon the theory of modeling which can be derived from a dimensional analysis of the physical phenomena involved in the behaviour of the structure.

In general structural modeling problems are mechanical, thus the measures of length, force, and time are most important. The theory of dimensions states that the equations for some physical quantities, of interest, X_1, X_2....., X_n, i.e,

$$F(X_1,X_2,X_3,.....,X_n)=0$$

can be expressed equivalently in the form:

$$G(\pi_1,\pi_2,\pi_3,.....,\pi_m)=0$$

where the π terms are dimensionless products of the physical quantities $X_1,X_2,....,X_n$. Generally, it can be stated that the number of dimensionless products (m) is equal to the difference between the number of physical variables (n) and the number of fundamental measures (r) involved i.e., $m=n-r$ [33]. This is Buckingham π theorem.

The question to be resolved in applying the π theorem pertains to the formulation of appropriate π terms. There are a number of formal techniques which involve setting up the appropriate dimensional equations. Consider an elastic structure made of homogeneous isotropic material whose vibration conditions are to be determined. Let S denotes the scale, that is, the factor by which one dimension in the prototype must be multiplied to obtain the corresponding dimension in the model. Also let subscript l refer to linear dimensions, t to time, and f to forces. Given S_l, S_t, and S_f, the scale of all other variables of interest can be obtained. The scales for the most usual variables given in Ref. [35], are written in the second column of Table 4.1.

Ordinarily in dynamic models, the scaling factors for length S_l and modulus of elasticity S_E are chosen and then all the other factors can be expressed as function of S_l and S_E. As can be seen from third column of Table 4.1, the density scale is equal to S_E/S_l which is normally different from one. This implies that the model should be made of different material than the prototype, in practice this condition is rather difficult to satisfy. The sixth column of Table 4.1 gives the scales corresponding to the case when the gravity forces are neglected [35].

When strength and post-yield response are important and gravity effects cannot be neglected, dynamic similitude theory dictates strict physical requirements that the model

must satisfy. Fortunately, for steel framed buildings the mass can often be assumed to be concentrated at floor level, permitting a simplification of the modeling constraints through artificial mass simulation (AMS). Modeling by AMS involves the addition of structurally uncoupled mass to augment the density of the model and permits selection of a model structural material without regard for mass density scaling (Table 4.1). This technique was widely used [31,51,103] in small scale steel frames. The nonlinear response of some steel-framed buildings to earthquakes has been investigated [94], and the correlation between prototype and model tests indicated that the model provided accurate simulation of the prototype and duplicated the energy-dissipation mechanism. Minor discrepancies in correlation were attributed to fabrication techniques that limit the applicability of this modeling method.

4.3 PRACTICAL DESIGN

A typical ten-storey frame of those used in commercial office buildings [21] was initially taken as a prototype for a small scale model design. The model was a three by three bay ten-storey building, both interior and exterior spans were 5.4m and the storey heights 3.6m. The structure was made of W305x350 columns and I406x178 beams. A factor of 1:12 was selected for length, and the scaling factor for the elastic modulus was fixed at unity.

Since solid round bars were to be used for the main members the similitude requirements of the dimensional analysis for the cross sectional area and the second moment of inertia (S_l^2, S_l^4) were not satisfied. For this reason, it was not possible to follow the exact requirements of dimensional analysis. However, some relaxation of the above condition is possible, provided that the effect is quantifiable, and can be compensated for [67]. This is discussed in Section 4.6.

The model was designed to resist the El-Centro earthquake scaled to give a maximum ground peak acceleration of 1g, the main frame members were selected to remain at all times elastic, only the knee elements would undergo plastic deformations. The diagonal braces should not buckle under compression. The other components such as the beam

connectors, and the screwed connectors (see Section 4.4.4) were designed to resist the induced forces and the fatigue performance was checked because of the prolonged cyclic nature of dynamic tests.

A series of preliminary tests on a small shaking table [104] was carried out on a single cell incorporating the first manufactured set of bracing components (Fig. 4.1). The performance of the system was examined in which yielding of the knee elements was observed. On the basis of the experimental observations minor changes to the knee elements and the connectors were made to improve their degree of fixity, to localise the yielding, and to control the strength level better.

4.4 DESIGN DETAILS OF A TEN-STOREY SMALL SCALE MODEL

As stated earlier the small scale model was not designed to duplicate a particular structure, but to simulate the behaviour of a range of typical multi-storey frames. A detailed description of the design procedure will be discussed in this section.

4.4.1 STRUCTURAL DIMENSIONS

The one twelfth scaling factor (S_l=1/12) was selected for length to fit up to a twelve-storey building within the headroom of the shaking Table. As mentioned before the basic configuration was a three by three bay ten storey structure. The storey height was 300mm and the bay span 450mm.

4.4.2 MOMENT RESISTING FRAME

The columns and beams of the four lower storeys are made of 19.1mm and 15.9mm solid round bars. Those of the upper storeys are reduced to 15.9mm and 12.7mm respectively. A total of 192 columns (285mm long), and 288 beams (425mm long) were made and joined together by specially manufactured block connectors so that the centre line lengths of the columns and beams once mounted coincided with the model storey height and the bay width.

4.4.3 BLOCK CONNECTORS

The beams and the columns are connected by blocks made of steel cubes, designed to ensure rigid nodes, and easy fitting, and also to allow different structural configurations. The beams and columns are linked to these blocks by means of 'Hydrostud' fittings Fig. 4.2(a) which determined the minimum dimensions of the cubes. The next largest available size of square bar (63.5x63.5mm) was chosen. It should be noted here that the size of the block connection is considerable when compared to the frame member lengths (about 20% and 15% of the storey height and the bay width respectively) which is common in small scale models [51]. Fig. 4.2(b) shows a typical block connection. A total of 176 blocks were made in four types, 16 blocks for fixing the bottom storey columns on steel plates base to be clamped to the platform, 16 intermediate blocks that permit the transition from 19.1mm diameter columns to 15.9mm columns, 48 blocks for the lower storey member connections, and 96 for the upper storeys. The most important features of these connection blocks are that they permit a relatively easy mounting of many building configurations, and damaged elements can be easily replaced.

4.4.4 KNEE BRACING SYSTEM

The small scaling makes the manufacture of the bracing system very difficult. However, by designing a relatively gross connection it was possible to realize the required knee element fixity, the brace pinned connections, the easy replacement of the yielded knee elements, whilst making the whole system removable. A unit bracing system is composed of thirteen pieces. Two knee elements made from solid bars 8mm in diameter, and 105mm long designed to be clamped to the columns and beams by means of four connectors. The knee element strength is controlled by a variable depth groove at the ends Fig. 4.3(a). Each of the two braces is composed of tension bar Fig. 4.3(b) (8mm diameter, 225mm long), and two screwed connectors, one is left hand threaded, the other is right hand threaded Fig. 4.3(c), which enables the tension to be adjusted in the brace elements. The central beam connector Fig. 4.4(a) ensures a pinned connection from the

braces to the beam in such a way that their centre lines coincide at one point in the middle of the beam.

4.4.5 FLOOR PLATES AND ADDED MASSES

In order to realise the AMS condition, an extra mass is needed at floor levels. To this end 6 mm thick steel plates were used to simulate the building floor, and to serve as supports for the lead masses. In order to minimise alterations to the structural stiffness, the plates were pinned to the edge of the block connections.

4.5 CYCLIC TESTING OF THE KBS

4.5.1 AIM

The aim of these tests was to investigate the cyclic behaviour of the small scale knee bracing system, and to determine experimentally the knee element characteristics. These are :

(1) Plastic moment capacity at midspan of the knee element

(2) Plastic moment capacity at the ends of the knee element

(3) End fixity coefficient, and

(4) Knee element stiffness,

which will be used for the analytical model, and finally the energy dissipation capacity was examined through the hysteretic loop stability.

4.5.2 TEST APPARATUS AND SPECIMENS

A knee bracing set composed of a diagonal brace and a knee element mounted on a beam and a column is shown in Fig. 4.5. The subassemblage was subjected to two loading schemes, (1) monotonic increasing tension or compression of the brace element until the failure of the knee element, and (2) cyclic loading with several cycles of gradually increasing amplitude. These tests were carried out using a Schenck servo-hydraulic testing machine using displacement control. The diagonal brace force and the

displacement of the knee element at midspan were recorded directly from the Schenck, and the knee element strains were measured by means of foil strain gauges. A total of ten knee element specimens were tested. Cyclic displacements were applied to specimens 3 and 9, and monotonically increasing displacement to all the other specimens, a list of the different specimen and the corresponding loading is given in Table 4.2.

4.5.3 KNEE ELEMENT GEOMETRIC CHARACTERISTICS

The brace axial forces recorded from the Schenck were plotted against the corresponding displacements which were assumed to be the knee element midspan deformation by neglecting the brace elongation which was less than 2% of the total displacement, Fig. 4.6. The geometric characteristics mentioned previously in Section 4.5.1 can be determined experimentally from the force-displacement curves, simply by finding the coordinates of the first and the second yielding points. Under the assumptions of Section 2.3, the theoretical coordinates of these two points are:

$$P_{y1} = 8\ M_p\ (3 + 2C)\ /\ (l_k\ (3 + 4C)) \tag{4.1}$$

$$d_{y1} = M_p\ l_k^2\ (3 + 8C)\ /\ (24\ EI_k\ (3 + 4C)) \tag{4.2}$$

$$P_c = 8\ M_p\ /\ l_k \tag{4.3}$$

$$d_c = M_p\ l_k^2\ (1 + 4C)\ /\ (24\ EI_k) \tag{4.4}$$

where :

P_{y1} : first yield force

d_{y1} : first yield displacement

P_c : second yield (collapse) force

d_c : second yield (collapse) displacement

M_p : plastic moment

E : Young's modulus

I_k : moment of inertia of the knee element

l_k : knee element length

C : end-fixity coefficient.

Because of the inaccuracy in determining the yield points, and to simplify the mathematical model of the KBFs further, fully rigid knee element ends are assumed i.e. C=0. The coordinates of the collapse point become :

$$P_c = 8\ M_p / l_k \tag{4.5}$$

$$d_c = M_p\ l_k^2 / 24\ EI_k \tag{4.6}$$

From the same force-displacement curve in Fig. 4.6, the yield point is defined by the intersection of the elastic line and the horizontal line of the collapse load. Consequently the knee element stiffness was reduced to nearly a third of the previous value to compensate for the effect of semi-rigidity of the knee element semi-rigid connections, the plastic moment remains practically unchanged.

4.5.4 BRACE-KNEE ELEMENT BACKLASH

The inevitable formation of gaps is due mainly to the knee element-brace connections. As can be seen in Fig. 4.7, where the brace force is plotted against the knee element midspan displacement, the hysteretic loops are shifted at the origin. This increases the required storey drift to obtain the same area that would be enclosed by a loop without the gap. Consequently the energy dissipation mechanism will be less efficient.

This type of nonlinear behaviour can be analytically modelled by a bilinear hysteretic model (knee element), and a conservative hardening elastic model (brace element) as shown in Fig. 4.7.

4.5.5 KNEE ELEMENT HYSTERETIC LOOP STABILITY

Good energy dissipation is the result of full hysteretic loops which a have large enclosed area and do not degrade in later cycles. Such loops are said to be stable. The loops formed at the midspan of the knee element (force at midspan vs bending strain of the knee element), shown in Fig. 4.8(a,b), are relatively stable. The degree of their stability is measured by the variation of the elastic slope during several severe cycles, as shown in Fig. 4.8(c) where the successive loading and unloading slopes derived from the hysteretic loop of Fig. 4.8(a) were plotted. Insignificant degradation can be observed in the unloading slopes.

4.5.6 KNEE ELEMENT STRAIN-DISPLACEMENT RELATIONSHIP

Because of the limited number of channels to monitor the test frames during the seismic testing, the stain-displacement recorded during monotonically increasing tests was used to convert the strain time histories of the seismic tests into displacement time-histories (see Section 5.4.3). The accuracy of this method will be examined by comparing the measured and computed displacement time histories. It can be demonstrated that the strain at the knee element midspan and the deflection at that point are directly proportional (linear relationship). However once the plastic hinge is formed, this relationship is no longer valid because of local rotations (Fig. 4.9). In reality, the yielding behaviour of the knee element is a complicated process and the strain at midspan is by no mean uniform. Thus local strain measurement cannot give a true picture of the bending strain distribution. The general nature of yielding, however, is clearly portrayed by the local strain. The displacement-strain curve, Fig. 4.9 is characterised by three more or less distinct phases, very sharp slope near the origin caused by the backlash, then the elastic and after that the plastic range where the increase in strain is accompanied by small change in displacement.

4.6 EFFECT OF THE SIMILARITY DISTORTIONS

4.6.1 GENERALITIES

The primary objectives of the model testing are to investigate the dynamic behaviour of knee braced steel frames, and to get a better understanding of the performance of their energy dissipation mechanisms without being interested in duplicating the exact response of a particular prototype, provided that the response of the model is within the range of similar real buildings. Thus an analytical study was carried out in order to quantify the discrepancies between the scaled model and the prototype structure due to the distortion in the similarity requirements, and to correct it by a mass distribution adjustment.

4.6.2 SIMILITUDE CORRECTION

The main members (columns and beams) of the knee braced frame remain elastic at all times, the only part that is subjected to yielding is the knee elements which also constitutes the main source of damping. Therefore the knee elements' geometric characteristics were kept under the similarity laws, and an attempt to duplicate the overall dynamic properties of the structures was made by using a mechanical simulation which for a given length scale coefficient S_l requires

$$K_p M_p^{-1} = S_l \, K_m \, M_m^{-1} \tag{4.7}$$

because of the uniform distribution of the stiffness and masses in the structures. K is taken as the total initial stiffness of the KBF which is the sum of the lateral equivalent stiffness of the MRF and KBS (Section 3.2.3), M is the floor mass.

The mass adjustment procedure as schematically shown in Fig. 4.10 consists of determining the mass distribution of the small scale model using equation (4.7) which ensures that the ratio of the storey stiffness to the floor mass of one dimensional model is similar to the prototype ratio.

4.6.3 CORRELATION BETWEEN THE MODEL AND THE PROTOTYPE

The discrepancies in response between the small scale model and the prototype structure was quantified through a comparative study of the responses of the two structures to the El-Centro earthquake in the elastic and plastic range as well as a study of their dynamic properties, i.e., natural frequencies, and mode shapes.

The model and prototype frequencies were within 10% (Table 4.3), and the mode shapes were very similar (Fig. 4.11). The maximum lateral deflection, the knee element maximum plastic rotation, and the accumulated plastic rotations were chosen for comparison. The scaled response parameters of the model were plotted together with those of the prototype in Fig. 4.12. Although there are relatively large discrepancies in the ductility demand of the knee elements between the prototype and the model, represented by the maximum knee element plastic rotations in Fig. 4.12(c), the distribution through the height was quite similar. The plastic deformation of the knee elements in the model are larger because the knee bracing system represents a larger portion of the total lateral stiffness in the model which leads to a weak restoring post-yielding system in the small scale model, moreover the cross section area of the model brace element is larger than the similar prototype brace, which means that for a similar drift storey, the knee element corresponding to a heavy brace will undergo a larger plastic deformations. The dissipated hysteretic energy in the two structures is very similar in quantity and distribution with height. The only difference caused by the incorrect modeling of the moment resisting frame stiffness in the model can be seen in the upper storeys, particularly at the fifth (transition) storey as shown in Fig. 4.12(a) where the hysteretic energy distribution is represented by the amount of the accumulated plastic rotations of the knee element of each storey. The top floor displacement time-histories in Fig. 4.13 shows the elastic and plastic responses of the prototype and model. The phase delay in the elastic range is because the first natural frequency of the prototype which dominated the response is 7% higher. The period elongation in the

nonlinear phase which is again more pronounced in the model is due to its weak post-elastic stiffness

4.7 CONCLUSIONS

The small scale dynamic model has proved to be a powerful tool in extending our knowledge and understanding the structural behaviour in many complex situations where analytical techniques are inadequate or to validate the existing analytical procedure by developing mathematical models that correlate well with the experimental results, detailed examples of small scale modeling and testing can be found in Ref. [31,33,50,51,69,94,103]. However true replica models are practically impossible to build and test because of the severe restrictions imposed on the model. Alternate scaling laws given in Table 4.1 have been shown to simulate adequately the behaviour of the structure, and some particular distortions of the similitude requirements can be accounted for.

The method used in this section was successful in correcting the unsatisfied similitude conditions using an overall mechanical simulation. As demonstrated the dynamic properties as well as the response parameters of primary interest, i.e, horizontal floor displacement, knee element ductility, and the energy dissipation capacity of the small scale model are within the range of true scale buildings.

Chapter 5

EARTHQUAKE SIMULATION FACILITIES AND DATA SIGNAL PROCESSING

EARTHQUAKE SIMULATION FACILITIES AND DATA SIGNAL PROCESSING

5.1 INTRODUCTION

To perform dynamic testing on a test specimen, major pieces of various apparatus and instruments are required. A typical shaker-test set-up (Fig. 5.1) can be divided into several subsystems, depending on the basic function of the various equipment and instruments employed. The main subsystems are as follows:

(1) The signal-generating system

(2) The excitation system

(3) The response-sensing system

(4) The signal-conditioning system

(5) The response-signal-recording system

A specified excitation signal is generated by the signal generator. This signal is converted into a dynamic motion by the excitation system and applied to the test specimen. Dynamic response of the test specimen must be monitored, using various sensors and transducers. The response signals must be conditioned, using signal-conditioning devices, before they are recorded for subsequent analysis and processing. Even the input signal must be conditioned before it is used for actuating the shaker [28]. A description of the mentioned phases applied to seismic tests and the operations of the data acquisition system constitutes the core of this chapter.

5.2 TEST FACILITIES

The seismic tests reported in this thesis were the first research project to be carried out on the six axis earthquake simulator (Fig. 5.2) in the Earthquake Engineering Laboratory of the Civil Engineering Department at the University of Bristol. The seismic test facilities are fully described in Ref. [15,19,104] so only features pertinent to this experiment will be discussed here.

5.2.1 EARTHQUAKE SIMULATOR

5.2.1.1 Description and specification

The shaking table consists of a 3m x 3m cast aluminium platform weighing 3.8 tonnes. The platform has the shape of an inverted pyramid and is reinforced by stiffening diaphragms. Test specimens are attached to the table by steel bolts which thread into a regular grid of M12 bolt holes. The platform sits inside a reinforced concrete seismic block that has a mass of 80 tonnes. The block is located in a pit in the earthquake simulator laboratory and supported by 950mm diameter air-spring vibration isolators. Hydraulic power for the earthquake simulator is provided by a two stage hydraulic pump driven by a 132 kW electric motor providing up to 300 l/min at a working pressure of 185 bar. The platform is attached to the block by eight hydraulic actuators each one is rated at 50 kN and has a maximum stroke of ±150 mm. The four vertical actuators each have a static section to carry the static load of the platform plus specimen [19].

The table drive system will be described later in Section 5.2.2.2 however an interfacing between analogue and digital control and acquisition systems can be achieved via the front panel of the analogue control unit ACU which converts a set of six voltage signals, one for each degree of freedom, to a set of eight voltage commands, one for each actuator.

The specification of the earthquake simulator are :

size:	3m x 3m
axes:	6
construction:	4 pieces cast aluminium
mass:	3.8 tonnes
maximum payload:	15 tonnes
maximum payload height:	4.2 m
maximum height of payload above centre of gravity:	1 m

vertical (Z) actuators:	4 at 50kN
vertical acceleration (no payload):	5.6g
vertical acceleration (10 tonnes payload):	1.2g
vertical displacement:	+/-150mm
yaw rotation:	+/-5.2°
vertical velocity:	0.5m/s
yaw velocity:	1.5rad/s
longitudinal (X) and lateral (Y) actuators:	4 at 50kN
horizontal acceleration (no payload):	3.1g
horizontal acceleration (10 tonnes payload):	1.6g
horizontal displacement:	+/-150mm
pitch/roll rotation:	+/-3.4°
horizontal velocity:	0.5m/s
pitch/roll velocity:	1.5rad/s
operational frequency range:	0-100Hz
hydraulic supply:	132kW;300 l/min
supply pressure:	185 bar (working),210 bar (max)

5.2.1.2 **Performance characteristics**

Fig. 5.3 shows the transfer function between supply voltage and table acceleration for the X axis. The strong resemblance to the response of a single degree of freedom oscillator is due to the resonance of the platform mass on the (compressible) oil columns in the actuators. The other flexibility that influences the performance curve is that of the horizontal actuator bearings (reducing performance around 50Hz).

When the isolation air bearings are inflated the seismic block effectively isolates the rest of the building from the vibrations of the earthquake simulator. Lifted on the bearings

the block has rigid body resonances in the region of 2Hz, so the earthquake simulator is normally used with the block down while driving with time history signals to provide closely controlled response accelerations.

Acceptance testing of the earthquake simulator included a set of performance trials in which it was driven at selected frequencies in the range 0.5-100Hz in the X,Y, and Z axes in turn with no load and with a test mass of 10 tonnes. The harmonic component of the response at the driving frequencies is presented for each case in Fig. 5.4. Up to approximately 2Hz the maximum acceleration is limited by the actuator stroke. For slightly higher frequencies (around 2-4Hz) maximum acceleration is limited by the rate at which oil can be supplied to the actuators. At higher frequencies peak acceleration depends on supply pressure, number of actuators, and resonant effects as discussed above. [19]

5.2.1.3 Generation and matching of time histories for seismic testing

Time histories can be provided in two ways:

(1) As time histories adjusted to produce accelerations from the earthquake simulator to match specified records.

(2) As histories synthesized so as to produce acceleration signals from the earthquake simulator having acceleration response spectra matching a specified set of values.

The procedure or algorithm by which times histories were derived to produce the desired acceleration record when applied as a command signal to drive the earthquake simulator during the seismic tests can be summarised as:

$$DRIVE(n+1) = DRIVE(n) * TARGET/ACQUIRED(n)$$

where:

DRIVE(n)	is the drive signal for the n^{th} iteration of the algorithm
TARGET	is the required acceleration time history
ACQUIRED(n)	is the acceleration measured while driving with DRIVE(n)

and the multiplication and division is with fast Fourier transform (FFTs) of the corresponding time domain signals, a summary of the procedure is given in Fig. 5.5 [19]. The matching can involve up to six degrees of freedom simultaneously, during the seismic test uniaxial and biaxial matching were used. Two or three cycles of the iteration were necessary to obtain the closest match possible. Typical accelerations generated by the shaking table (i.e. the simulated earthquake) and corresponding original earthquake records with the same peak value are shown in Fig. 5.6 for comparison. The simulated record lacks the low frequencies since they were filtered from the table motion to limit the displacement. In general the characteristics of the original earthquake were only moderately well reproduced by the simulated motion, but were good enough for the purpose of these experiment. A possible nonlinear and more stable algorithm could have been used to improve the simulated signal but it converged more slowly and several cycles would have taken too much time.

5.2.2 INSTRUMENTATION AND DATA ACQUISITION SYSTEM

The data-acquisition and processing system performs several important functions in addition to the control of the system. Shown in Fig. 5.1 the data acquisition and processing system consists of the response sensors, the amplifiers, filters, the ADCs, and the digital computers, with associated input-output devices [28]. The main functions of a digital data-acquisition and processing system are described here.

5.2.2.1 **Instrumentation and signal conditioning**

The range of instrumentation used in the seismic tests included Dytran accelerometers, and foil strain gauges. The signals from the accelerometers are amplified by a Dytran 12 channel power unit/amplifier 4125, and a bridge balance supply transducer conditioner Flyde FE-492-BBS is used to convert the output variation of the resistance of the strain gauges to a voltage signal and then amplified by a charge amplifier Fylde FE-128-CA. The amplified signals are filtered by a multi channel programable Fern EF6 filter unit . The sixteen channels used were digitised at a rate of

256 samples per second thus setting the Nyquist frequency at 128Hz. This sampling rate was high enough to encompass the highest horizontal natural frequency of the frames, moreover it was chosen to be a power of two to facilitate the data processing.

5.2.2.2 Table control and data acquisition system

Associated with the shaking table were two dedicated computers: a Tandon PCA-20 and an IBM PC-AT. Normally the IBM PC-AT was used for driving the table and the PCA-20 for acquiring response data from the earthquake simulator and test specimens. The control and data acquisition system is shown in Fig. 5.7. Signal output is via a Data Translation DT2821 DAC board for eight channels at aggregate rates of up to 3.3kHz. Signal input is via a Data Translation DT2821 ADC board providing a data sampling at an aggregate rate of up to 50kHz into up to 16 (single ended) channels [19]. Software which provide analogue signals to drive the table has been written by Principia Mechanica Ltd. This comes with two modules PRFG6 which provides sine waveform signals, and PRSTF6 which outputs specified time histories. The acquisition computer used for acquiring data during testing of specimens, uses the DASYST program [20]. DASYST may be used to display the data on the screen for quick checks, to plot the data on a HP7475 plotter or to write the data to ASCII format files for later processing.
A convenient way to perform system identifications is to drive the table and acquire the data using the Solatron S1200 spectrum analyser. The S1200 is used as a signal generator to drive the table, generally with a band limited random signal at the same time twin channels of data may be analysed using digital techniques to produce frequency spectra. The resulted spectral data may be plotted or downloaded to one of the earthquake simulator computer for later processing.

5.3 PRINCIPLES OF SIGNAL PROCESSING

Signal analysis in realistic terms means data reduction. Any practical measurement in a dynamic environment will involve acquisition of a mass of data and the prime purpose of the analysis is to reduce this to manageable parameters describing

some relevant features of the physical process. The aims of this section is to describe the range of techniques to be used for processing the seismic test results. Rigourous proofs are not included as they can be found in many good explanation books [12,74,89]

5.3.1 FILTERING

The main function of filtering is extraction of unwanted components in a signal. In this sense, any dynamic system can be considered as a filter. The range of the frequency components that are allowed through a filter depends on the frequency response function of the filter. For an analogue circuit, the frequency-response function is normally a smooth function, and therefore a sharp cutoff is not feasible. Filters however can be idealised into several categories. The main categories are low-pass filters (do not allow high-frequency input-signal components above the cutoff frequency f_c), high-pass filters (do not allow low-frequency input-signal components below f_c) and band-pass filters (allow frequency components within a frequency band and reject the remaining components). Digital filter design is adequately treated in Ref. [12].

5.3.2 SAMPLING OF TIME HISTORIES

Conversion of continuous analogue signals obtained from different instrumentations (accelerometers, and strain gauges in this particular tests) into a sampled form involves a number of requirements to be met in which accuracy, economy and format provide the essential features. The most important of the difficulties that arise when a continuous signal is sampled is undoubtedly that of aliasing. The nature of this problem is that the same data points can described a number of time series histories which are indistinguishable to the digital computer. Assuming the function $x(t)$ to represent a sinusoid of frequency f_0, then the same points could equally well be taken to represent sinusoids of frequencies f_i called aliased frequencies and related to the sampling period h by

$$f_i = i/h \pm f_0 \tag{5-1}$$

The highest frequency above which an unambiguous reconstruction of a digitised signal is not possible is known as Nyquist frequency and is given as

$$f_N = 1/2h \tag{5-2}$$

Obviously the highest frequency of interest should be within this range. To prevent aliasing low pass anti-aliasing filters should filter out all frequencies above $1/2h$ before they reach the ADC. The inadequacy of practical filters modifies our choice of sampling rate such that a rather higher rate is required than is suggested by the sampling theorem [28].

The sampling theorem also applies to the time domain, so that the lowest frequency that can be resolved from the sampled signal of length T is

$$f_m = 1/T \tag{5-3}$$

The representation of a variable amplitudes by numerical values is termed quantisation. This is effected by an analogue to digital converter (ADC). The ADC will have a limited range, say ± 10V, split into say 2048 equal intervals. The range of the input should match the range of the ADC to achieve the best resolution of the variation of the signal [18].

5.3.3 FREQUENCY ANALYSIS

A signal which is repetitive is a periodic function of time. Any periodic function of time $g(t)$ can be represented by the Fourier series

$$g(t) = a_0 + \sum_{n=1}^{\infty} a_n \cos n\omega t + \sum_{n=1}^{\infty} b_n \sin n\omega t \tag{5-4}$$

where a_n and b_n are the coefficients to be evaluated, and are given by the expressions

$$a_n = 2/T \int_{-T/2}^{+T/2} g(t) \cos n\omega t \, dt \tag{5-5}$$

$$b_n = 2/T \int_{-T/2}^{+T/2} g(t) \sin n\omega t \, dt \tag{5-6}$$

where $\omega = 2\pi/T$, and T is the periodic time.

The term a_0 is given by the average value of $g(t)$ in a period T

$$a_0 = 1/T \int_{-T/2}^{+T/2} g(t)\, dt \tag{5-7}$$

An alternative but convenient way of writing the periodic function $g(t)$ is in terms of complex quantities

$$g(t) = \sum_{n=-\infty}^{+\infty} G_n \exp(jn\omega t) \tag{5-8}$$

$$G_n = 1/T \int_{-T/2}^{+T/2} g(t) \exp(-jn\omega t)\, dt \tag{5-9}$$

The Fourier series technique can be extended to non-periodic waveforms by making $T \rightarrow \infty$. In the limit $\omega = 2\pi/T \rightarrow d\omega$, $1/T = \omega/2\pi \rightarrow d\omega/2\pi$ and $n\omega \rightarrow n\, d\omega$ which becomes a general value defined as ω, then the eqs. (5-8) and (5-9) become the integral pair

$$g(t) = 1/2\pi \int_{-\infty}^{+\infty} G(\omega) \exp(j\omega t)\, d\omega \tag{5-10}$$

$$G(\omega) = \int_{-\infty}^{+\infty} g(t) \exp(-j\omega t)\, d\omega \tag{5-11}$$

Eqs (5-10) and (5-11) are known as Fourier integral pair.

In the case of the analysis of digitised data, it is necessary to consider a finite version of the Fourier series and to derive a discrete form of the Fourier transform. Assuming a sample record of finite length T divided into N equally spaced points, having adjacent points separated by a duration h, the discrete Fourier transform can be obtained from eqs (5-8) and (5-9) as

$$g(n) = \sum_{i=-N/2}^{+N/2} G(i)\exp(j2\pi in/N) \tag{5-12}$$

$$G(i) = (1/N) \sum_{n=-N/2}^{+N/2} g(i)\exp(-j2\pi in/N) \tag{5-13}$$

and eqs (5-12) and (5-13) can be written in the form

$$G(i) = (1/N) \sum_{n=0}^{N} g(i)\exp(-j2\pi in/N) \tag{5-14}$$

$$g(n) = \sum_{i=0}^{N} G(i)\exp(j2\pi in/N) \tag{5-15}$$

These equations are referred to as the Discrete Fourier Transform(DFT) and Inverse Fourier Transform (IDFT) respectively. A major use of the discrete Fourier transform is the translation of a time series into an equivalent frequency series, to this end Fast Fourier Transform algorithms for digital computers have been devised to reduce considerably the required number of operations.

5.4 EXPERIMENTAL DATA PROCESSING

Three computer programs were used to acquire, process, and help analyse the data. ASYST was mainly used to acquire and store the experimental data for further processing. PAFEC SPIDERS and the local program GRAF were used for a number of purposes. They have most of the functions needed for data processing which can be grouped as follows:

(1) data presentation and plotting

(2) miscellaneous (input/output etc.)

(3) curve fitting (system identification)

(4) data manipulation

(5) signal processing

The structure and the use of GRAF and SPIDERS are fully described in Ref. [18,100]. In addition to these programs several smaller programs were written to perform specific tasks. The displacements, forces, and energies derived from accelerations and strain recorded during the seismic tests are described below.

5.4.1 FLOOR DISPLACEMENTS

The acceleration time histories were integrated twice and corrected by the modified Trifunac baseline correction to remove high amplitude low frequency sinusoids. Unfortunately no displacement records were available to check the accuracy of this method, but in general the computed displacements are in good agreement with those predicted analytically (as will be seen later in Chapter 7). Errors introduced by similar numerical integration were found to be very small [16].

5.4.2 DIAGONAL AXIAL FORCES AND COLUMN BENDING MOMENTS

The axial forces and column bending moments were derived by multiplying the measured elastic strains by appropriate elastic constants based on the assumptions that the strain distribution is linear across sections and that the strains do not exceed their elastic limits.

The brace force was computed by

$$F = EA\epsilon \tag{5.16}$$

where:

F : brace force

E : Young's modulus

A : cross sectional area

ϵ : measured strain

The measured elastic bending moment at the strain gauge location is defined as

$$M = EI\epsilon/y \tag{5.17}$$

where:

I : moment of inertia of the column

y : half the column depth

ϵ : measured bending strain

5.4.3 KNEE ELEMENT MIDSPAN DISPLACEMENT

The strain time histories recorded at mid point of the knee elements were converted to displacements using the strain-displacement relationship determined during the quasi-static test (Section 4.5.6). The strain-displacement relationship was first approximated by polynomials of 2nd and 3rd degree by fitting the curve of Fig. 4.9, then a conservative bilinear model was used to approximate the elastic and plastic phase. The latter showed a better matching with the analytical results.

5.4.4 TOTAL ENERGY INPUT

The energy input E_I is defined as the work done by the ground motion to the structure, and equal to the product of the base shear and ground displacement (Section 3.2)

$$E_I = \int_0^u Q \, du \tag{5.18}$$

The base shear is the sum of the inertia forces of all stories, which were obtained by multiplying the masses by their corresponding total accelerations. Inaccuracies both in measured accelerations and the location of the mass centres of the stories may affect the results of these calculations.

Using the trapezoidal rule, the integral of Eq. (5.18) can be expressed as:

$$E_I^{(j)} = E_I^{(j-1)} + 1/2 \sum_{i=1}^{N} [m_i(u_i^{(j)} + u_i^{(j-1)})(u_g^{(j)} - u_g^{(j-1)})] \tag{5.19}$$

where :

m_i : lumped mass at the i^{th} floor

u : total acceleration of the i^{th} floor

u_g : displacement of the ground

N : number of floor

The number of degrees of freedom is reduced to the number of storeys by considering only the lateral movement of each floor of the frame [33]

5.4.5 ENERGY DISSIPATED BY KNEE ELEMENTS

The area enclosed by hysteretic loops of an element represents the energy dissipated by the element, that is

$$E_H = \int_{loop} F\, dx \tag{5.20}$$

The same scheme was applied to perform the integration of the giving:

$$E_H = E_{H(i-1)} + 1/2\,(F_{(i)} + F_{(i-1)})(x_{(i)} - x_{(i-1)}) \tag{5-21}$$

where :

F_i : normal component of the brace force on the knee element

x_i : displacement at midspan of the knee element

The elastic strain energy of the knee element is also included in this expression, but it should be noted that the stored energy is small compared with the energy dissipated by the knee element. So the above expression could be used as a good estimate of the knee element hysteretic energy. The procedure adopted to measure the energy dissipated by the knee element is not very accurate, because it involves a lot of intermediate calculations. However it gives a good qualitative measure of the overall ability of the structure to absorb the energy imparted to it, and its distribution through the height of the model (Section 6.2.7.2)

5.5 CONCLUSION

The obvious advantage of the earthquake simulator is that it subjects the test structures to true earthquake type excitations, or predefined spectrum of synthesized signals. The extent to which this can be achieved is controlled by a set of hardware and software constraints. The quality of tests then is principally related to the test facilities. Generally the shaking table was successful in reproducing the main characteristics of the different type of earthquake records used during the seismic tests. The reliability of the results however depends also on the errors introduced at each stage of the processing these were evaluated and attempts made to develop procedures to mitigate the effect of these errors in the estimation of the different response quantities.

Chapter 6

SHAKING TABLE TEST

SHAKING TABLE TEST

6.1 INTRODUCTION

The importance of the shaking table test of small scale models was discussed in Chapter 4 and 5. This chapter, however, presents the results of three series of tests that attempted to simulate the structural behaviour of KBFs under earthquakes.

It was intended to cover three major aspects of the KBFs that would be practically very difficult to realise and very risky to perform in full scale structures at this early stage where little information is available about the KBSs.

The first series of tests deals with the energetic aspect of the frames and their capacity to dissipate the imparted energy, the second investigates the performance of different bracing arrangements in medium-rise buildings under a wide range of earthquake types, and the third series focuses on the torsional coupling behaviour of space KBFs.

6.2 TEST SERIES I: ENERGY QUANTIFICATION

6.2.1 OBJECTIVES

The main objective of those tests is to investigate the dynamical behaviour of knee braced frames from the energetic point of view, and in particular the energy absorption efficiency of the knee bracing system, and its effect on the total input energy. The associated objectives of this test included a development of mathematical models for the knee braced test structure, and the evaluation of the effect of the knee element's strength on the response to different earthquake excitations, with a comprehensive description of the techniques and procedures used in performing the shaking table tests, and outlining most of the difficulties encountered in these tests.

6.2.2 TEST STRUCTURE

The availability of instrumentation to monitor the response of the test structure was the major limitation, because the experimental determination of the

various forms of energy requires a large number of channels to monitor the whole structure. Fortunately the design of the original skeleton of the ten-storey structure (Section 4.2) allows the assembly of a large variety of building configurations. To reduce the number of monitored variables, the simple four-storey structure shown in Fig. 6.1 was used.

The moment resisting frame (MRF) is a three-bays long, and one-bay deep. A disposable knee bracing system (KBS) was placed in each side of the middle bay bracing the longitudinal axis. Stiff bracing was built transversally into each of the end bays to increase the torsional stiffness of the structure and eliminate any significant torsional coupling. This produced an essentially two-dimensional test.

6.2.2.1 **Mass distribution**

Lead blocks were added to the structure to introduce the desired inertia forces. The distribution of the masses Fig. 6.2 is constrained by (1) the similitude requirements, (2) the practicality of loading the blocks into the clearances of stories, (3) the fixing method, which should minimise the interaction with the frame stiffness, and (4) the symmetric distribution of masses.

6.2.2.2 **Specimens and frames**

The same frame was tested either on its own as a moment resisting frame (MRF), or with knee bracing of two different strengths, the strongly knee braced frame (SKBF), and the weakly knee braced frame (WKBF).

6.2.2.3 **Instrumentation**

A detailed description of the different instruments and their purposes was presented in Section 5.2.2, the present discussion is limited to indicate their locations. Six "Dytran modalometers" (accelerometers) were used to measure the horizontal acceleration at various levels in the structure. As seen in Fig. 6.3, five accelerometers were mounted on one of the exterior columns in an end bay, and the sixth was placed on the top of the

transversally opposite column to detect any acceleration from torsional motion of the structure. Considering the symmetries of the building, only four sets of foil strain gauges were installed to monitor the strain time-history of a single brace and the corresponding knee element in each storey. The axial strains in the braces were measured using quarter bridge circuits, and half bridge circuits were used to record the loading strains at midspan of the knee elements. A total of fourteen channels were used to measure the response of the frames to earthquake ground motion.

6.2.3 TEST PROGRAM AND SEQUENCE OF TESTS

Two earthquake records were selected and intended to cover (1) near-field, short duration, impulsive type ground motion as for example that represented by Parkfield record, and (2) far-field, long duration, relatively severe and symmetric type cyclic excitation, as for example that represented by the El-Centro record [111].

Three different intensities, expressed in terms of the peak acceleration of the ground motion, were used to study the performance of the model frames. These intensities were chosen so that the main frame would remain elastic at all times, and under intensity I very little or no yielding should occur in the knee elements, at intensity II a few knee elements should undergo plastic deformations without severe damage, under motions of intensity III considerable yielding should occur in most of the knee elements and some might fail, and finally at the end of the tests the WKBF was subjected to a very severe motion of intensity IV. The ground motion accelerations that met these requirements were :

Intensity	**Parkfield**	**El-Centro**
I	0.54 g	0.37 g
II	0.62 g	0.52 g
III	0.96 g	0.74 g
IV	----	1.76 g

The model was 1:12 of a prototype length scale, and so the time of the earthquake records was speeded by a factor of $1/\sqrt{12}$. The acquired data was 8s and 4s long for El-Centro and Parkfield respectively.

The test program started with the MRF identification test described in Section 6.2.4, which was also carried out at the end of the test series of each frame. Then a set of preliminary tests was performed at low accelerations for time-history matching. The main testing began on the strongly knee braced frame (SKBF). The frame was subjected to the two earthquake records beginning with the least intense tests for each earthquake and then proceeding to the next higher intensity. Most of the tests were performed twice either for repeatability comparison or because faults were detected in the acquired data. Each damaged knee element was replaced before the next test. After all the knee elements had been substituted by a weaker set (WKBF) the tests were repeated. Additional tests in which a sine wave of linearly increasing amplitude was applied to the WKBF. The frame was then converted to the original MRF by taking off the removable bracing system, and the same earthquake testing sequence was applied. A complete listing of the tests performed in this series is given in Table 6.1

Every test run is identified by a code, which indicates:

(1) Source signal

EC : El-centro earthquake

PK : Parkfield earthquake

RD : Band limited random signal

SI : Sine wave.

(2) Type of frame

MR : Moment resisting frame

SK : Strongly knee braced frame

WK : Weakly knee braced frame.

(3) Intensity

0 : Very small amplitude

1 : Intensity I

2 : Intensity II

3 : Intensity III

(4) Run number

0 : First run

1 : Second run

2 : Third run.

For instance ECMR20 stands for the moment resisting frame(MR), subjected to El-Centro earthquake(EC), intensity II (2), first run (0). Note that intensity IV was used only at the end of the WKBF test to cause severe damage in some knee elements.

6.2.4 SYSTEM IDENTIFICATION

The modal characteristics of the three frames were determined from pseudo-random base motion containing a range of frequencies 0-50Hz, using the Solartron 1200 signal processor (Section 5.2.2.2) as a generator to drive the shaking table at low amplitudes, and as an analyser for the response of the structure. The frequency response curves (transfer functions) Figs .6.4 to 6.6 generated from these tests were used to establish the dynamic parameters, namely the modal damping ratios and the natural frequencies using the curve fitting of the response of a single degree of freedom oscillator in GRAF program [18].

In order to verify these results a continuous sinusoidal waveform was used to excite the frames near their natural frequencies and by monitoring the response a manual control sine sweep converged on the resonant frequencies. These were found to be:

	mode	pseudo-random	freq. sweep	damping ratio %
MRF				
	1	5.31 Hz	5.16 Hz	2.01%
	2	16.65 Hz	16.32 Hz	1.57%
	3	31.39 Hz	30.80 Hz	1.75%

SKBF			
1	8.66 Hz	8.64 Hz	4.29%
2	25.82 Hz	25.60 Hz	4.68%
3	39.17 Hz	42.51 Hz	-----
WKBF			
1	8.41 Hz	8.40 Hz	3.55%
2	26.26 Hz	25.81 Hz	5.55%
3	42.41 Hz	41.73 Hz	-----

The associated mode shapes were measured by exciting the frame structures at the desired natural frequencies and recording the accelerations at each floor level relative to the moving base. The measured and predicted mode shapes of the three frames are plotted for comparison with their corresponding transfer function modulus in Fig. 6.4 to 6.6.

6.2.5 SINUSOIDAL FORCED VIBRATION TEST

The test was performed in order to examine the behaviour of the knee bracing system, specifically the diagonal brace elements, the knee elements, and the formed hysteresis loops. The test was carried out with a linearly increasing sinusoidal base motions having excitation frequency near the fundamental natural frequency of the weakly knee braced frame (8.5Hz). The resulting Fourier amplitude spectra of the second and third floor acceleration presented in Fig. 6.7 confirm the shape of the second mode determined earlier. As it can be seen the second mode participation is considerable in the second floor acceleration, but negligible in the third floor because this is a stationary node in the second mode of vibration. The harmonic frequencies that appear in the Fourier spectra of the second floor acceleration, the fourth storey brace force, and knee element strain is probably due to backlash (looseness) in the brace connections which alters the storey stiffness. This phenomenon is better illustrated in Fig. 6.8 where a horizontal portion can be seen in the brace force time-histories at low amplitudes around the origin, these portions shift up and down from the origin as the amplitude increases. In this particular test pronounced high frequency peaks appeared in the brace strain

time-histories but were not accompanied by similar peaks in the knee elements strains, distorting the hysteresis loops which are shown in Fig. 6.9.

6.2.6 MRF RESPONSE TO SIMULATED EARTHQUAKE MOTIONS

The test results for the MRF were selected for presentation as representative of the response of an elastic system. Since the behaviour of the test structure subjected to the same earthquake type motion was similar with a variation occurring in amplitude of response, only the time histories of the two tests are presented. These are the response of the frames to El-Centro and Parkfield earthquakes at intensity III.

The measured table and floor acceleration time-histories recorded during the test ECMR30 and PKMR30 are presented in Fig. 6.10 and 6.11. The maximum table accelerations recorded during the test were 0.81g and 0.96g respectively, and the maximum recorded absolute accelerations of the top floor were 1.98g and 2.55g, corresponding to amplifications of 2.44 and 2.65 respectively. It should be noted that the maximum response acceleration does not coincide with the peak table acceleration, however the maximum response of the braced frames occurred nearly at the same time as the peak table acceleration. In general the peaks of the input energy time-histories are associated with the maximum response of a system [111], this can be easily identified when considering the energy input curves of Fig. 6.12, the one corresponding to the MRF has two distinct big jumps, and both are characterised by large fluctuations during the strong parts of the earthquake motions, as with every linear system with insufficient damping to dissipate the imparted energy, the energy is temporarily stored as kinetic energy or strain energy, before being radiated to the ground (platform) or dissipated by damping.

6.2.7 KBF RESPONSE TO SIMULATED EARTHQUAKE MOTIONS

These tests were designed to study the response characteristics of a linear and a nonlinear knee braced frame, specific example chosen are PKSK10 (SKBF subjected to Parkfield earthquake intensity I), PKWK30 (WKBF subjected to Parkfield earthquake

intensity III), and ECWK40 (WKBF subjected to a very severe El-Centro earthquake). Other test results are presented in form of maximum responses or in a comparative study to demonstrate certain characteristic features of knee braced frames.

6.2.7.1 Elastic behaviour of KBFs

Unfortunately the data from test ECSK10 was lost, and no perfectly linear response of the KBF is available. The PKSK10 test where minor yielding in the knee elements in the lowest storey occurred, and the frame behaved essentially like an elastic system has been used as a substitute. The time-histories of the table acceleration, first storey brace force, first storey knee element strain, and the top floor acceleration are plotted in Fig. 6.13. They are characterised by major peaks occurring one second into the motion corresponding to the maximum base acceleration. Because of the backlash of the braces the small amplitudes before and after the main peaks were not felt in both the brace and the knee element. The input energy time-history is similar to the MRF because of the elastic character of the frame Fig. 6.12.

6.2.7.2 Nonlinear behaviour of KBFs

All the frames having weak knee elements and subjected to the different earthquake motions with different intensities registered yielding in some of the knee elements. The yield level in the knee element is low compared with the full plastic bending moment, and so some yielding may occur even at small amplitudes. Also, in general strong specimens suffered less damage than the weaker ones. The amount of yielding and the amplitude of the inelastic response varied with the intensity of the shaking table motion depending mainly on the strength of the knee elements.

The test, PKWK30, is selected to represent the response of the KBF to the Parkfield earthquake. Time-histories of acceleration, brace force, and mid-span knee element strain time histories are displayed in Fig. 6.14. The major inelastic deformations occurred at the time of the table peak acceleration. A close examination of the acceleration and strain time-history shows that the peaks following the first major ones,

are much more damped than those of the elastic test (PKSK10). In terms of the acceleration, a reduction in amplification of 20% was registered as the ground motion was increased from intensity I to intensity III. During this test the knee elements of the lower storeys underwent large inelastic deformations in few excursions, consequently the energy dissipated is concentrated at that time, resulting in a big step in the hysteretic energy time history, which is also not distributed uniformly through the height of the building, as seen in Fig. 6.15. The results for the first and second stories were affected by the strain gauge becoming detached early in the test. The curves were expected to be near to each other and also show some rise towards the end of the test. The efficiency of the knee bracing system as a dissipator mechanism can be seen by the reduction of the input energy fluctuation, as the intensity of the earthquake motion increases Fig. 6.16. Most of the energy is dissipated in the two lower storeys. Fig. 6.17 shows the hysteresis loops for each storey, the breakdown of the strain gauge at the first and second storey level can be clearly seen in the figure.

At the end of the braced frame tests, the WKBF was subjected to a very severe table motion (intensity IV). The maximum table acceleration reached 1.76g, and the top floor acceleration 2.93g that is an amplification factor of 1.66. The acceleration time-histories are shown in Fig. 6.18, the high frequencies contained in the input ground acceleration excited the second mode of vibration which therefore appears in the output of all the stories except the third which is node in this mode.

A small initial pretension introduced in the brace element, accidentally when tightening the brace elements, often resulted in markedly unidirectional strain and brace force time-histories at low amplitudes, as for example that presented by the top storey brace force in Fig. 6.19. This phenomenon is not so noticeable in the lower storeys because of the shift in origin caused by the knee elements yielding. Another feature is that the brace force is limited by the strength of the knee elements. This can be seen from the uniform oscillation of the brace force between a maximum and minimum value during the strong parts of the time-history, therefore the diagonal braces are prevented from buckling or yielding. Most of the tested knee braced frames did not suffer any

permanent displacements despite the relatively large inelastic deformation of the knee elements. No permanent distortions were apparent after testing, and a simple examination of the knee element strain time-histories in general and particularly in this test Fig. 6.19 confirm this since the knee elements are the only parts in which yield has occurred. The reason for this is that the overall restoring force from the MRF which always remains in the elastic range is sufficient to force the structure to return to its initial position and the knee elements are not strong enough to cause any permanent distortion to the structure. From the energetic point of view, the plot of the input energy (ECVW IV test) in Fig. 6.16 with almost no peaks shows the efficiency of the knee elements in dissipating the energy taken up by the structure immediately. The limited number of channels recorded does not permit the calculation of the total dissipated energy, instead the hysteresis loops formed in the first storey knee element and the time-history of the energy dissipated by this element are plotted in Fig 6.20.

6.2.8 CONCLUSIONS

With the minimum required monitoring instrumentation a satisfactory achievement of the objectives of these series was accomplished. The experimental results portrayed the general trend of most of the KBS characteristics that had been analytically established in Chapter 3, such as the energy dissipation capacity, the force reduction in braces, and the energy input characteristics of elastic and inelastic systems. Among other points to come out of these tests, an important one concerns the nature of the knee element-diagonal brace connection that should be carefully designed to minimise the backlash which may weaken the energy dissipation capacity of the frame.

6.3 TEST SERIES II : TEN-STOREY 2-D KNEE BRACED FRAMES

6.3.1 OBJECTIVE

This section describes a series of shaking table experiments in which ten-storey small scale steel frames were subjected to different earthquake type motions of

sufficient intensity to cause inelastic deformations in the knee elements. The main purpose of the experiments was to study the behaviour of knee braced medium-rise frames. Three modified knee braced frames and a moment resisting frame were used to compare the efficiency of different configurations of knee bracing systems. One of these configurations was tested with three levels of knee element strength and all the frames were subjected to six different input motions at different levels of intensities. An additional aspect of the study is to accumulate experimental data that would provide a rigourous test for evaluating the accuracy of existing computer programs used to analyse nonlinear dynamic behaviour of structural frames.

6.3.2 EXPERIMENTAL STRUCTURE AND INSTRUMENTATION

A three by one bay, ten-storey model was used for these series of experiments (Fig. 6.21). The geometric characteristics and the mass distribution are indicated in Fig. 6.22, the four lower storeys are basically the same as those used in test series I (Section 6.2), except that the floor masses are different and new beam connectors were designed to facilitate the modification of the frame configuration. The upper six storeys are made of 5/8" columns and 1/2" beams as described in Section 4.4. A total of four frame configurations were tested, a moment resisting frame (MRF), and three braced frames, which were an X knee braced frame (XKBF), a K knee braced frame (KKBF), and an N knee braced frame (NKBF) Fig. 6.23.

An instrumentation system was assembled to monitor the experiments and obtain data for analysis. The instrumentation consisted of five accelerometers and ten strain gauges for each structure. The motion of the shaking table was measured directly from the output of the control panel. Since the shaking table was restricted to move in only one horizontal direction parallel to the braced bays of the frame, one accelerometer channel was adequate to monitor the table acceleration. The location of the sensors on the four frames are shown in Fig. 6.24 (the NKBF was instrumented the same way as the XKBF with weak knee elements). The five accelerometers were used to measure the 2^{nd}, 4^{th}, 6^{th}, 8^{th}, and the top floor accelerations. Nine of the strain gauges were used to monitor

the bending strains of the knee elements and some of their corresponding brace elements to estimate the ductility distribution throughout the height of the frames as well as to plot the hysteresis loops. One strain gauge was installed at the base of an exterior column on the bottom storey.

6.3.3 EXPERIMENTAL PROCEDURE (TESTING SEQUENCE)

The testing was performed in three main phases, which were 1) signal matching, 2) identification tests, and 3) performance of the earthquake tests. The first phase was performed once at low amplitudes at the beginning of the test series, as described in Section 5.2.3. The second and the third phases were repeated for each frame configuration. The identification tests were described in detail in Section 6.2.4. The third phase consisted of subjecting each frame to five earthquake record motions and a white noise signal input at least at two intensity levels. Table 6.2 lists the test sequence where each run is named according to the earthquake input, the bracing system configuration, and the knee element strength level.

The first two letters indicate the name of the input motion

PK : Parkfield earthquake

EC : El-Centro earthquake

KY : Koyna earthquake

FE : San Fernando s16e component

FW : San Fernando w74e component

RD : White noise signal

The third letter indicates the bracing system configuration

K : K configuration

X : X configuration

N : N configuration

MR : moment resisting frame

The fourth letter indicates the knee element strength level

W : level 1 (weak)

M : level 2 (medium)

S or U : level 3 (strong)

The number at the end of each name indicates the run number, generally associated with increasing intensities. For example PKXM2 denotes the X knee braced frame (XKBF) incorporating knee elements with medium strength (M) subjected to Parkfield earthquake (PK) at intensity level 2.

6.3.4 SYSTEM IDENTIFICATION

Following the same procedure in Section 6.2.4, the resonant frequencies and their corresponding damping ratios for each frame were found to be:

	mode	freq (Hz)	damp. ratio
MRF			
	1	2.69	0.52 %
	2	7.56	0.60 %
	3	13.00	0.31 %
XKBF			
	1	5.00	2.12 %
	2	16.75	4.27 %
	3	30.20	-
KKBF			
	1	5.04	2.53 %
	2	14.45	3.24 %
	3	28.30	-

It should be noted that the XKBF and the NKBF have basically the same dynamic characteristics, thus only the XKBF natural frequencies and mode shapes are presented. The transmissibility functions and their corresponding mode shapes of all the frames are shown in Fig. 6.25-27

6.3.5 RESPONSE OF THE DIFFERENT FRAME CONFIGURATIONS

A comparison of the response of the four frames to the different types of earthquake motions (Fig. 6.28-30) show that the braced frames, KKBF, XKBF, and NKBF behaved more or less similarly under all the input motions at all levels of intensity. However, the moment resisting frame (MRF) underwent larger deformations in terms of top floor acceleration and column bending strains. The peak acceleration at the

roof level of the MRF was often as high as those of the braced frames with the exception of the Parkfield earthquake where the acceleration was much lower. An important feature of the braced frames is that after major peaks the response is much more damped, because of the high structural and hysteretic damping.

6.3.6 EFFECT OF EARTHQUAKE MOTION TYPES

The frames were tested for their response to five different earthquake input motions and one generated signal motion. The earthquakes used varied from those with short strong motion duration, such as the Parkfield earthquake, to earthquakes with long strong motion duration for example the 1940 El-Centro earthquake. This variable is important because the amount of cumulative damage incurred by structures increases with number of cycles of loading, and also because the duration of strong motion is used in evaluating one of the measures of strength of shaking, namely the root-mean-square acceleration [30]. Fig. 6.31 shows the distribution of the acceleration peaks of the earthquakes where the maximum accelerations are normalised to 1g. It can be seen that the El-Centro earthquake has a greater number of relatively large peaks whereas the Parkfield earthquake has a few larger peaks. The FFTs of these earthquake records illustrating the frequency content of each earthquake were presented in Section 5.2.1.3. The scaled time signals vary from those with a predominantly low frequency content to those with a predominantly high frequency content. The Parkfield earthquake has most of its frequency content between 4Hz and 7Hz, while Koyna earthquake record has a broad range of frequency content the most significant peaks are between 8Hz and 30Hz. The frequency content of San Fernando earthquake (Pakoima dam) has three major peaks near 3Hz, 8Hz and 15Hz. The El-Centro has a significant amount of frequency content between 4Hz and 8Hz which gradually decreases to nearly zero at frequency of about 25Hz. The FFT of white noise input cover a frequency 0-20Hz has a more or less constant Fourier amplitudes for that range of frequency.

The response of the KKBFM to the different earthquake inputs at intensity level 2 is presented in this section. The top floor acceleration and the bending strain at

the column of the bottom storey were used as global response parameters to investigate the performance of the knee braced frame. Figs.6.32-34 show the acceleration, displacement and bending strain time-histories. It is apparent that the effectiveness of the bracing system depends greatly on the type and the frequency content of the earthquake. This can be well demonstrated when considering the response of the frames to Parkfield, El-Centro and Koyna earthquake. The first and the second are both rich in frequencies near the fundamental resonant frequency of the frame, but belong to different types of earthquake. Parkfield and Koyna earthquake, however are both impulsive but with distinct frequency contents. Parkfield earthquake resulted in a relatively high amplification ratio of acceleration which reached 5.2. In this particular case the impulsive character of the earthquake does not allow the knee bracing system to dissipate energy over several cycles because the first plastic deformation of the knee elements coincided with the major peaks of the earthquake, which led to a hysteresis loops with practically only one big cycle. Despite the impulsive character of Koyna earthquake the acceleration amplification factor was less than 2.4, because the earthquake has the dominant portion of its frequency contents far away from the fundamental frequency of the frame. Although the El-Centro earthquake is rich in frequencies near the fundamental frequency of the frame, the acceleration amplification factor was about 3 (less than that induced by Parkfield earthquake), because the structures escape the resonance by an early yield of the knee elements which helped to detune the frames and absorb the energy over several cycles. The conclusion is that the efficiency of the KBS is significantly reduced under impulsive earthquake with frequency content coincident with the frame resonant frequencies.

6.3.7 EFFECT OF THE KNEE ELEMENT STRENGTH

As discussed in Chapter 2, the knee element strength effect can be felt in local member forces, the diagonal brace force, column and beam bending moments at the knee element connections, and obviously on the energy dissipation capacity of the structure. Strongly knee braced frames (frames with high knee element strength)

dissipate energy in a few discrete intervals during the strong parts of the input motion, while frames incorporating weak knee elements tends to dissipate the energy continuously even at relatively small amplitudes. The global response of the frames with different knee element strength is represented here by the top floor acceleration and bending strain of the column of the bottom storey. Figs .6.35 and 6.36 show these parameters and are very similar in terms of maximum amplitudes. There is a slight tendency for frames incorporating weaker knee elements to have lower acceleration amplitudes but increased lateral deformations under most of the earthquake input motions. The oscillations following major peaks in the response time-histories are more damped in strongly knee braced frames than in the weaker ones. It was also noticed that stronger knee elements are more likely to suffer permanent distortion. It was difficult in practice to vary the strength of the knee elements without alterating their stiffness, so the range of variation was limited. The influence on the frame responses is not therefore very great. The semi-rigidity of the knee element connections also has a great effect on the local response of the knee elements because it expands the apparent elastic range and decreases the effect of the strength variation effect as discussed in Section 2.4. The combination of all these limitations made the study of the strength effect difficult.

6.3.8 EFFECT OF THE INTENSITY OF EARTHQUAKES

The response of an elastic system is usually taken to be linear, so any response parameter of the system is proportional to the intensity level of the input excitation. Beyond the elastic limit, however, the behaviour of the system can be highly variable because of the change in structural properties. Therefore this section will limit itself to observations of the behaviour of the braced frames as the intensity level of the input motion is increase. The XKBF was subjected to El-Centro earthquake at five intensity levels in which the peak table acceleration varied from 0.07g to 0.34g. Fig. 6.37 shows a significant decrease in the amplification factor for the top floor acceleration as the intensity is increased which then stabilises when the input acceleration reached 90% of the original peak acceleration of El-Centro. The variation of the amplification factor

of the global responses with the input intensity depends on the type of earthquake. For example the ratio of the maximum top floor acceleration to the table acceleration varied from 4.57 to 3.29 under El-Centro earthquake, but it remained practically unchanged under the Parkfield earthquake. Because the knee elements yield, the frames lost part of their overall stiffness, and the Fourier spectra of the top floor acceleration corresponding to intensity 1 and 5 shown in Fig. 6.38 are characterised by a clear shift of the apparent resonant frequency.

6.3.9 KNEE ELEMENT DUCTILITY DISTRIBUTION

The strength of the knee elements and the overall storey stiffness are the main parameters that govern the ductility distribution through the height of the knee braced frames subjected to earthquake loading. During these tests series no attempt was made to modify the overall frame stiffness. The strength of the knee elements, and the type and intensity of the input motions were the only variable parameters. The ductility demand measured by the ratio of maximum knee element bending strain to the initial yield strain, shown in Fig. 6.39, is characterised by its uniformity through the height of the frames under most of the input motions. Another important feature is that the knee element ductility was distributed according to the fundamental mode shape of the knee element deformation (Section 3.4.3) for limited yielding, but for large nonlinear deformations the distribution patterns could be significantly different, as was the case for the PKKM2 test which will be investigated further in Section 6.3.11. In this particular test it is worthwhile noting the influence of structural faults on the nonlinear behaviour of the structure, such a case can be totally or partially unpredictable. A close examination of the ductility distribution of the PKKM2 test shows that large plastic deformation took place in the bottom storey to the detriment of the second storey. This is probably due to an unpredictable over-softening of the lowest storey. However, the large deformation of the knee element at the fifth level can be justified by the sudden variation of the main frame stiffness (MRF) at that level.

6.3.10 HIGHER MODE PARTICIPATION TO THE FRAMES RESPONSES

The response of low-rise buildings is generally governed by the fundamental mode, however the higher mode participation in tall buildings may be very significant and occasionally is much more important than the first mode. There is an example in these tests, the MRF when subjected to earthquake loading (Fig. 6.40) shows the high participation of the second mode. We can also note that the participation of higher modes in flexible structures is more frequent than in stiffer ones, because the frequency content of most of the earthquakes is relatively low.

6.3.11 DAMAGE OBSERVATIONS

Yielding and subsequent permanent distortion of the knee element are the only damage observed in the test structure. Although some of the knee elements experienced tremendous nonlinear deformation, no appreciable damage occurred in bending. Some of the knee element-brace connections became loose because the holes at midspan became slightly elongated. Fig. 6.41 shows an unusual permanent distortion of a knee element, at the end of the PKKM2 test (KKBF with knee elements strength 2 under Parkfield earthquake intensity 3). This distortion was present through the height of the frame, but greatest at the bottom storey. This is probably due to the impulsive character of the earthquake and more importantly to the directional nature of the earthquake.

Major excursions of knee element yielding were evident. Fig. 6.42 shows typical evidence of knee element yielding in terms of hysteretic behaviour. After each test all the knee elements were closely examined, most of them remained straight without any visible damage. The strain gauges usually remained undamaged. A few installed on the knee elements, however, peeled off prematurely before the prescribed maximum gauge strains were reached.

6.3.13 CONCLUSIONS

A summary of the general observations relating to the dynamic behaviour of the medium-rise KBF models which can be conservatively assumed to hold in full scale buildings are noted now.

(1) The modal damping can be significantly increased in structures incorporating the KBSs.

(2) The X and K configurations exhibited similar behaviour.

(3) Impulsive earthquakes having frequency contents near the resonant frequencies of the frame may reduce the KBS efficiency.

(4) Discontinuity in structural construction may alter the ductility distribution through the height of the building leading to a concentration of inelastic deformation in a particular storey.

(5) Noticeable period elongation was associated with high amplitude vibrations.

(6) Permanent distortions of the knee elements are unusual, and their effect on the overall structural distortion is minimal.

6.4 TEST SERIES III : TORSION IN KNEE BRACED FRAMES

6.4.1 OBJECTIVE

Torsional vibrations of buildings can be attributed to two main causes referred to as the coupling effect, and the accidental effect.

The aim of these series of tests is to examine the performance of the knee bracing system in torsionally coupled frames in the elastic and plastic region. Two types of structural eccentricity were tested, the first was manufactured from an offset of the centre of the mass from the centre of rigidity by changing the mass distribution on each floor (mass eccentricity), and the second was created by removing the bracing from one side of the building (stiffness eccentricity). An important objective within this study was to investigate the initiation of torsional oscillations of nominally symmetric frames subjected only to translational excitations. To gain a better understanding of the effect

of the location of the KBS in the plan of the structure, frames with either the inner bays braced (stiffened core), or the outer bays braced (stiffened periphery) were tested. Finally the performance of the KBFs under multi-component seismic excitation was investigated by subjecting the frames to two horizontal earthquake components simultaneously.

6.4.2 TEST FRAMES AND INSTRUMENTATION

A four storey frame, three bays wide and three bays deep was tested with a range of knee bracing configurations. The IKBF (inner bays braced) and the OKBF (outer bays braced) test structures can be seen in Fig. 6.43. The symmetric, mass eccentric, stiffness eccentric, and strength eccentric frames are schematically represented in Fig. 6.44. The test models were monitored using 6 accelerometers and ten strain gauges located as shown in Fig. 6.45. Two of the accelerometers recorded the table acceleration in each horizontal direction. The others monitored the structural response. Two of the strain gauges were used to monitor the bending strain in the X and the Y-directions at the base of a corner column in the model. The remaining eight strain gauges monitored the strains of one knee element and the corresponding brace in each of the two lower storeys in two orthogonal planes in the model.

6.4.3 TEST PROGRAM

The structures shown in Fig. 6.43 were subjected to two types of earthquake. The N-S component of El-Centro earthquake in the X-direction of the table and the S16E and S74W horizontal components of San Fernando earthquake. Forced vibration tests were also conducted to measure the initial dynamic characteristics of the models before testing with the earthquakes. A complete chronological listing of the tests in this series is presented in Table 6.3. Every test is identified by a filename as indicated in Section 6.2.3, where :

I : indicates the configuration with central core braced (inner)

O : indicates the configuration with peripheral edge braced (outer)

SY : symmetric structure

AF : stiffness eccentric structure

AM : mass eccentric structure

AS : strength eccentric structure

EC : NS component of El-Centro earthquake (X-direction)

XY : simultaneous action of the two components of San Fernando

XX : S16E component of San Fernando earthquake (X-direction)

YY : S74W component of San Fernando earthquake (Y-direction)

6.4.4 IDENTIFICATION TEST

The identification test technique described in Section 6.2.4 was used to establish the natural frequencies and their corresponding mode shapes. Single degrees of freedom of the table were employed to excite the lateral and torsional modes of the frames. Some typical frequency response functions of the model are shown in Fig. 6.46. The first six natural frequencies and damping ratios determined from the transfer functions are listed below :

	Mode	nature	freq (Hz)	damp. ratio %
OKBF (symmetric frame)				
	1	(Lx)	9.19	3.70
	2	(Ly)	9.60	3.50
	3	(T)	15.50	3.62
	4	(Lx)	28.47	3.04
	5	(Ly)	30.73	4.33
	6	(T)	49.73	1.58
IKBF (symmetric frame)				
	1			
	2	(Lx)	7.63	2.49
	3	(Ly)	7.83	3.27
	4	(T)	9.31	1.55
	5	(Lx)	21.93	2.90
	6	(Ly)	23.76	4.08
		(T)	26.26	1.54
OKBF (mass asymmetric)				
	1			
	2	(Lx)	9.38	3.34
	3	(Ly)	9.81	5.52
		(T)	16.26	3.74

4	(Lx)	31.13	4.35
5	(Ly)	31.24	-
6	(T)	43.71	1.14

IKBF (mass asymmetric)

1	(Lx)	7.76	2.05
2	(Ly)	8.87	2.50
3	(T)	9.78	1.56
4	(Lx)	22.07	2.94
5	(Ly)	24.63	4.14
6	(T)	27.59	1.32

Where Lx, Ly denote lateral or a predominantly lateral modes in the X and Y-direction respectively, and T denotes a torsional or a predominantly torsional mode. The mode shapes were determined, using the travelling accelerometer technique, with the reference accelerometer fixed along an X or Y direction. The amplitudes from at least two points on each floor were needed to determine the mode shapes of the space frames. Fig. 6.47 shows some typical mode shapes represented by the horizontal displacement of the top floor. It should be noted that levels of damping show a wide degree of variation. The only trend discernible is that the lateral modes in the Y direction (corresponding to the inverted K bracing) are higher than in the X direction. No obvious reason presents itself to explain this phenomenon. The measured shapes are plotted together with the predictions from the numerical models of the OKBF. The accuracy of the mathematical models will be discussed later in Chapter 7. The effect of imperfect symmetry will be studied in the following section.

6.4.5 INITIATION OF TORSION IN NOMINALLY SYMMETRIC STRUCTURES

6.4.5.1 Accidental eccentricity

A building which is nominally symmetric may respond in torsion due to an accidental eccentricity, an unsymmetrical distribution of strength or because the horizontal ground motion has a rotational component about the vertical axis.

Accidental eccentricity may due to unaccounted differences between the computed and actual stiffness and mass, as well as the participation of nonstructural elements in the building's response. In this section, an attempt to quantify the effect of accidental

eccentricities on the elastic and plastic response is made. Particular attention is given to the mode shapes, the amplitude of the induced out of plane response, and the amplification or reduction of the torsional coupling in the plastic range. As shown in Fig. 6.47 the measured lateral mode shapes of the symmetric frames were slightly distorted especially those corresponding to the IKBFs which were more vulnerable to torsional coupling when they were excited near their lateral resonant frequencies. A perfectly symmetrical model when subjected to a translational ground motion along an axis of symmetry should respond only in that direction. However acceleration at the top floor and bending strain at the base of the column were registered in the direction at right angles to the input motion in the symmetric structures. In order to compare the effect of the accidental eccentricity in different frames a ratio, RT_{xy} was defined as the maximum response (column strain, or top floor acceleration) in the Y-direction to the maximum response in the X-direction. For different frames under different earthquakes, this ratio varied from 0.20 to 0.30, which means that a nominally symmetric structure had accidental eccentricities that induced orthogonal responses which reached 30% of the response parallel to the input motion. It should be noted that the ratio RT_{xy} was almost constant for elastic and plastic behaviour and was only loosely dependent on the intensity of the ground motion. Less than 6% difference between the elastic and the plastic ratios was observed when the intensity of the earthquake doubled. In other words there was no amplification of torsion due to the knee elements yielding as a result of the accidental eccentricities.

6.4.5.2 Strength eccentricity

A nominally symmetric frame with a strength eccentricity was manufactured by fitting lower strength knee elements into one side of the model. Such frames are symmetric in the elastic range and only asymmetric after yield. The equivalent structural eccentricity caused by unbalanced yielding of the knee elements depends on the degree of the strength eccentricity, and the level of stiffness reduction and the location of the KBS. During nonlinear dynamic loading, the induced eccentricity is function of time. An

OKBF (outer bay braced frame) was selected to be used in this experiment because the strength eccentricity would result in a significant structural eccentricity.

Although the strength eccentricity measured by the ratio of the plastic moment of the normal knee elements M_p to the weakened ones M_{pw} was relatively high (M_p/M_{pw}=1.82), the torsional translational coupling induced at high intensity level (peak table acceleration reached 0.76g) was insignificant. Fig. 6.48 shows the relative displacements of the SW corner (ch.11) and the SE corner (ch.12) of the top floor in the X-direction, together with the induced perpendicular displacement in Y-direction (ch.15). At low amplitudes both ch.11 and ch.15 were almost coincident (symmetric structure). The oscillations in y-direction recorded by ch.15 started to be significant only at the beginning of the strongest part of the response, and were accompanied by a slight separation of ch.11 and ch.12, a sign of the initiation of torsion in the model due to unbalanced yielding of the knee elements.

The amplification of the induced torsion was probably prevented because of the existence of strong restoring force from the remaining elastic elements (MRF and few unyielded knee elements) in addition to the effect of the hysteretic damping developed by the yielded knee elements.

6.4.6 EFFECT OF KBS LOCATION ON THE TORSIONAL RESISTANCE OF FRAMES

In order to examine the effect of the location of the KBS on the torsional capacity of structures, a study was carried out comparing the response of two eccentric frames having different geometric bracing arrangements. The asymmetry of thc frames in these tests was due to an unbalanced mass distribution. Fig. 6.44 shows a typical floor having an eccentric mass distribution where two added lead blocks of 10kg each were removed from the eastern side of each floor. This shifted the centre of mass to the western side by 29mm (2% of the structure's width). Both the central core braced frame (IKBF), and the peripherally braced frame (OKBF) were subjected to the El-Centro earthquake at two intensities to excite the frames elastically and inelastically.

The torsional translational coupling was most clear in the top floor accelerations. The torsional mode participation in the response of the OECAM1 test is noticeable by the magnitude of the peak in the FFT of the acceleration time histories shown in Fig. 6.49(a). It is clear that the peaks of the first lateral and torsional frequency (f_L=9.81, f_T=16.26) were comparable in terms of magnitude. However the torsional component of the inelastic response (OECAM2) was considerably damped out by effect of the knee element yielding Fig. 6.49(b). The torsional component of the SW corner (ch.11 X-direction) of the top floor acceleration of the inner braced frame was equally important to the translational component as illustrated by the FFTs of Fig. 6.50.

The relationships between the displacement of the SW and SE corners of the top floor are shown in Fig. 6.51. The orbit of the IKBF Fig. 6.5(b) shows a circular shape indicating a strong coupling of the two components of the displacement. On the other hand, the coupling is less effective in the case of the OKBF Fig. 6.5(a) where the displacements of the two corners tend to coincide with the diagonal line corresponding to perfectly symmetric deformations. The ratio of the maximum acceleration recorded by channel 15 in the Y-direction to the corresponding one in the X-direction reached 0.51 in the IECAM1 test, and 0.30 in the OECAM1. The time-histories of the bending strain recorded at the base of the column of the bottom storey, plotted in Fig. 6.52, show that the induced bending moment in the direction orthogonal to the input motion was relatively important in the IKBF. The maximum strain in Y-direction attained 71% of the maximum strain in X-direction. The ratio RT_{xy} corresponding to the OKBF remained constant when the intensity was doubled, but the one corresponding to the IKBF increased from 0.40 to 0.71 for the same variation of the intensity. The strong torsional lateral coupling which characterised the IKBF response shows that the absolute level of eccentricity is not as important as the torsional resistance of the frame itself.

Apparently the high torsional coupling observed in the response of the central core braced frame was due to three main reasons. The first is that the structural damping associated with the torsional mode of the IKBF was about half of that corresponding to the OKBF (see damping ratios listed in Section 6.4.3). The second can be attributed to

the inefficiency of the KBSs to damp out the torsional oscillations during the inelastic phase. A third possible reason could be included if the closeness of the uncoupled lateral and torsional natural frequencies effectively amplify the response [41], because the IKBF had its first torsional frequency close to the fundamental lateral frequency. Their ratio was 1.16 compared to 1.73 in the OKBF, however the results from Ref. [102] indicated the absence of such effects.

Nevertheless the importance of the KBS location in the horizontal plan of the structures will be illustrated by a close examination of its influence on the structural damping associated with torsional modes, the torsional stiffness, and the energy dissipation capacity of the KBS. These three parameters, as discussed in the previous paragraph, governed to a certain extent the degree of the torsional coupling in the frames.

Part of the torsional stiffness of a KBF is provided by the KBS and defined with respect to the centre of mass by :

$$TK = \Sigma\, TK_{ix}\, Y_i^2 + \Sigma\, TK_{iy}\, X_i^2 \qquad (6.1)$$

where TK_{ix}, TK_{iy} are the translational stiffness of KBSs in X and Y-directions respectively, and X_i, Y_i, the distances between the KBSs and the centre of mass.

Obviously the torsional stiffness of a KBF increases as the distances between the KBSs and the centre of mass increase.

The structural damping associated with the torsional modes of vibration tends to decrease as the KBSs get nearer to the centre. One possible explanation is that nearer KBSs are less affected by torsion, consequently the contribution of the mechanical friction of the different components of the KBS, especially the joints, to the torsional damping is lower. For the same reason the hysteretic energy developed by the knee elements of inner KBSs is less than the amount absorbed by those located far from the centre.

6.4.7 STIFFNESS ECCENTRICITY

In order to investigate the behaviour of KBFs with large eccentricities, the bracing system of the eastern side of the OKBF was removed, illustrated schematically in Fig. 6.44. The resulting eccentricity was estimated using the following method. Letting TK_{ix}, TK_{iy}, MK_{ix}, and MK_{iy} represent the translational stiffness of the i^{th} resisting element (KBS and MRF respectively) and K_x, K_y the resulting structural translational stiffness in the X and Y-directions respectively, the eccentricity e was defined with respect to the centre of mass by :

$$e = (\Sigma\, TK_{ix}\, Y_i + \Sigma\, MK_{ix}\, Y_i\,) / K_x \tag{6.2}$$

The translational stiffness of the KBS and the MRF were estimated by the expression developed in Section 3.2.3 :

$$TK_{ix} = (384\, E\, I_k\, A_d \sin(\alpha + \phi) \cos^2\phi) / (192\, I_k\, l_d + A_d\, l_k^3) \tag{6.3}$$

$$MK_{ix} = (48\, EI_c) / H^3[\, 1 + (I_c\, L)/(I_b\, H)] \tag{6.4}$$

Using equation (6.2) for the stiffness distribution shown in Fig. 6.44, the distance between the centre of mass and the stiffness centre of a typical floor can be written as follows :

$$e_i = (TK_{ix}\, L_t) / 2(\, 4\, MK_{ix} + TK_{ix}) \tag{6.5}$$

where :

A_d : brace cross sectional area

ϕ : angle between brace element and the beam

α : angle between the knee element and the beam

l_k : knee element length

l_d : brace element length

L : bay width

H : storey height

L_t : overall width of floor

I_c : column moment of inertia

I_b : beam moment of inertia

E : Young's modulus.

The eccentricities e_i/L_t were found to be 15% in the lower storeys and 26% in the upper storeys. Of course these values are just a guide to the degree of eccentricities and they are by no means the exact values as the expressions 6.3, and 6.4 were only used to estimate the stiffness of the KBS and the MRF (their accuracy was discussed in Chapter 3).

The stiffness eccentric OKBF was subjected to the El-Centro earthquake, the direction of the motion was at 90° to the axis of symmetry. The resulting acceleration time histories (OECAF2 test) in X and Y-direction are plotted together with their corresponding Fourier spectra in Fig. 6.53. The response is characterised by strong torsional-translational coupling; the ratio RT_{xy} (the maximum acceleration in Y-direction to the maximum in the X-direction) reached the value 0.60. It also remained almost unchanged in other tests when the ground motion intensity was doubled. This shows the ineffectiveness of the KBS in attenuating the torsional coupling, and will be discussed later in this section.

A comparison between the coupled response of the asymmetric frames (IECAM2, OECAM2) and the uncoupled response of the symmetric frames (IECSY2, OECSY2) revealed a reduction of about 30 % in the bending strain and the top floor acceleration. This runs against the trend observed in the mass eccentric frames. A typical comparison between the response of the stiffness asymmetric and the corresponding symmetric structure, show large increase in the coupled response. The amplification factors defined by the ratios of the maximum responses (bending strain and absolute acceleration) to the peak table acceleration were more than 60% higher in the asymmetric frame. This is not due to the coupling effect alone. The principal cause is the absence of the KBS in the

eastern side of the model, not only as stiffener but also as dissipator mechanism. As can be clearly seen in Fig. 6.54 where the bending strain time-histories of the eccentric (OECAF2 test) and the symmetric (OECSY2 test) are plotted, the response of the latter was markedly lower. The eccentric frame underwent larger elastic deformations without being able to dissipate energy through the knee elements because the braced side of the model was restrained and led to a shift of the deformations to the unbraced side, the knee bracing systems in the Y-direction were almost inactive since they can only dissipate energy when they are deformed in their plane.

This example and the one before in Section 6.4.6 demonstrate the crucial importance of the location of the knee bracing systems within the plan of the structure, and showed that poor location of the KBSs may lead to an inefficiency of the system.

6.4.8 MULTI-COMPONENT EARTHQUAKE EXCITATION

The effect of all three components of an earthquake should be considered for an elastic structure to estimate the true margin of safety against yielding. For inelastic structures all the inputs must be considered simultaneously because the inelastic behaviour at a section depends on interaction between all the forces acting on the section [102].

The purpose of this section is to investigate experimentally the fundamental properties of the KBFs under two horizontal components of ground motion. To achieve this most of the test frames were subjected to the S16E and S74W horizontal components of San Fernando earthquake at two level of intensity. These tests were conducted in three phases. The frames were excited by the S16E component along the x-axis, then by S74W component along the y-direction, and finally they were subjected to both of them simultaneously.

The results from the OXXSY2, OYYSY2, and OXYSY2 tests for a symmetric frame, and the OXXAF1, OYYAF1, OXYAF1, OXXAF2, OYYAF2, and OXYAF2 tests for a stiffness eccentric frame in the elastic and plastic phase were chosen to be representative of the response of KBFs to multi-component earthquake input, since they were the most

important in terms of inelastic behaviour and degree of eccentricity. The remaining tests, however, also exhibited the same type of response.

The effect of multi-component earthquake excitation is examined through a comparison between the superposed responses of the frame under unidirectional excitation and the corresponding response from the bidirectional tests. The time-histories of the relative displacement of the top floor of the symmetric OKBF under the unidirectional S16E and S74W input which caused yield in the knee elements are plotted in Fig. 6.55 together with the response to the same components when applied simultaneously. The beginning of the time-histories have been adjusted by changing the origin of the time axis. As illustrated in this figure, the responses to the unidirectional and bidirectional excitations were identical.

Two important points can be deduced from such a behaviour. The first one is that the displacement along the two components of ground motion of these frames were resisted independently by a set of elastic structural elements (columns) and a set of mutually perpendicular knee bracing systems, there is little or no effect on the yield of the knee elements caused by out-of-plane deformation of the bays. Provided that only the knee elements undergo plastic deformation, the response of the KBFs can be obtained independently for each component even though the frame is nonlinear. If, however, the columns were to reach the yield limit, the behaviour must then be examined under the simultaneous action of the two components.

The second point which concerns the reliability of this dynamic testing is the repeatability of the tests. As can be seen from Fig. 6.55 the same results can be obtained from repetitive tests in normal circumstances.

The response of the asymmetric structure to bidirectional excitation in the nonlinear range is more complex as it involves two fundamental parameters which are mutually dependent, the torsional-translational coupling and the nonlinear behaviour which force the centre of stiffness to vary with time, consequently the effect of the multi-component earthquake on the torsional response of the KBSs is difficult to determine, nevertheless

the results of the tests enable some qualitative conclusions about the performance of the system to be drawn.

The response of the frame to the unidirectional and bidirectional input were very similar in the elastic range as can be seen in Fig. 6.56. The curves with dashed lines represent the measured bending strain at the base of the column during the OXYAF1 test (bidirectional input), and the continuous line is the sum of the responses derived from the unidirectional tests OXXAF1 and OYYAF1. In the X-direction the two curves matched very closely, but a few perturbations at low amplitudes in Y-direction can be seen. The peaks, however, were less than 2% different.

The principle of the superposition of multi-component excitations that had been successful in representing the elastic response of symmetric and eccentric frames as well as the inelastic response of symmetric frames is no longer valid for the nonlinear deformation of eccentric structures. Although the overall wave pattern of the response of the frame to the unidirectional and bidirectional inputs were quite similar (see Fig. 6.57), the phase and amplitude during the strongest part of the earthquake were slightly different. The bidirectional response was much more damped because the knee elements underwent larger inelastic deformations which was reflected by a pronounced period elongation characterising the bidirectional response, this can be better seen in Fig. 6.58 where the strongest part of the response was replotted in larger scale. The maximum bending strain in X-direction corresponding to the bidirectional response was about 18% lower than that reached by the unidirectional response. The unsymmetric KBFs tend to dissipate more energy under two-dimensional input because of the yielding interaction, the same phenomenon was noticed in symmetric structures resisted by structural elements susceptible to yield interaction in columns [44]. Similarly it has been reported in Ref.[76] that the interaction has the effect of reducing the energy input to the frame.

The discrepancies between the unidirectional and bidirectional response can be attributed mainly to the alteration of the knee element ductility by the induced torsional vibration and the complex nature of the variation of the structural eccentricity with time. It

should be noted however that the interaction effect seemed generally to be minor considering the high level of eccentricity of the model.

6.4.9 CONCLUSIONS

The experimental results obtained in this investigation show for the first time certain features of the KBS behaviour in space frames which are essential for a good implementation of the torsional resistance of KBFs.

Based on the data presented, the following conclusions may be drawn :

(1) The torsional oscillations initiated in nominally symmetric structures with unbalanced knee element strength seemed to be insignificant compared with other sources.

(2) Modal damping is sensitive to the location of the KBS and more broadly to the structural and nonstructural elements that may contribute to this form of damping when excited by that particular mode of vibration.

(3) Both the modal and hysteretic damping associated with torsional modes of vibration are necessary to damp out or prevent the initiation of torsional oscillations.

(4) The KBS operates only in its own plane. This means that each principal direction of a nonlinear symmetrical structure can be analysed independently in each principal direction and the results superposed provided that only the KBS is yielding.

(5) The degree of eccentricity in itself is meaningless, but it is the ability of the structure to resist torsion which is critical. A small eccentricity may result in very severe damage to a structure with feeble torsional resistance.

(6) The location of the KBS in the plan of the structure is crucial for the torsional stiffness and more importantly for the energy dissipation capacity of the frame. Peripheral knee braced frames (OKBFs) show better performance in resisting torsion than core knee braced frames (IKBFs)

Chapter 7

ANALYTICAL CORRELATION

ANALYTICAL CORRELATION

7.1 INTRODUCTION

For more than 30 years, ambient and forced vibration studies have been performed on many full scale multistorey buildings and laboratory scale models [24,51,80,92,108]. The existence of this database of experimental findings offers an opportunity to evaluate the modeling procedures that may be applied in the seismic analysis of buildings. The acquired knowledge of complex structural behaviour, and the computational power of modern computers has lead to a more exacting and deterministic approach in the aseismic design of multistorey buildings [73].

The foremost objective of this study is to use the results of the experimental work as basis for checking and developing numerical models which reflect the observed dynamic properties of frame structures. At this stage practically no information regarding the dynamic behaviour of knee braced frames is available. Therefore detailed mathematical models and analytical techniques are required to represent their structural behaviour. In this respect, simple and refined models are discussed in terms of accuracy by comparing the predicted results with the experimental data. It was also of interest to study how best to model the nonlinearities of a knee element by using the available elements in existing programs, and to quantify the discrepancies resulting from the complicating factors such as the semi-rigidity of the knee element connections, the backlash in the brace, and the size of the connection blocks.

7.2 FORMULATION OF MATHEMATICAL MODELS FOR THE EXPERIMENTAL STRUCTURES

The main objective of the mathematical modeling is to reduce a system with many degrees of freedom to one with the minimum number of degrees of freedom which still retains the significant properties of the system and is able to characterise the behaviour within a tolerable error [110].

The frame structures were designed to minimise the number of parameters involved in the dynamic behaviour, so that the influence of each parameter could be studied in greater detail.

The finite element program DRAIN-2D [53], briefly described in Section 3.2, was used to generate and solve the equations of motion of the two dimensional frames. However the general purpose finite element package, ANSYS [29,61], was used to predict the natural frequencies, mode shapes of the frames and to perform the nonlinear dynamic analysis of the three dimensional structures.

In order to generate a complete analytical model, the structure's geometric, mass, damping, and stiffness properties had to be defined closely since the accuracy of the numerical model is greatly dependent on the exactness of these factors. In certain circumstances a direct estimation of element characteristics can be sufficiently accurate, but in many cases the characteristics of the elements and subassemblages can only be determined experimentally.

7.2.1 GEOMETRY OF THE EXPERIMENTAL STRUCTURES

Nodes were defined at the intersection of the column and beam assembly centre lines. The flexible length of columns and beams of the first numerical model were extended to the nodes. However later rigid links were introduced at the end of columns and beams to simulate the block connection (Section 7.4), while maintaining the original dimensions of the frames.

7.2.2 MASS DISTRIBUTION

Two and three dimensional lumped mass systems were developed to model the inertia. The mass of the structure is concentrated at node points. This idealisation will introduce a very little error since most of the structural mass is concentrated at floor levels and the centre of gravity is close to the centre line of the nodes. The total mass of a floor is taken as the sum of the mass of the block connections, plates, added mass (blocks of lead), and the mass of the beams at that level plus an equivalent mass of the

columns of one storey. The entire mass of each floor is evenly divided on the four nodes of the corresponding level of the two dimensional models shown in Fig. 7.1. The mass distribution of the 3-D model will be discussed in Section 7.6.1.

7.2.3 DAMPING PROPERTIES

One procedure for defining a system damping matrix is to employ a particular form of proportional damping, called Rayleigh damping defined by

$$C = \alpha M + \beta K \tag{7.1}$$

where in the case of nonlinear system, K could represent the initial tangent stiffness matrix, alternatively C can be modified with each change in stiffness. The constants α and β can be chosen to produce specified modal damping factors for two given modes [27].

If a natural frequency, f_i and a modal damping ξ_i, are selected from a particular experimental data, α and β should satisfy the following relation

$$\xi_i=\alpha/2\omega_i + \beta\omega_i/2 \tag{7.2}$$

Both damping terms are strong functions of the frequency as shown in Fig. 7.2. For α=0 and b=$2\xi_i/\omega_i$, higher frequencies will be damped less than the lower ones. The effect is inverted when $\alpha = 2\omega_i\xi_i$ and β=0, however their sum is nearly constant over the frequency range f_1 and f_2 [29]. Fig. 7.3 shows the FFT of the response of the computed model corresponding to the cases where α=0, $\beta=2\xi_i/\omega_i$ (dashed line), and $\alpha=2\omega_i\xi_i$, β=0 (solid line) when excited by the recorded table acceleration during ECMR3 test. For the following analyses it was assumed that the damping matrix was proportional to the stiffness and mass matrices except for the case of the MRF of test series I where the damping matrix for the MRF was proportional to the mass matrix alone, because the predicted response matched the measured one better. The substitution of the measured first and second modes and the corresponding damping ratios into Eq. 7.2 gives :

	FRAME	α	β
Test series I	MRF	1.512	0.0
	WKBF	2.940	0.000387
	SKBF	1.986	0.000342
Test series II	MRF	0.376	0.00031
	KKBF	1.090	0.000509
	XKBF	0.504	0.000844
Test series III	OKBF (sym.)	2.790	0.000444
	OKBF (asym.)	2.038	0.000531

7.1.4 ELASTIC STIFFNESS PROPERTIES

Beam and column flexibility were accounted for by using elementary beam theory. The element forces and deformations are shown in Fig. 7.5(a) The axial and flexural stiffness of the beam-column element [53] are given by

Axial stiffness

$$dF_1 = (EA/L)\, dv_1 \tag{7-3}$$

Flexural stiffness

$$\begin{bmatrix} dF_2 \\ dF_3 \end{bmatrix} = EI/L \begin{bmatrix} K_{ii} & K_{ij} \\ K_{ji} & K_{jj} \end{bmatrix} \begin{bmatrix} dv_2 \\ dv_3 \end{bmatrix} \tag{7-4}$$

In which :

A : equivalent uniform cross sectional area

I : moment of inertia

E : modulus of elasticity

L : length of element

K_{ii}, K_{jj}, K_{ij} : stiffness coefficients, $K_{ij} = 2.0$, $K_{ii} = 4.0$ values for uniform element

dF : force

dv : deformation

The material properties of the main members were determined by uniaxials test on steel specimens Fig. 7.4.

7.2.5 KNEE BRACING SYSTEM CHARACTERISTICS

The brace elements were modelled by truss elements. The mode of inelastic behaviour was assumed to be yielding in tension and elastic buckling in compression. The only element deformation considered is its axial extension, the stiffness in terms of deformations is given by :

$$dF = (EA/L)\, dv \tag{7.5}$$

The yield tension and elastic buckling were determined by

$$P_y = A\sigma_y$$

$$P_{cr} = (\pi^2\, EA)/(kL/r)^2 \qquad P_{cr} < P_y$$

$$P_{cr} = P_y \qquad P_{cr} \geq P_y$$

P_y : yield in tension

P_{cr} : critical load (Euler buckling load)

σ_y : yield stress

kL : effective length

r : radius of gyration.

The beam element described in Section 7.1.4 was used to represent the knee elements. The elastic and inelastic characteristics, that is the flexural stiffness and the yield moment were obtained from the quasi-static loading tests (Section 4.5). Yielding may take place only in concentrated plastic hinges at the element ends [24]. DRAIN2D allows the user to enter the characteristics of the bilinear moment-rotation relationship at the element level, together with an approximate axial-bending moment interaction curve to take account of the yield moment reduction.

Finally, in the 3-D models the hinges were idealised by element 40 of the ANSYS program. This element becomes a spring-slider when both the gap and the damper are removed. A sketch of this element is shown in Fig. 7.5(b). It is defined by two nodal points and two stiffness constants K_1, K_2. K_1 can be based upon the semi-rigidity of the knee element connection, or a very high value can be input to account for rigid nodes. The second constant, K_2, represents the strain hardening effect which was approximated by 3% of the elastic stiffness of the knee element.

7.3 ANALYTICAL CORRELATION WITH TEST SERIES I

In this test series the validity of model 1 in predicting the global and local seismic responses of the structures is examined by comparing the experimental results with the analytical predictions.

The predicted natural frequencies of the frames were markedly lower than those determined experimentally, however the refined model (Section 7.4) predicted the first two natural frequencies to within 3.5% error.

	mode	expt.	model 1	model 2
MRF	1	5.31	4.36	5.13
	2	16.65	14.46	16.88
	3	31.39	27.90	32.31
WKBF	1	8.41	8.15	8.61
	2	26.26	24.33	26.11
	3	42.41	40.74	45.27

The mode shapes of the two numerical models were very similar. The experimental modes and those predicted by model 2 were plotted in Figs.6.4-6 (Chapter 6). All the mode shapes matched well except the third. Some experimental difficulties were encountered in exciting the frame at this resonant frequency.

7.3.1 SEISMIC RESPONSE OF THE MRF

In order to distinguish between discrepancies related to the main frame (MRF) and those due to the KBS, correlation studies of the MRF were complemented with studies of the KBFs. The analytical model representing the MRF was subjected to the motion recorded in test ECMR3. The time history of the relative displacement of the fourth floor computed by DRAIN-2D is compared with the corresponding experimental time history derived from the measured acceleration in Fig. 7.6. The measured time history (solid line) which was lagging increasingly behind the predicted values (dashed line) tends to match better during large amplitudes, on the other hand the measured large amplitudes are much more damped. It is believed that a good match could be reached between the calculated and the experimental data, but no attempt was made to increase the damping as it was believed that it had a much less significant role in the nonlinear responses. In fact this was not so as will be discussed.

7.3.2 SEISMIC RESPONSE OF THE KBFS

The test ECVW4 was selected for details analysis because the knee elements experienced considerable plastic deformation. In general model 1 appeared to be adequate in predicting the global response of the structure. The plot in Fig. 7.7 indicates good correlation in terms of the relative displacement of the top floor, despite the poor phase correlation obtained in some small amplitude intervals. The use of base line correction procedure when integrating the acceleration time history may affect the shift due to permanent distortions, if there were any, but no apparent permanent shift can be seen in the predicted displacement. The input energy was used as a global response parameter to assess the accuracy of the mathematical model. The discrepancy between computed and measured time histories of the total input energy during the PKVW3 and ECVW4 tests shown in Fig. 7.8 can be associated with errors in predicting the local deformations of the knee elements during the strongest part of the test. This produced a shift of 20% to 25% of the computed curves, yet the overall pattern has been satisfactorily conserved. Fig. 7.9 presents a comparison between measured and computed

values of the first storey brace force and the knee element midspan deformation. The poor correlation between the observed and computed brace force is mainly due to the small backlash and the pretension in the brace elements, consequently the measured amplitude is slightly smaller and offset from the origin. Considering the procedure described in Section 5.4.3 to obtain the knee element deformation, the measured response is enveloped by the predicted deformations along the time history. Two major disagreements in terms of amplitudes of the brace force and the knee element deformation can be clearly noticed. The first occurred at the beginning of the test at t=0.5s where the analytical model failed to predict three consecutive peaks, and the second occurred around t=3.4s. Their effect can be easily seen in the input and hysteretic energy time histories plotted in Fig. 7.8 and 7.10.

7.4 REFINED MODEL

Although model 1 was successful to a certain extent in predicting the response of the different frames when subjected to severe earthquake motions, an attempt was made to improve this model to match better the natural frequencies and the response of the frames at low amplitudes. Different matching techniques can be used, for instance Kabe and Rea [51] established new stiffness coefficients K_{ji},K_{jj}, and K_{ij} (Section 7.2.4) such that the horizontal interstorey stiffness of the models matched the experimental structures. However the matching procedure adopted here was based on realistic compensation for the influence of physical components that had not been accounted for in model 1.

The discrepancy between the numerical and experimental model was essentially due to the effect of the size of the connection blocks, the semi-rigidity of the connections and the stiffening effect of the floor plates. To take account of both the degree of rigidity and the dimensions of the connection blocks, rigid end elements were used. By trial and error the length of these rigid links were determined such that the fundamental frequency of the model matched the ten-storey MRF's without floors (steel plates). The length of the rigid ends would have been exactly equal to the connection block

dimensions if there were perfectly rigid connections, but the connection length was actually about 30% less than the actual block dimensions. The same procedure was used to account for the floor effect (steel plates), and the beams flexural stiffness was increased by 10%. Model 2 is in fact a simplified version of a more sophisticated model 3 which can idealise the frame connections without reducing the link lengths, and involves semi-rigid connections with nonlinear moment rotation relationships (Fig. 7.11). Some difficulties may arise in determining the model characteristics, but it is feasible by considering the local and global behaviour of the frame. However this model is expensive in terms of computing time and was judged to be unnecessary in this study, as the behaviour of the block connections of this size are not present in actual buildings. The use of this model is restricted to these particular frames and may not be generalised. However, as will be shown in Section 7.5, model 2 is accurate enough when due account is made of the experimental uncertainties.

7.5 ANALYTICAL CORRELATION WITH TEST SERIES II

The measured and predicted first natural frequencies of the braced and unbraced frames are listed below :

	mode	expt.	model 2
MRF	1	2.67	2.66
	2	7.54	7.44
	3	13.0	13.00
KKBF	1	5.04	5.11
	2	16.96	14.45
	3	27.32	25.02
XKBF	1	5.00	5.01
	2	16.76	14.36
	3	27.05	24.93

Compared with the four storey frames (test series I), the third mode matched the experimental one better (Figs .6.5-7 Chapter 6).

7.5.1 ELASTIC RESPONSE

The shaking table accelerations recorded during the low amplitude tests was used as the base excitation for the analytical model in order to check the accuracy of model 2 in the linear range of behaviour. The top floor displacement and the column bending moment of the unbraced frame (MRF) obtained experimentally and the DRAIN-2D computed values are plotted on a common axis in Fig. 7.12. In general very good agreement is obtained between the response of the analytical model and the experimental frame under the different input motions, the errors in predicting the maximum displacements were less the 10%. Again the differences in the response amplitude at the end of the time histories indicates that the damping factor used in the analytical model was underestimated. The response of the braced frames was also accurately predicted (12% error) by the numerical model as shown in Fig. 7.13.

7.5.2 NONLINEAR RESPONSE

When subjecting analytical model 2 to the motions recorded in tests PKKM2, PKXW5, and ECXW6 which caused nonlinear deformations in the knee elements, significant discrepancies in terms of phase and amplitude were apparent, particularly in the PKKM2, but the wave patterns were similar, as shown in Fig. 7.14. The ratio of the experimental period to the predicted period measured by the number of peaks between two coincident peaks during the strongest part of the earthquake reached 12/11. The ratio of the maximum experimental amplitude to the corresponding maximum predicted amplitude was 1.54. The period elongation observed in the experimental responses is mainly due to the nonlinear behaviour of the frame connections which affect both the stiffness and the energy dissipation capacity of the frame. To take account of this phenomenon, the knee element flexural stiffness was decreased by 20% so as to match the experimental period. The numerical model so modified matched the maximum

experimental displacement within 10% error, and a remarkable improvement in the phase was achieved. The delay in the experimental phase during the large amplitudes was compensated during the lower amplitudes as can be clearly seen in Fig. 7.15.

7.6 ANALYTICAL CORRELATION WITH TEST SERIES III

In this section particular attention was given to the torsional behaviour of the KBFs. An effort to examine the parameters that affect most this mode of behaviour was made in order to establish adequate models in terms of accuracy and simplicity which simulate best the torsional as well as the lateral behaviour of 3-D buildings.
Both the modal and transient dynamic analyses were carried out using ANSYS. Fig. 7.16 shows the plot of the 3-D model.

7.6.1 MODAL CORRELATION

The natural frequencies predicted by model 1 were 10% to 15% lower than those determined experimentally. However a similar refined model to model 2 discussed in Section 7.4 accounted for the floor and connection blocks by increasing the flexural stiffness of the column by 12.5% instead of the links at the end of the members to reduce the size of the numerical model. The first three frequencies predicted by this model and those determined experimentally are listed below :

frame	**mode**	**nature**	**expt.**	**predict.**
OKBF	1	(L_x)	9.19	8.86
(sym.)	2	(L_y)	9.60	8.88
	3	(T)	15.58	15.33
OKBF	1	(L_x)	9.38	9.29
(mass asym.)	2	(L_y)	9.81	9.34
	3	(T)	16.26	15.38

The accuracy of predicting the torsional frequencies as studied by comparing the results of three different models (derived from the refined model) and having practically the same lateral frequencies but different torsional ones. Three different mass arrangements were used. As shown in Fig. 7.17(a), the floor masses were distributed evenly between the 16 nodes of the floor in the first model, in the second one the mass was distributed according to the node locations, where internal nodes was assigned twice the mass of

intermediate nodes and four times a node situated at the corner of the frame, as shown in Fig. 7.17(b). A third model was introduced to reduce the number of DOF in the structure. This model had one lumped mass at each floor. Using the mass distribution of Fig. 7.3(b), the single mass characteristics were determined as follows :

$$M_{xi} = M_{fli} \tag{7.6}$$

$$M_{yi} = M_{fli} \tag{7.7}$$

$$J_i = \Sigma M_i l_i^2 \tag{7.8}$$

where :

M_{xi} : structural mass in the X-direction of the i^{th} floor

M_{yi} : structural mass in the Y-direction of the i^{th} floor

J_i : torsional inertia of the i^{th} floor

M_{fli} : total mass of the i^{th} floor

l_i : the distance between the centroid and a lumped mass of the distribution shown in Fig. 7.17(b).

The torsional frequencies determined by the uniform mass distribution were 22% lower than the experimental frequencies. The second distribution however was more realistic and the lowest torsional frequency increased by 20%. The results of the third model which were practically the same as the second, matched the experimental frequencies with less than 2% low in the symmetric frames and only 7% low in the mass eccentric structure. Thus this model was used to predict the seismic responses of the frames.

7.6.2 LINEAR DYNAMIC CORRELATION :

The numerical models representing the symmetric, mass and stiffness eccentric frames were subjected to the table accelerations recorded during the OECSY1, OECAM1, and OECAF1 tests respectively. The top floor displacement along the X and Y-directions of the experimental and analytical models were plotted in Fig. 7.18-20. Generally the predicted and measured responses were in very good agreement in terms of phase and amplitude. The error in predicting the maximum response in the X-direction of most of these tests varied from 3% to 25%. The largest error was observed

in the case of the symmetric structure caused by an underestimate of the structural damping (Fig. 7.18). The analytical model failed to predict accurately the top floor displacement in Y-direction of the mass eccentric frame OECAM1 in Fig. 7.19. The maximum measured displacement was four times bigger than the predicted peak. This was due to the small effect of the 2% eccentricity which was not strong enough to overcome the accidental eccentricities. Also, the very small amplitudes (0.12mm) registered in this direction were very sensitive to the induced experimental error. However, the error in the Y-direction of the stiffness eccentric frame was only 17% because of the strong eccentric character of the frame (Fig. 7.20)

7.6.3 NONLINEAR DYNAMIC CORRELATION

The previous linear 3-D analysis were carried out using ANSYS version running on the Apollo DN4000 workstations. Using the matrix reduction and the displacement pass options [29], it was possible to perform several runs within a reasonable time (about 3 hours each run). The nonlinear transient dynamic analysis, however, is the most expensive type of structural analysis in ANSYS especially for large systems because the program decomposes the stiffness matrix for each load step and each unconverged iteration within a load step. In addition no option is available to separate the displacement and stress pass which increase both the time and the storage space. For these reasons, the nonlinear dynamic analysis of the 3-D models was not possible on the workstations. Instead the ANSYS version running on the mainframe computer IBM3090 was used. Even so, it was not possible to analyse all the structures for all earthquake inputs, because of limitations in storage space and computer time. Therefore only the strongest part of the time-histories of two selected frames were considered. The frames were chosen to represent a symmetric structure (OECSY3), and a strength eccentric structure (OECAS7) subjected to the strongest scaled El-Centro earthquake (0.76g).

The predicted dynamic response to the table motion recorded during the OECSY3 was plotted as a dashed curve together with the corresponding experimental response in a solid line in Figs.7.21. This correlation was made in an attempt to quantify the deviation

of the predicted response in the X-direction from the experimental response due to the torsional translational coupling effect caused by a small accidental eccentricity. Apparently no specific sign of this effect can be detected from the time-histories of Fig. 7.21. Like most of the previous nonlinear correlations with the 2-D frames where torsion was prevented, the response of the 3-D numerical model was in good agreement with the experimental response. In terms of amplitudes the peak displacement of the top floor was predicted within 22% error, the phase and the signal pattern were well reproduced.

The numerical model of the strength eccentric model succeeded to a certain extent to replicate the experimental X-displacement as shown in Fig. 7.22(a) and (b). A total disagreement, however, between the measured and predicted Y-displacement can be clearly seen in Fig. 7.22(c). The experimental response was characterised by a wider range of frequency components than the predicted response. It was thought that a superposition of extraneous signal might be the cause of the discrepancy, therefore an attempt to extract a signal from the experimental response which matches the predicted response by a pass-band filter was made and failed, which means that such a signal is not present. In addition to the table acceleration in the X-direction the numerical model was then subjected to a noisy acceleration signal (low amplitude) registered in the Y-direction of the table, but the response in both direction was not affected significantly. A possible reason of the incompatibility seems to be the lateral-torsional coupling initiated at an early stage by an accidental eccentricity, thus different initial conditions coincided with knee element yield in the experimental model and the numerical model.

As a recapitulation, the discrepancies between the response of the numerical models considered in this chapter and the experimental results were in general of two categories, assuming that the solution algorithms of the programs used are accurate enough (Section 3.2).

The first resulted from an incompatibility in damping mechanisms. Included in this category are the structural, and hysteretic damping. The modal damping determined at

low amplitudes was generally underestimated. The hysteretic damping resulting from the knee element yield could not be accurately predicted because of the error induced by the indirect method used to determine the characteristics of the hysteretic loops of the knee elements (Section 4.5). Any discrepancy in this area would affect the amplitude of the response. The second source of error may be the incorrect determination of the stiffness properties of the physical model.

As discussed earlier, the stiffness characteristics of the structural elements can be accurately determined, even the nonstructural elements were successfully compensated for. However, the nonlinearity of the overall behaviour of the frames is due principally to the behaviour of the connections, which was a major source of error. This can be overcome provided that the expected range of amplitudes is known, say small amplitudes in the elastic and moderate inelastic range, or high amplitudes in exceptionally severe conditions. For the former case the closer the stiffness of the numerical model is to the actual value the better, and this requires every possible parameter that may affect the stiffness of the structure to be taken into account, such as the refined model of Section 7.4. However, for the second case where large deformations are expected to occur in the structure, more flexible models in which for instance the effect of nonstructural elements is omitted, perform better as did those in Section 7.3 (model 1). Inconsistencies in this category can be normally detected by variable phase lag in the response time-histories. Results from Ref. [73] shows similar behaviour for full scale structures.

7.7 CONCLUSIONS

The correlative analyses of the several frames discussed in this chapter demonstrate various important aspects relating particularly to the KBFs and more generally to seismic analyses of multistorey buildings. From the results of these analyses general observations and conclusions concerning modeling approaches are made in this section.

(1) The natural frequencies predicted by simple analytical models with full flexible member lengths were significantly lower than those determined experimentally at small amplitude vibrations.

(2) These simple models were able to predict with a fair degree of accuracy the seismic responses of the frames at high amplitudes. The phase lagged behind however at low amplitudes.

(3) The refined models on the other hand achieved very good correlation with the experimental seismic responses at low amplitudes, but a clear phase disagreement was observed during large oscillations.

(4) In general, the analytical mode shapes correlated well with those from the experimental studies for both the refined and the simple models.

(5) The structural damping determined during the identification tests at small amplitudes was often exceeded in the tests, and showed some dependency on the level of excitation.

(6) The total input energy is a good overall indicator for the assessment of the analytical models. Any error in predicting yield can be easily detected from the difference in the time-history of the input energy.

(7) The equivalent single mass per floor technique was successful in 2-D and 3-D modeling and more efficient.

(8) DRAIN2D was more efficient than the ANSYS in performing nonlinear dynamic analyses both in terms of time and output control.

Chapter 8

CONCLUSIONS AND RECOMMENDATIONS FOR FUTURE WORK

CONCLUSIONS AND RECOMMENDATIONS FOR FUTURE WORK

8.1 CONCLUSIONS

The analytical and experimental work presented in this thesis evaluated several aspects of the knee bracing system related to its ability to resist earthquakes. On the basis of these results, the KBFs show an effective adequacy to meet most of the criteria demanded by the earthquake resistant design of multistorey buildings. Detailed comments and conclusions were included at the end of each chapter, the following conclusions are a summary of the main results.

(1) By varying the geometric characteristics of the knee element it is possible to control the initial elastic stiffness, the strength, the distribution of the structural element forces, and the energy dissipation capacity of the frame. On the ground of the comprehensive parametric analyses, the range of the length, relative stiffness and the geometric configuration of the knee element was defined and guidelines to refine the design of the knee element for specific cases were established.

(2) An expression to estimate the ductility demand in a knee braced frame has been developed, and the end-fixity effect on the dynamic characteristics of the frame was quantified.

(3) Simple analytical expressions to estimate the elastic and post-elastic equivalent lateral stiffness of KBFs were developed to serve for hand calculations in the preliminary design.

(4) In addition to the conventional structural parameters, the energy concept was used to illustrate the high capacity of KBFs to dissipate energy. Uniform distribution of ductility and energy dissipation distribution through the height can be easily achieved.

(6) The yield of the knee elements provides the frame with a wide range of contained yielding, which acts as safety valve to limit the loads exerted on the braces and hence buckling and yielding of these are prevented.

(7) An important feature of the knee bracing system is its capability to enforce a preselected yield sequence, and to control the range of the contained yielding in the KBF.

(8) True replica models are practically impossible to build and test because of the severe restrictions imposed on the model. A proposed overall mechanical scaling, however, simulated adequately the behaviour of the structure, and some particular distortions of the similarity requirements were successfully accounted for.

(9) The experimental results portrayed the general trend of most of the KBS characteristics that had been established analytically (4) and (6).

(10) Among other points encountered during the first series of tests, an important one concerned the nature of the knee element-diagonal brace connection that should be carefully designed in full scale structures to minimise the backlash which may weaken the energy dissipation capacity of the frame.

(11) The modal damping may be significantly increased in structures incorporating the KBSs.

(12) Like any other system the KBFs performance depends on the earthquake type.

(13) Imperfection in structural construction may alter the ductility distribution through the height of the building, leading to a concentration of inelastic deformation in a particular storey. However, permanent distortions of the knee elements are unusual, and their effect on the overall structural distortion is minimal.

(14) Initiation of torsional oscillations in nominally symmetric structures with unbalanced knee element strength seemed to be insignificant.

(15) Modal damping is sensitive to the location of the KBSs and more broadly to the structural and nonstructural elements that may contribute to this form of damping when excited by that particular mode of vibration. Both the modal and hysteretic damping associated with torsional modes of vibration are necessary to damp out or to prevent the initiation of torsional oscillations.

(16) The KBS is a uni-directional resisting element which means that space symmetric KBFs can be studied as 2-D models when only the knee elements are expected to yield.

(17) The degree of eccentricity in itself is meaningless, but it is the ability of the structure to resist torsion which is critical, as a small eccentricity may result in a very severe damage to a structure with feeble torsional resistance.

(18) The location of the KBS in the horizontal plan of the structure is crucial for the torsional stiffness and more importantly for the energy dissipation capacity of the frame. Peripheral knee braced frames (OKBFs) show better performance in resisting torsion than core knee braced frames (IKBFs)

(19) From the extensive numerical modeling of the KBFs, simple analytical models with full flexible member lengths underestimate the frame frequencies determined at low amplitudes. These models, however, were able to predict accurately the seismic responses of the frames at high amplitudes. The refined models that accounted for the floor and connection rigidity and having natural frequencies matched with the experimental frequencies, achieved very good correlation with the experimental seismic responses at low amplitudes, generally in the elastic phase; however, a clear phase disagreement was observed during large oscillations.

(20) The structural damping determined during the identification tests at small amplitudes was sometimes underestimated, and showed some dependency on the excitation intensity.

8.2 RECOMMENDATIONS FOR FURTHER RESEARCH

The above conclusions constitutes the first step in the advancement of a new bracing system for earthquake resisting steel structure which is capable to meet the seismic design requirements. However more analytical and experimental work is needed to explore other aspects of the KBS in order to reach the standard of the practice implementation. These can be summarised as follows:

(1) An optimisation study of the shape and mode of yield of full scale knee elements accompanied by cyclic test of knee braced subassemblages to determine *more realistically* the hysteretic loop characteristics and to investigate the out-of-plan deformation of the knee element.

(2) Large scale seismic tests, or full scale pseudo-dynamic test are required to validate experimentally the yield sequence of the structural members.

(3) A study of KBFs incorporating frictional devices at midspan and ends of the knee element is worthy. The advantage of this is to separate the energy dissipation and the force distribution role of the knee element.

(4) The implementation of the techniques for practical design of KBFs need to be developed to assist the engineer in the structural design process.

REFERENCES

[1] Anagnostides G., *'Design of economical means of enhancing the energy-absorption capability of braced frame structures,'* Ph.D thesis, University of London, Imperial College of Science and Technology, London, 1988.

[2] Anagnostopoulos S. A., *'Inelastic Beams for Seismic Analysis of Structures,'* Jnl. of Structural Engineering, ASCE, vol. 107 No. 12, Dec. 1981, 1757-1767.

[3] Aristizabal-Ochoa J. D., *'Disposable Knee Bracing: Improvement in Seismic Design of Steel Frames,'* Jnl. of Structural Engineering, ASCE, vol. 112 No. 7, Jul. 1986, 1544-1552.

[4] Arnold C., *'Soft first storeys: Truths and Myths,'* Proc. 8th World Conf. on Earthquake Engineering, vol V, San Francisco, USA 1984

[5] Arnold P., Adams P.F., and Lu L.W., *'Strength and behaviour of an inelastic hybrid frame,'* Jnl. of Structural Engineering, ASCE, vol.94, No. 1, Jan. 1968, 243-266.

[6] Austin M. A., and Pister K. S., *'Design of seismic-resistant friction-braced frames,'* Jnl. of Structural Engineering, ASCE, vol. 111, No. 12, Dec. 1985, 2751-2769

[7] Austin M. A.,and Pister K. S., *'Optimisation-Based Computer-Aided Design of Earthquake Resisting Steel Structures,'* Proc. 8th World Conf. on Earthquake Engineering, vol. V, San Francisco, USA 1984, 451-458.

[8] Balendra T., Lam K., Liaw C., and Lee S., *'Behaviour of eccentrically braced frame by pseudo-dynamic test'*, Jnl. of Structural Engineering ASCE, vol. 113, No. 4, April 1987, 673-688.

[9] Bathe K. J. and Wilson E. L., *'Stability and accuracy analysis of direct integration methods,'* Earthquake Engineering and Structural Dynamics, vol. 1, 1973, 283-291.

[10] Bathe K.J, and Wilson E. L., Numerical Methods in Finite Element Analysis, Prentice Hall 1976.

[11] Bathe K.J, Wilson E.L, and Peterson F.E., *'SAP IV - A structural analysis program for static and dynamic response of linear systems,'* Report No EERC 73-11, Earthquake Engineering Research Centre, University of California, Berkeley, 1973.

[12] Beauchamp K. G., Signal Processing, using analog and digital techniques, George Allen & Unwin, 1973

[13] Bertero V. V., Uang C. M., Llopiz C. R., and Igarashi K., *'Earthquake simulator testing of concentric braced dual systems'*, Jnl. of Structural Engineering, ASCE, vol. 115, No. 8, Aug. 1989, 1877-1894

[14] Bittner J. L., ANSYS tutorial Newmark integration solution technique, Swanson Analysis Systems Inc, Rev.4.3, 1988.

[15] Blakeborough A., Severn R. T., and Taylor C. A., *'The new UK national six-axis earthquake shaking table,'* Proc. of the 8th European Conf. on Earthquake Engineering, vol. 4, Lisbon, Portugal 1986.

[16] Blondet J. M., Yep J. F., and Kelly J. M., *'Shaking table evaluation of strong motion data processing techniques.'* Proc. of the 9th World Conf. on Earthquake Engineering, vol. IV, Tokyo, Japan 1988.

[17] Booth E. D., Dallard P. R., and Willford M. R., *'The accuracy of response spectrum analysis for the seismic response of typical building structures'*, Proc. of the Conf. on Civil Engineering Dynamics, Bristol 1988.

[18] Brownjohn J. M. W., *'Assessment of structural integrity by dynamic measurement,'* PhD thesis, Civil and Mechanical Engineering Department, University of Bristol, Bristol 1988.

[19] Brownjohn J. M. W., EERC Earthquake Simulator, Technical Instruction 23001, Earthquake Engineering Research Centre of Bristol University, Feb 1989.

[20] Brownjohn J. M. W., Use of ASYST for Data Acquisition (DASYST), Technical Instruction 23002, Earthquake Engineering Research Centre of Bristol University, Feb 1989.

[21] Chen C.K., *'Seismic analysis of building frames with semirigid connections,'* Proc. of the 8th World Conf. on Earthquake Engineering, vol. V, San Francisco, USA 1984, 725-732.

[22] Chung L. L., Reinhorn A. M., and Soong, T. T., *'Experiments on active control of seismic structures,'* Jnl. of Engineering mechanics, ASCE, vol.114, No 2, Feb. 1988, 241-256

[23] Clough R. W., and Penzien J., Dynamics of Structures, McGraw Hill Book Company, 1975.

[24] Clough R. W., and Tang D. T., *'Earthquake simulator study of a steel frame structure vol I'*, No. EERC 75/6, Earthquake Engineering Research Centre, University of California, Berkeley, 1975.

[25] Conover J. L., ANSYS tutorial Incremental Newton-Raphson solution technique, Swanson Analysis Systems Inc, Rev.4.3, 1988.

[26] Constantinou M. C., and Tadjbakhsh I. G., *'The optimum design of a base isolation system with frictional elements,'* Earthquake Engineering and Structural Dynamics, vol.12, 1984, 203-214.

[27] Craig R., Structural Dynamics: An introduction to computer methods, Wiley, New York 1981.

[28] DeSilva C. W., Dynamic Testing and Seismic Qualification Practice, Lexington Books, D.C. Heath and Company, Toronto 1983.

[29] DeSalvo G. J., Gorman R. W., Engineering Analysis System (ANSYS) User's Manual, Swanson Analysis Systems Inc, Rev.4.3, vol. I and II, 1988

[30] Despeyroux J., *'Some lessons to be drawn from the El Asnam earthquake of 10 October 1980,'* Proc. of the 8th World Conf. on Earthquake Engineering, vol. V, San Francisco, USA 1984, 549-556.

[31] Dumanoglu A. A., and Severn R. T., '*Dynamic behaviour of clasp-type buildings*,' Earthquake Engineering and Structural Dynamics, vol. 13, 1985, 481-505.

[32] EERI, Reducing Earthquake Hazards: Lessons Learned from Earthquakes, Publication EERI No. 86-02, Nov. 1986.

[33] Filiatrault A., and Cherry M., '*Performance evaluation of friction damped braced steel frames under simulated earthquake loads*', Earthquake Spectra, vol. 3, No. 1, 1987.

[34] Fitzgerald T. F., Anagnos T., Goodson M., and Zsutty T., '*Slotted bolted connections in aseismic design for concentrically braced connections*,' Earthquake Spectra, vol. 5, No. 2, 1989, 383-391.

[35] Gajanan S. M., Harris H. G., White R. N., Mirza M. S., Structural Modeling and Experimental Techniques, Prentice-Hall, 1983.

[36] Giberson M. F. '*Two nonlinear beams with definitions of ductility*', Jnl. of Structural Engineering, ASCE, vol. 95, No.2 1969, 137-155.

[37] Goel S. C., and Berg G. V., '*Inelastic Earthquake Response of Tall Steel Frames*,' Jnl. of Structural Engineering, ASCE, vol. 94 No.8, Aug. 1968, 1907-1935.

[38] Goel S. C., and El-Tayem A. A., '*Cyclic load behaviour of angle X-bracing*,' Jnl. of Structural Engineering, ASCE, vol. 112, No 11, Nov. 1986, 2528-2539.

[39] Hanson R. D., '*Comparison of static and dynamic hysteresis curves*,' Jnl. of the Engineering Mechanics, ASCE, vol.100, No 5, Oct. 1966, 87-113.

[40] Haroun N. M., and Shephred R., '*Inelastic behaviour of X-bracing in plane frames*,' Jnl. of Structural Engineering, ASCE, vol. 112, No 4, 1986, 764-781.

[41] Hejal R., and Chopra A. K., '*Earthquake response of torsionally coupled frame buildings*,' Jnl. of Structural Engineering, ASCE, vol.115, No.4, Apr. 1989, 834-851.

[42] Hilber H. M., Hughes T. J. R., and Taylor, R. L., '*Improved numerical dissipation for time integration algorithms in structural dynamics*,' Earthquake Engineering and Structural Dynamics, vol.5, 1977, 283-292.

[43] Hjelmstad K. D., and Popov E. P., '*Characteristics of eccentrically braced frames*,' Jnl. of Structural Engineering ASCE, vol. 110, No. 2, Feb.1984, 340-688.

[44] Hoerner J. B., '*Modal coupling and earthquake response of tall buildings*,' Ph.D thesis, California Institute of Technology, Pasadena, California, 1971.

[45] Huixian L., '*The sole course of mitigating earthquake risk*,' Proc. of the 9th World Conf. on Earthquake Engineering, vol. 2, Tokyo, Japan 1988, 21-28.

[46] Hüffmann G., '*Spring-damper systems for the support of structures to prevent earthquake damage*,' Proc. of the 7th World Conf. on Earthquake Engineering, vol. 8, Istambul, Turkey 1980, 53-61.

[47] Ikeda K., and Mahin A., '*Cyclic response of steel braces*,' Jnl. of Structural, ASCE, vol. 112, No 2, Feb.1986, 342-361.

[48] Jain A. K., and Goel S. C., *'Designing multistorey braced frames for earthquakes,'* Proc. of the 7th World Conf. on Earthquake Engineering, vol. 4, Istambul, Turkey 1980, 9-17.

[49] Jeary A. P., and Ellis B. R., *'The accuracy of mathematical models of structural dynamics'* Proc. Design for Dynamic Loading, Longman Group Ltd., London 1982.

[50] Kabe A. M., and Rea D., *'Inelastic earthquake response of steel structures,'* Jnl. of Structural Engineering, ASCE, vol. 109, No. 3, Mar. 1983, 705-719.

[51] Kabe A., and Rea D., *'Earthquake induced inelastic deformation in small scale steel construction,'* Dissertation presented to the University of California, Los Angeles, in partial fulfilment of the requirements for the degree of Ph.D,June 1980.

[52] Kahn L. F., and Hanson R. D., *'Inelastic cycles of axially loaded steel members,'* Jnl. of Structural Engineering, ASCE, vol. 102, No 5, May 1976, 947-959.

[53] Kanaan A. E., and Powell G. H., *'DRAIN-2D A general purpose computer program for dynamic analysis of inelastic plane structures,'* Reports No. EERC 73-6 and EERC 75-22, Earthquake Engineering Research Centre, University of California, Berkeley, Sept. 1973, and Aug. 1975.

[54] Kasai K., and Popov E. P., *'Cyclic web buckling control for shear link beams,'* Jnl. of Structural Engineering, ASCE, vol. 112, No. 3, March 1986, 505-523.

[55] Kasai K., and Popov E. P., *'General behaviour of WF steel shear link beams'*, Jnl. of Structural Engineering, ASCE, vol. 112, No. 2, Feb. 1986, 362-382.

[56] Kasai K., and Popov E. P., *'On seismic design of eccentrically braced steel frames,'* 8th World Conf. on Earthquake Engineering, vol. V, San Francisco, USA 1984, 387-394

[57] Kasai K., and Popov E. P., *'Study of seismically resistant eccentrically braced steel frame systems,'* Report No. UCB/EERC 86/01, Earthquake Engineering Research Centre, Univ. of California, Berkeley March 1986.

[58] Kato B, and Akiyama H., *'Seismic design of steel buildings,'* Jnl. of Structural Engineering, ASCE, No 8, Aug. 1982, 1710-1720.

[59] Kelly J. M., *'Aseismic base isolation: review and bibliography,'* Soil Dynamics and Earthquake Engineering, vol.5, No.3, 1986,703-727.

[60] Key, D. E., *'The earthquake response of building structures with energy absorbing dampers,'* PhD thesis, Faculty of Engineering and Applied Science, University of Southampton, Southampton 1985.

[61] Kohnke P. C., ANSYS, Theoretical Manual, Swanson Analysis Systems Inc, Rev.4.2, 1983.

[62] Krawinkler H. and Mohasseb S., *'Effect of panel zone deformations on seismic response,'* Jnl. of Constructional Steel Research, vol. 8, 1987,233-250.

[63] Lui E. M., and Chen W. F., *'Steel frame analysis with flexible joints,'* Jnl. of Constructional Steel Research, vol. 8, 1987, 161-202.

[64] Malley J. O., and Popov E. P., *'Design considerations for shear links in eccentrically braced frames,'* Report No UCB/EERC 83/24, Earthquake Engineering Research Centre, University of California, Berkeley Nov. 1983.

[65] Malley J. O., and Popov E. P., *'Shear links in eccentrically braced frames,'* Jnl. of Structural Engineering, ASCE, vol. 110, No. 9, Sept. 1984, 2275-2295.

[66] Manheim D. N., and Popov E. P., *'Plastic shear hinges in steel frames'*, Jnl. of Structural Engineering, ASCE, vol. 109, No. 10, Oct. 1983, 2404-2419.

[67] Menu J.M.H. and Elnashai A. S., *'Earthquake time-history transformation for scale model dynamic testing,'* Proc. of the Conf. on Civil Engineering Dynamics, Bristol 1988.

[68] Midorikawa M., and Yamanouchi H., *'Analytical evaluation of K-braced structure seismic test,'* Jnl. of Structural Engineering, ASCE, vol. 115, No 8, Aug.1989, 1930-1949.

[69] Moncarz P. D., and Krawinkler H., *'Modelling of steel and reinforced concrete structures for seismic response simulation,'* Proc. Design for Dynamic Loading, Logman Group ltd., London 1982, 162-168.

[70] Morovich A. T., Nicoletti J. P., and Hartle E., *'Eccentric bracing in tall buildings,'* Jnl. of Structural Engineering, ASCE, vol. 108, No. 9, Sept. 1982, 2066-2080.

[71] Mueller P., *'On aseismic design, '* Proc. of the 8th World Conf. on Earthquake Engineering, vol. V, San Francisco, USA 1984, 411-418.

[72] Neal B. G. The Plastic Methods of Structural Analysis, Science Paperbacks, third edition 1977

[73] Neuss C.F., Maison B.F., and Bouwkamp J.G., *'A study of computer modeling formulation and special analytical procedures for earthquake response of multistorey buildings'*, Report for the National Science Foundation J. G. Bouwkamp, Inc., California, Berkeley Jan. 1983.

[74] Newland D. E., Random Vibration and Spectral Analysis, Longman Group Ltd., London 1975.

[75] Newmark N. M., Rosenblueth E., Fundamentals of Earthquake Engineering, Prentice -Hall, 1971.

[76] Nigam N. C., and Housner G. W., *'Elastic and inelastic response of framed structures during earthquakes'*, Proc. of the 4th World Conf. on Earthquake Engineering, vol. 2, Santiago, Chile 1969, A-89 to A-104

[77] Nordenson G. J. P., *'Notes on the seismic design of steel concentrically braced frames,'* Proc. of the 8th World Conf. on Earthquake Engineering, vol.V, San Francisco, USA 1984, 395-402.

[78] Pall A. S., and Marsh C., *'Response of friction damped braced frames,* Jnl. of Structural Engineering, ASCE, vol.108, No. 6, June 1982, 1313-1323.

[79] Paz M., Structural Dynamics, Van Nostrand Reinhold CompanyInc, New-York 1985.

[80] Penzien, J., *'Dynamic response of elasto-plastic frames,'* Jnl. of Structural Engineering, ASCE, vol. 86, No. 7, July 1960., 81-94

[81] Popov E. P. *'Panel zone Flexibility in seismic Moment Joints'* Jnl. Constructional Steel Research, vol. 8, 1987, 91-118.

[82] Popov E. P., *'Panel zone flexibility in seismic moment joints,'* Jnl. of Constructional Steel Research, vol 8, 1987, 91-118.

[83] Popov E. P., Amin N. R., Louie J. J. C., and Stephen R. M., *'Cyclic behaviour of large beam-column assemblies,'* Earthquake Spectra, Vol.1, No 2, Feb. 1985, 3-38.

[84] Popov E. P., and Black R. G., *'Steel struts under severe cyclic loading,'* Jnl. of Structural Engineering, ASCE, vol. 107, No 9, Sept.1981, 1857-1881.

[85] Popov E. P., Kasai K., Engelhardt M. D., *'Advances in design of eccentrically braced frames,'* Earthquake Spectra, vol.3, No 1, Jan. 1987, 43-55.

[86] Popov E. P., Takanashi K., and Roeder C. W., *'Structural steel systems: Behaviour under cyclic loading,'* Report No EERC 76-17, Earthquake Engineering Research Centre, University of California, Berkeley Oct. 1973.

[87] Popov, E. P., *'On California structural steel seismic design'*, Earthquake Spectra, vol. 2, No. 4, Feb. 1986 703-727.

[88] Raichur K. S., ANSYS tutorial mode superposition, Swanson Analysis Systems Inc, Rev.4.3, 1988

[89] Randall R. B., Frequency Analysis, Brüel and Kjaer, sep. 1977.

[90] Rea D., Bouwkamp, J.G., *'Dynamic behaviour of a high-rise diagonally braced building,'* Report No. EERC 71-5, Earthquake Engineering Research Centre, University of California, Berkeley 1971.

[91] Roeder C. W., and Popov E. P., *'Inelastic behaviour of eccentrically braced steel frames under cyclic loading,'* Report No. UCB/EERC 77/18, Earthquake Engineering Research Centre, University of California, Berkeley Aug. 1977.

[92] Roeder C. W., Foutch D.A., and Goel S.C., *'Seismic testing of full-scale steel building part I and II,'* Jnl. of Structural Engineering, ASCE, vol. 113, No. 11, Nov 1987.

[93] Roeder, C. W., and Popov E. P., *'Eccentrically braced steel frames for earthquakes,'* Jnl. of Structural Engineering ASCE, vol. 104, No. 3, March 1978, 391-412.

[94] Russel M., *'Small-scale modeling of the nonlinear response of steel-framed buildings to earthquakes,'* Proc. Design for Dynamic Loading, Longman Group Ltd., London 1982, 171-177

[95] Samali B., Yang J. N., and Liu S. C., *'Active control of seismic-excited building,'* Jnl. of Structural Engineering, ASCE, 111, No 10, Oct. 1985, 2165-2180.

[96] Scholl R. E., *'Brace dampers : An alternative structural system for improving the earthquake performance of buildings,'* Proc. of the 8th World Conf. on Earthquake Engineering, vol. V, San Francisco, USA 1984, 1015-1022.

[97] Shibata M., '*Influence of restoring-force characteristics of braces on dynamic response of braced frames,*' Proc. of the 7th World Conf. on Earthquake Engineering,vol. 4, Istambul, Turkey 1980.

[98] Skinner R. I., Beck J. L., and Bycroft G. N., '*A practical system for isolating structures from earthquake attack,*' Earthquake Engineering and Structural Dynamics, vol.3, 1979, 297-309.

[99] Skinner R. I., Kelly J. M., and Heine A. J., '*Hysteretic dampers for earthquake-resistant structures,*' Jnl. of Earthquake Engineering and Structural Dynamics, vol.3, 1975, 287-296.

[100] SPIDERS, Data Capture and Analysis, User's Manual, PAFEC Ltd 1988.

[101] Straudacher K., '*Structural integrity in extreme earthquakes the Swiss full base isolation system (3-D),*' Proc. of the 8th World Conf. on Earthquake Engineering, vol.V, San Francisco, USA 1984, 1039-1054

[102] Syamal P. K., and Pekau O. A., '*Dynamic response of bilinear asymmetric structures,*' Earthquake Engineering and Structural Dynamics, vol.13, 1985, 527-541.

[103] Tang D T., and Clough R. W, '*Shaking table earthquake response of steel frame,*' Jnl. of Structural Engineering, ASCE, vol. 105, No. 1, Jan. 1979.

[104] Taylor C. A., '*Development of the Bristol seismic shaking table and its use in embank*ment *dam research,*' Ph.D thesis, Civil Engineering Department, Bristol University, 1983.

[105] Tezcan S., Civi A., and Hüffmann G., '*Spring-dashpot vibration isolators against earthquakes,*' Proc. of the 7th World Conf. on Earthquake Engineering, vol. 8, Istambul, Turkey 1980,53-60

[106] Warburton G. B., The Dynamical Behaviour of Structures, Pergamon Press 1976.

[107] Wheeler W. K., and Hancock G., J., '*Dynamic response of discretely damped structures under harmonic and random excitation,*' Engineering Structures, vol. 7, oct. 1985, 237-244.

[108] Whittaker A. S, Uang C., and Bertero V. V., '*Seismic testing of eccentrically braced dual steel systems,*' Earthquake Spectra, vol. 5, No. 2, Feb. 1989, 429-449.

[109] Yamada Z. M., Kawamura H., Tani A., '*Finite resonance response of asymmetric* structures,' Proc. of the 9th World Conf. on Earthquake Engineering, vol. 5, Tokyo, Japan 1988, 97-104.

[110] Yang M. S., '*Seismic behaviour of an eccentrically X-braced steel structure,*' Report No. EERC 82/14, Earthquake Engineering Research Centre, University of California, Berkeley 1982.

[111] Zahrah T. F., and William J. H., '*Earthquake energy absorption in SDOF structures,*' Jnl. of Structural Engineering, ASCE, vol. 110 No 8, Aug. 1983, 1757-1772.

BIBLIOGRAPHY

[1] Acton F., Numerical Analysis That Work, Harper and Row, 1970.

[2] Anagnostopoulos S. A., *'Post-yield flexural properties of tubular members,'* Jnl. of Structural Engineering, ASCE, vol. 105, No. 9, Sep. 1979, 1757-1767.

[3] Applied Technology Council, Tentative Provisions for the Development of Seiemic Regulations for Buildings, Structural Engineers' Association of California, Publication ATC 3-06, U.S. Department of Commerce, Washington, June 1978.

[4] Biggs J. M., Introduction to Structural Dynamics, McGraw-Hill, 1964.

[5] Bresler B., Lin T. Y., and Scalzi J. B., Design of Steel Structures, John Wiley & Sons, 1968.

[6] Dong R. G., *'Vibration-absorber Effect under seismic excitation,'* Jnl. of Structural Engineering, ASCE, vol. 102, No. 10, Oct. 1976.

[7] Faires B., Numerical Analysis, Prindle and Webber, Schmidt 1985.

[8] Hilber H. M., Hughes T. J. R., and Taylor R. L., *'Improved numerical dissipation for time integration algorithms in structural dynamics,'* Earthquake Engineering and Structural Dynamics, vol. 5, 1977, 283-292

[9] Housner G. W., Earthquake Engineering, Prentice Hall, 1970.

[10] Iwan W. D., and Gates N. C., *'The effective period and damping of class of hysteretic structures,'* Earthquake Engineering and Structural Dynamics, vol. 7, 1979, 199-211.

[11] Jenkins w. M., Matrix and Digital Computer Methods in Structural Engineering, McGraw-Hill, 1969.

[12] König G., Wörner J., *'Influence of local nonlinearities on structural behaviour under dynamic excitations,'* European Earthquake Engineering vol. 2, No 1, 1988, 8-14.

[13] Lapidus L., Seinfeld J. H., Numerical Solution of Ordinary Differential Equations, Academic Press, 1971.

[14] Lian W., Jingxin Z., Zhili J., *'Elasto-plastic earthquake reponse analysis for multi-storeyd building taking account of torsion,'* Proc. of the 7th World Conf. on Earthquake Engineering, vol. 7, Istambul, Turkey 1980, 270-277.

[15] Lin A. N., and Verser B. A., Microcomputer Based Data Acquisition System for Dynamic Testing, Earthquake Spectra, vol. 3, No. 2, 1987, 299-313.

[16] McGuire W., and Gallagher R. H., Matrix Structural Analysis, John Wiley and Sons, 1979.

[17] Rao S. S., The Finite Element method in Engineering, Pergmon Press, 1982.

[18] Riddell R., *'Effect of damping and type of material nonlinearity on earthquake response,'* Proc. of the 7th World Conf. on Earthquake Engineering, vol. 7, Istambul, Turkey 1980.

[19] Rogers G. L., Dynamics of framed structures, John Wiley & Sons, 1959.

[20] Ruiz P., and Penzien J., *'Artificial generation of earthquake acceleregrams,'* NSF - GK - 1319, Earthquake Engineering Research Centre, University of California, Berkeley, March 1969.

[21] Tso, W. K., *'Induced torsional oscillations in symmetrical structures,'* Earthquake Engineering and Structural Dynamics, vol. 3, 1975, 337-346.

[22] Tso, W. K., *'Torsional vibration of symmetrical structures,'* Proc. of the First Canadian Conf. on Earthquake Engineering, Vancover, Canada, 1971, 178-186.

[23] Wilkinson, J. H., The Algebraic Eigenvalue Problem, Clarendon Press Oxford, 1965

[24] Wilson E. L., Farhaoomand I., Bathe K. J., *'Nonlinear dynamic analysis of complex structures,'* Earthquake Engineering and Structural Dynamics, vol. 1, 1973, 241-252

FIGURES

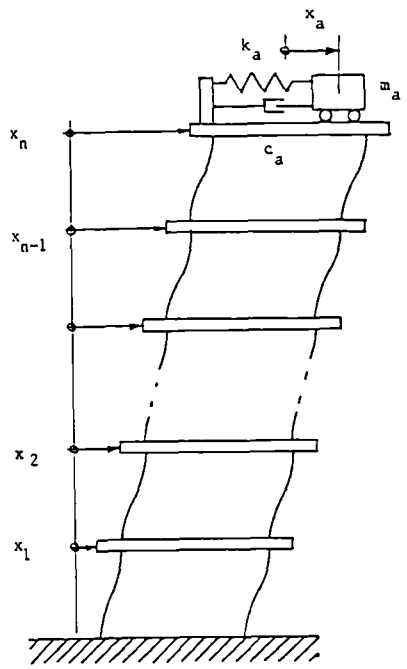

a-Structural modelling

of a roof level tuned mass damper

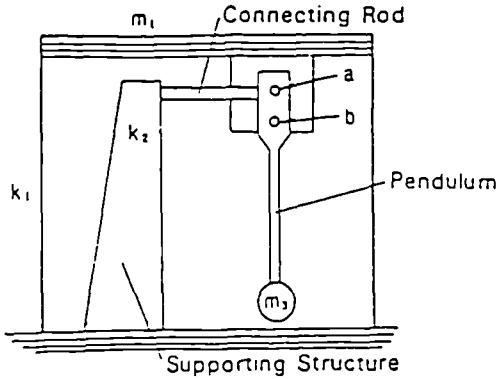

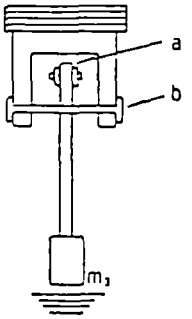

b-Pendulum dampers for storage tanks

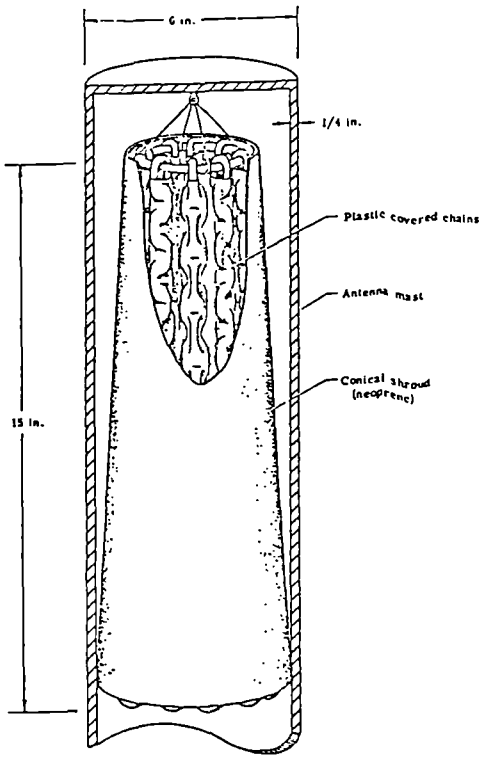

c-Hanging chain damper for antenna mast

Fig.1.1 Tuned mass dampers [60]

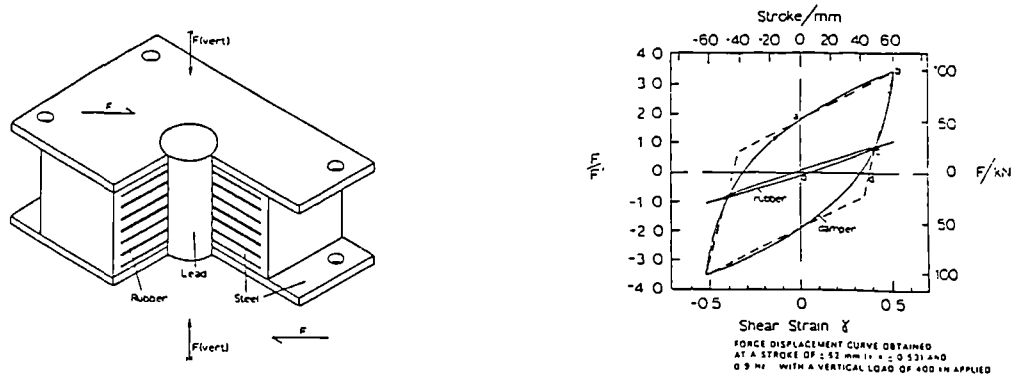

a-Lead-rubber damper [60]

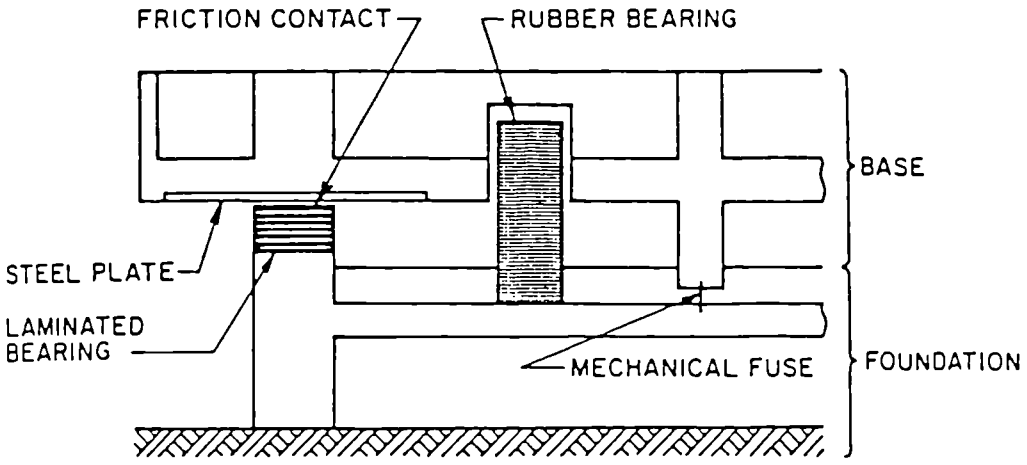

b-Typical isolator unit using rubber bearing and frictional elements [26]

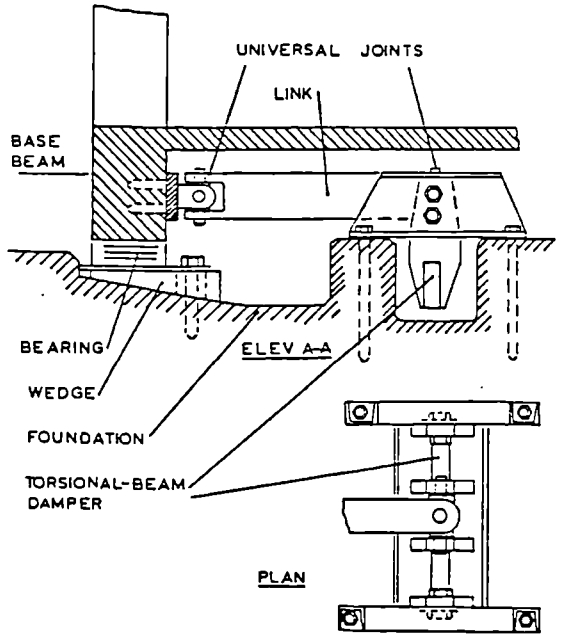

c-Typical isolator unit using a torsional-beam hysteretic dampers [98]

Fig.1.2 Base isolation systems

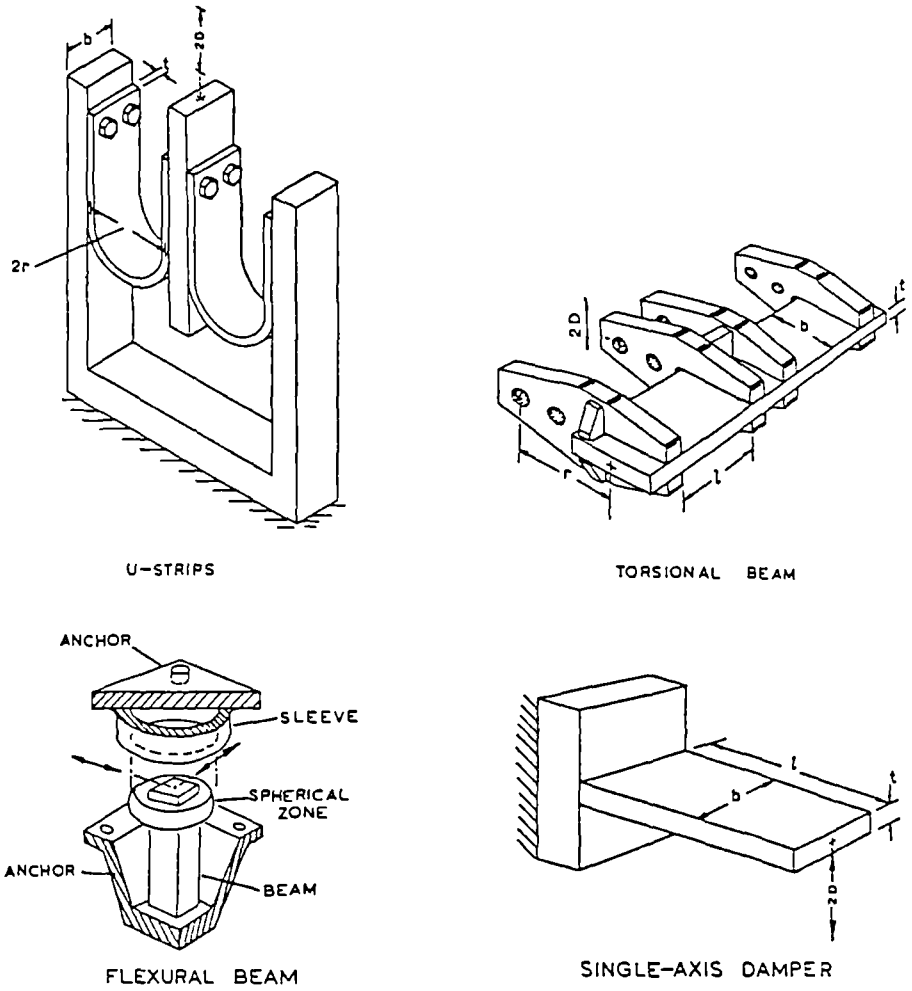

a-Typical hysteretic dampers [99]

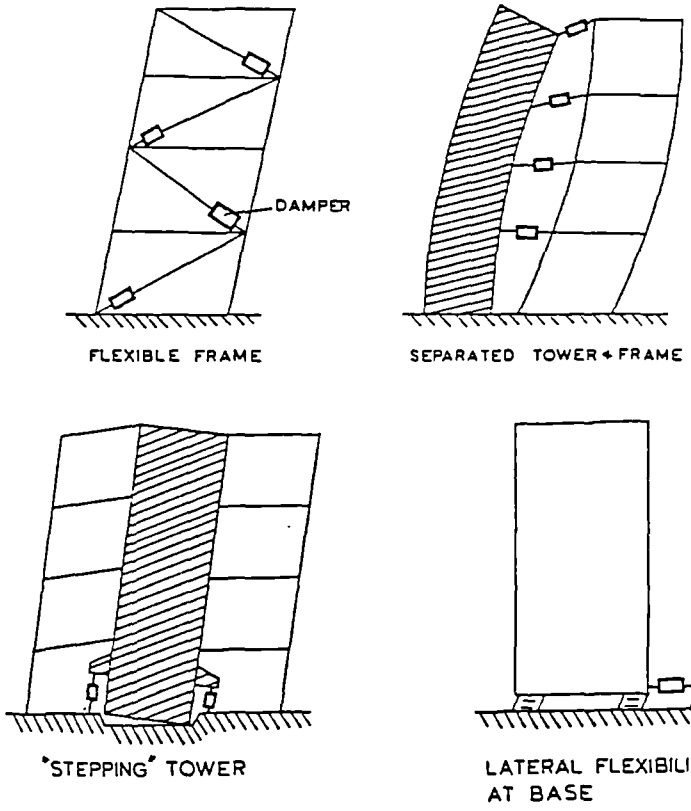

b-Structural situations in which hysteretic dampers may be used

Fig.1.3 Steel energy dampers

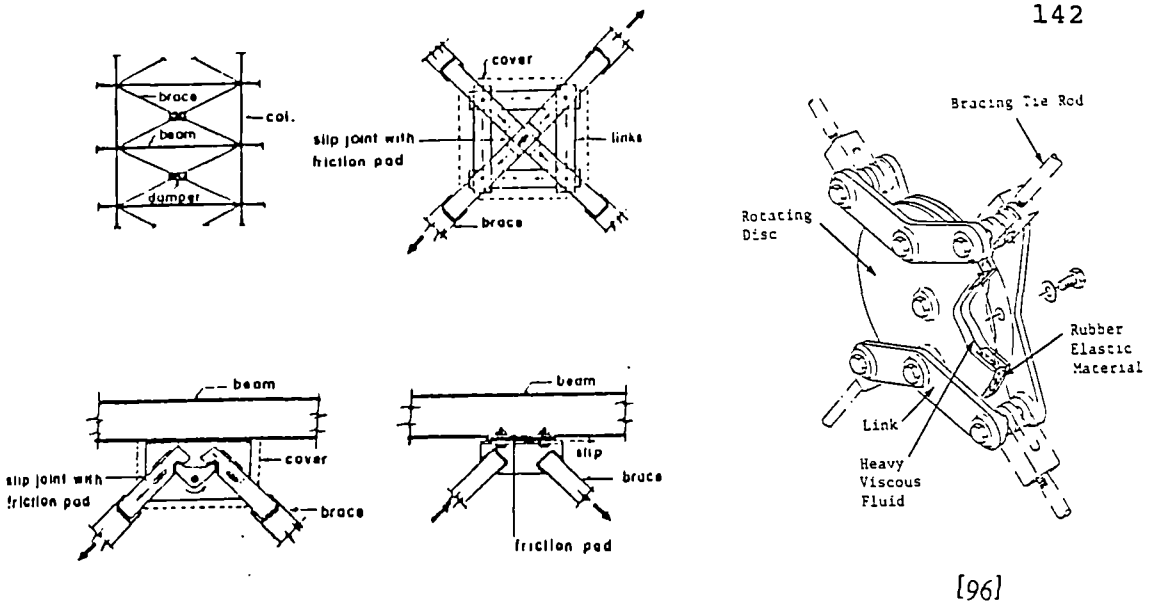

a-Friction and viscous devices for diagonal steel bracing

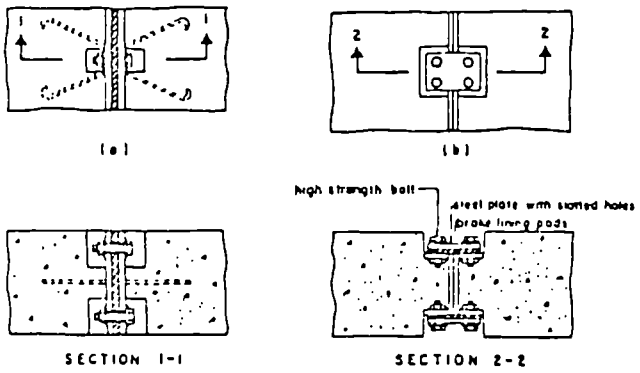

b-Typical detail of friction joints for concrete shearwall

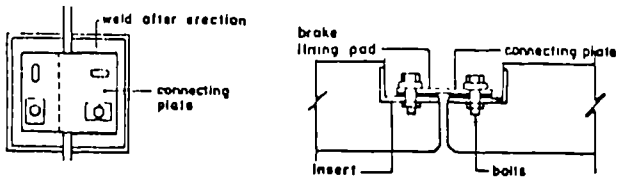

c-Typical detail of friction joint for precast concrete large-panel

Fig.1.4 Friction and viscous dampers [78]

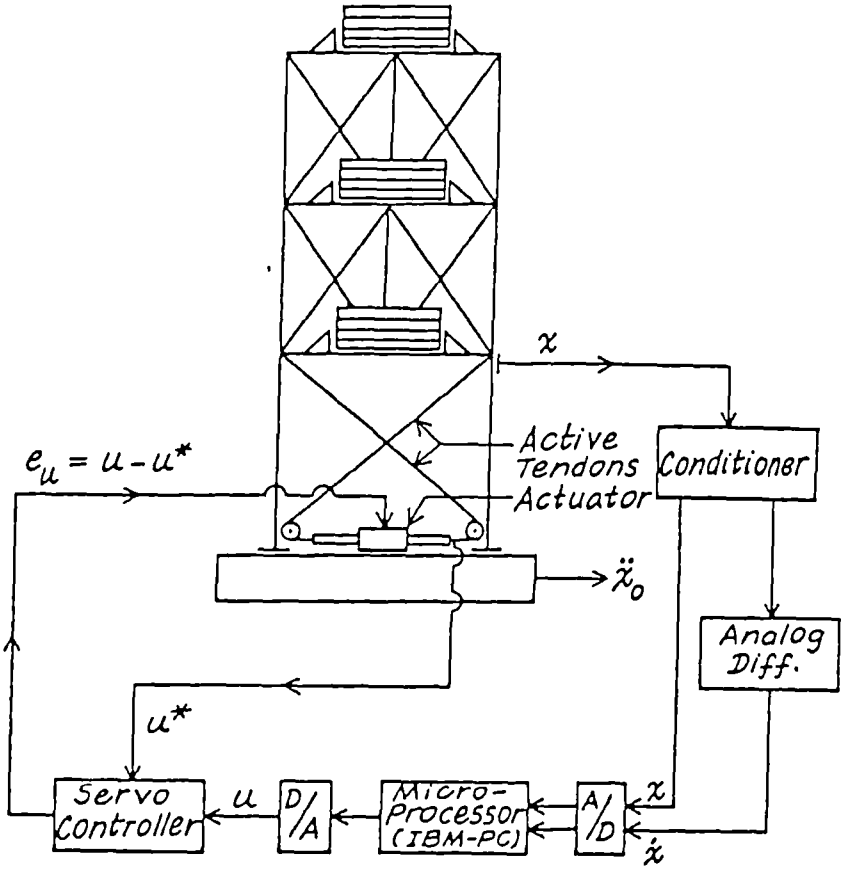

Fig.1.5 Diagram of a structural control system [22]

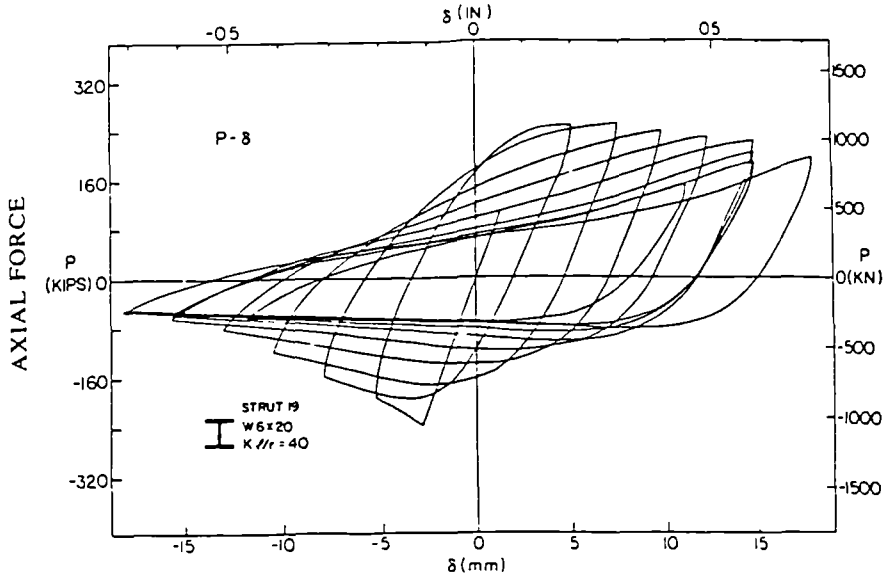

a-hysteretic loop of a steel brace under cyclic load

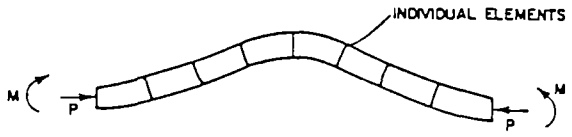

b-Finite element model

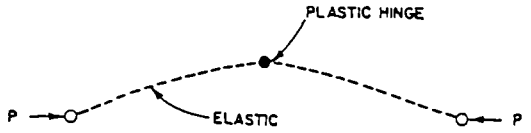

c-Physical theory brace model

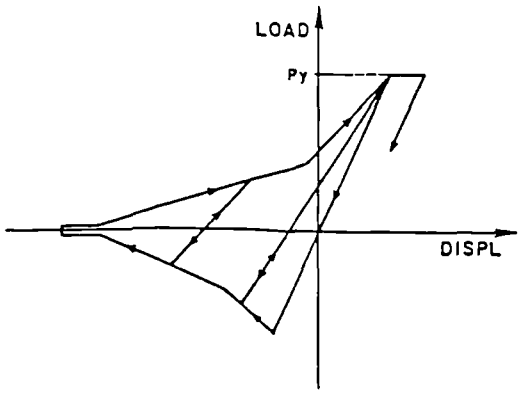

d-theoretical load-displacement model

Fig.1.6 Cyclic behaviour of struts in concentrically braced frames [47]

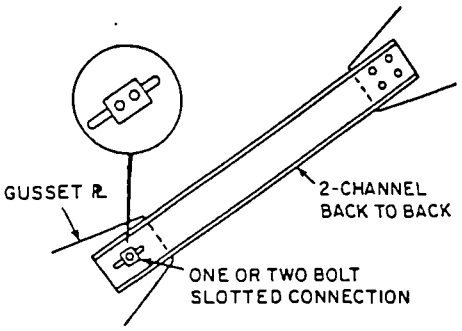

a-Typical slotted bolted connection configuration

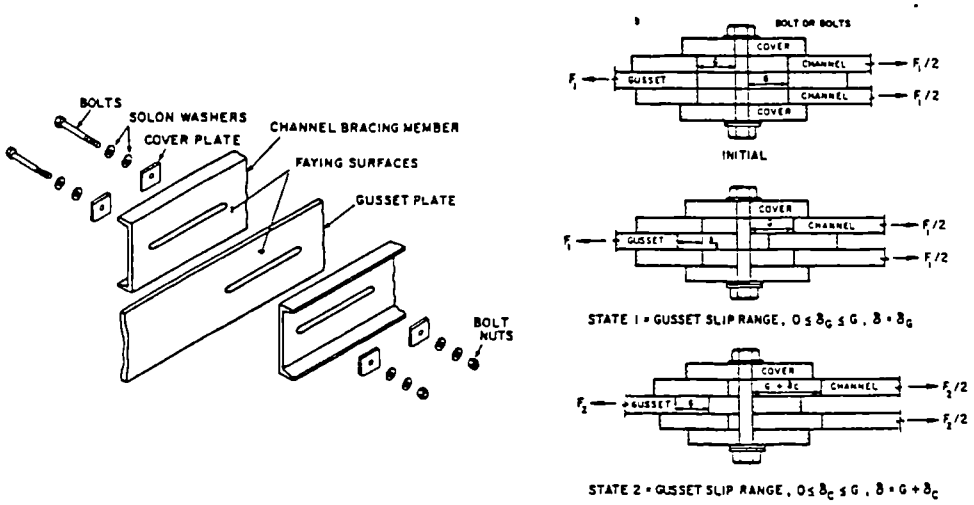

b-Slotted-bolted connection assembly

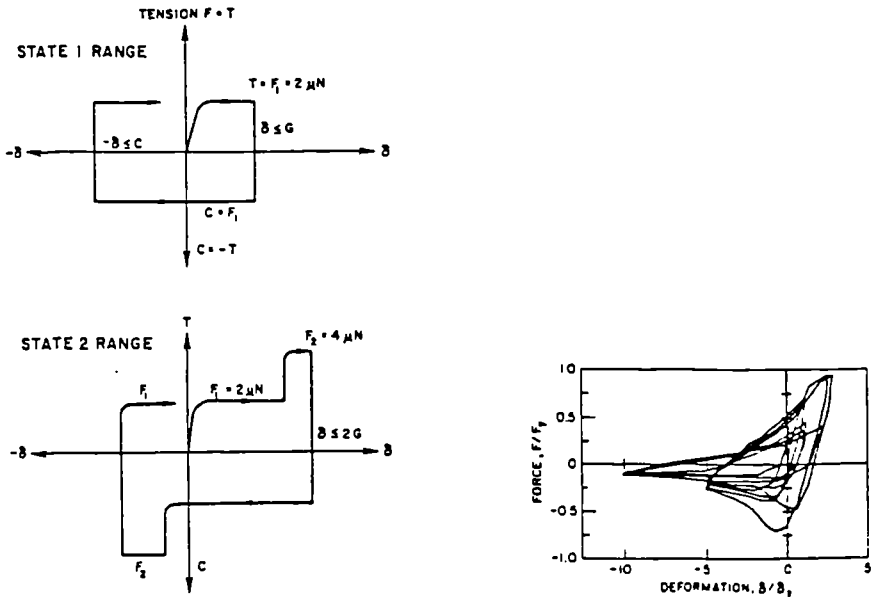

c-Idealised hysteresis loops for concentric braced frames with slotted-bolted connections

Fig.1.7 Slotted bolted connection [34]

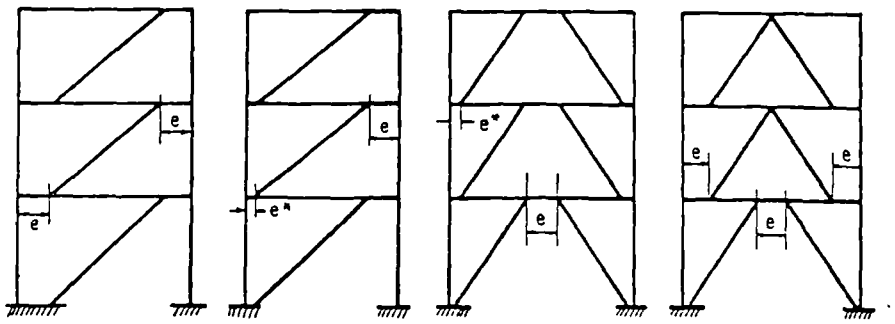

a-Recommended EBF types

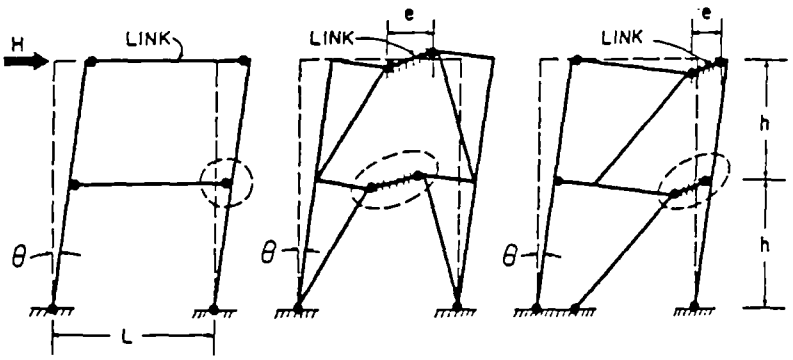

b-Plastic deformation mechanisms

Fig.1.8 Eccentrically braced frames [85]

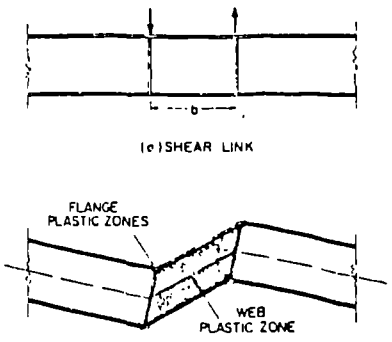

a-Deformed shape of plastic shear hinge

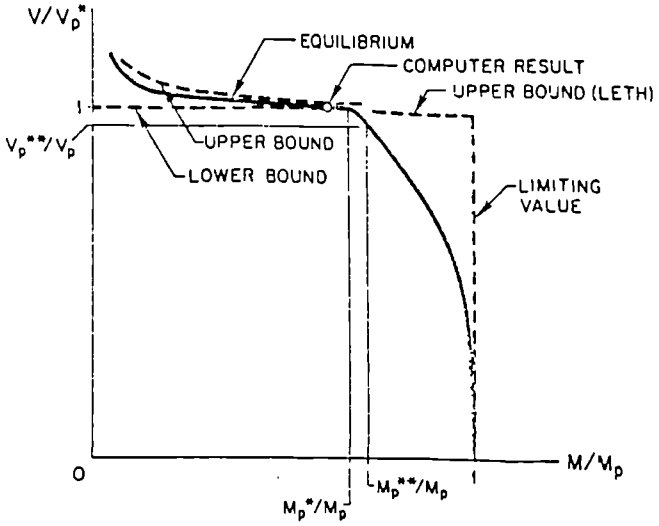

b-Shear moment interaction (W24x61)

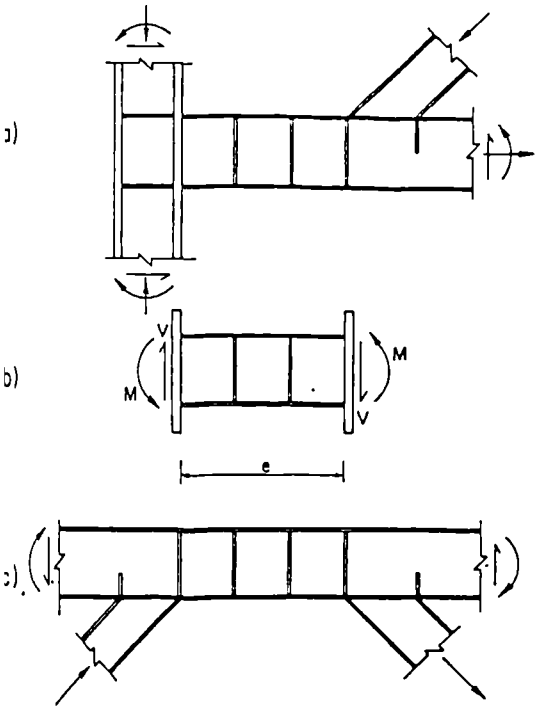

c-Active link model from two possible configurations

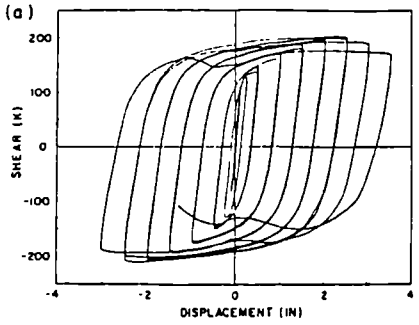

d-Force-displacement hysteretic loops

Fig.1.9 Plastic shear hinges in steel frames [65]

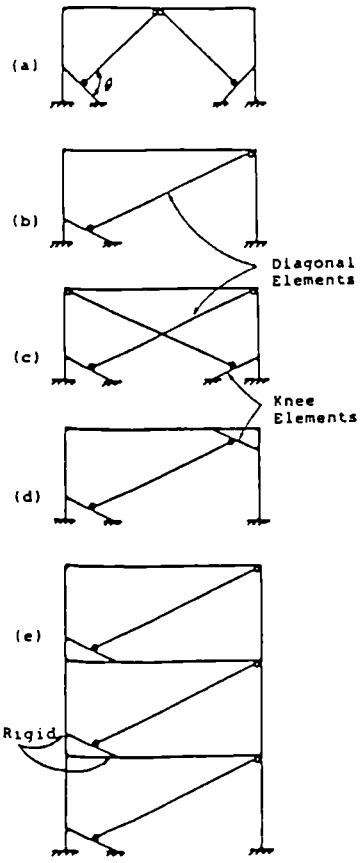

a-Typical KBF configurations

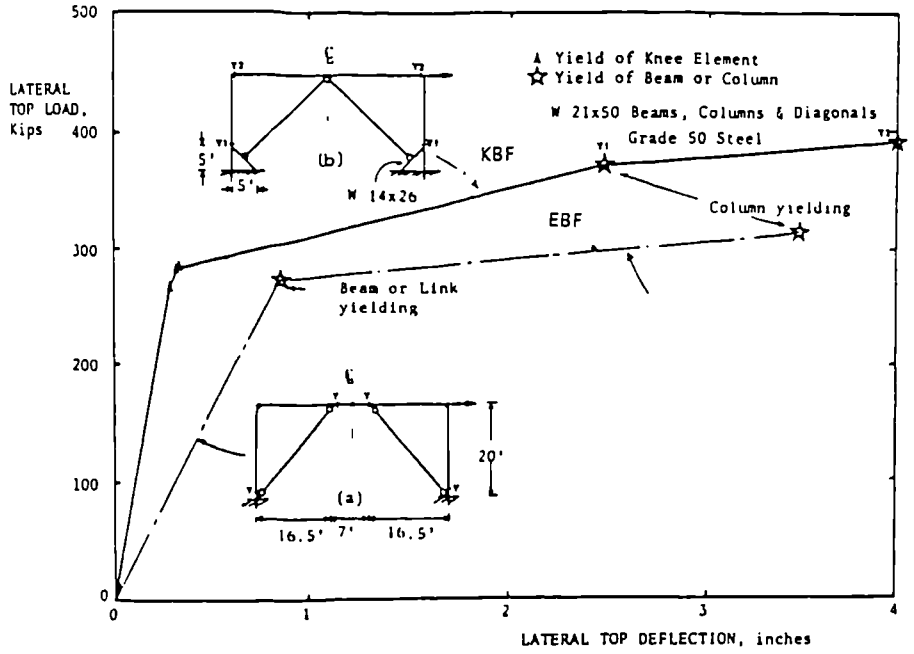

b-Load-deflection behaviour of a KBF and EBF

Fig.1.10 Knee bracing frames [3]

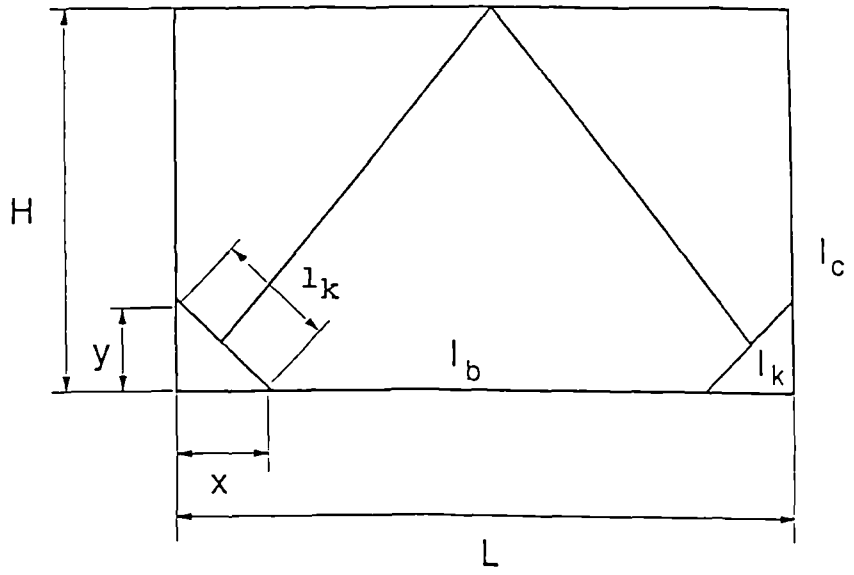

a-Single storey knee braced frame

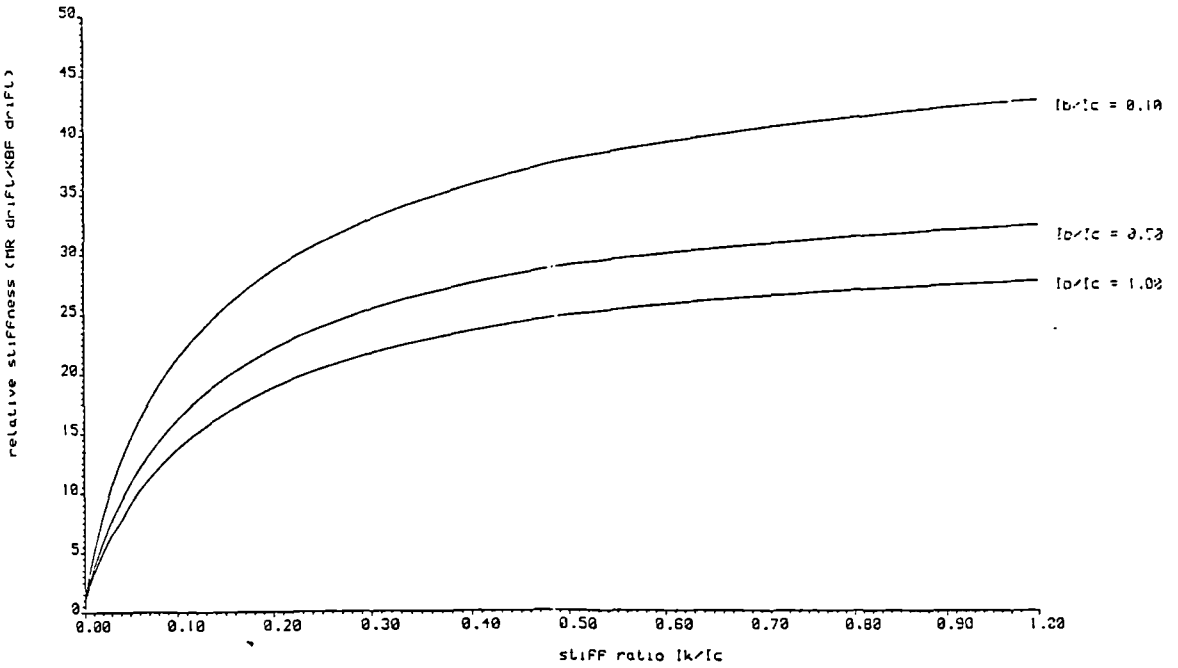

b- Relative lateral stiffness vs the knee element stiffness ratio

Fig.2.1 Effect of the knee element stiffness on the lateral stiffness of the frame

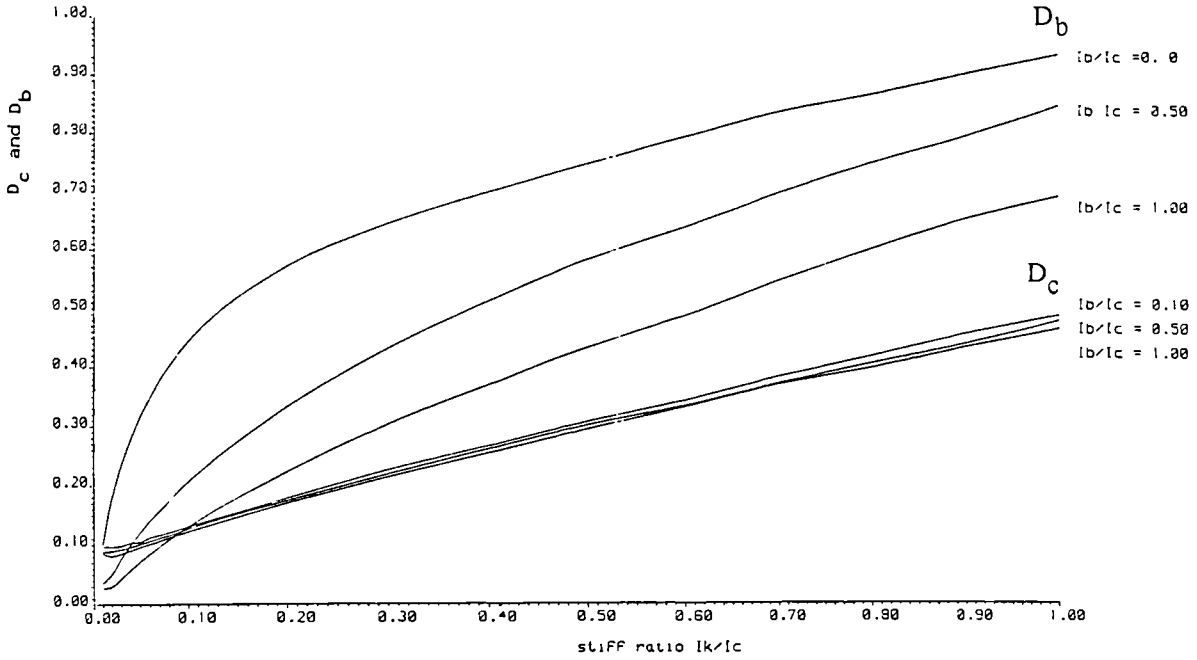

a- variation of the parameters D_c and D_b with I_k/I_c

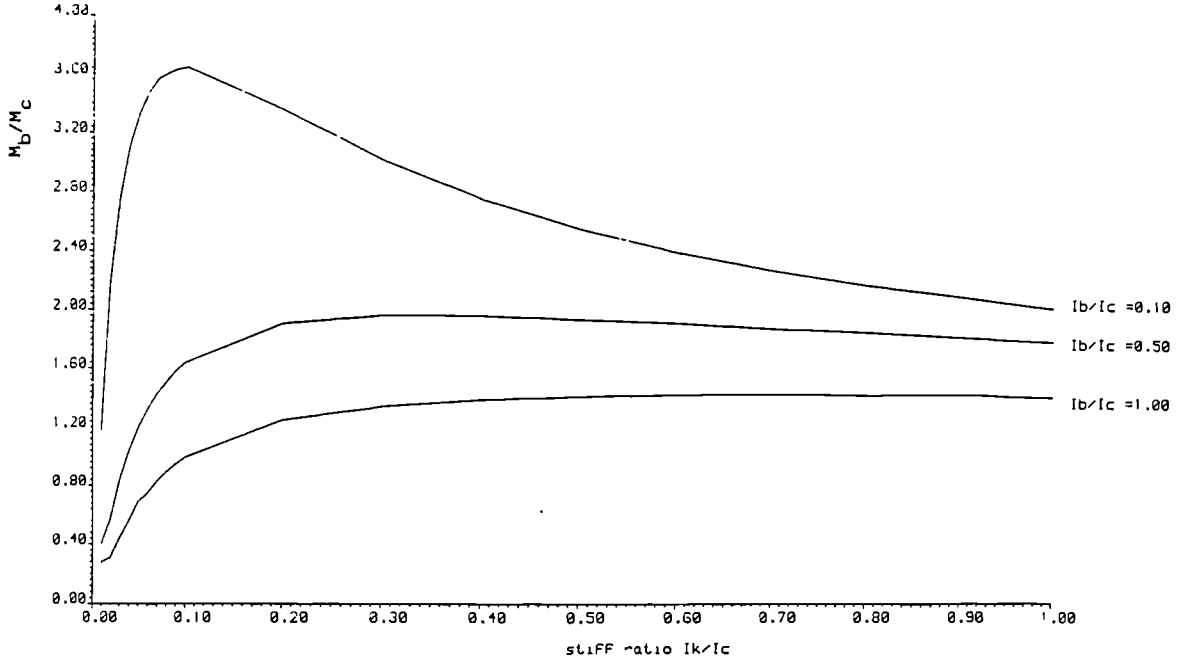

b- variation of the ratio M_b/M_c with I_k/I_c

Fig2.2 Yielding hierarchy of the knee element, beam, and column

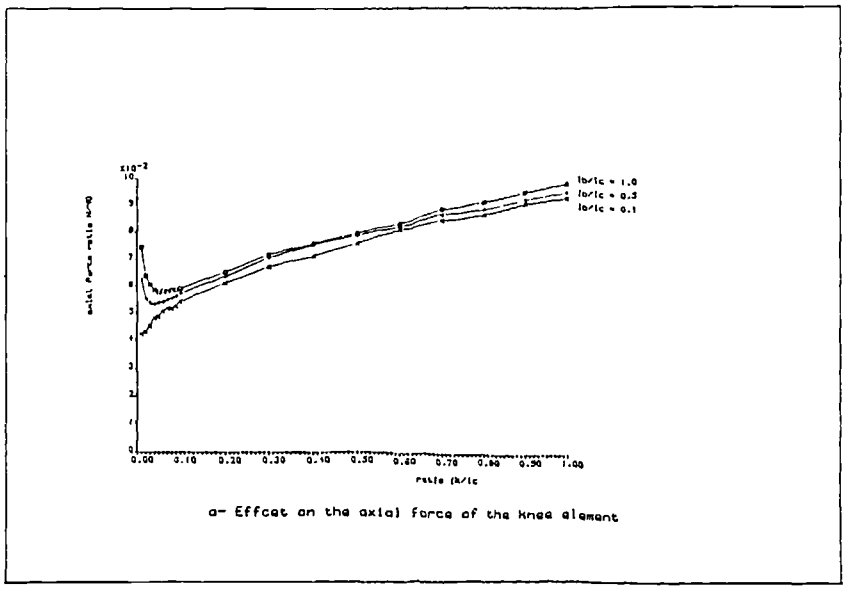

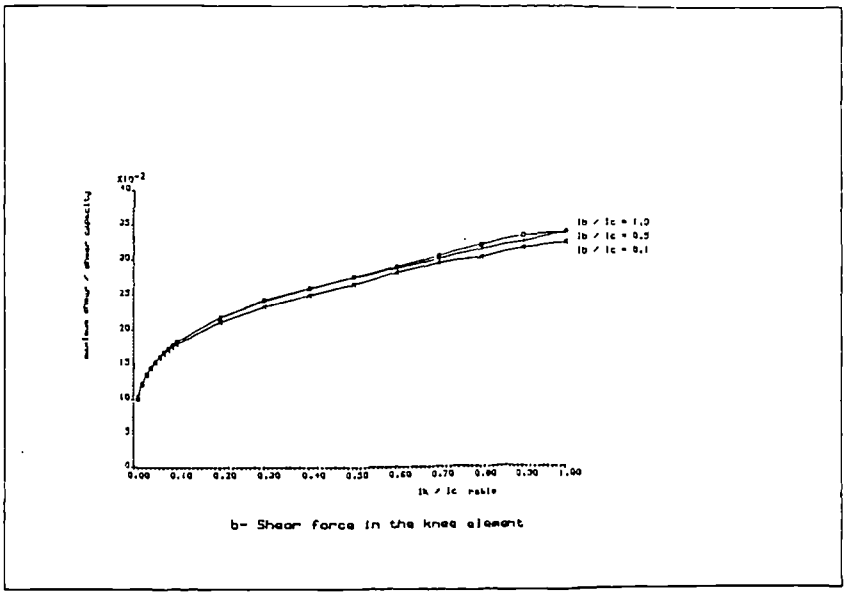

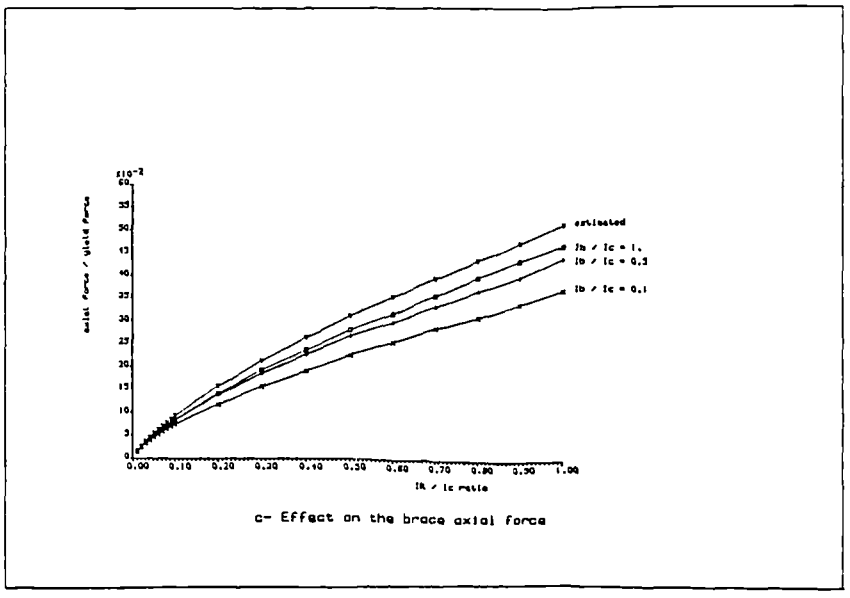

Fig.2.3 Axial and shear force variation in the knee element and the brace element

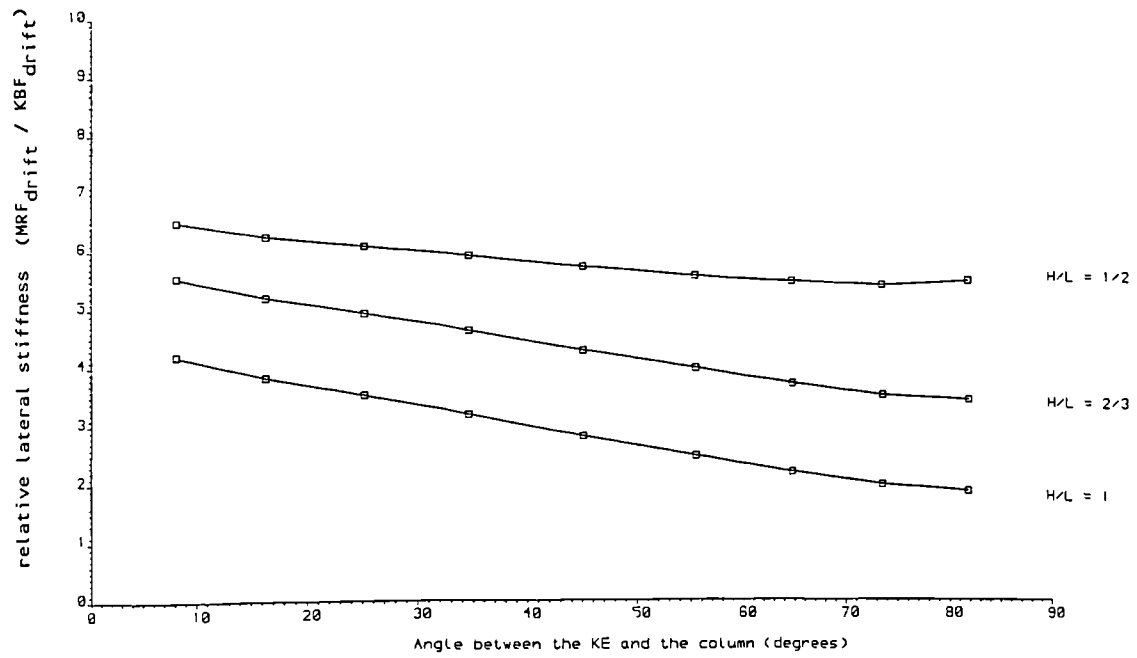

a- Effect on the lateral stiffness of the frame

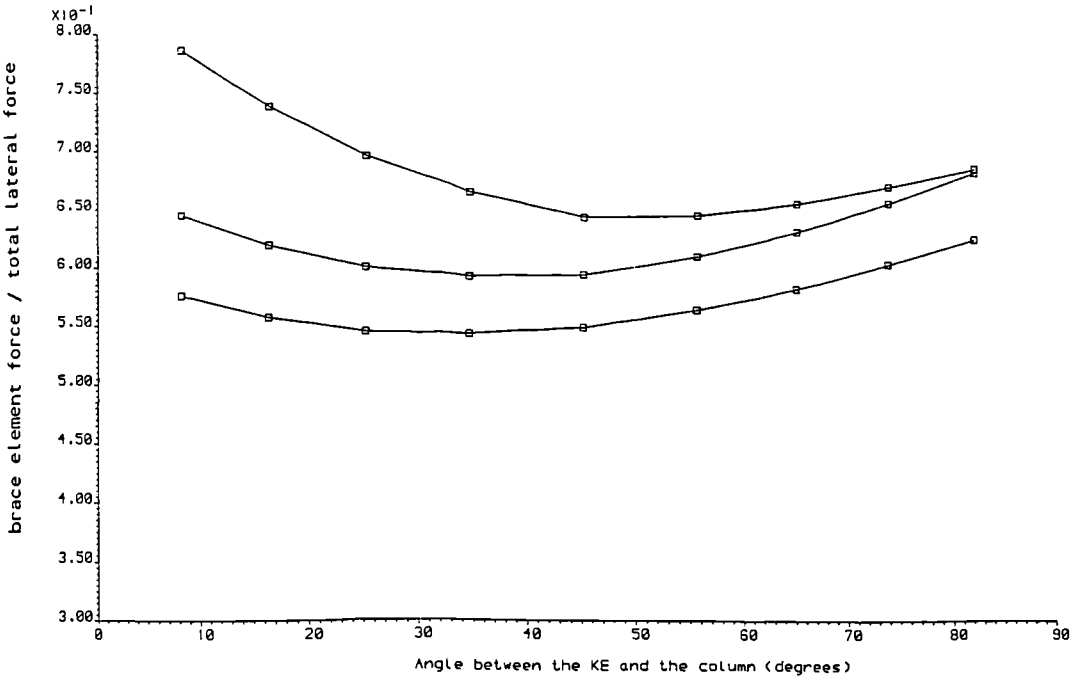

b- Effect on the brace element force

Fig.2.4 Effect of the knee element configuration

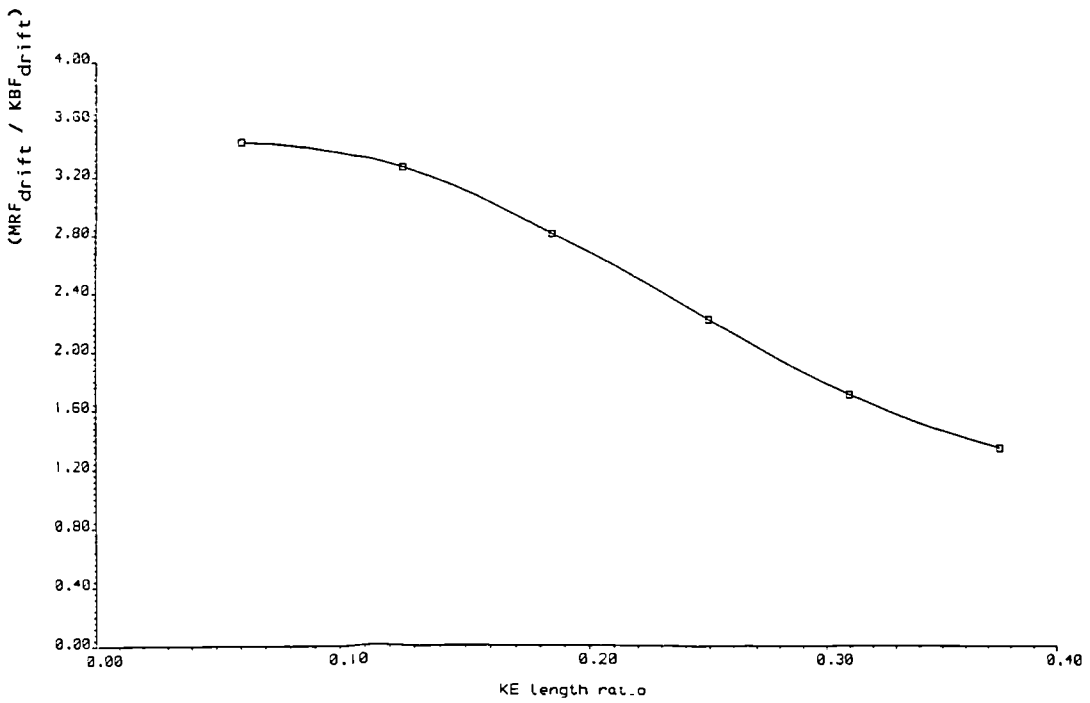

a- Effect on the lateral stiffness

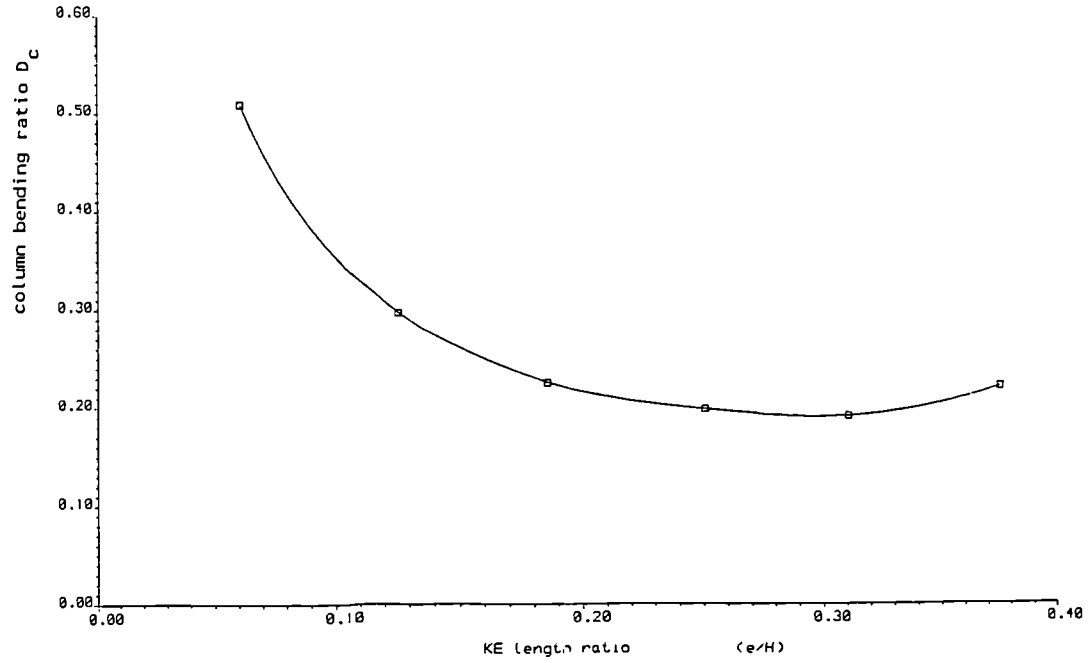

b- Effect on the parameter D_c

Fig.2.5 Effect of the knee element length

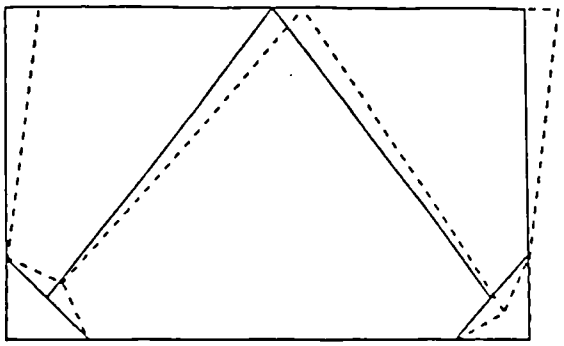

a- K-bracing configuration

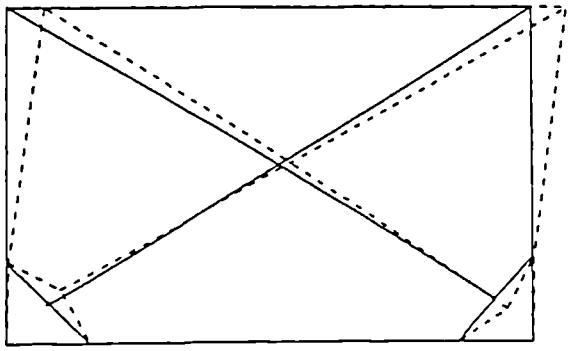

b- X-bracing configuration

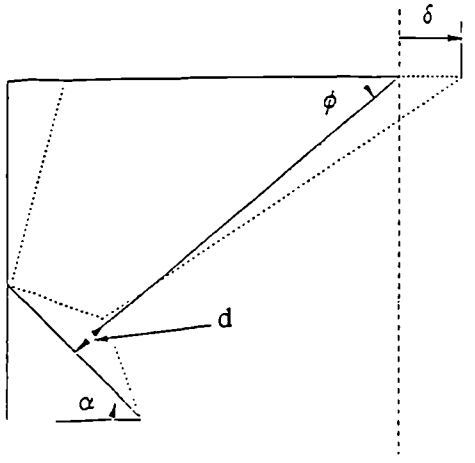

c- The geometry of plastic deformation
in the knee element excursion mechanism

Fig.2.6 X and K knee braced configurations

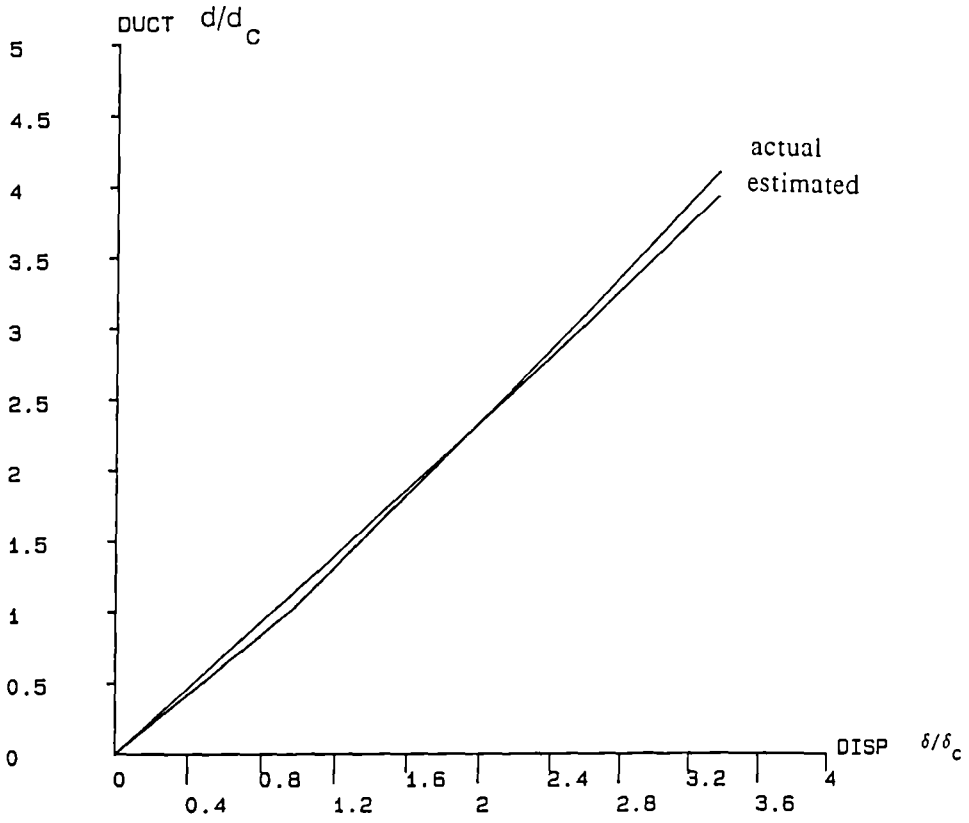

Fig.2.7 Knee element estimated and actual ductility

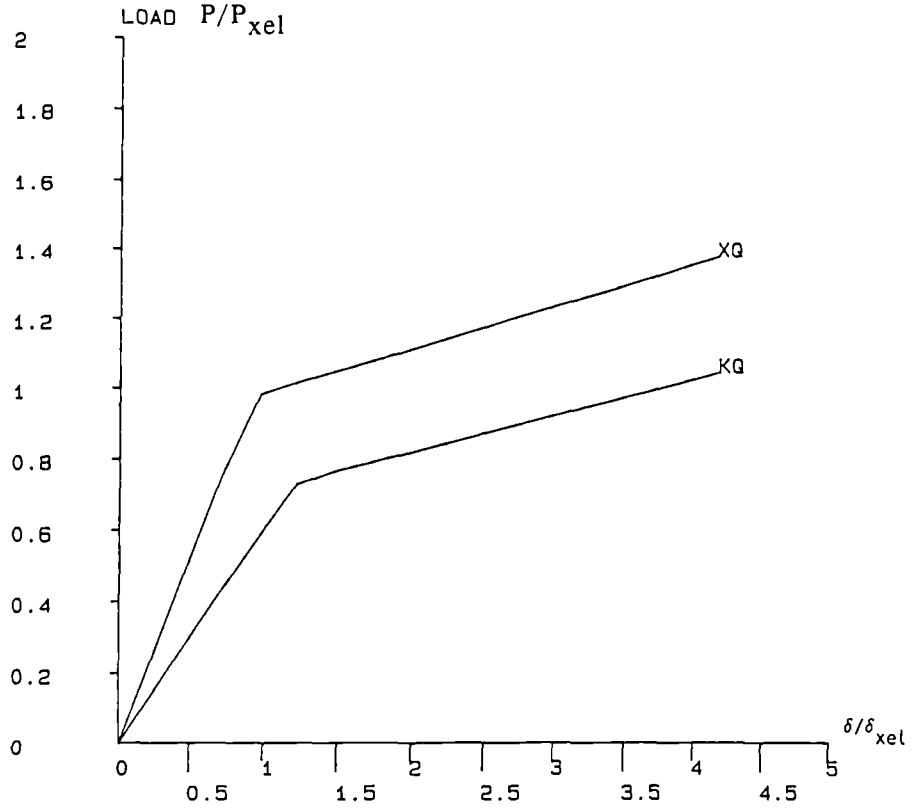

a- lateral load vs storey drift of the X and K configuration

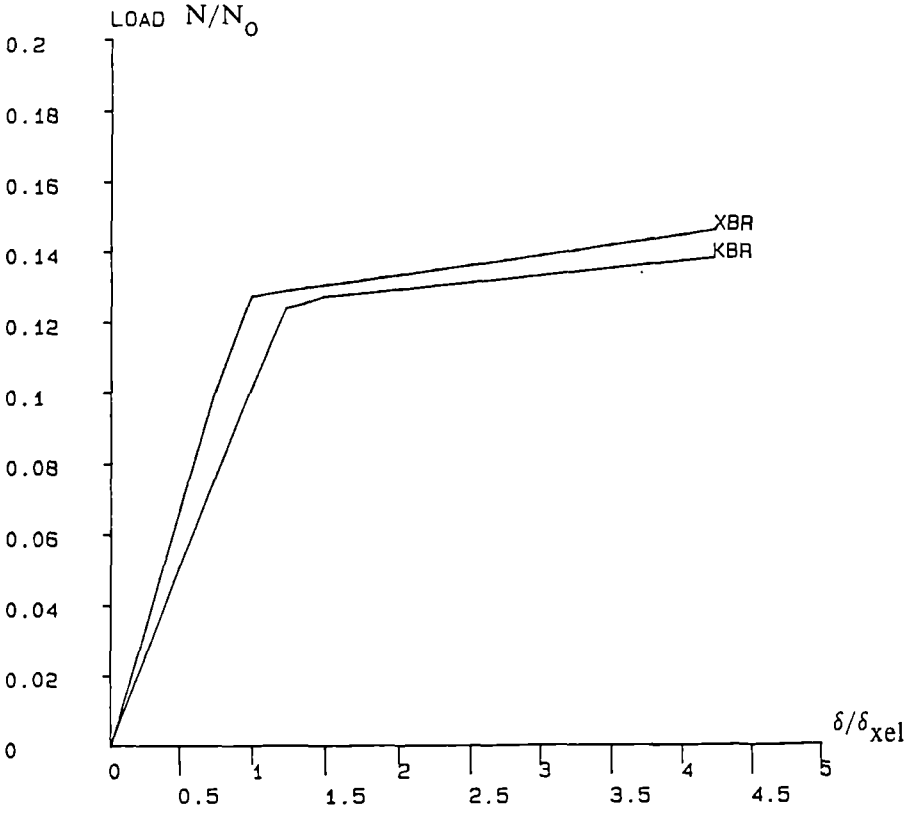

b- axial force of the brace element vs the stroey drift

Fig.2.8 Load-deflection of X and K-bracing configuration

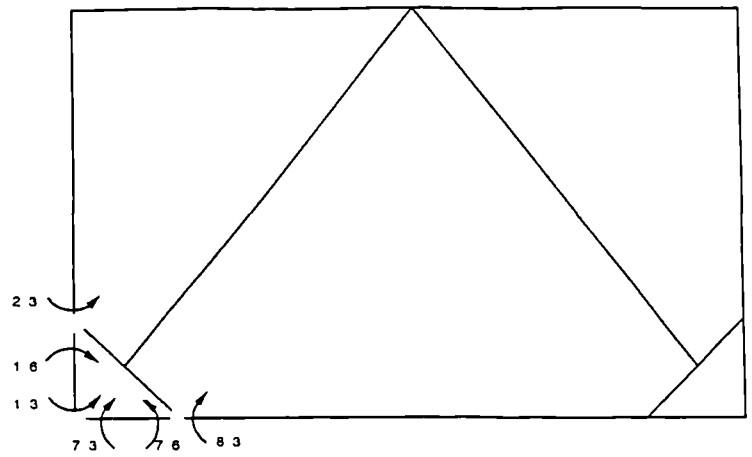

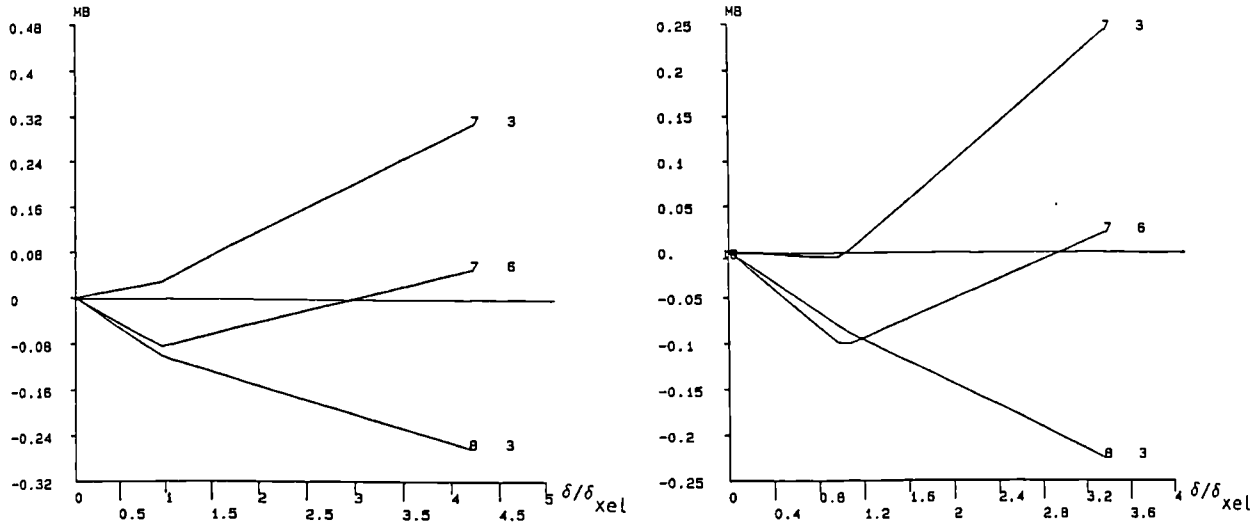

a- Bending moment in the beams of the X and K configuration

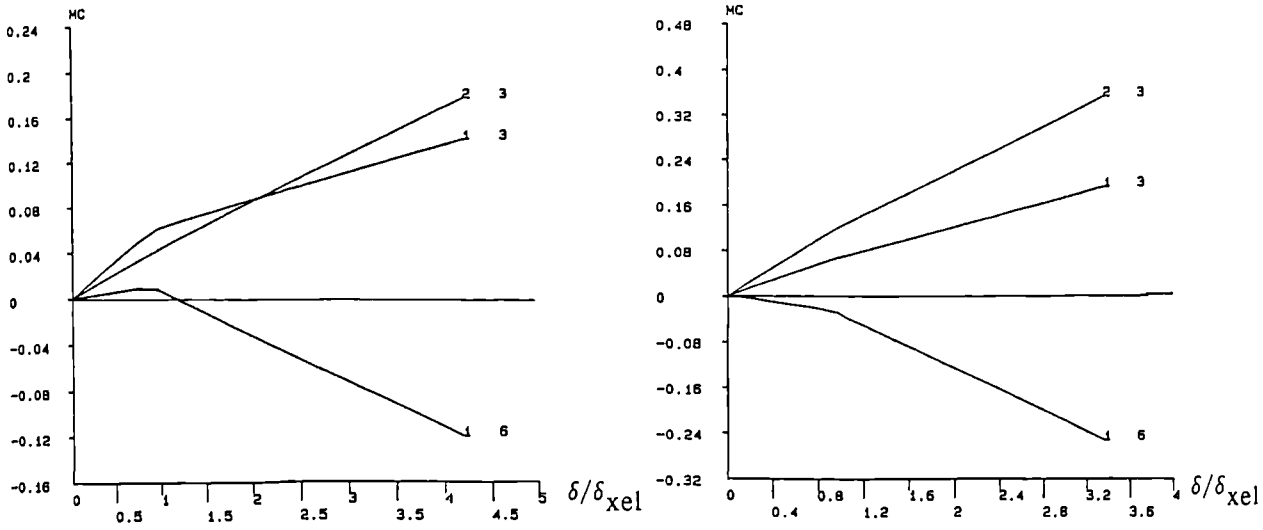

b- Bending moment in the columns of the X and Y configuration

Fig.2.9 Bending moment distribution in the elastic and post-elastic phase

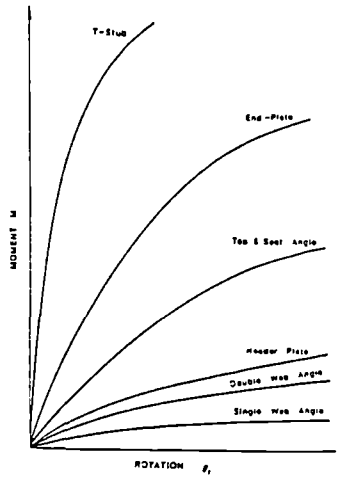

a- connection moment-rotation curves from ref. [63]

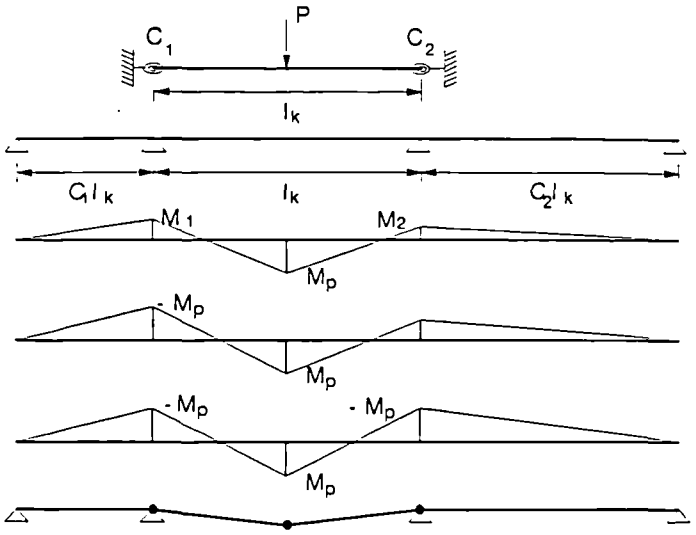

b- Partially fixed knee element and the equivalent continuous beam

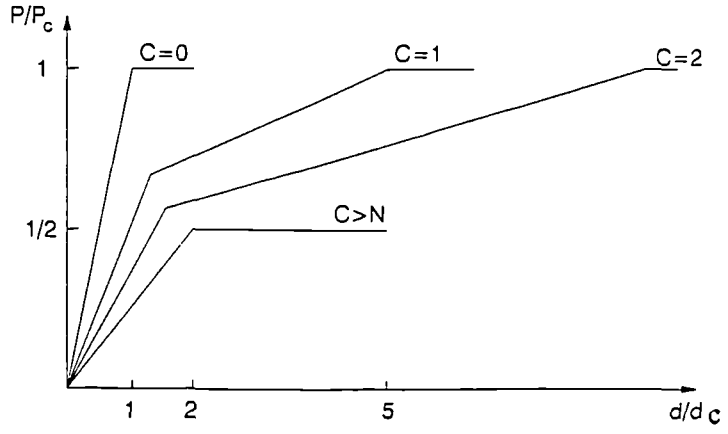

c- Load-deformation relations for $C_1=C_2=C$

Fig.2.10 Partial end-fixity of the knee element

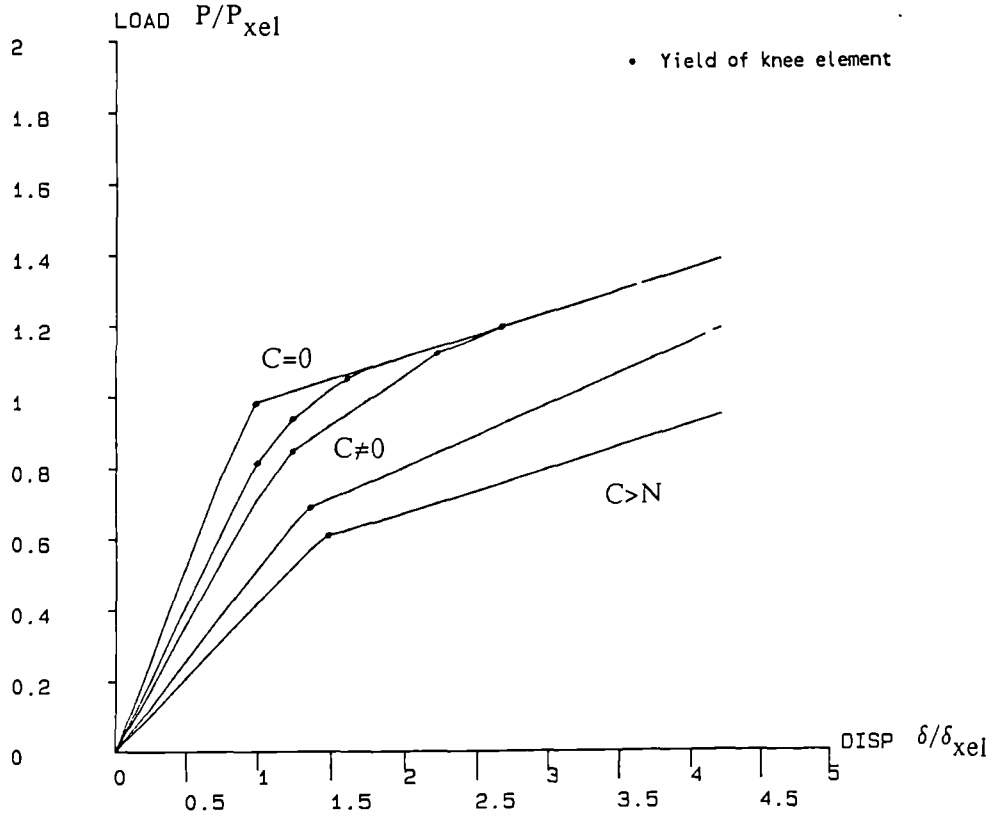

Fig.2.11 Load-deformation relations for partially fixed knee element.

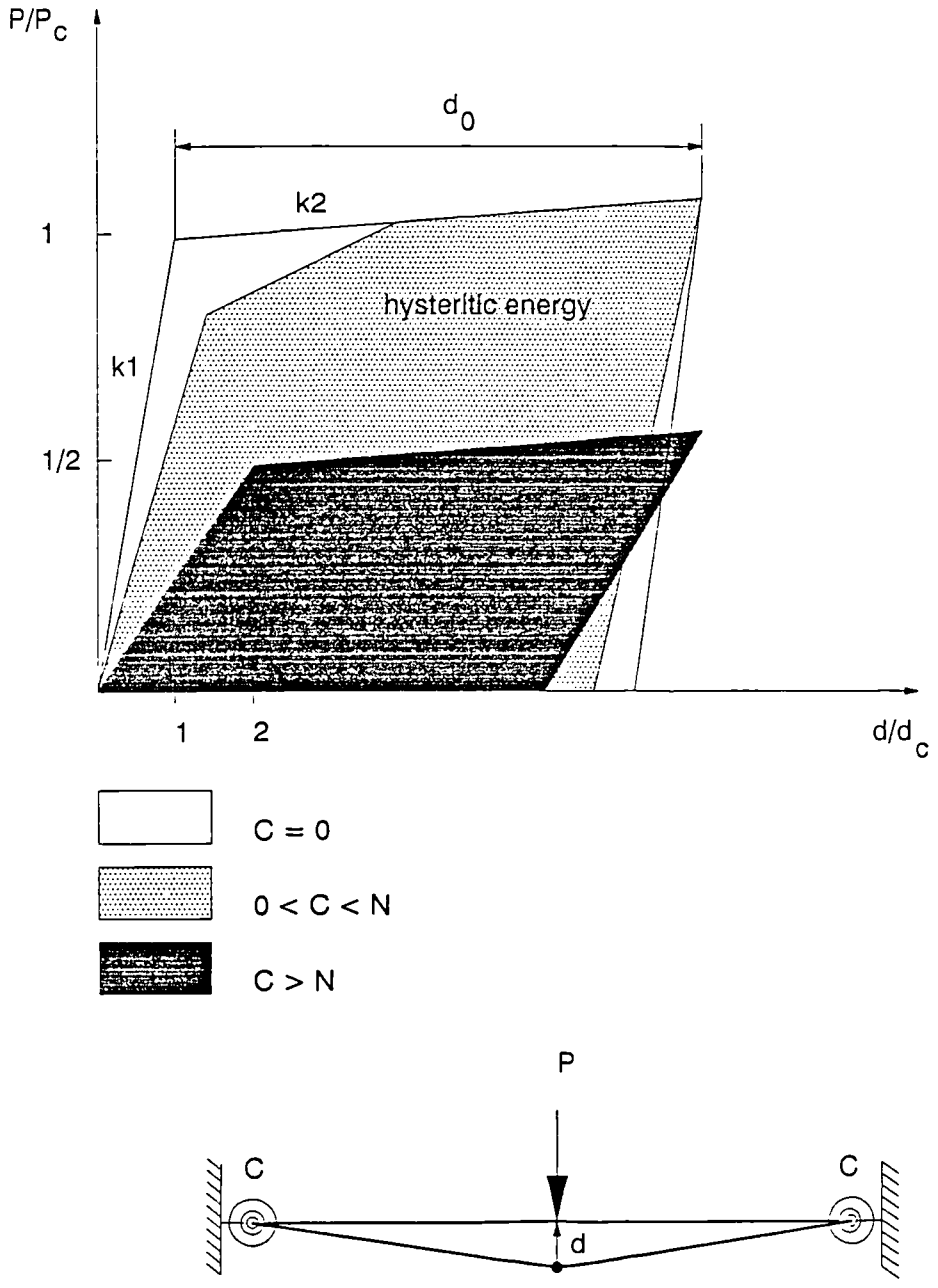

Fig.2.12 Effect of the end-fixity on the hysteresis loops

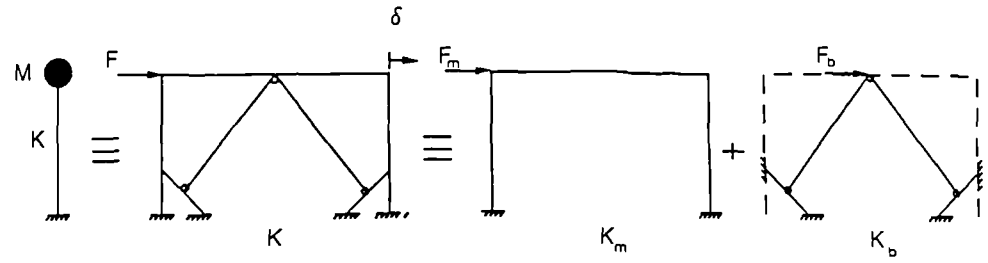

a- lateral stiffness of a KBF

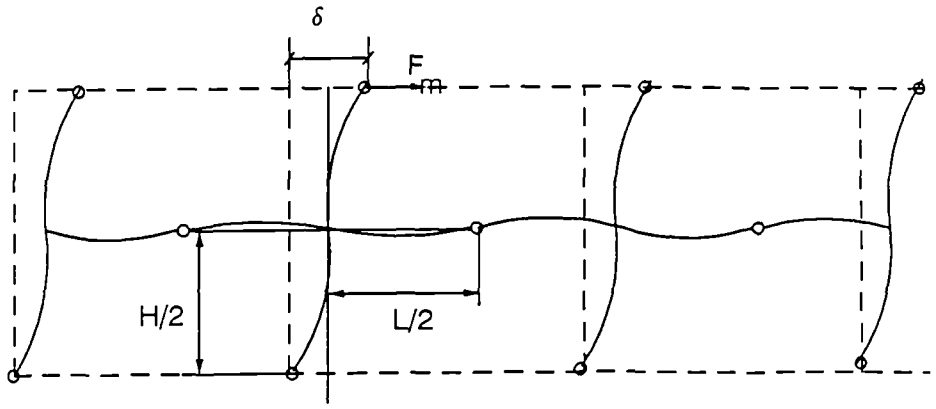

b- deflected shape of an interior column of a MRF

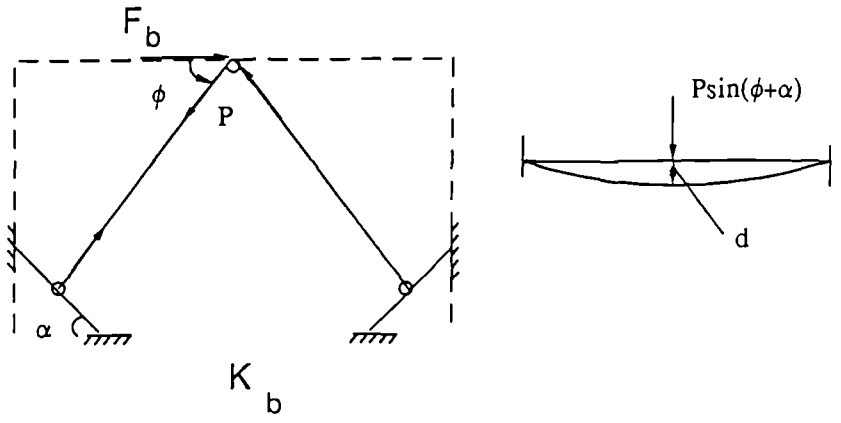

c- lateral stiffnee of a KBS

Fig.3.1 Equivalent lateral stiffness of a KBF

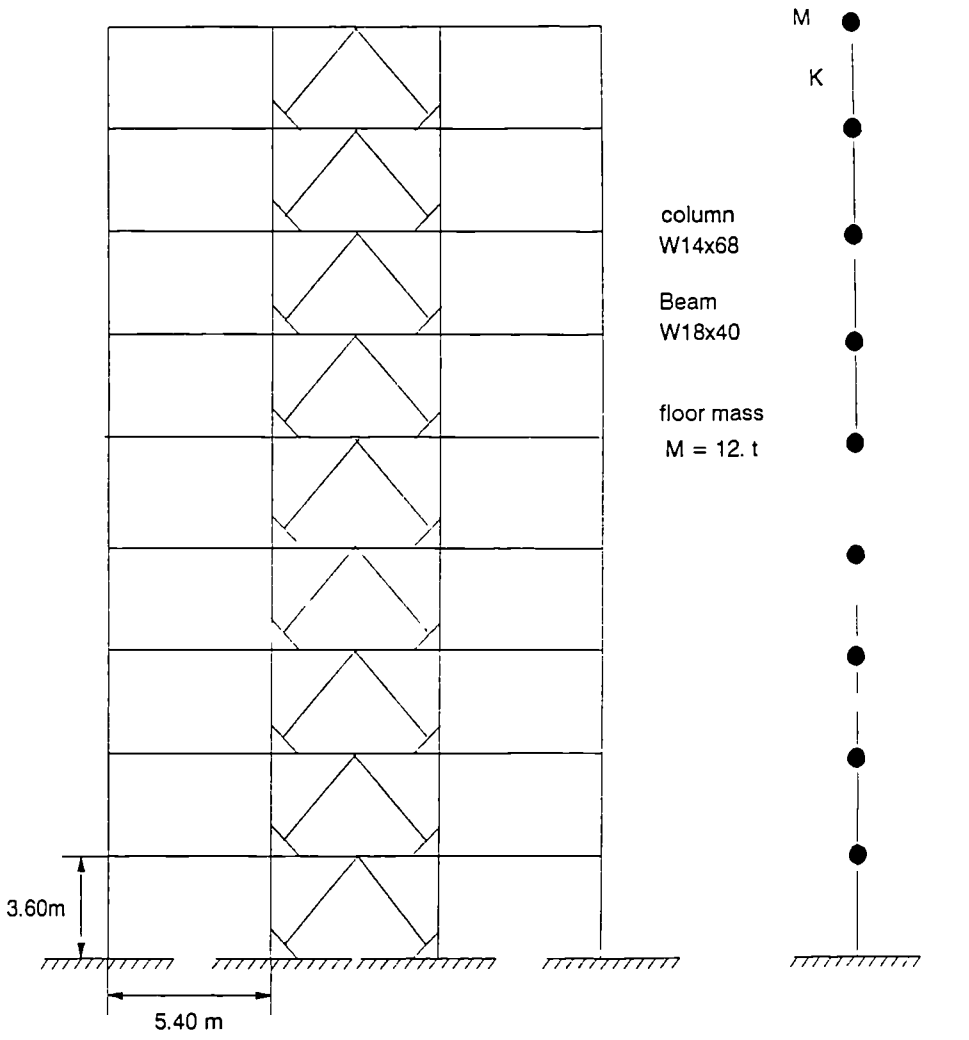

Fig.3.2 Prototype structure and the equivalent one dimensional model

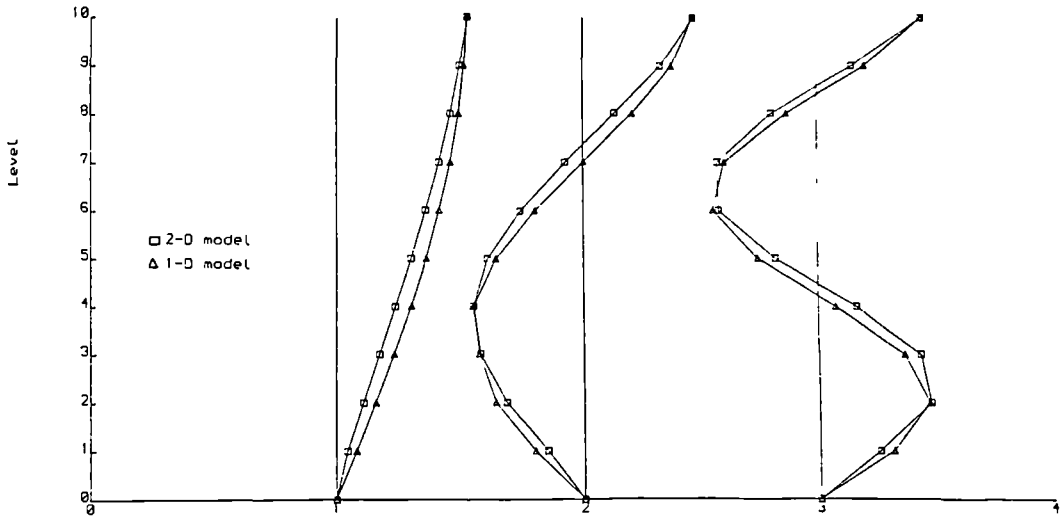

$f_{D1} = 1.56$ $f_{D2} = 1.48$ $f_{D1} = 4.66$ $f_{D2} = 4.59$ $f_{D1} = 7.65$ $f_{D1} = 8.26$

a- Mode shpes of the 2-D and equivalent 1-D model

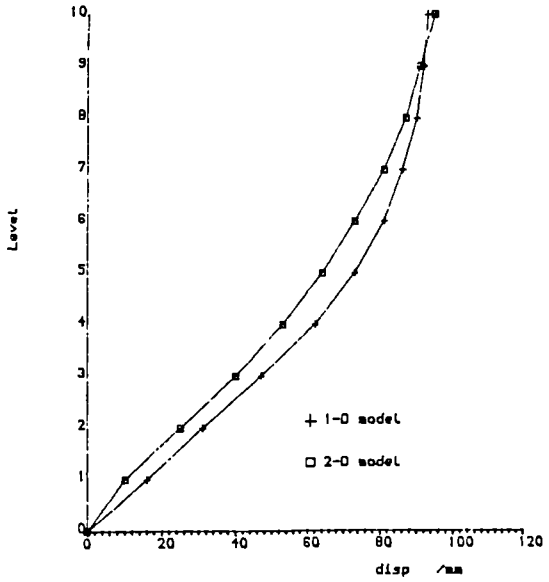

b- Maximum lateral displacement

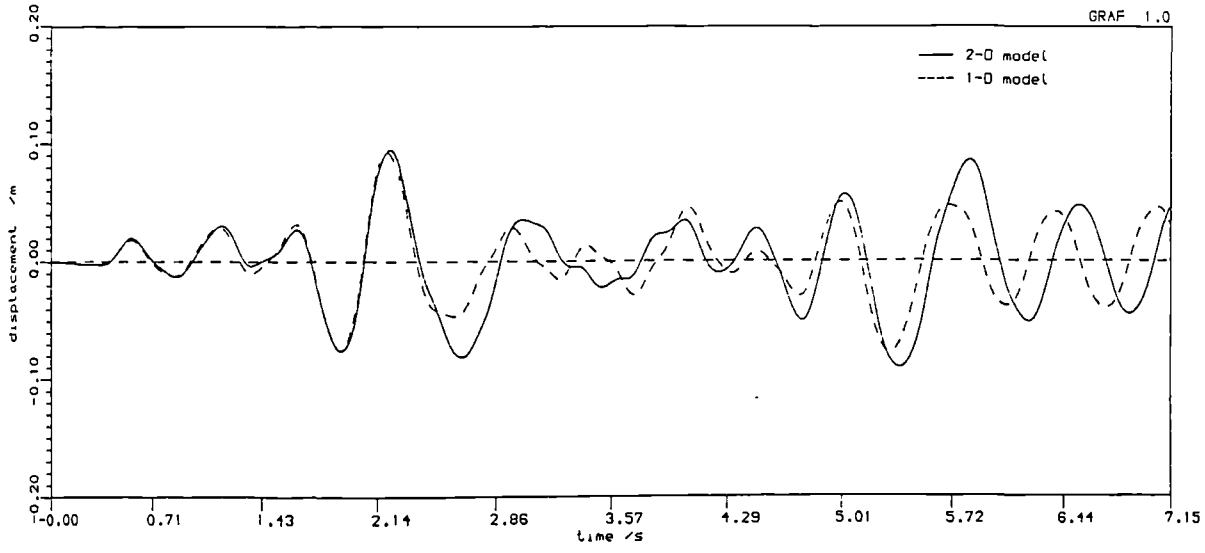

c- Top floor lateral displacement time history (1-D and 2-D)

Fig3.3 Response of the simplified model (1-D) to earthquake loading.

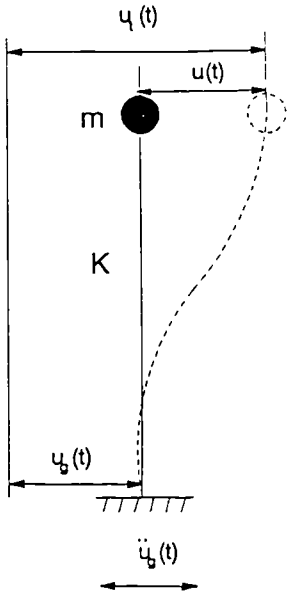

a- SDOF system subjected to a ground motion

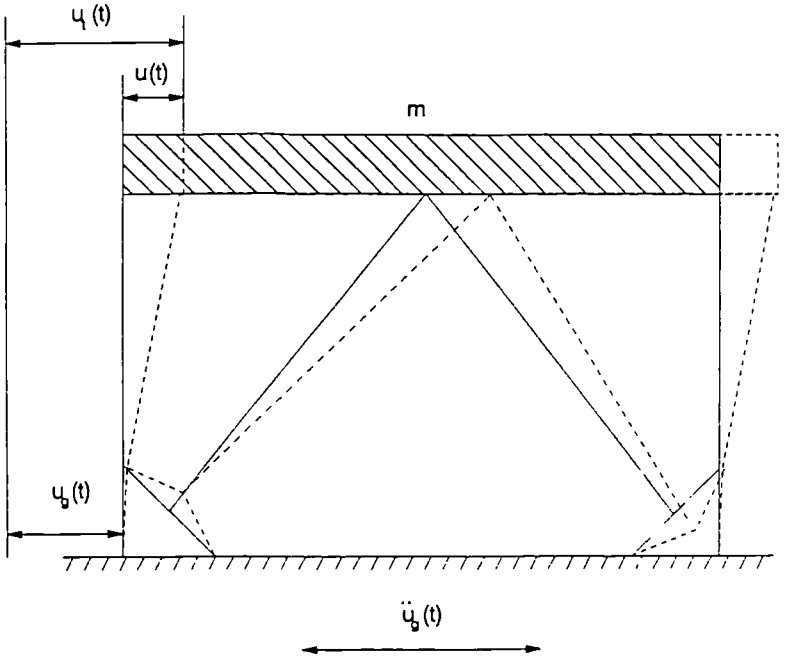

b- Single cell KBF subjected to an earthquake motion

Fig.3.4 Single storey knee braced frame and the equivalent mathematical model of a SDOF system subjected to a ground motion

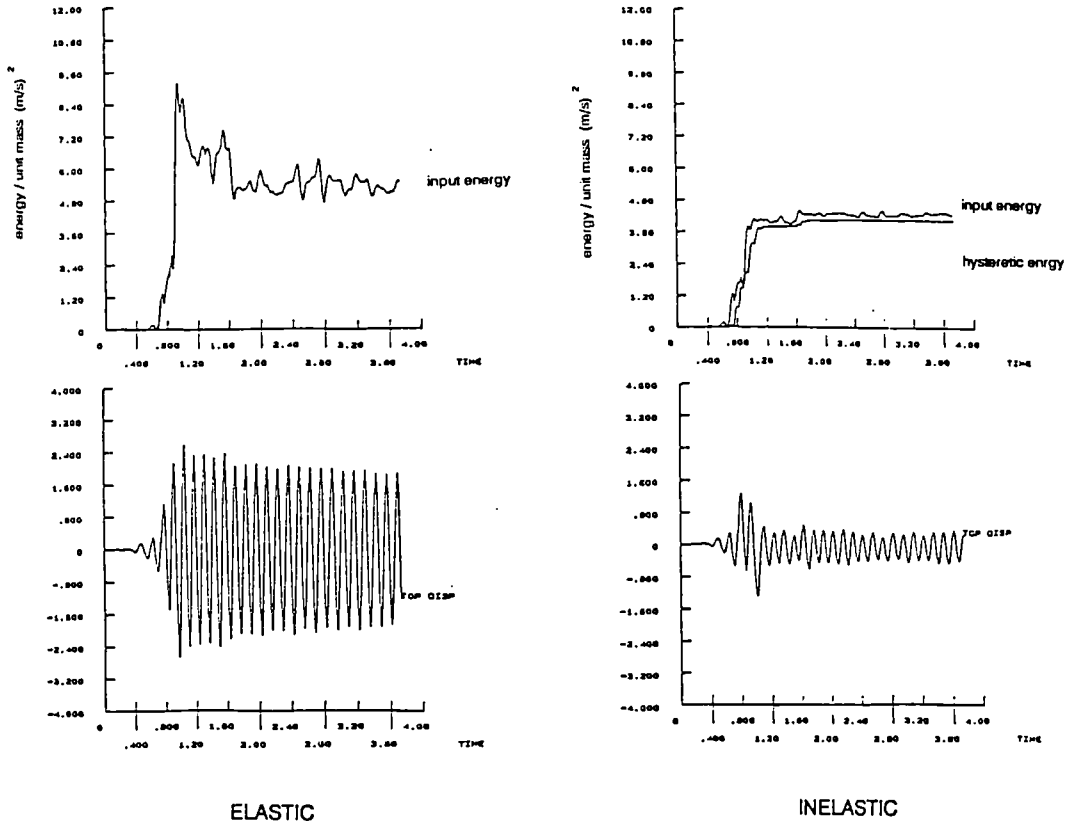

Response of the frame to Parkfield

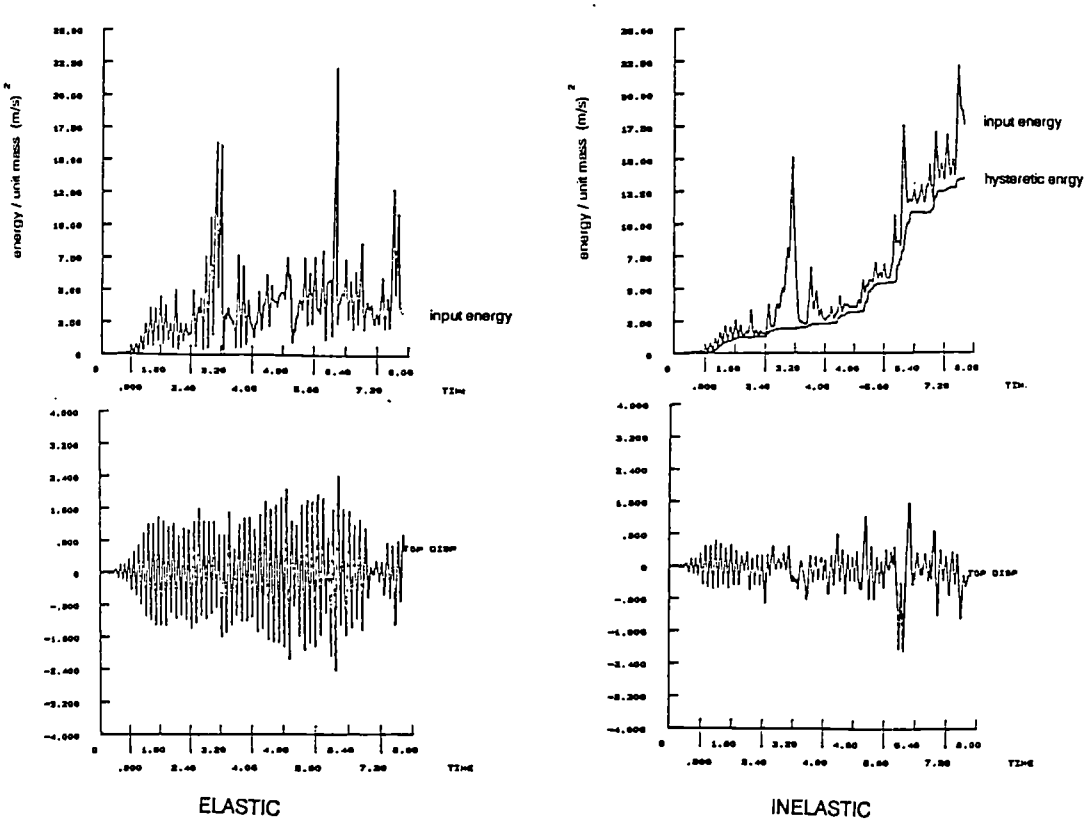

Response of the frame San Fernando

Fig.3.5 Energy time histories of the elastic and inelatic frames

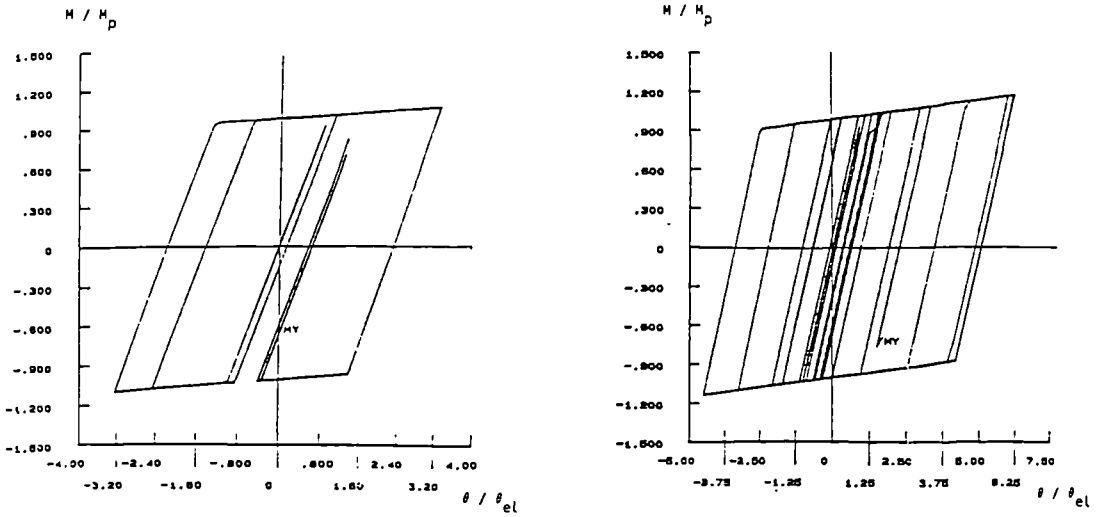

a- Hysteretic loops

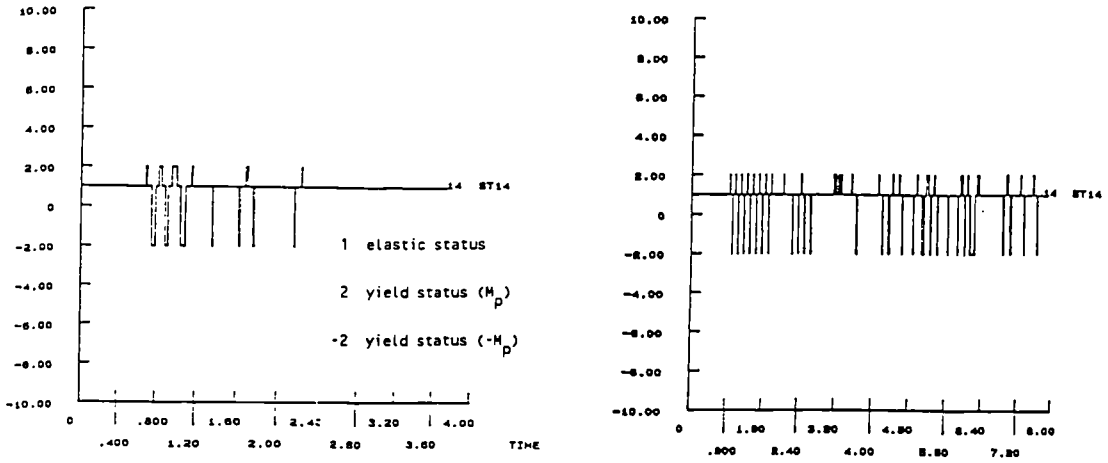

b- Yield sequence

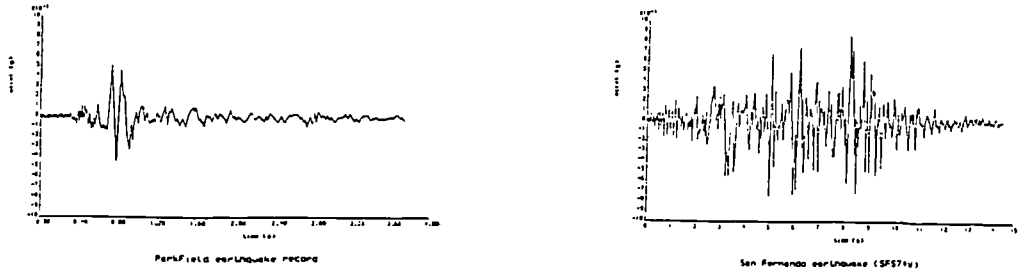

c- Earthquake inputs

Fig.3.6 Knee elements hysteretic loops and yield excursion time histories

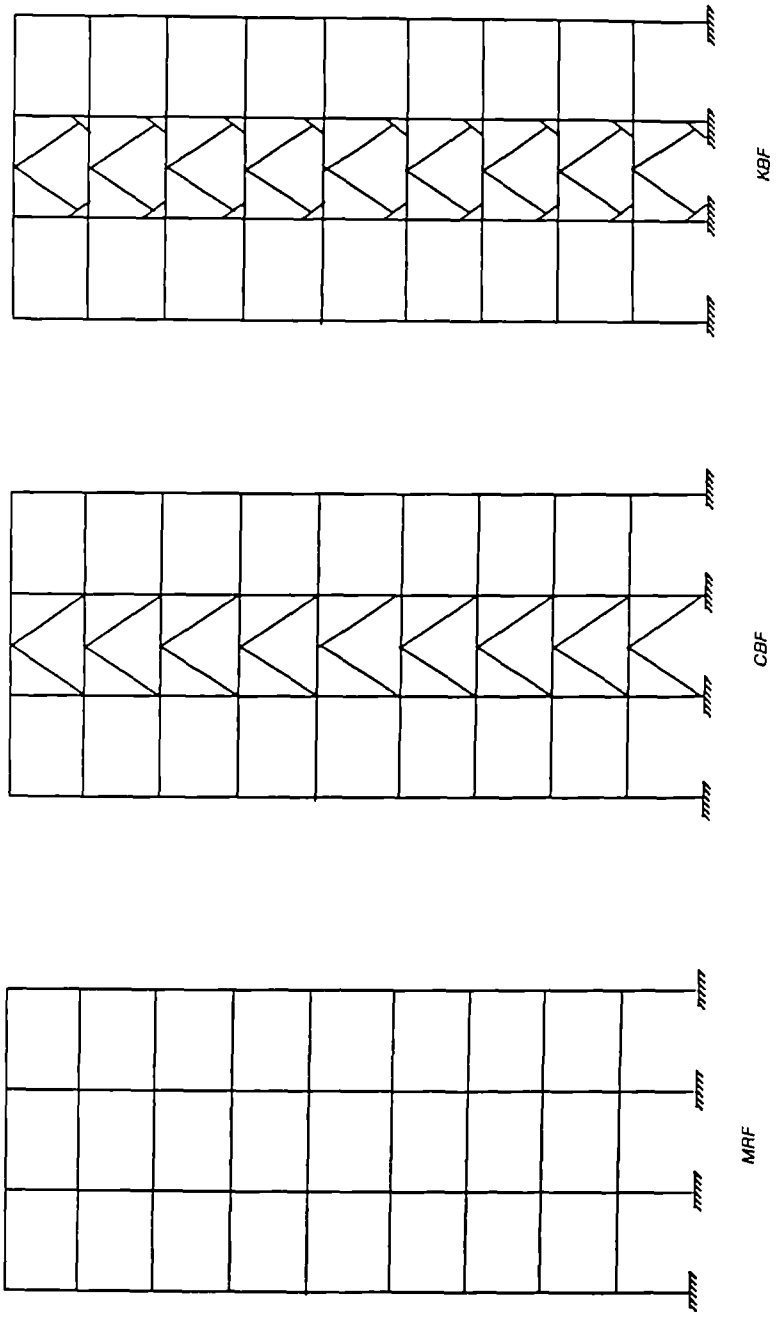

Fig.3.7 The three types of framing studied

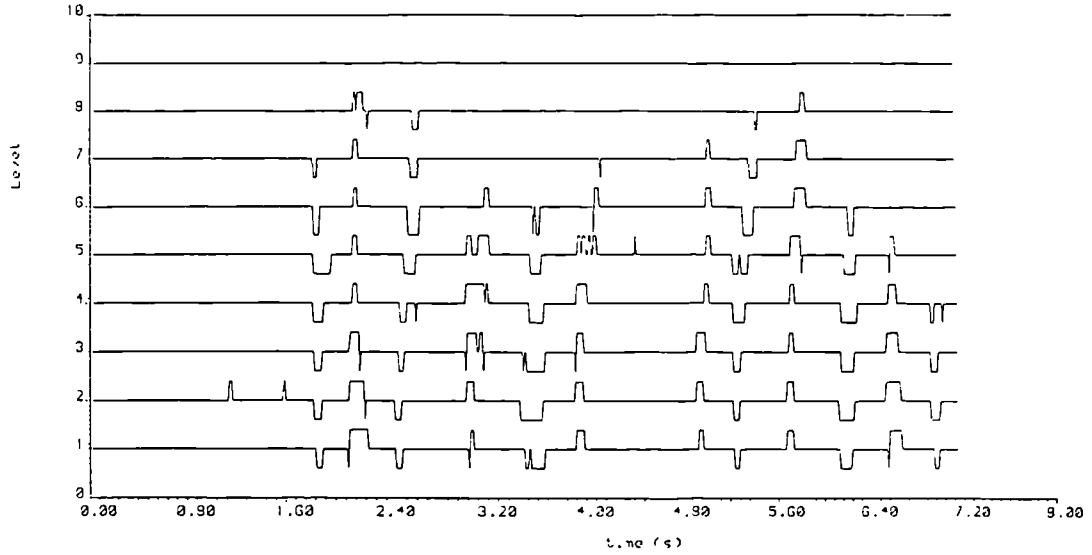

Time history of yielding excursions in the knee elements

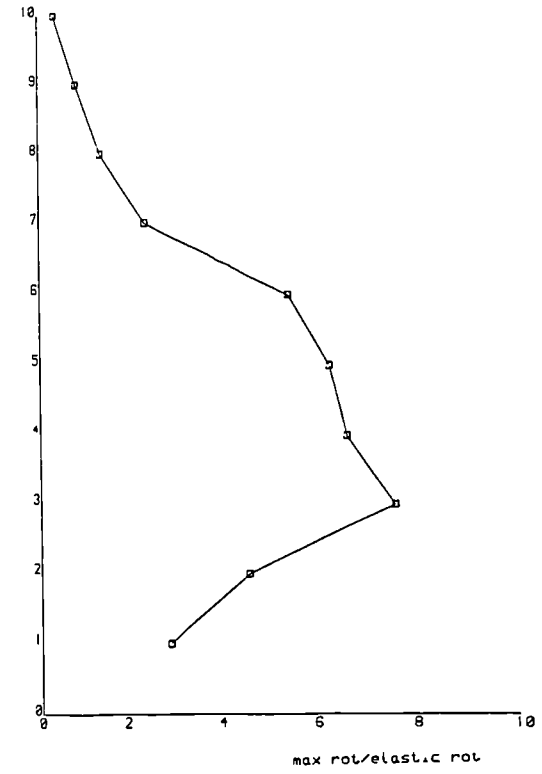

Maximum knee element ductility

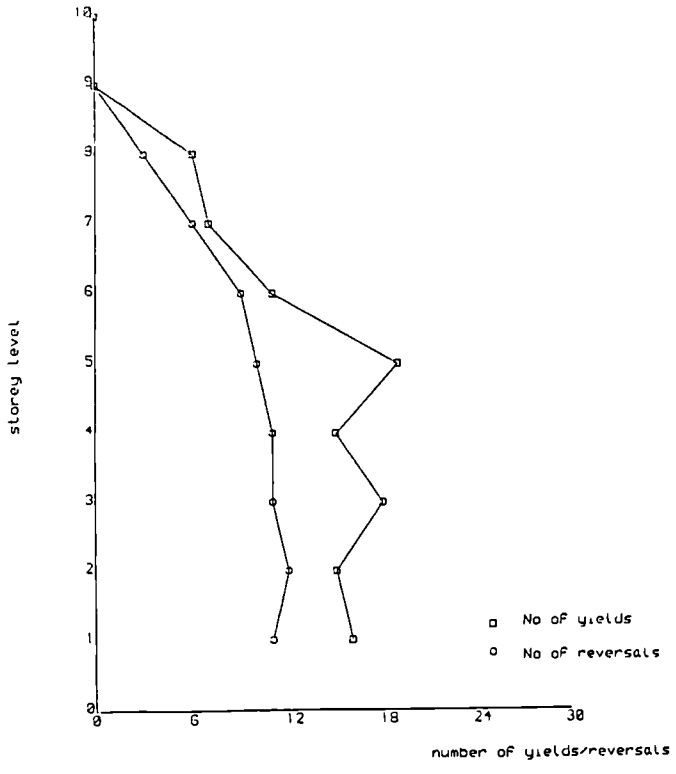

number of yield and reversal excursions

Fig.3.8 Parameters measuring the potential damage of knee elements

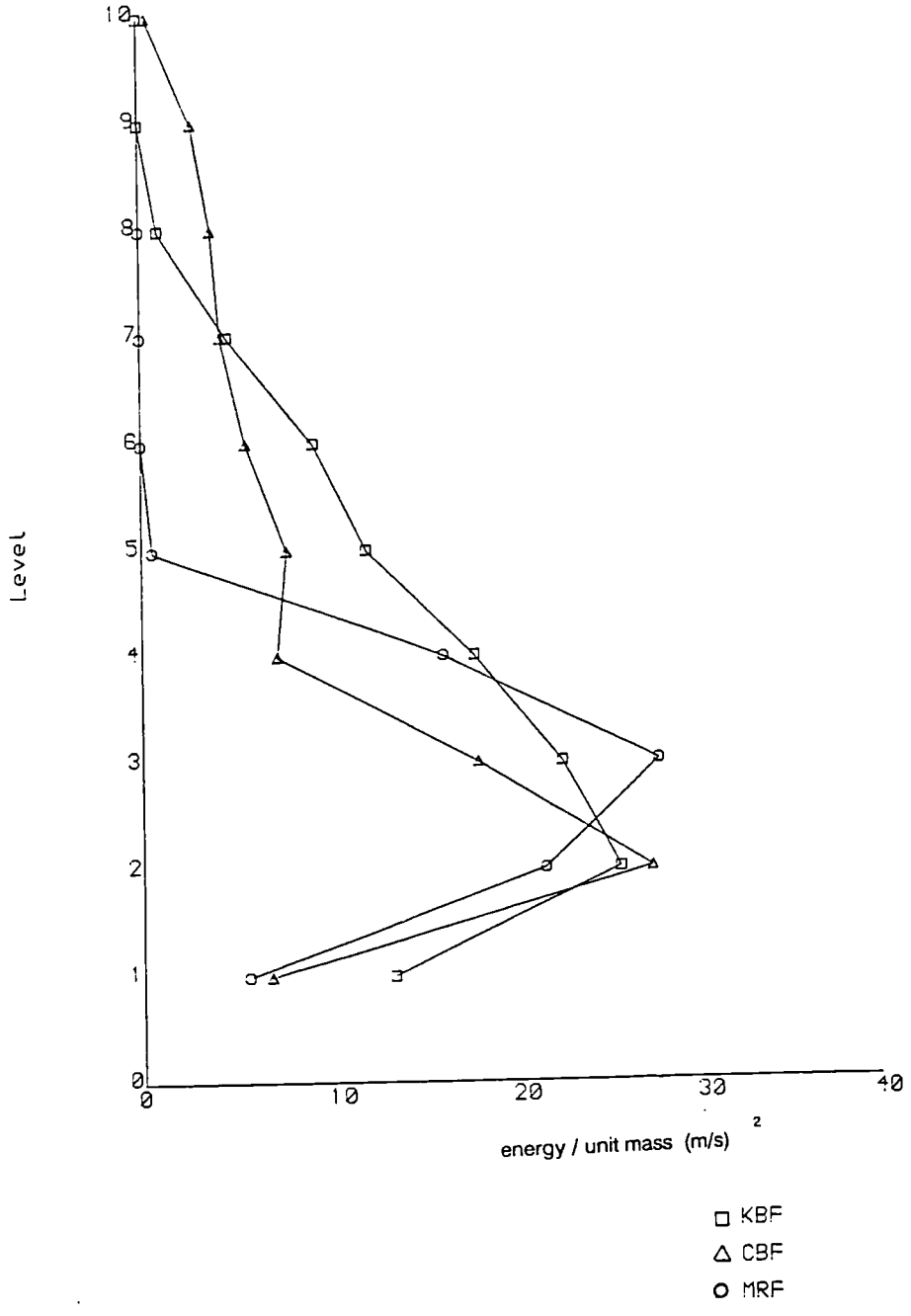

Fig.3.9 Hysteretic energy distribution through the height of the frames

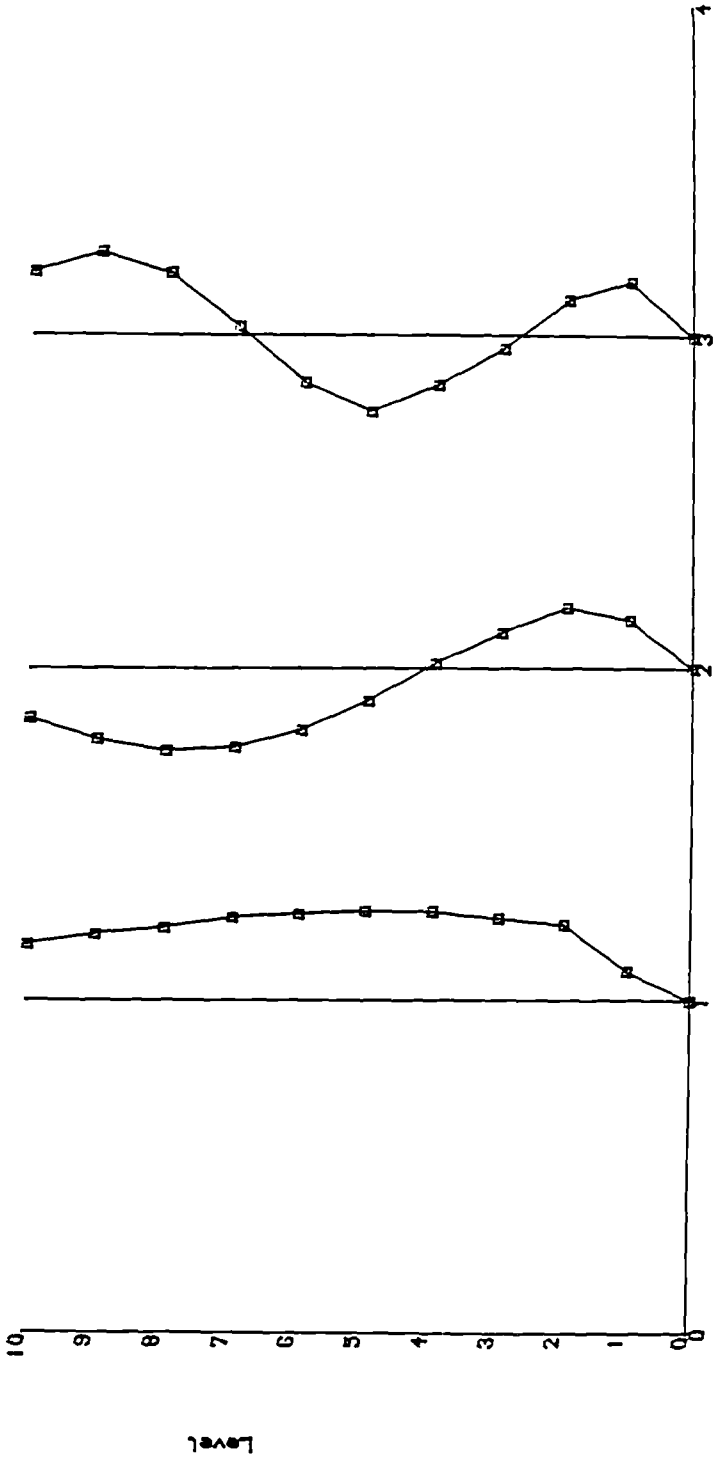

Fig.3.10 Mode shapes of the knee element deformations

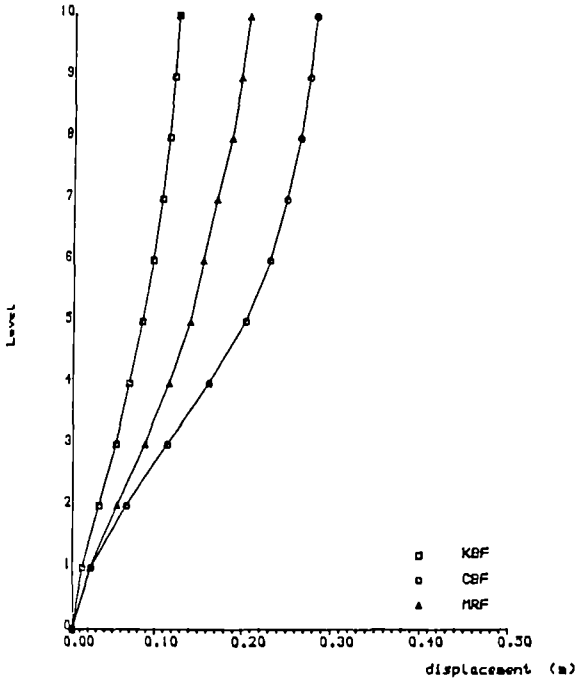

Maximum lateral deflection

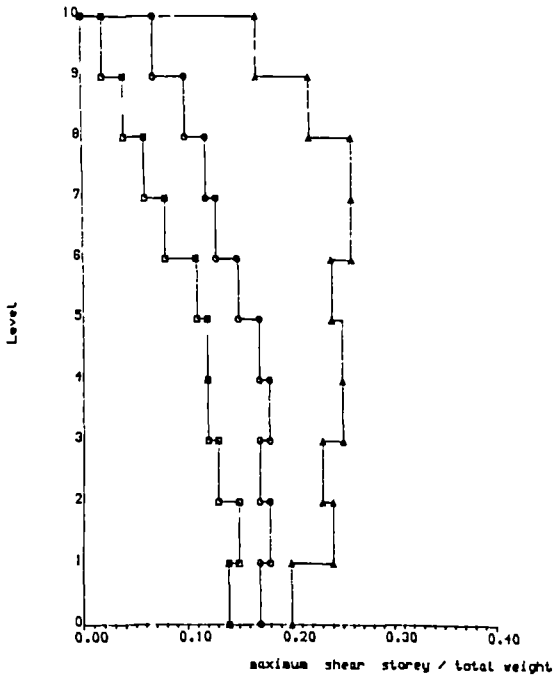

Shear envelope

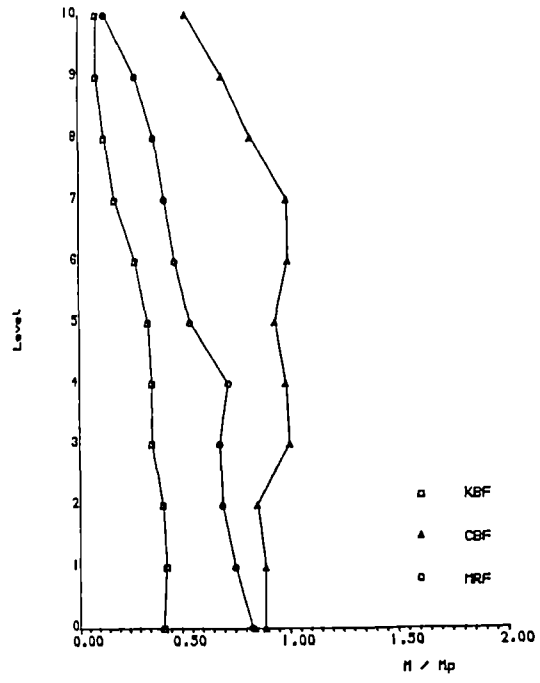

Bending momemt envelope

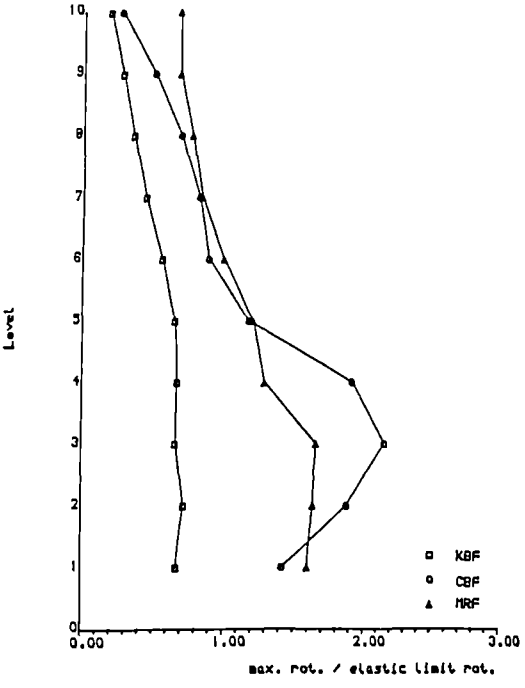

Beam ductility

Fig.3.11 Envelope responses of the KBF, MRF, and CBF

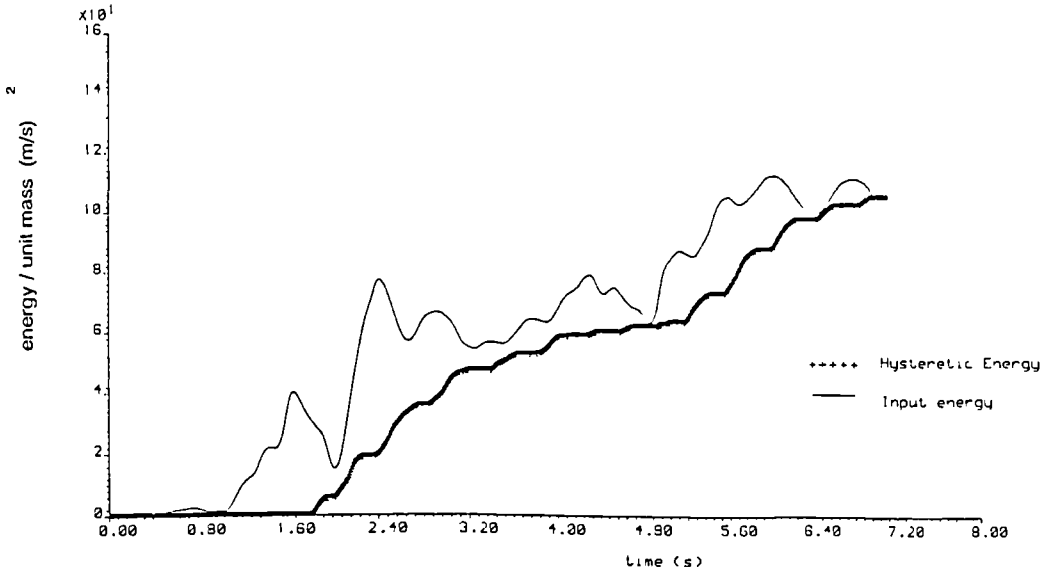

knee braced frame

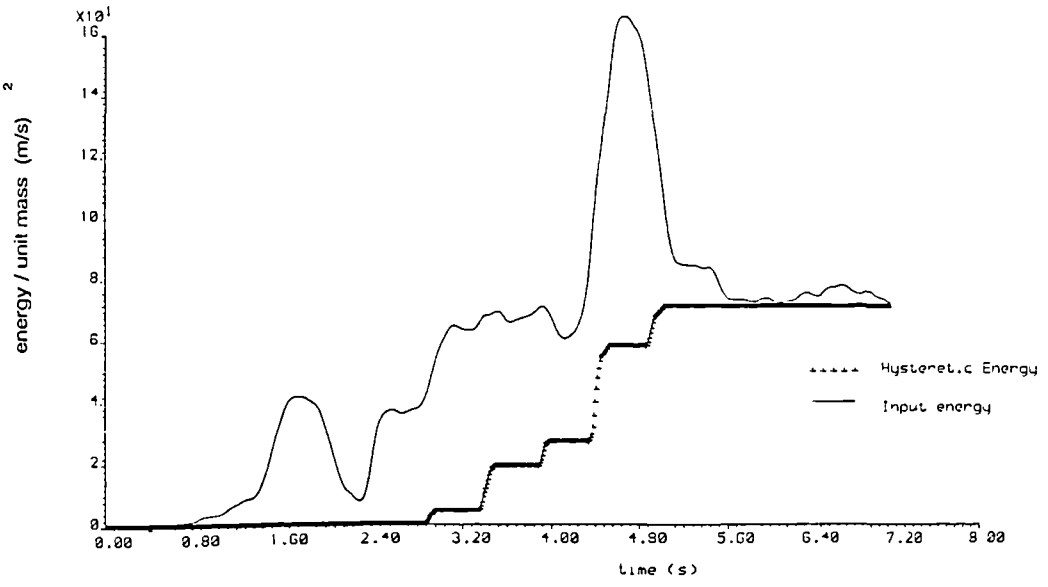

moment resisting frame

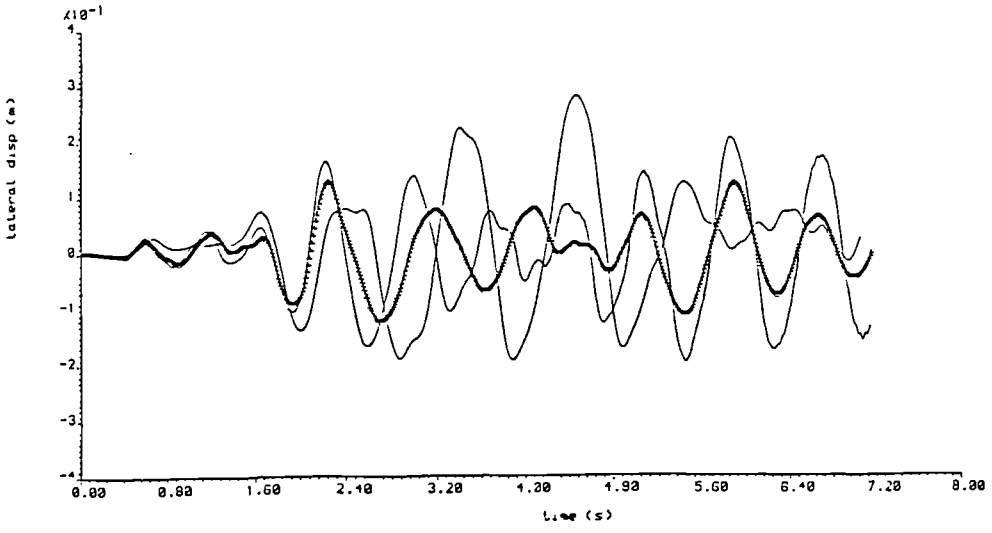

Fig.3.12 Energy and displacement time histories of the frames

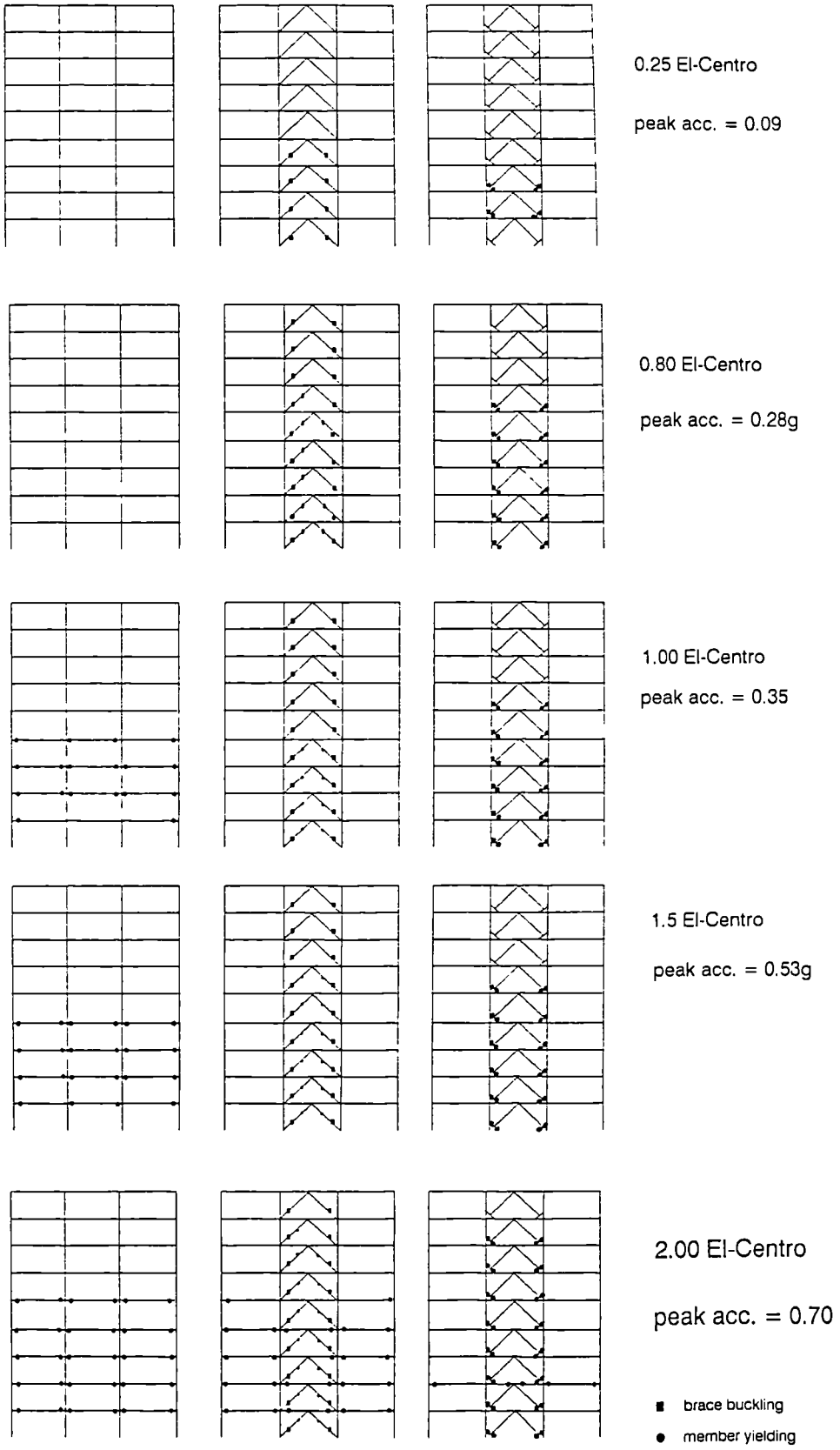

Fig.3.13 Structural damage caused by different earthquake intensities

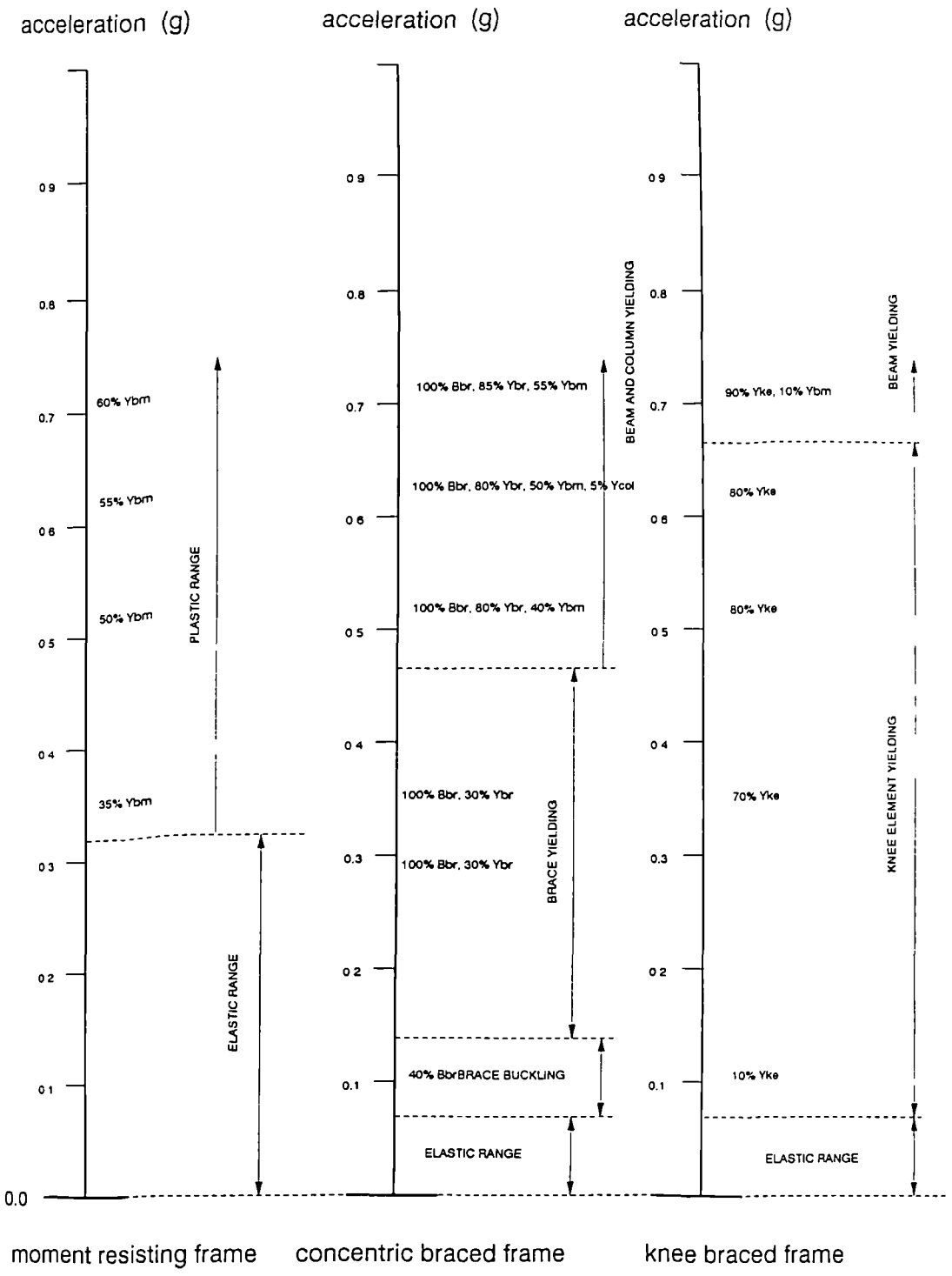

Ybm : yielded beam
Ycol : yielded column
Ybr : yielded brace
Bbr : brace buckling
Yke : yielded knee element

Fig.3.14 Yield sequence in the MRF, CBF and KBF

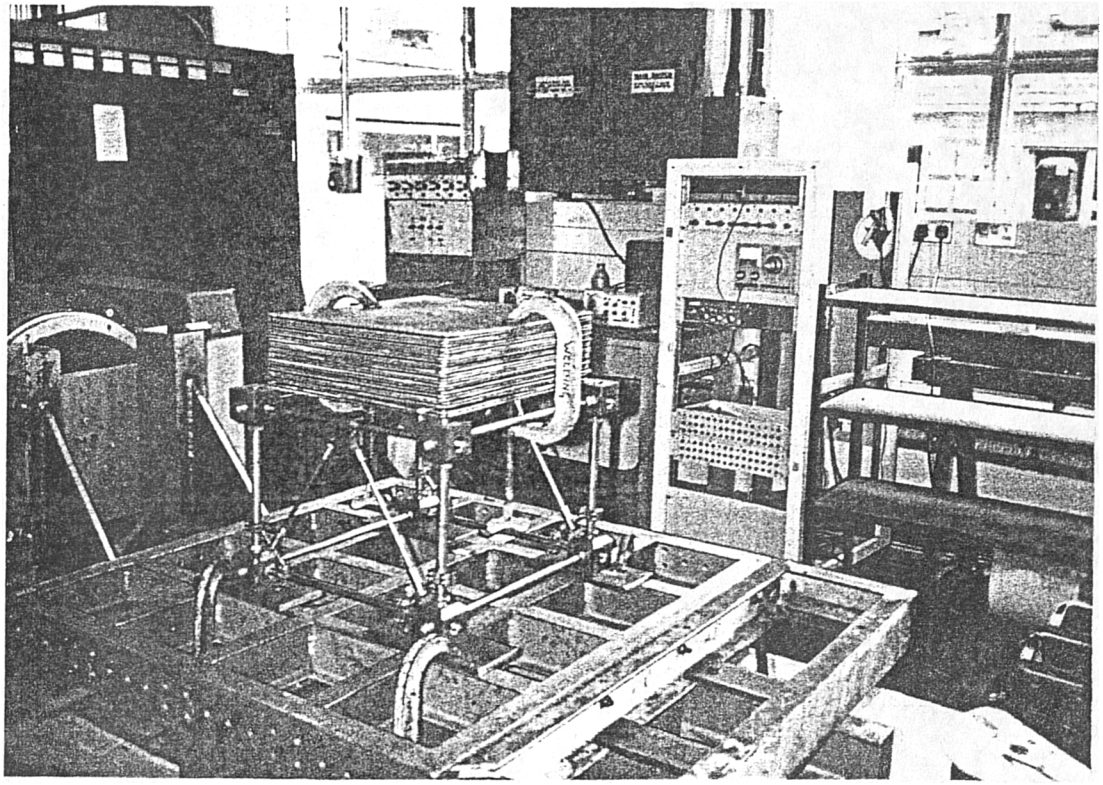

Fig.4.1 Knee braced single cell on the small shaker

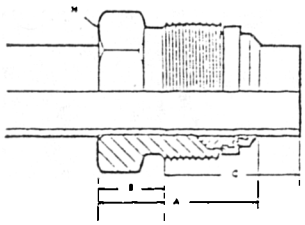

a- 'Hydraustud' fitting

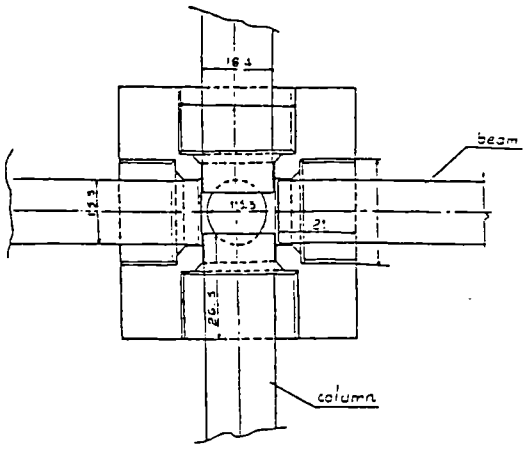

b- Block connector

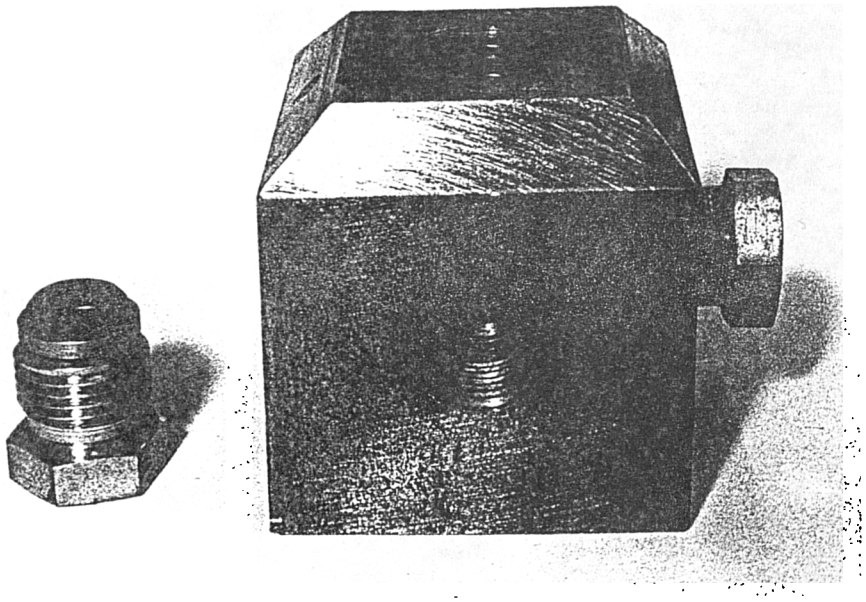

Fig.4.2 Typical connection block

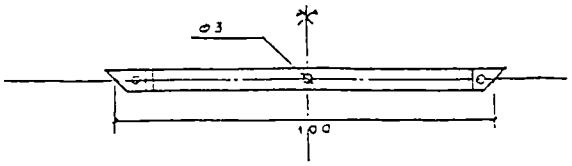

a- Knee element

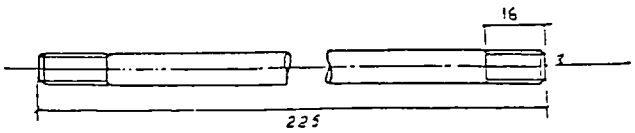

b- Brace element

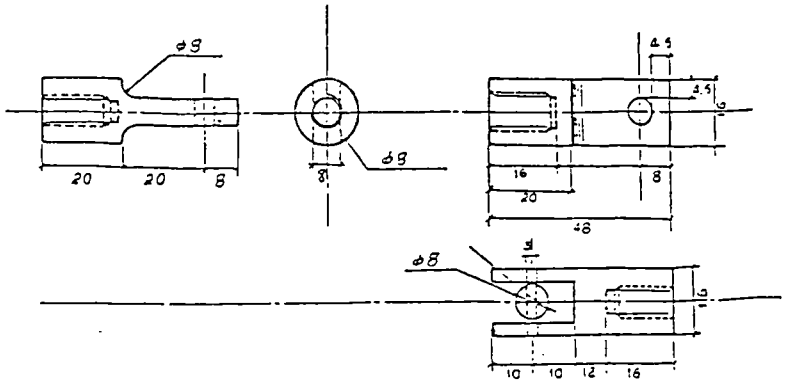

c- screwed connectors

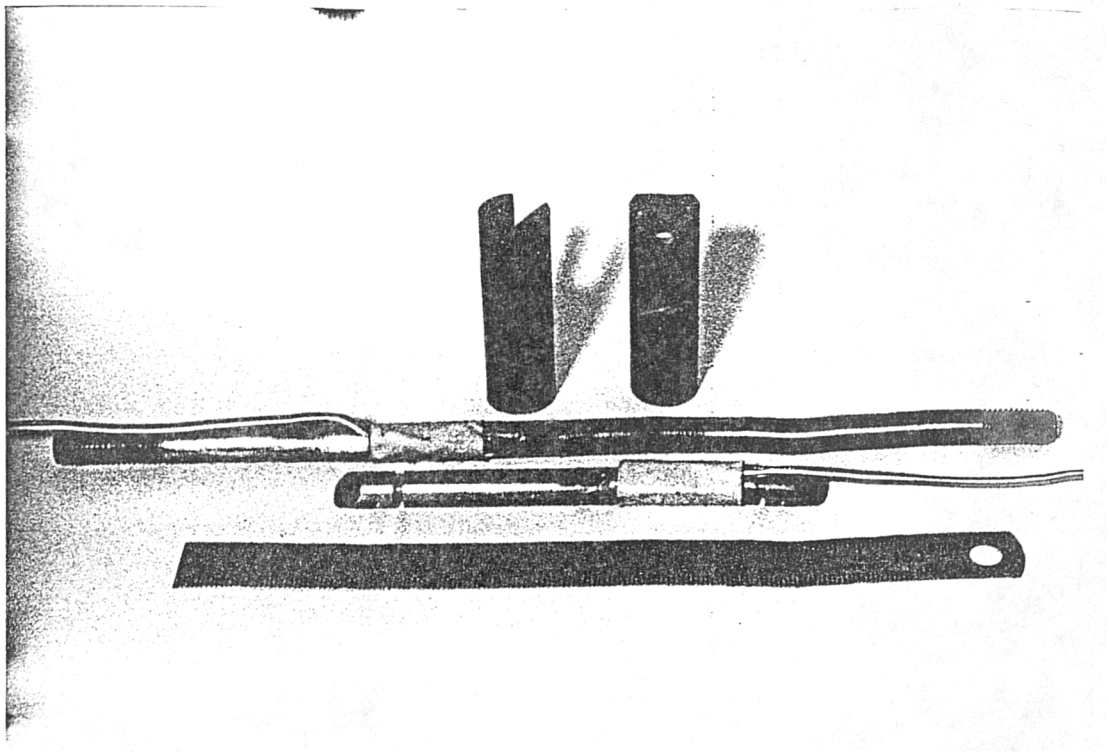

Fig.4.3 Knee element, brace element, and screwed connectors

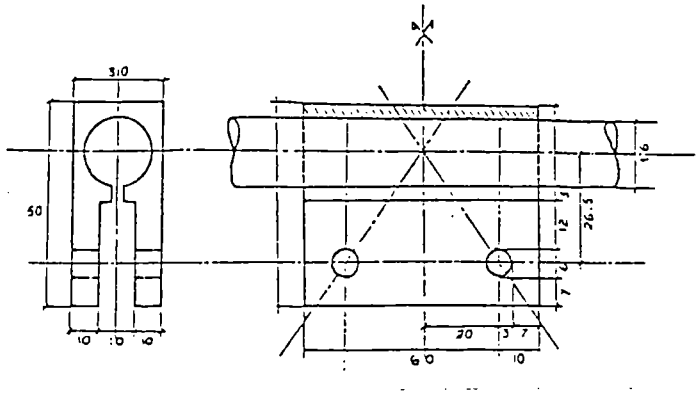

a- Central beam connector

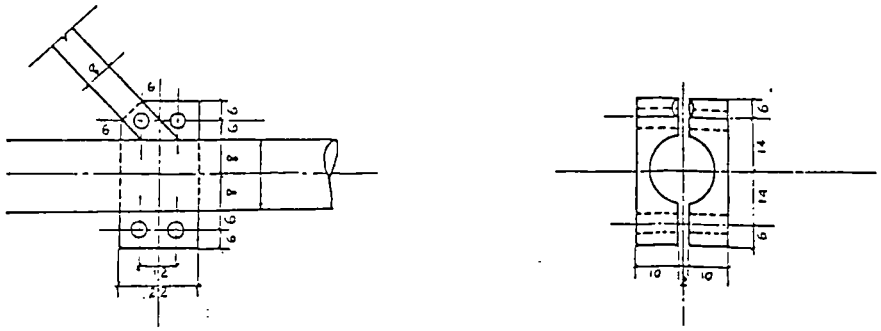

b- Knee element connectors

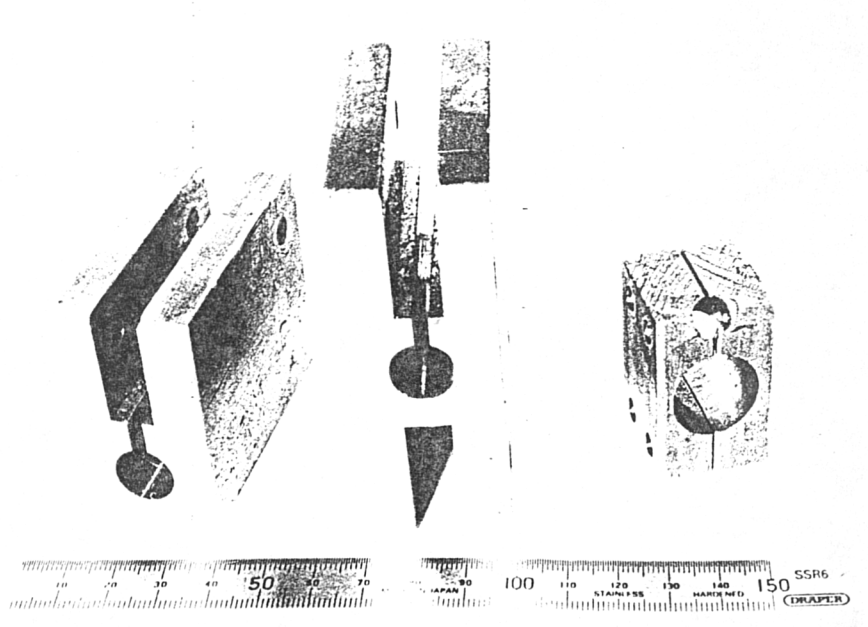

Fig.4.4 Central beam and knee element connectors

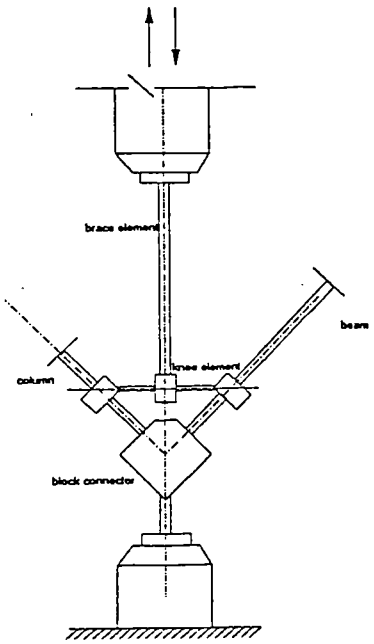

a- Cyclic test of knee bracing system set

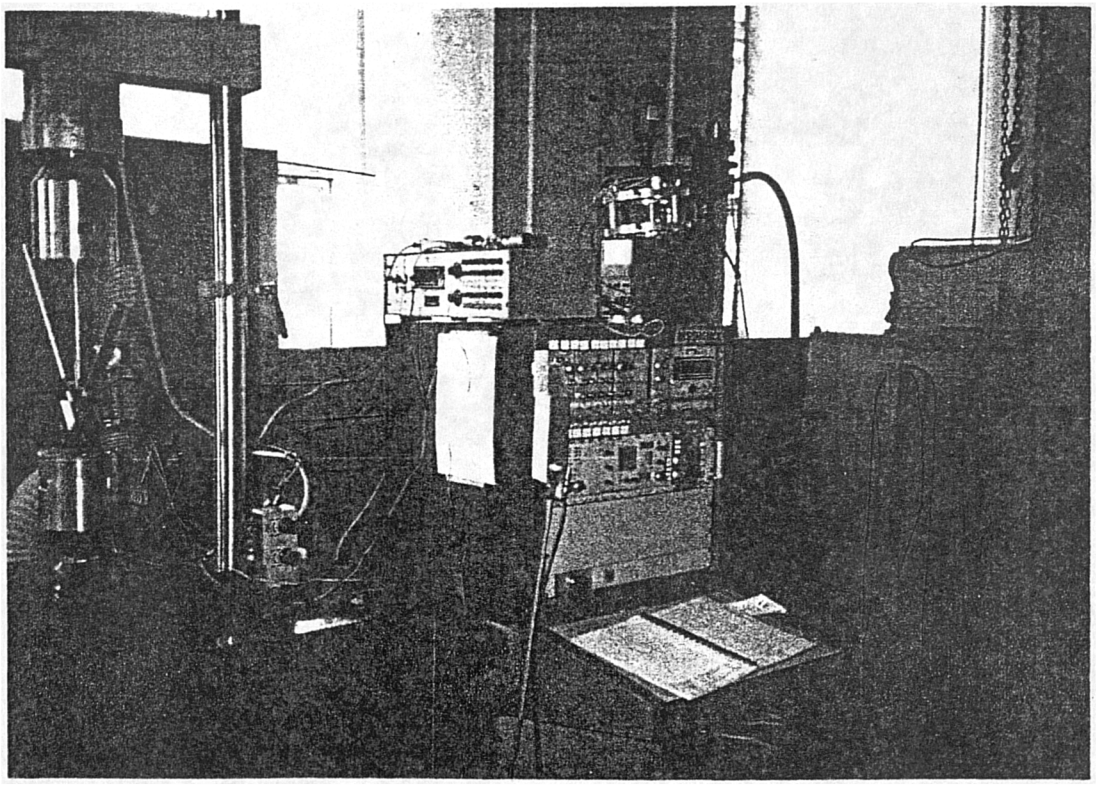

b- Cyclic test using the Schenck

Fig.4.5 Cyclic test apparatus

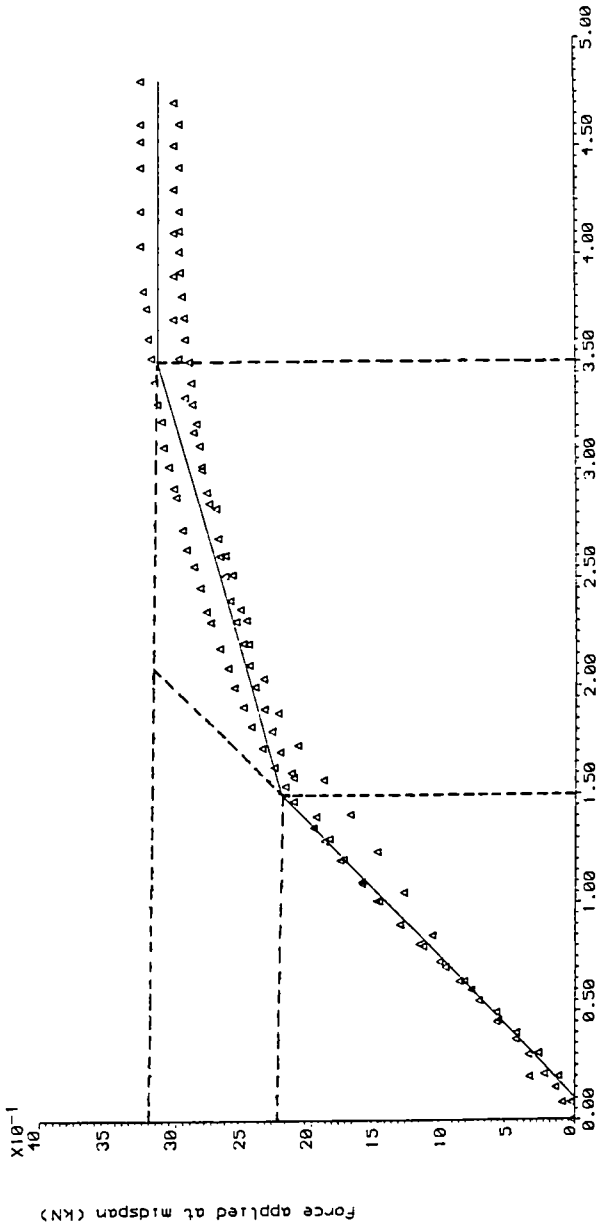

Fig.4.6 Typical brace force-knee element displacement relationship

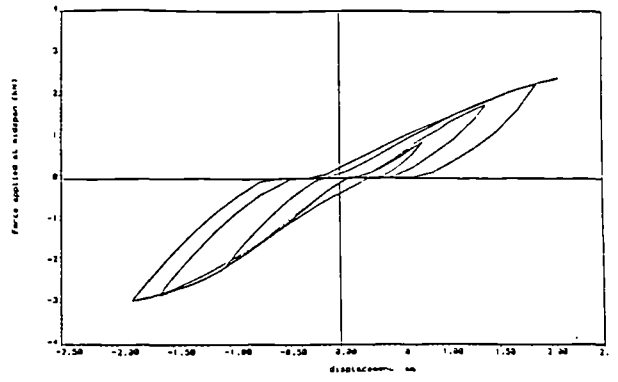

Force-displacement hysteritic loop (specimen 9)

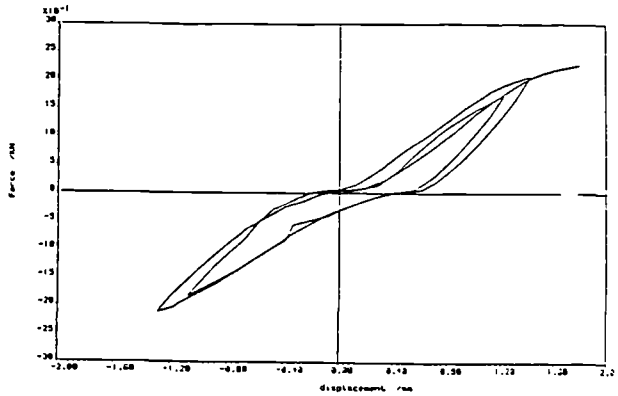

Force-displacement hysterit.c loop (specimen 3)

a- Brace force-knee element displacement relationship

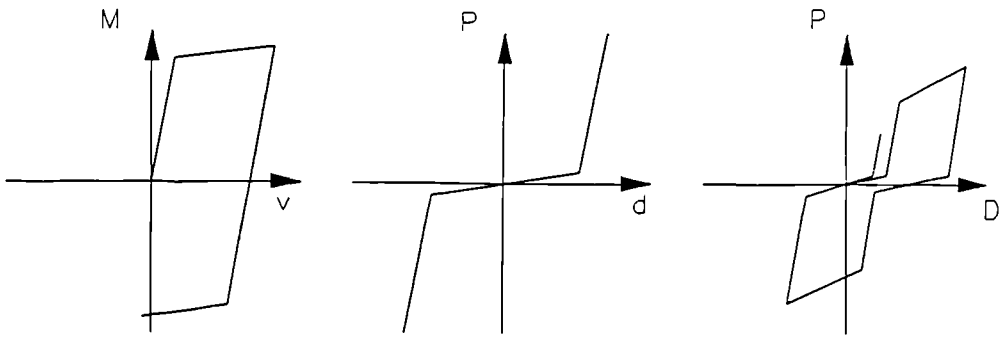

Bilinear model knee element

Conservative elastic hrdening brace element

System benaviour

b- Analytical models

Fig.4.7 Brace force-knee element displacement hysterisis loop and the corresponding

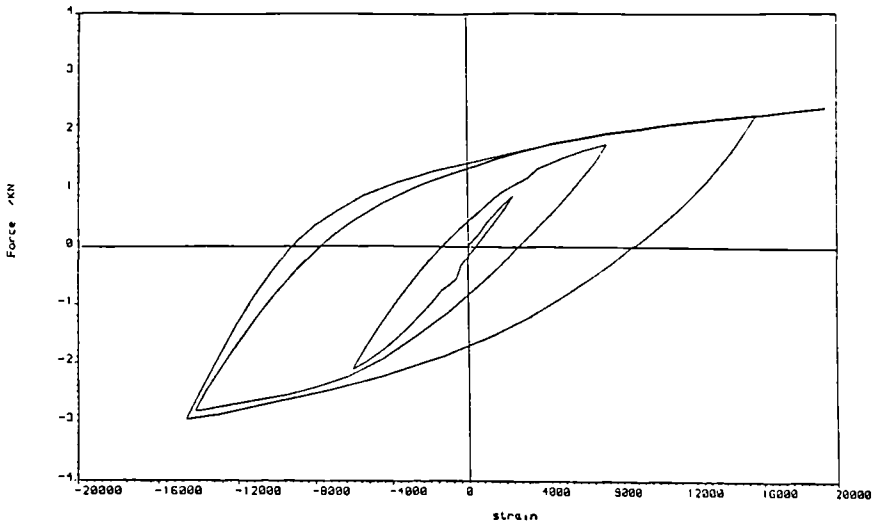

a- Force-strain hysteretic loop (specimen 9)

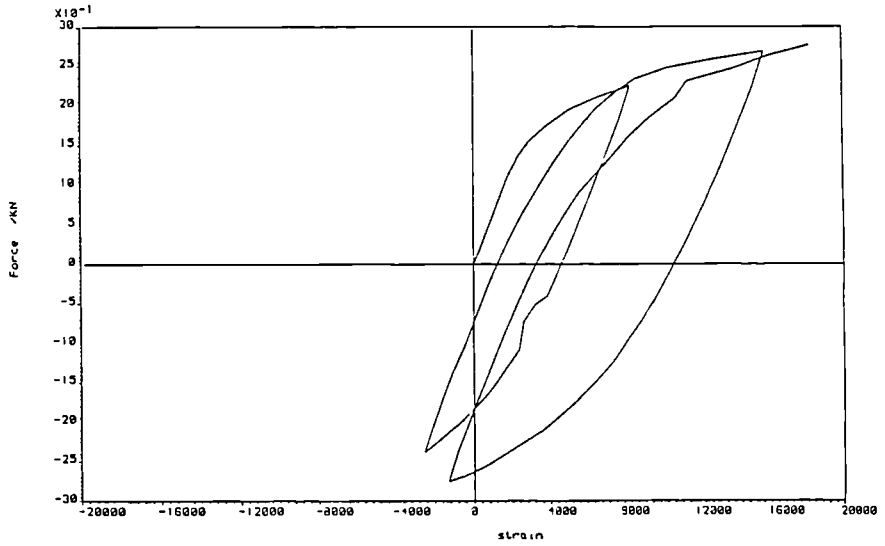

b- Force-strain hysteretic loop (specimen 3)

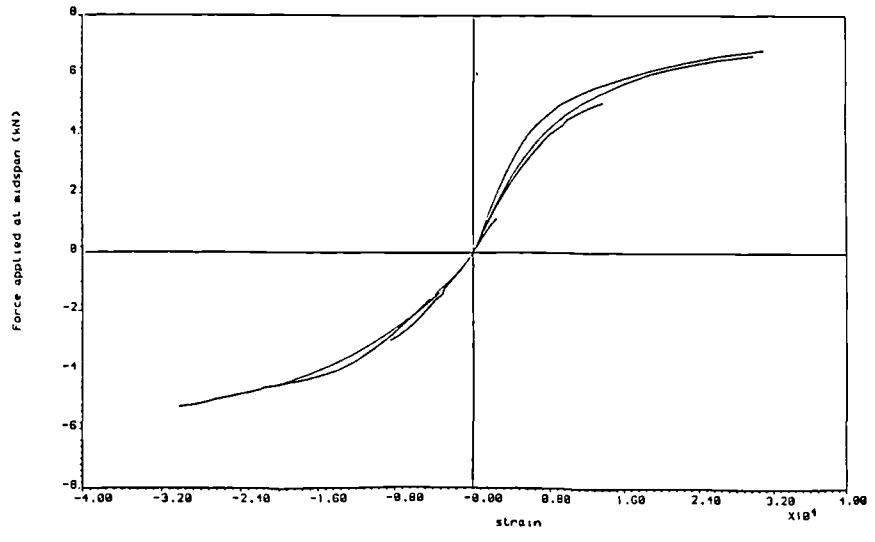

c- Slope degradation of the hysteretic loop

Fig.4.8 force-strain hysterisis loops of the knee elements

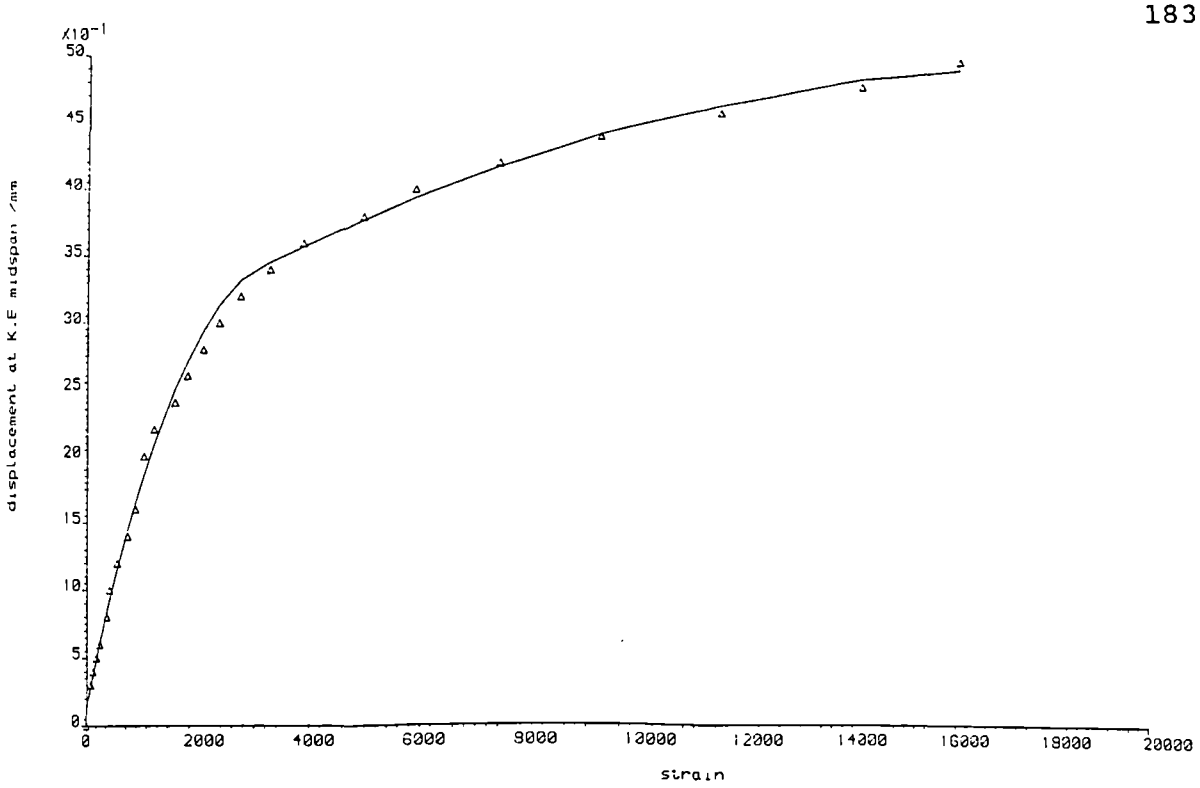

displacement-strain relationship

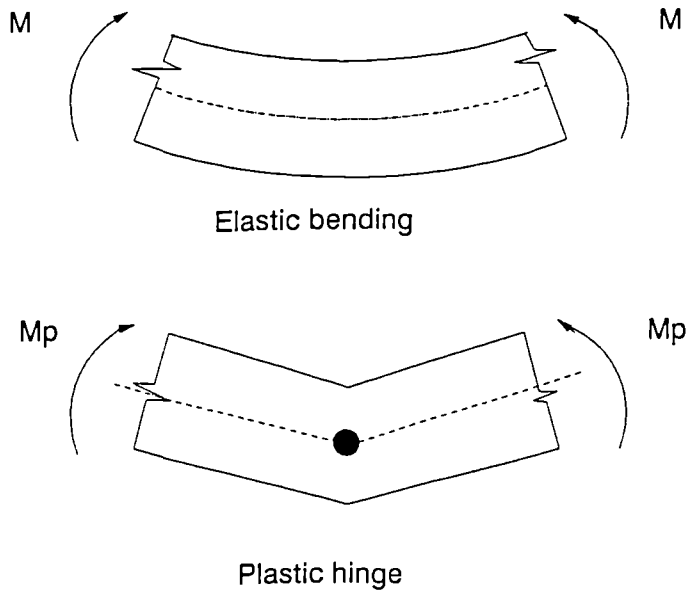

Fig.4.9 strain-displacement relationship and Plastic hinge formation

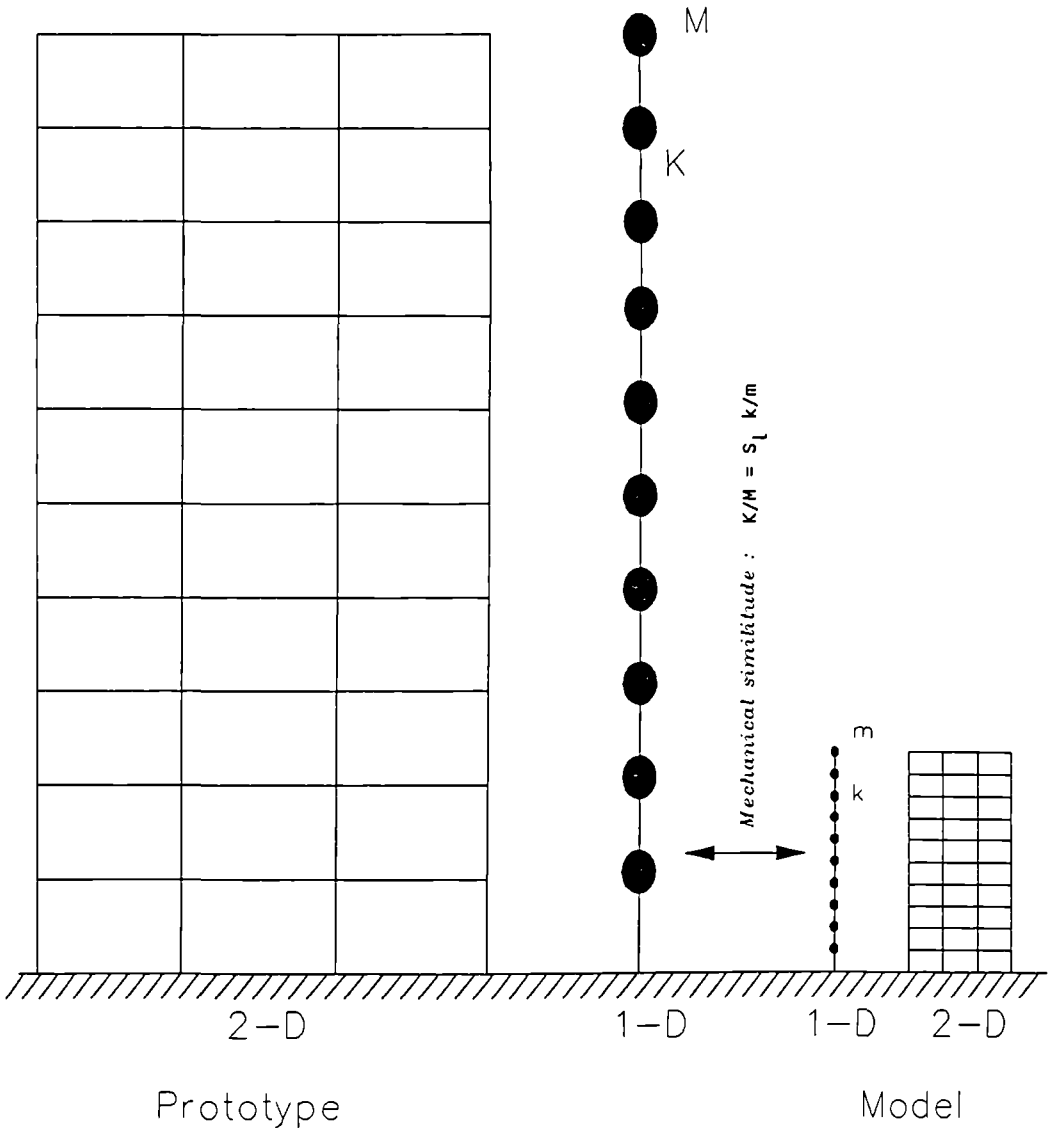

Fig.4.10 Mass adjustement procedure

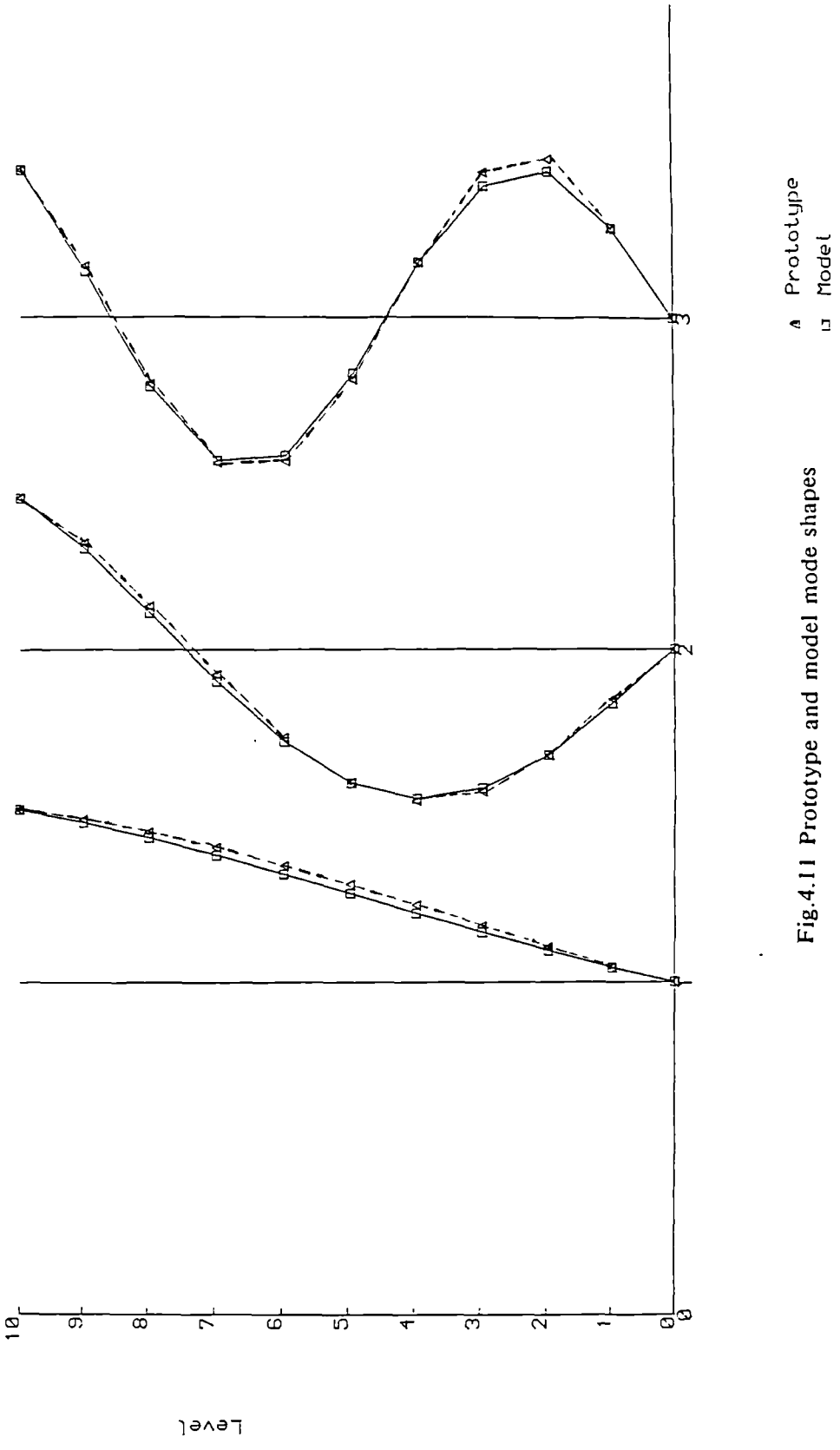

Fig.4.11 Prototype and model mode shapes

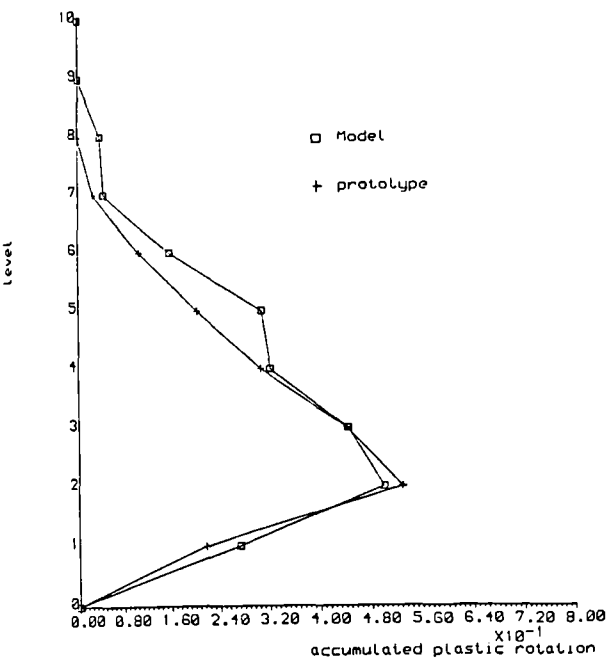

a- Hysteretic energy distribution

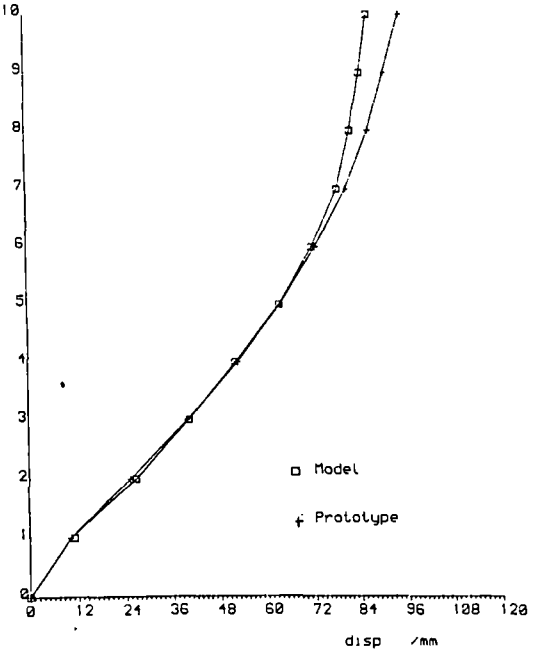

b- Maximum lateral displacements

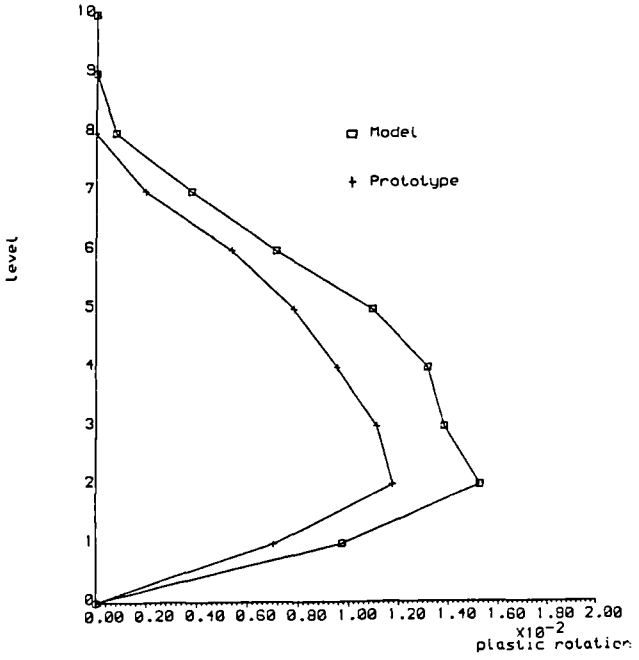

c- Maximum knee element plastic rotation

Fig.4.12 Maximum deflections, knee element ductilities and accumulated plastic deformations of the model and the prototype

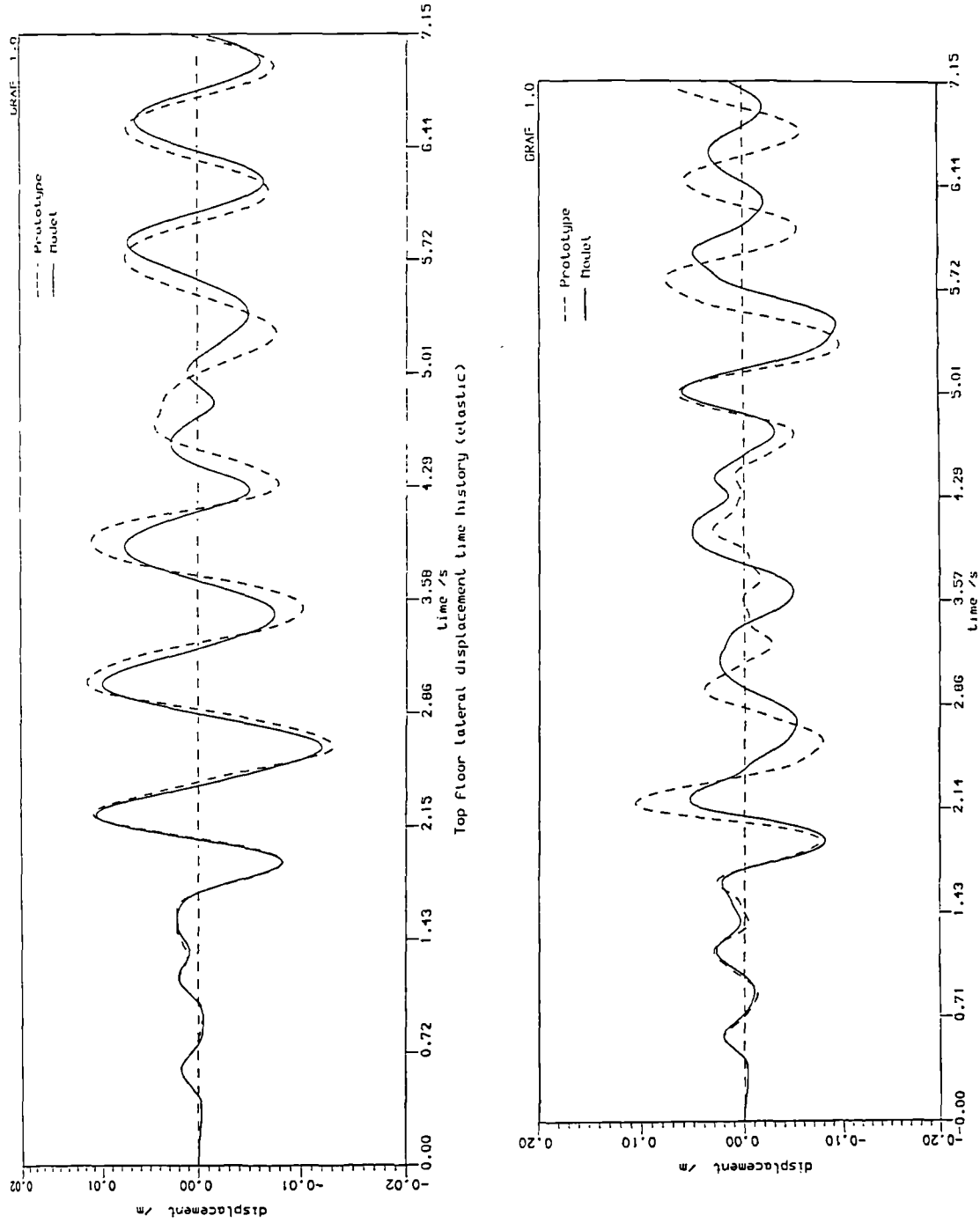

Fig.4.13 Time histories of the top floor displacement of the prototype and the model

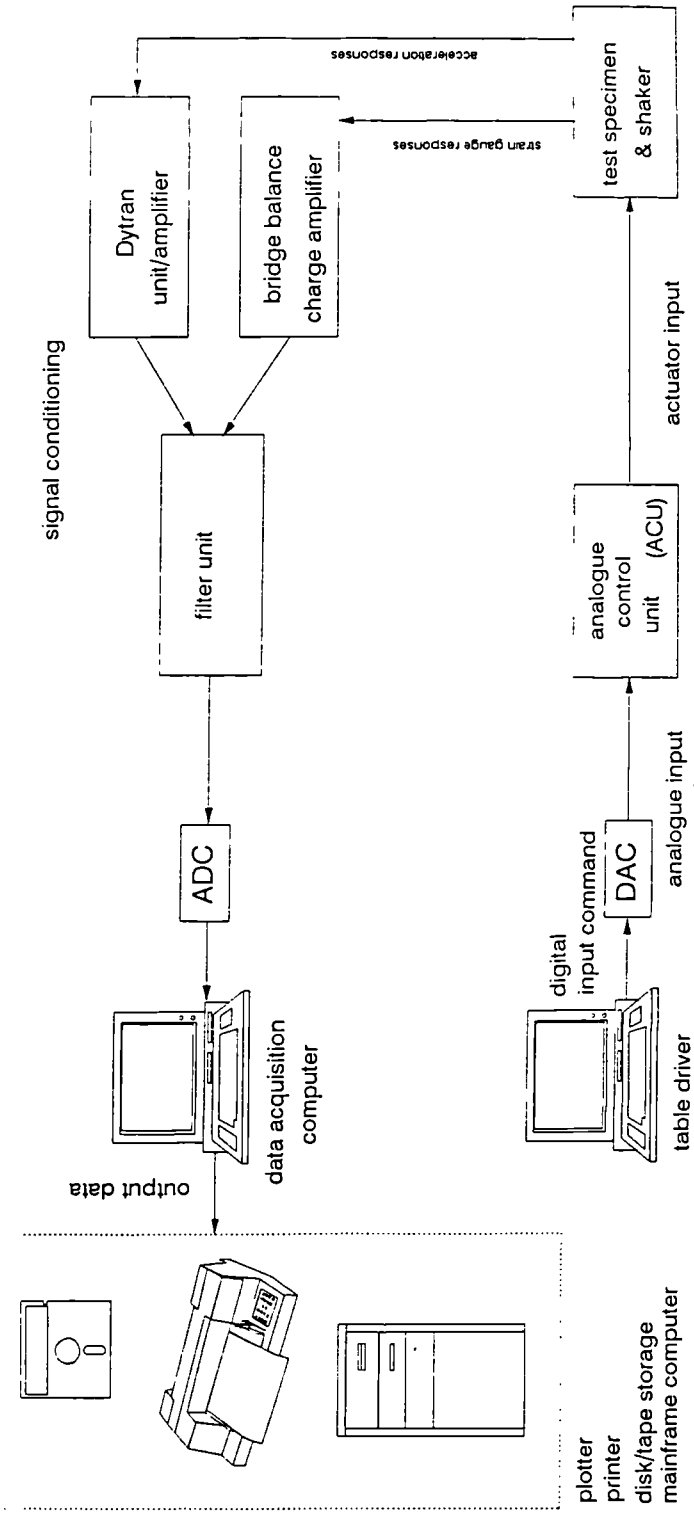

Fig.5.1 Typical setup of a digital control system in a shaker apparatus

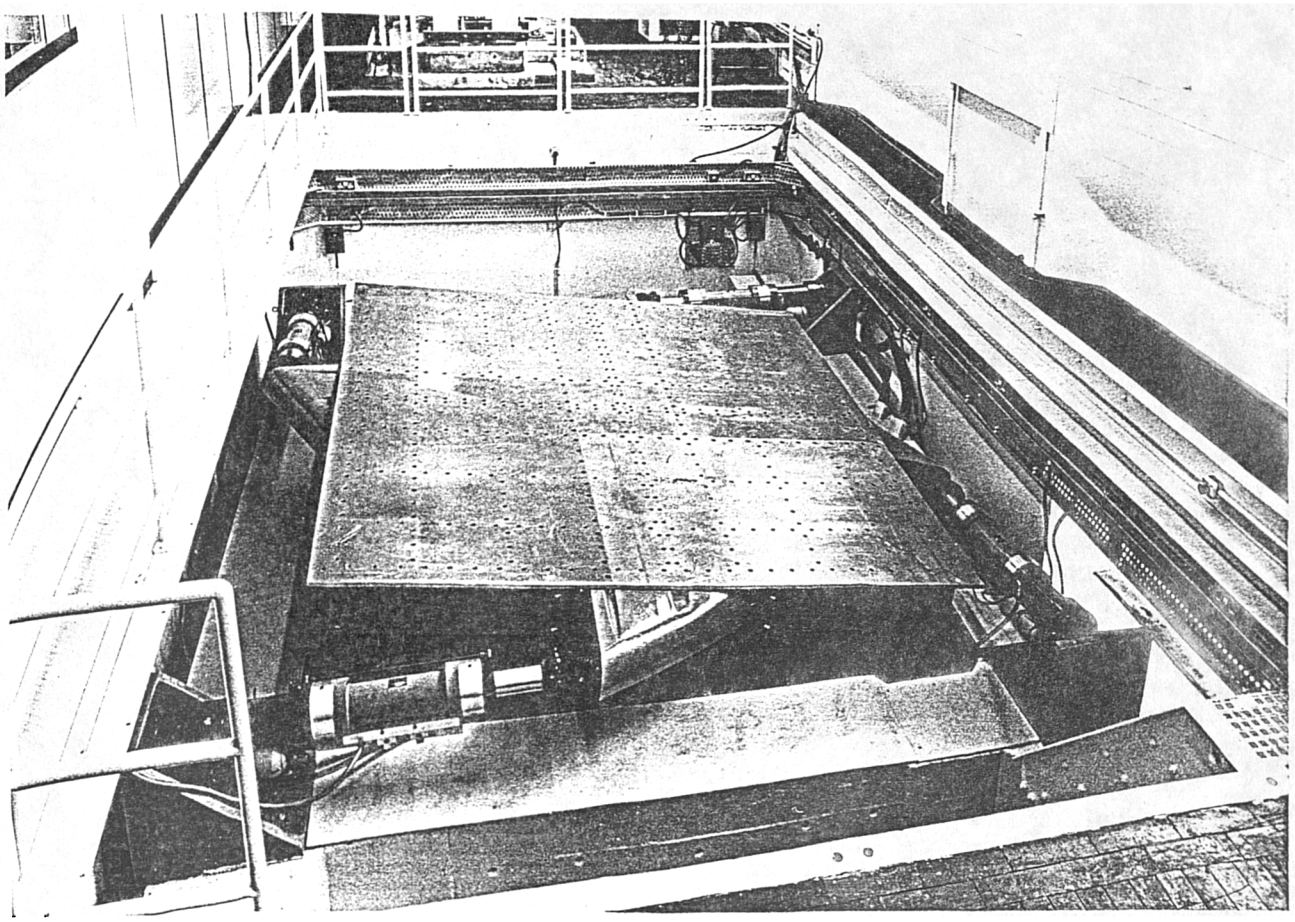

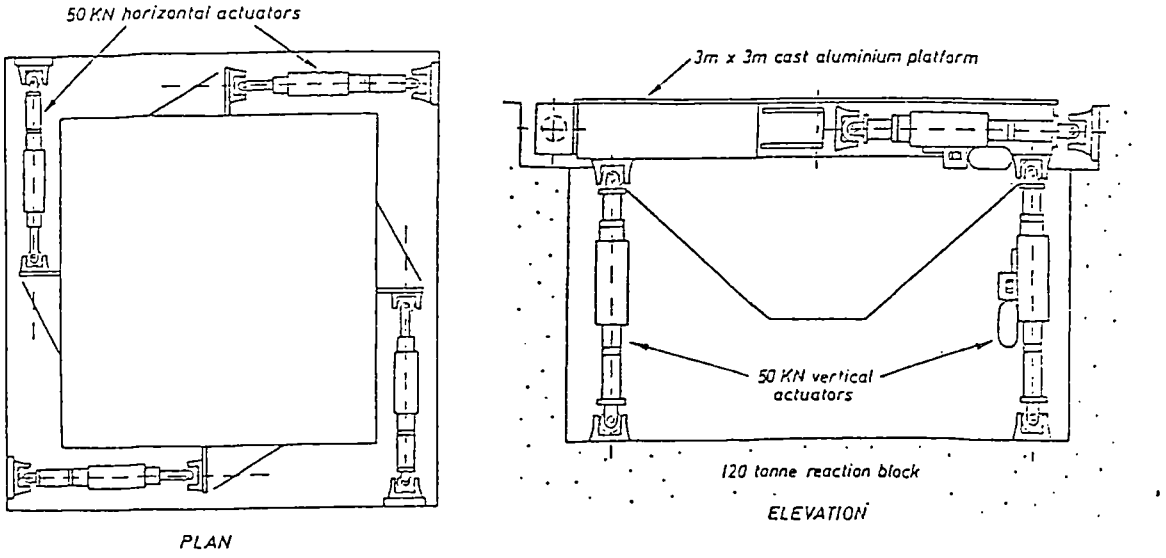

Fig.5.2 View and arrangement of the earthquake simulator from ref.[19]

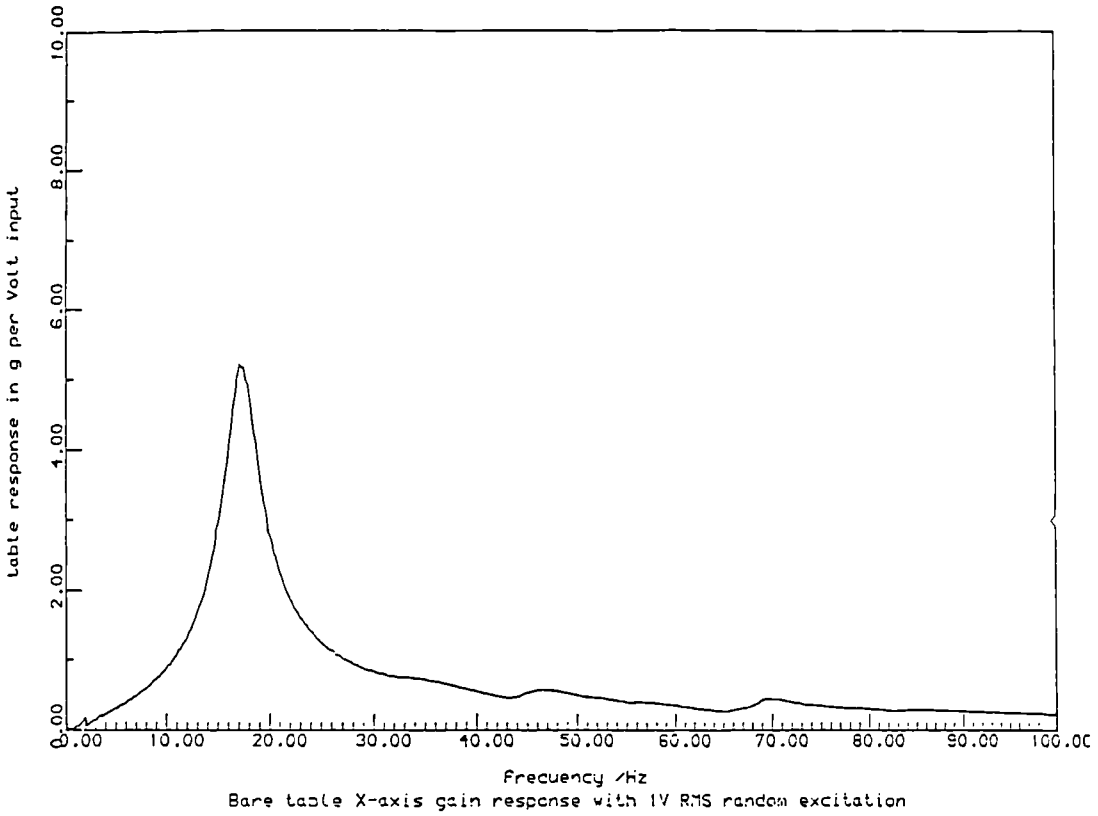

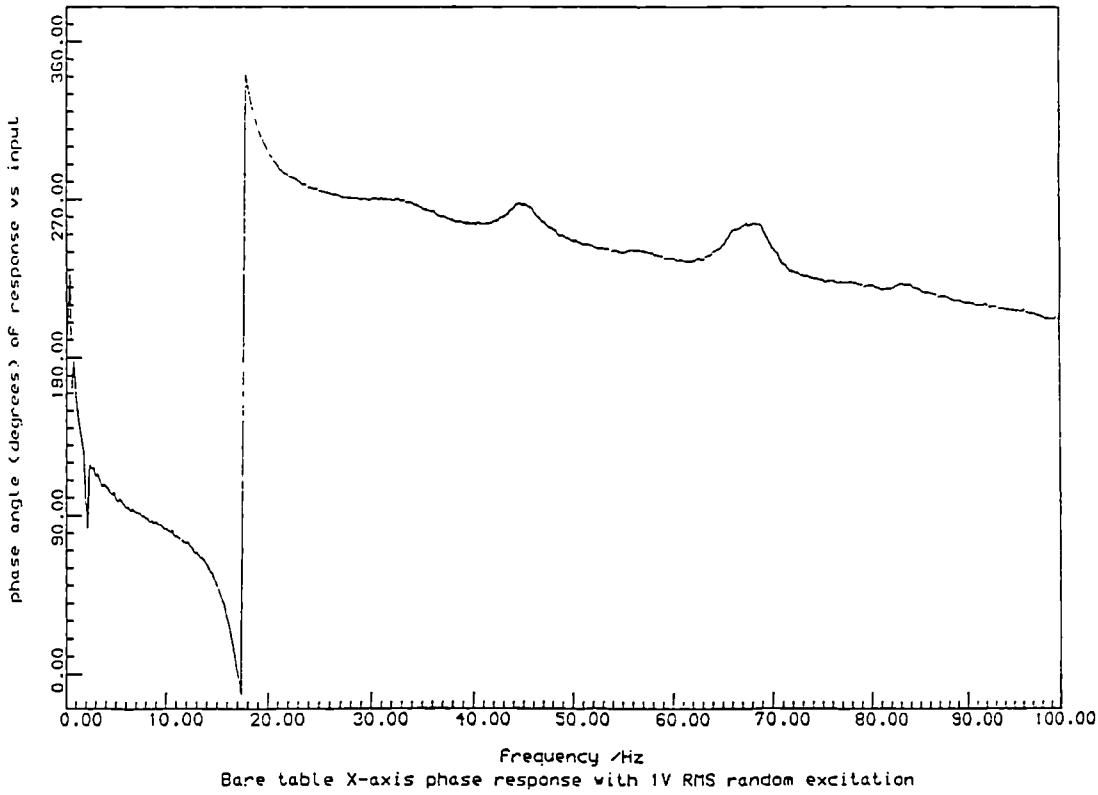

Fig.5.3 Response transfer function for the earthquake simulator X-axis from ref. [19]

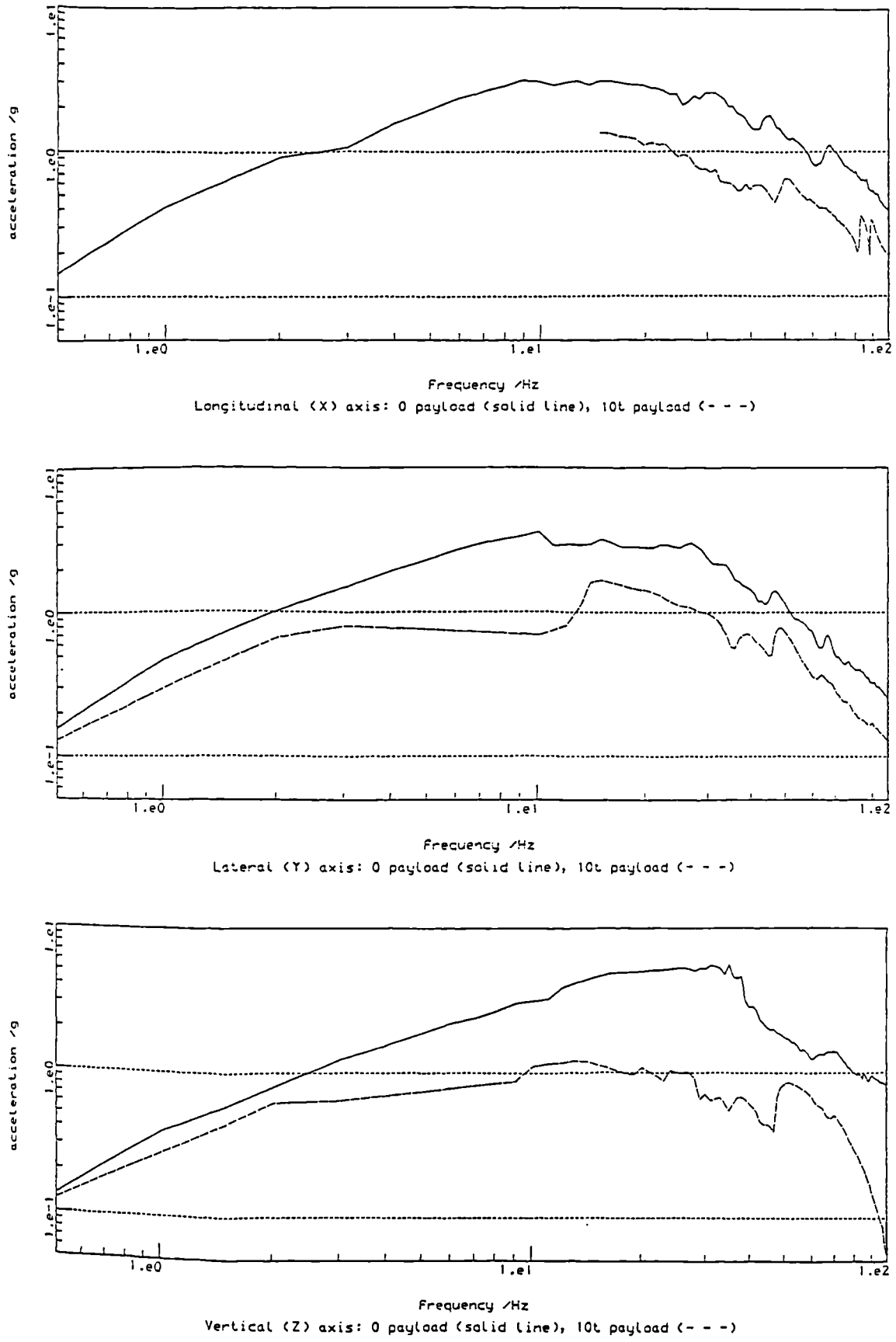

Fig.5.4 Earthquake simulator maximum single axis acceleration from ref.[19]

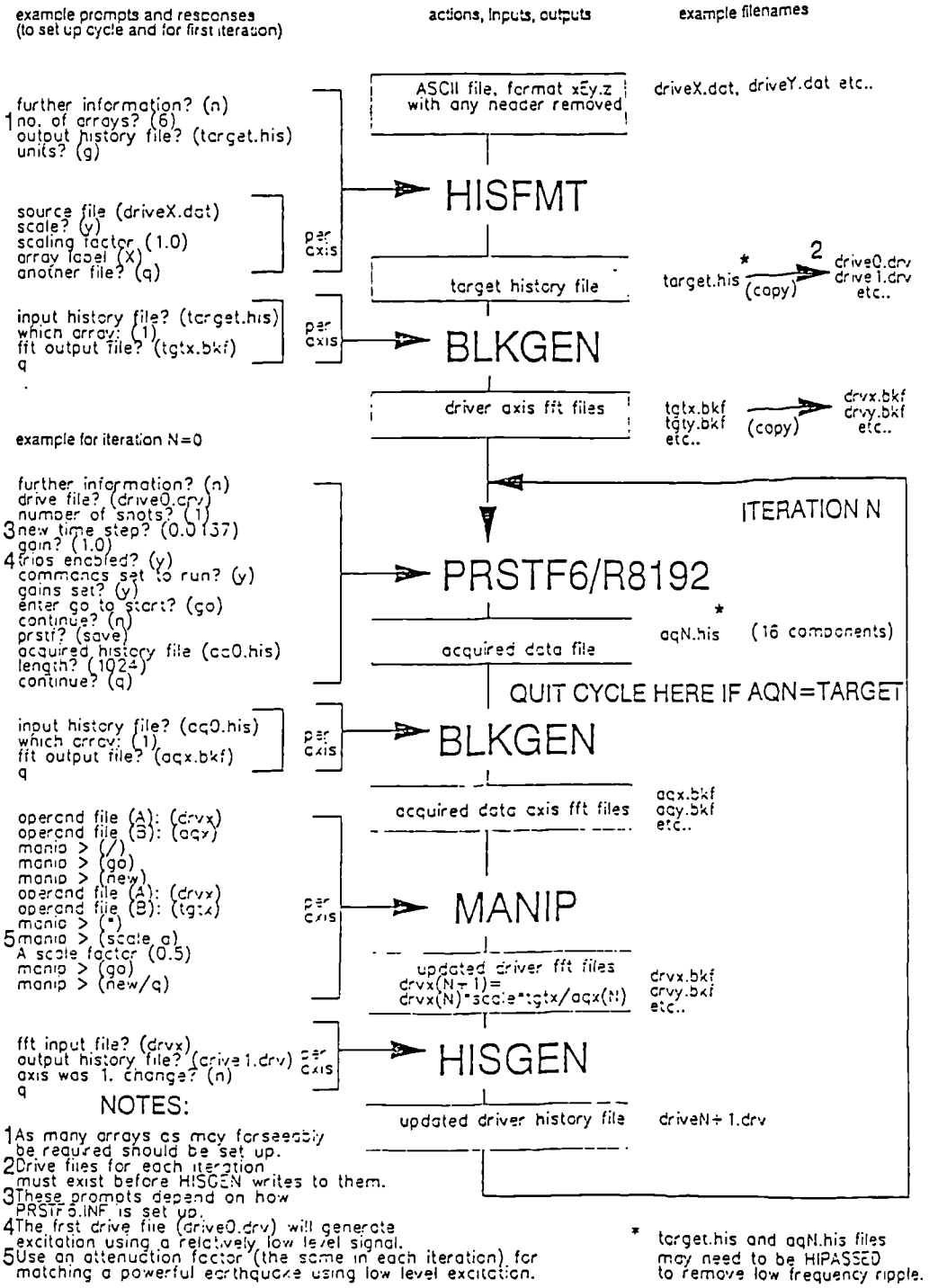

Fig.5.5 Linear algorithm for time history matching from ref.19

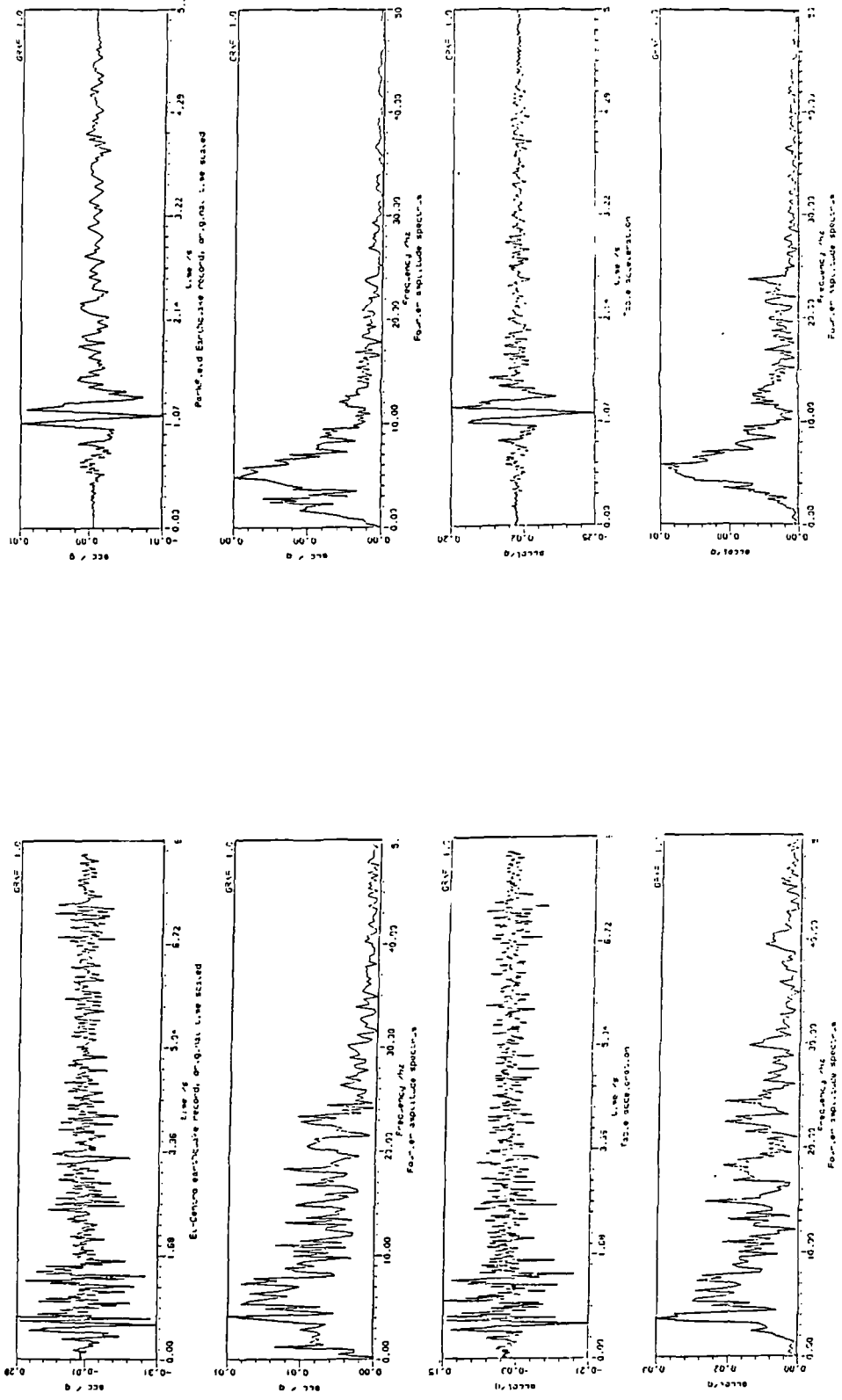

Fig.5.6 Simulated vs actual earthquake records

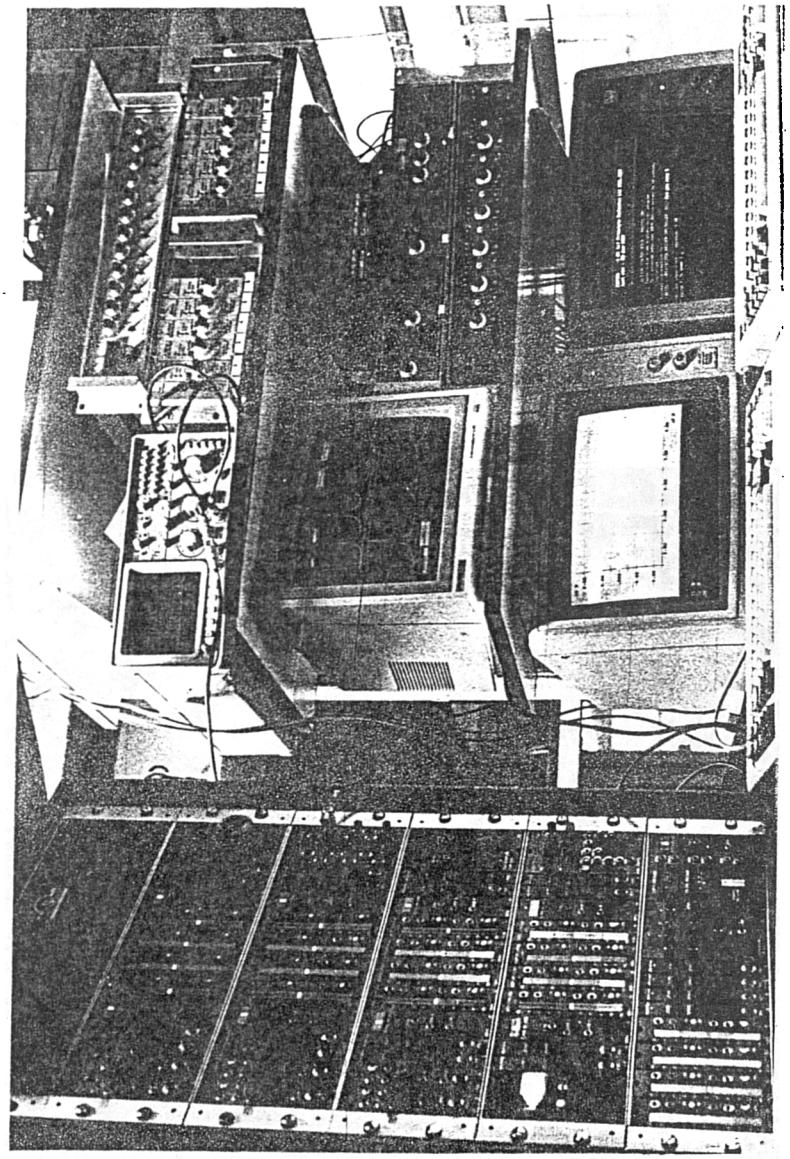

Fig.5.7 Shaking table control and data acquisition system

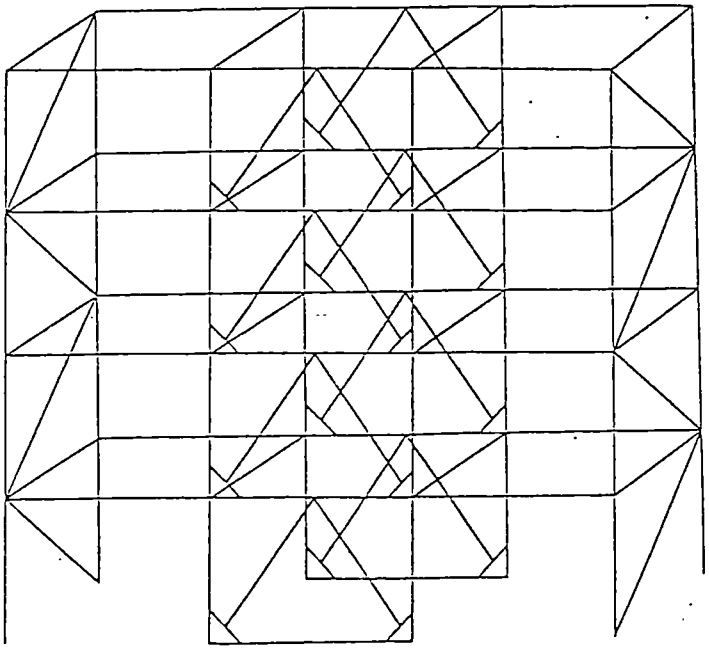

a-Skeleton of the four-storey KBF

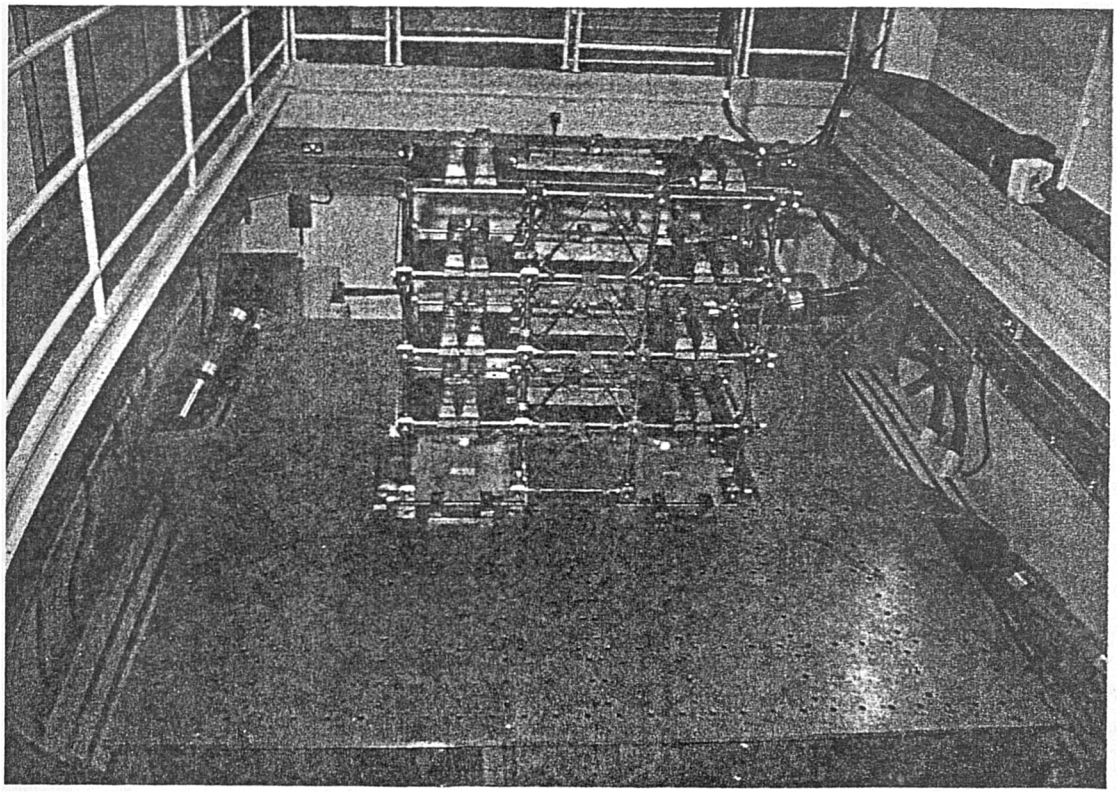

b-overall view of the test structure

Fig.6.1 structure of test series I

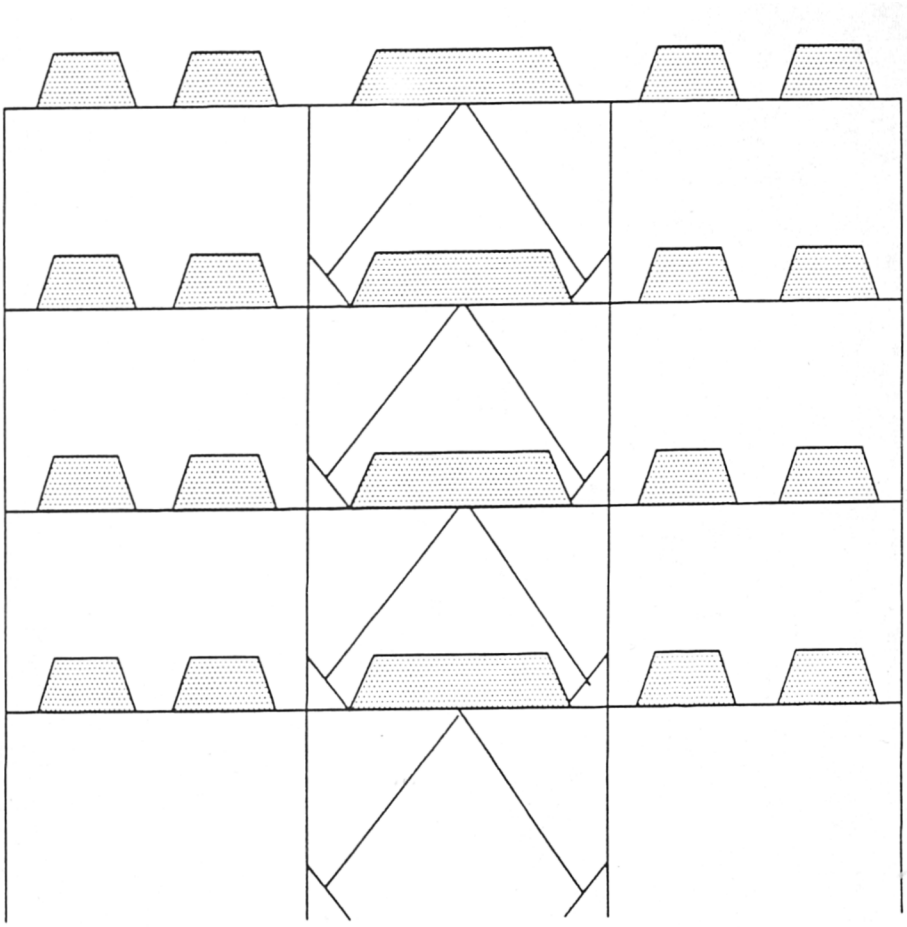

Fig.6.2 Added mass distribution

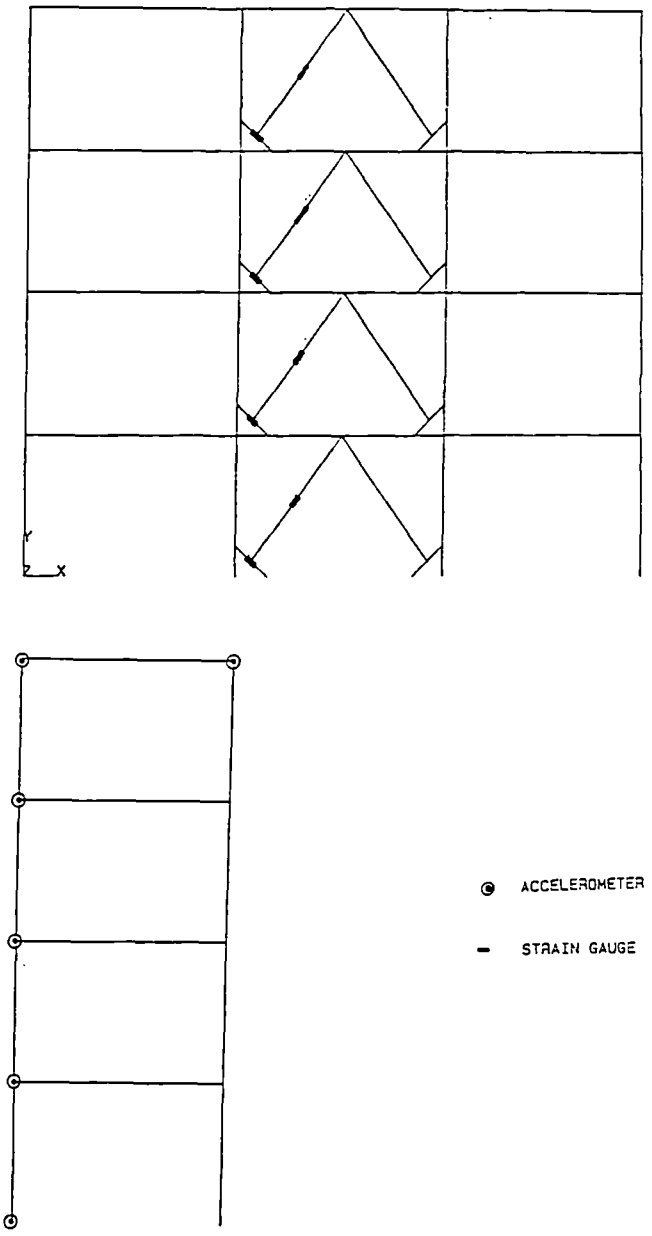

Fig.6.3 Sensors stations on the model

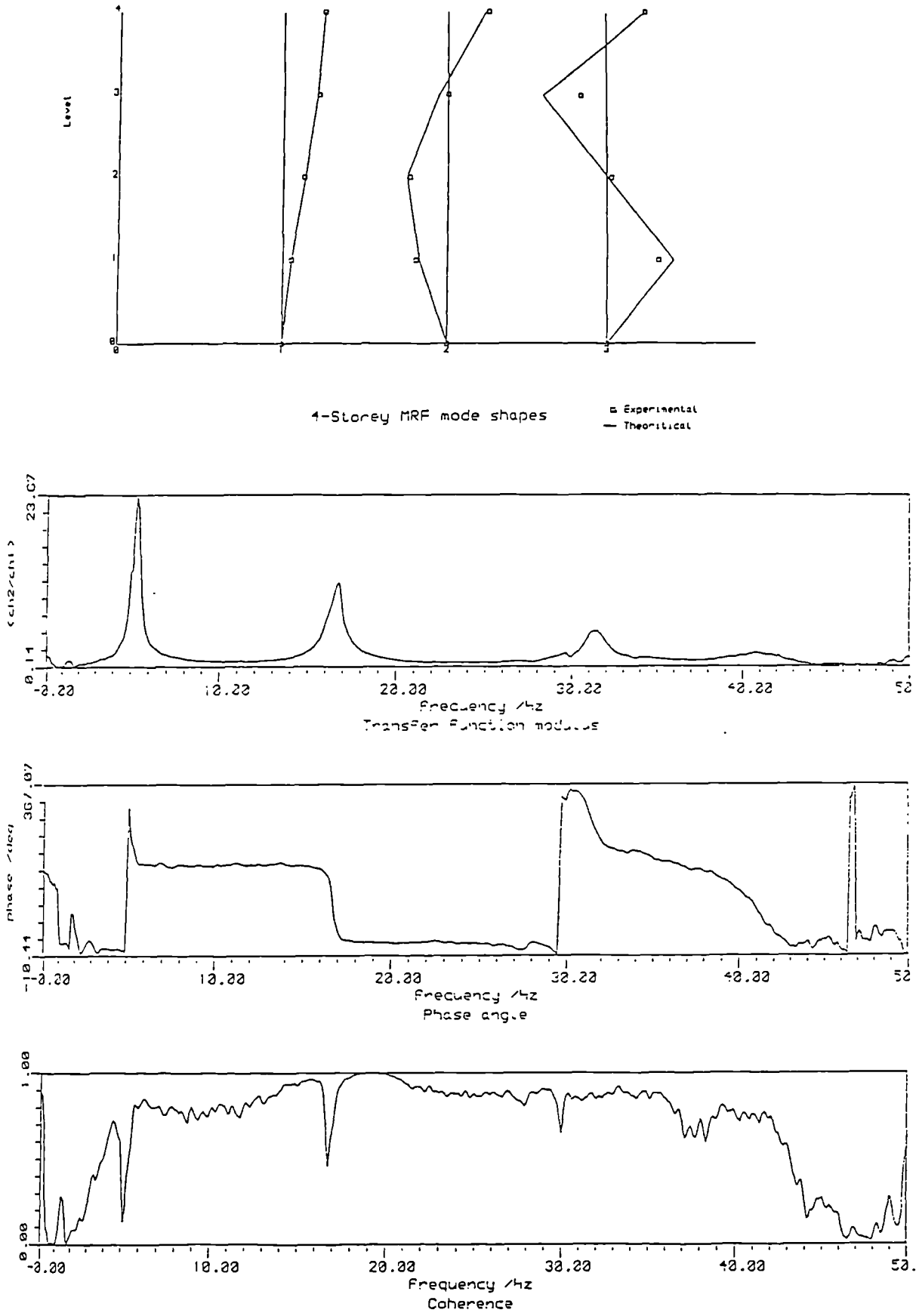

Fig.6.4 Mode shapes and the transmissibility function of the MRF before the seismic testing

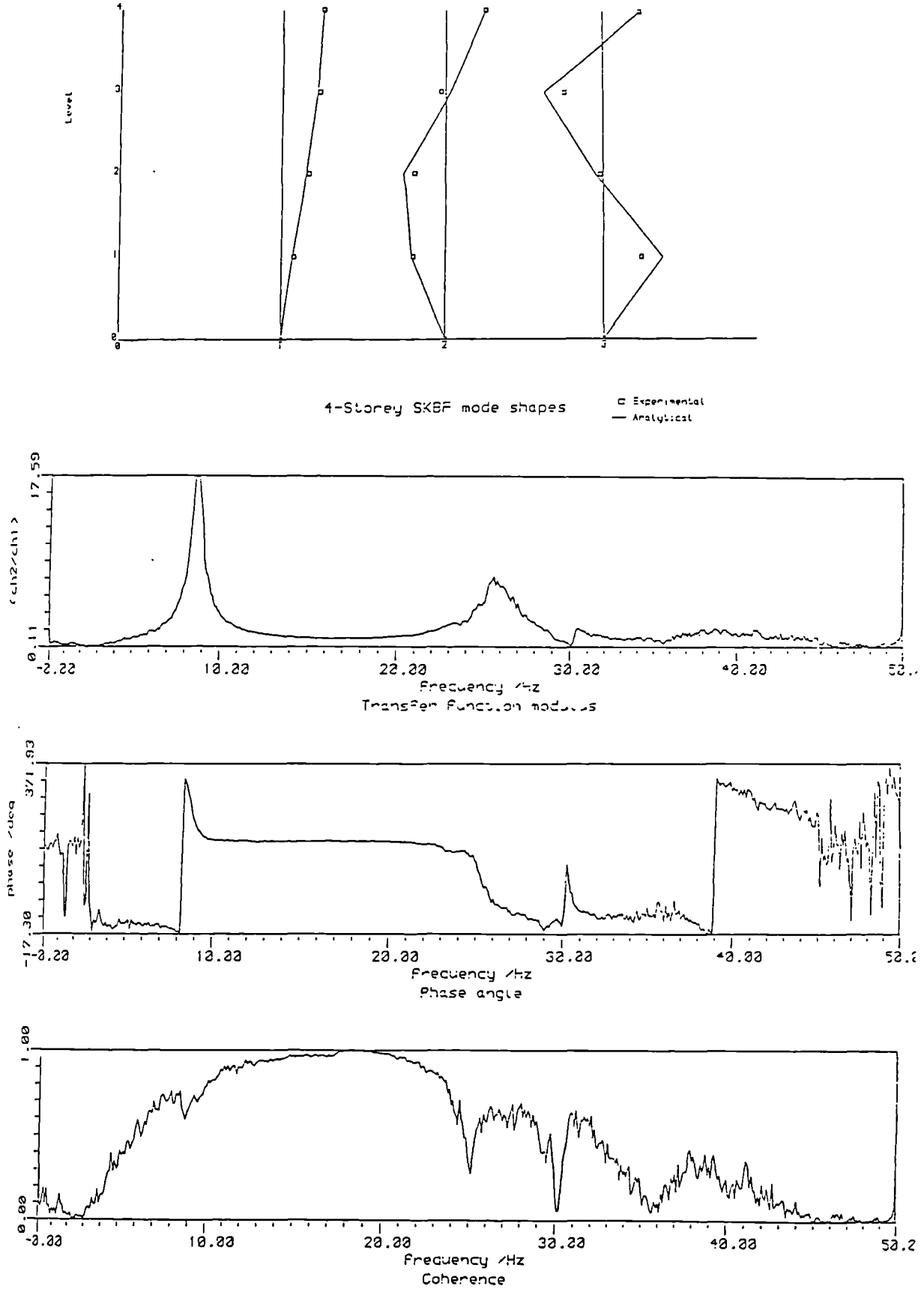

Fig.6.5 Mode shapes and the transmissibility function of the SKBF

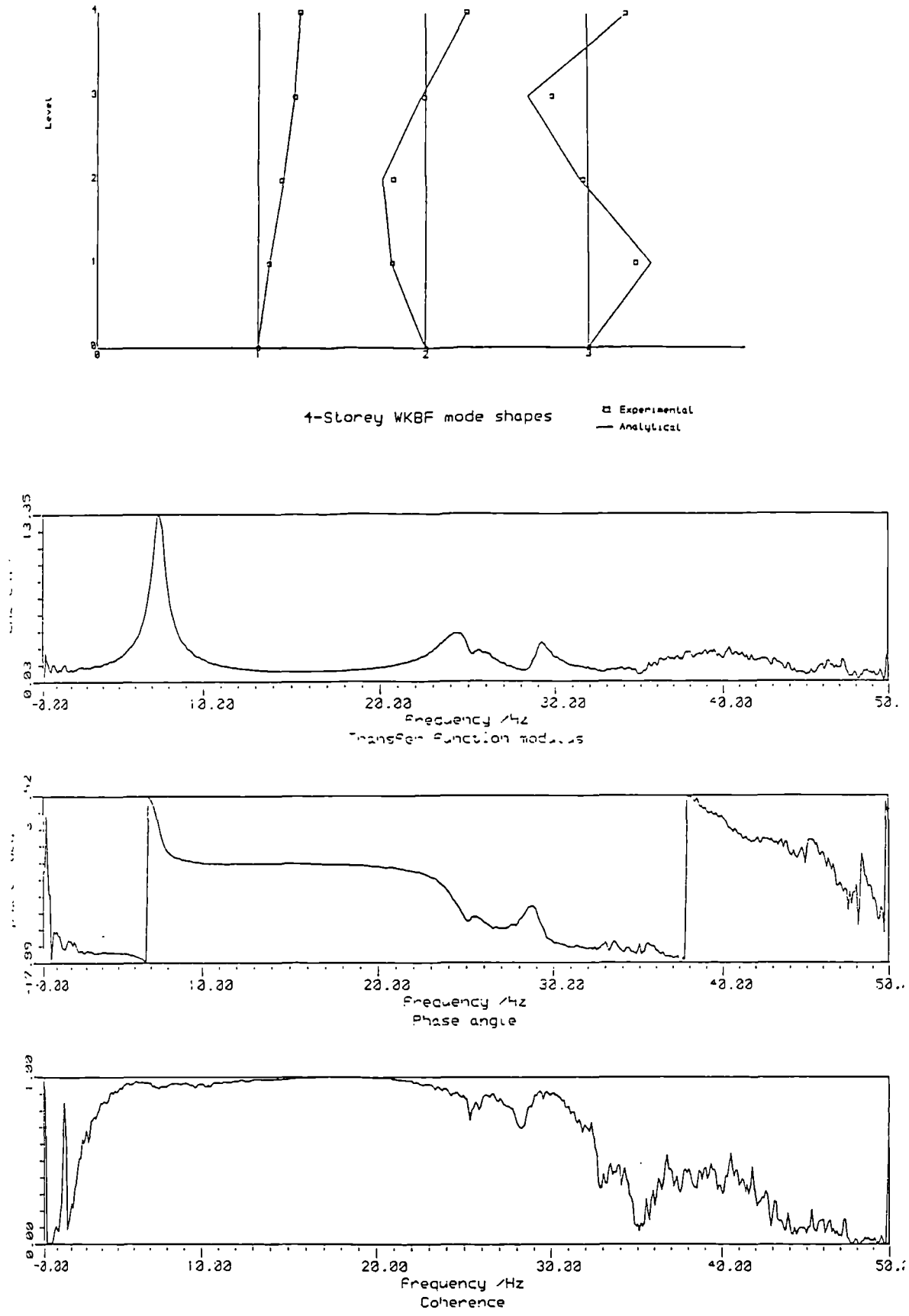

Fig.6.6 Mode shapes and the transmissibility function of the WKBF

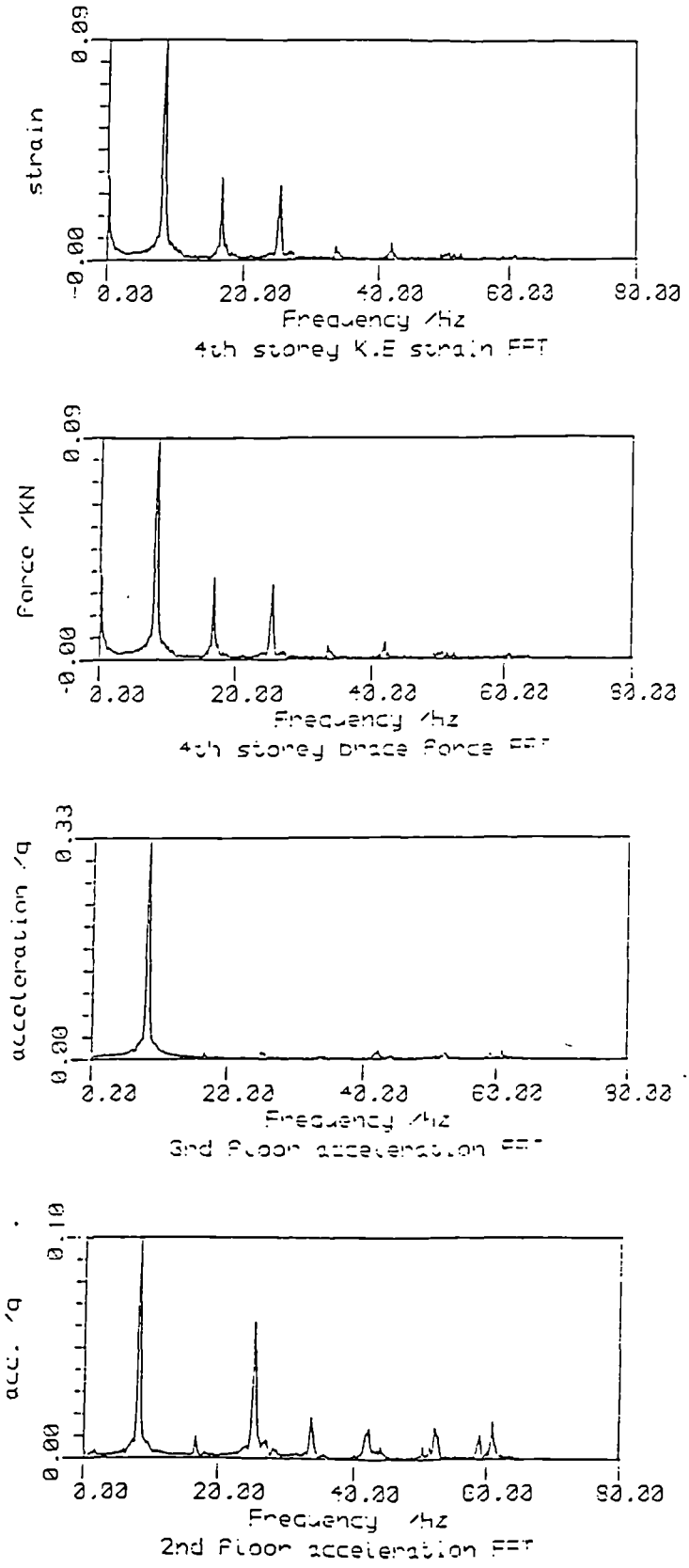

Fig.6.7 Fourier amplitude spectra of the WKBF response to a sine wave excitation

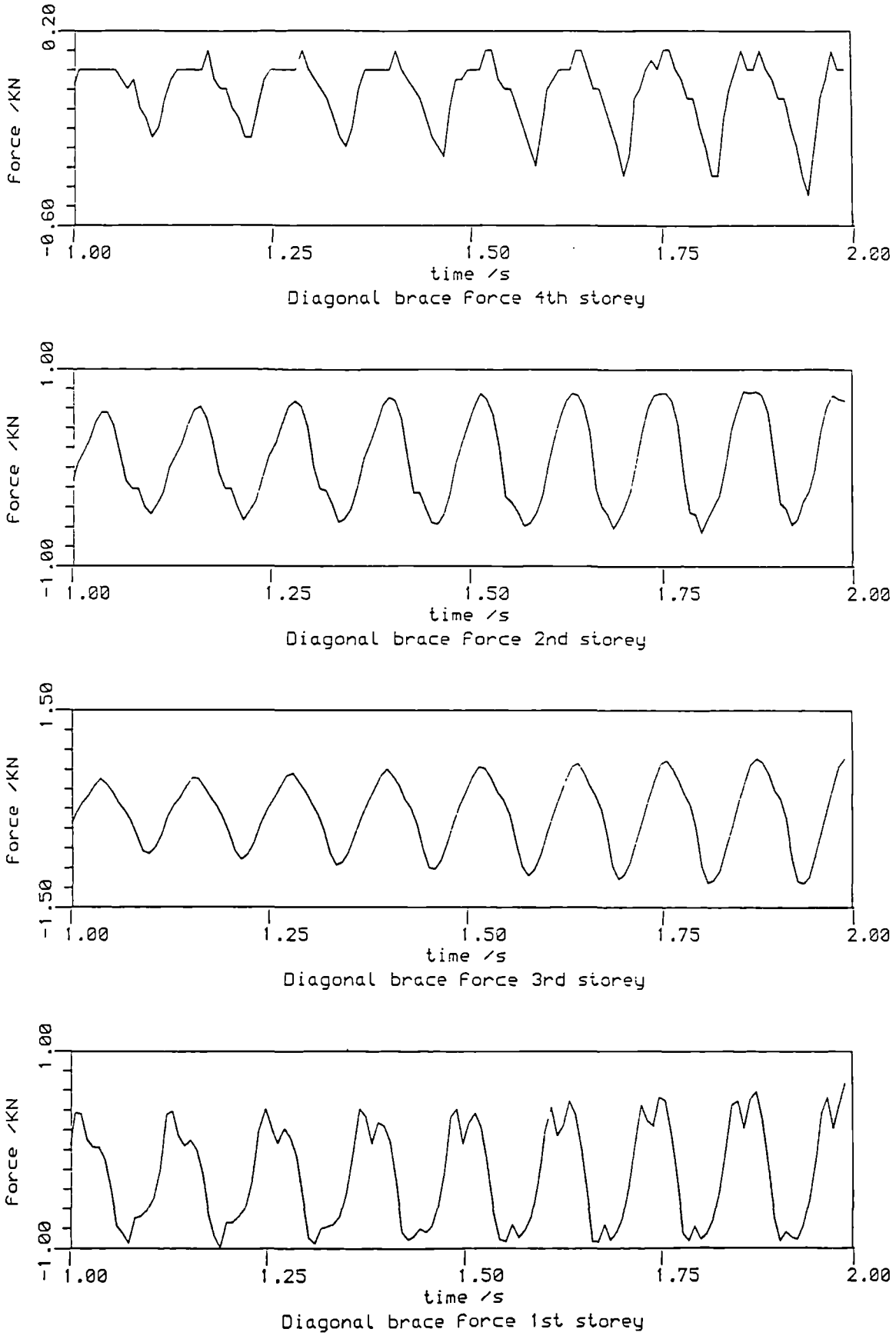

Fig.6.8 Brace force time-histories at low amplitudes

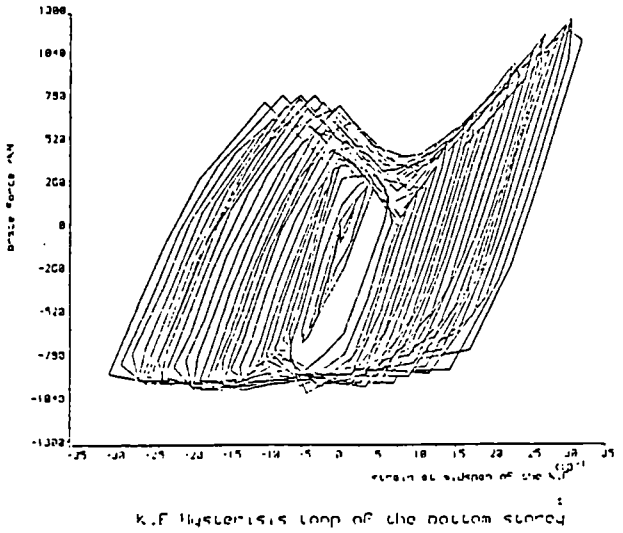

K.E Hysterisis Loop of the bottom storey

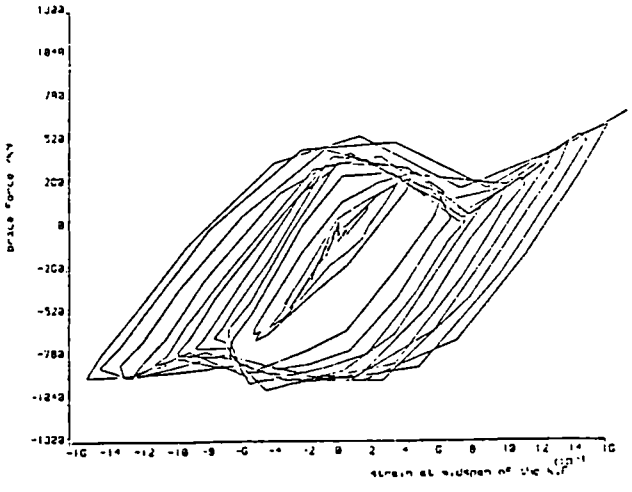

K.E Hysterisis Loop of the bottom storey (0.25sec)

Fig.6.9 Knee element hysterisis loops (SIWK00)

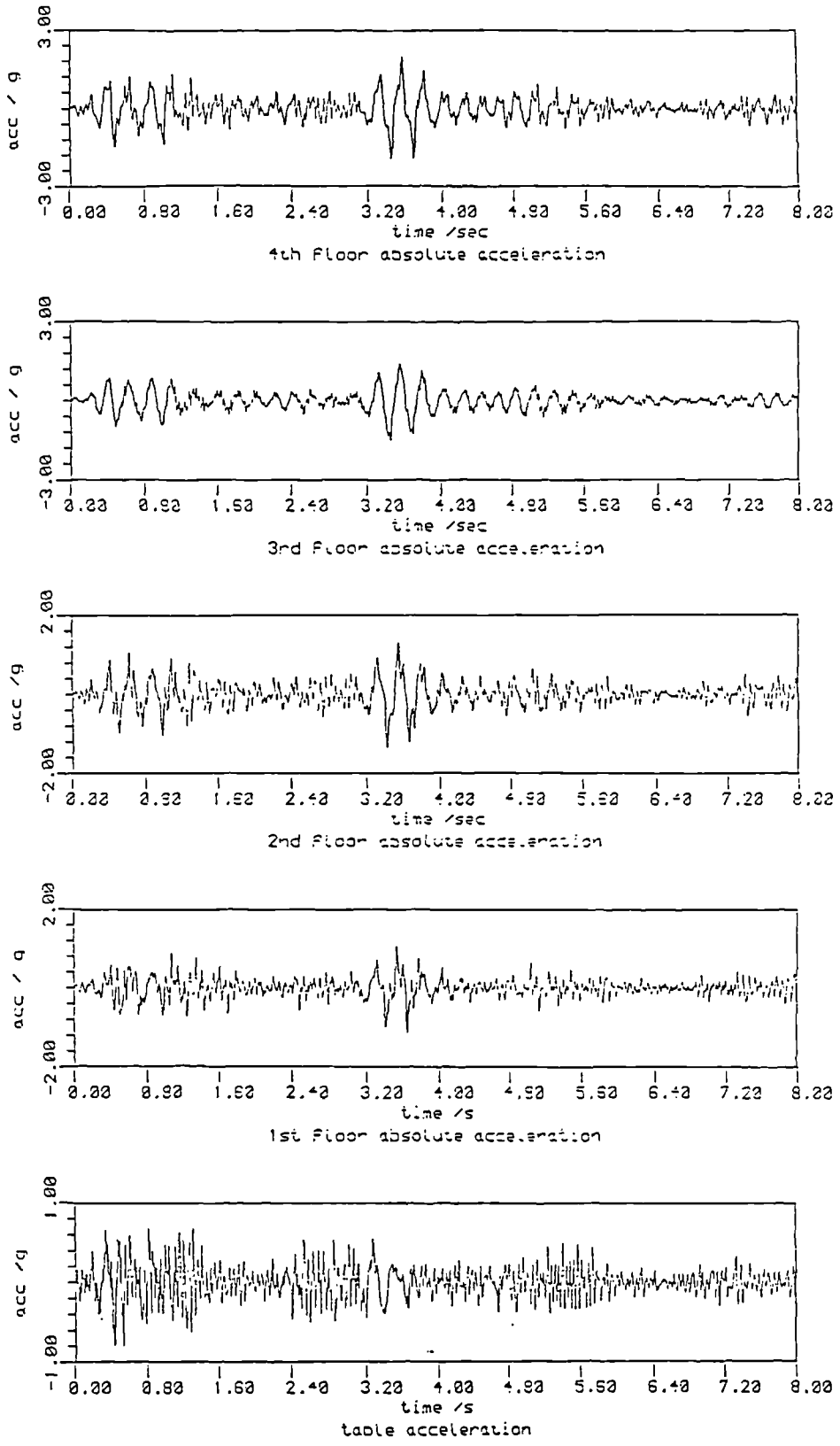

Fig.6.10 Acceleration time-histories recorded during ECMR30 test

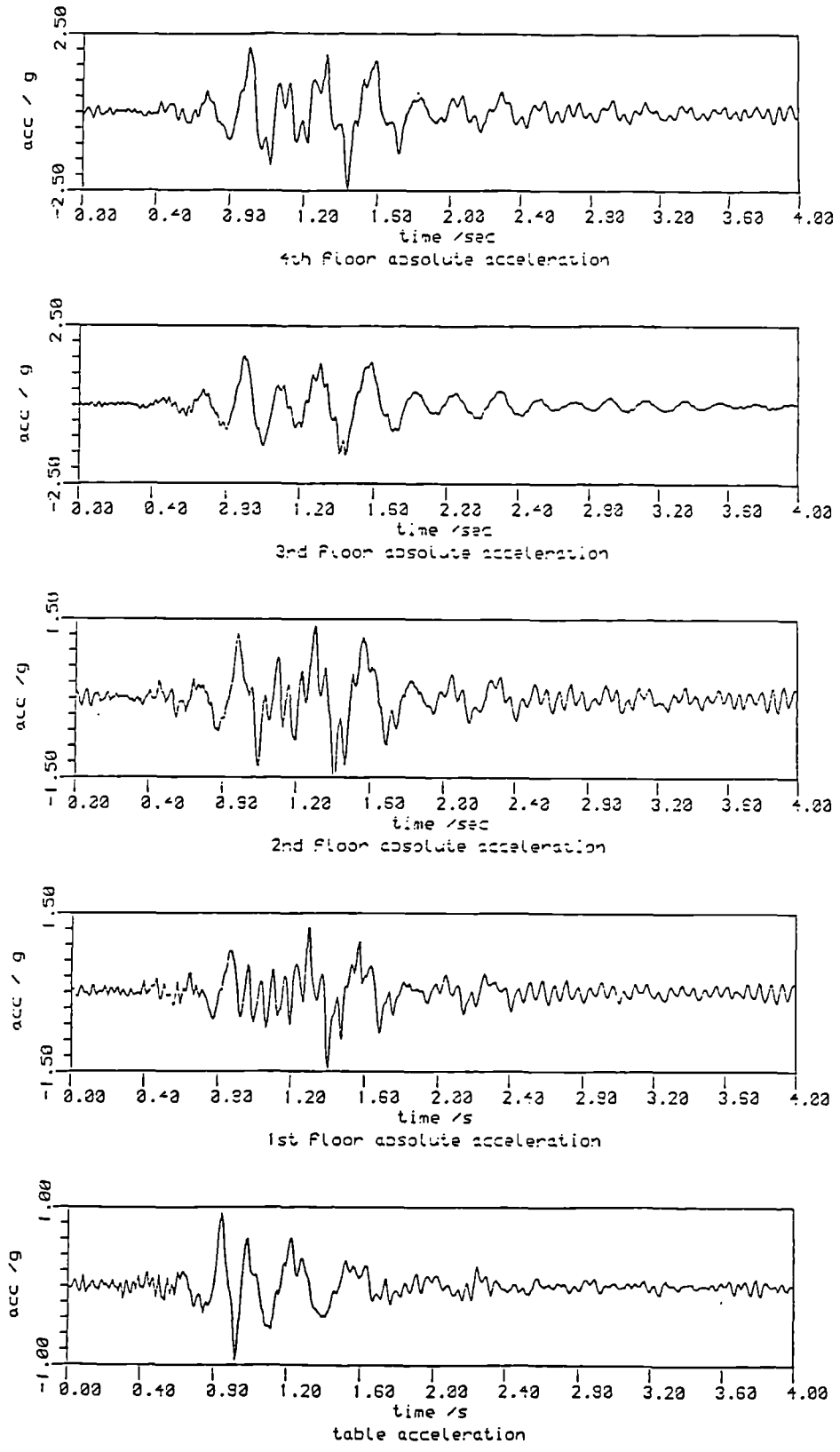

Fig.6.11 Acceleration time-histories recorded during PKMR30 test

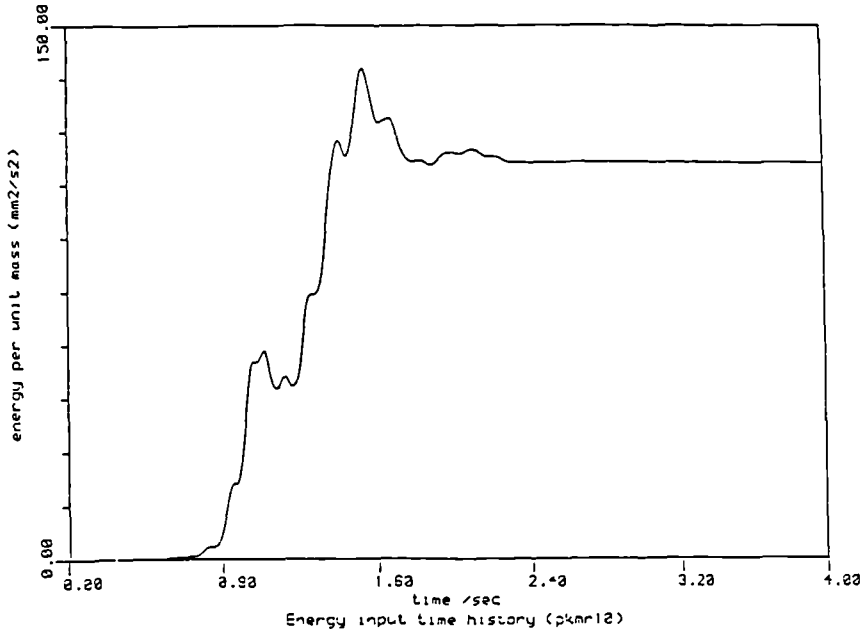

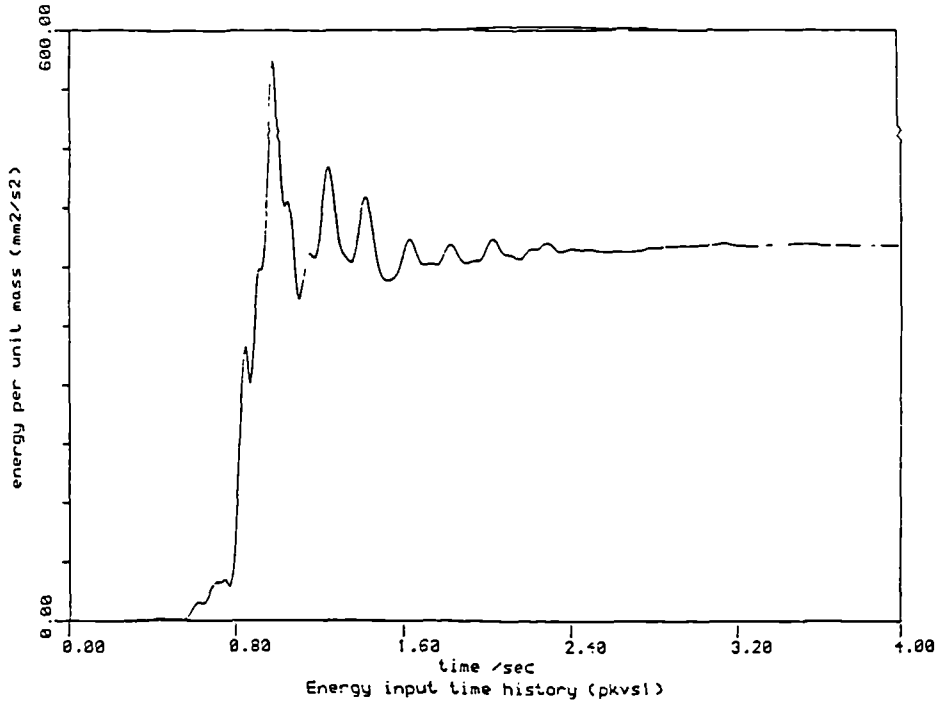

Fig.6.12Energy input time-histories of the MRF and the KBFs

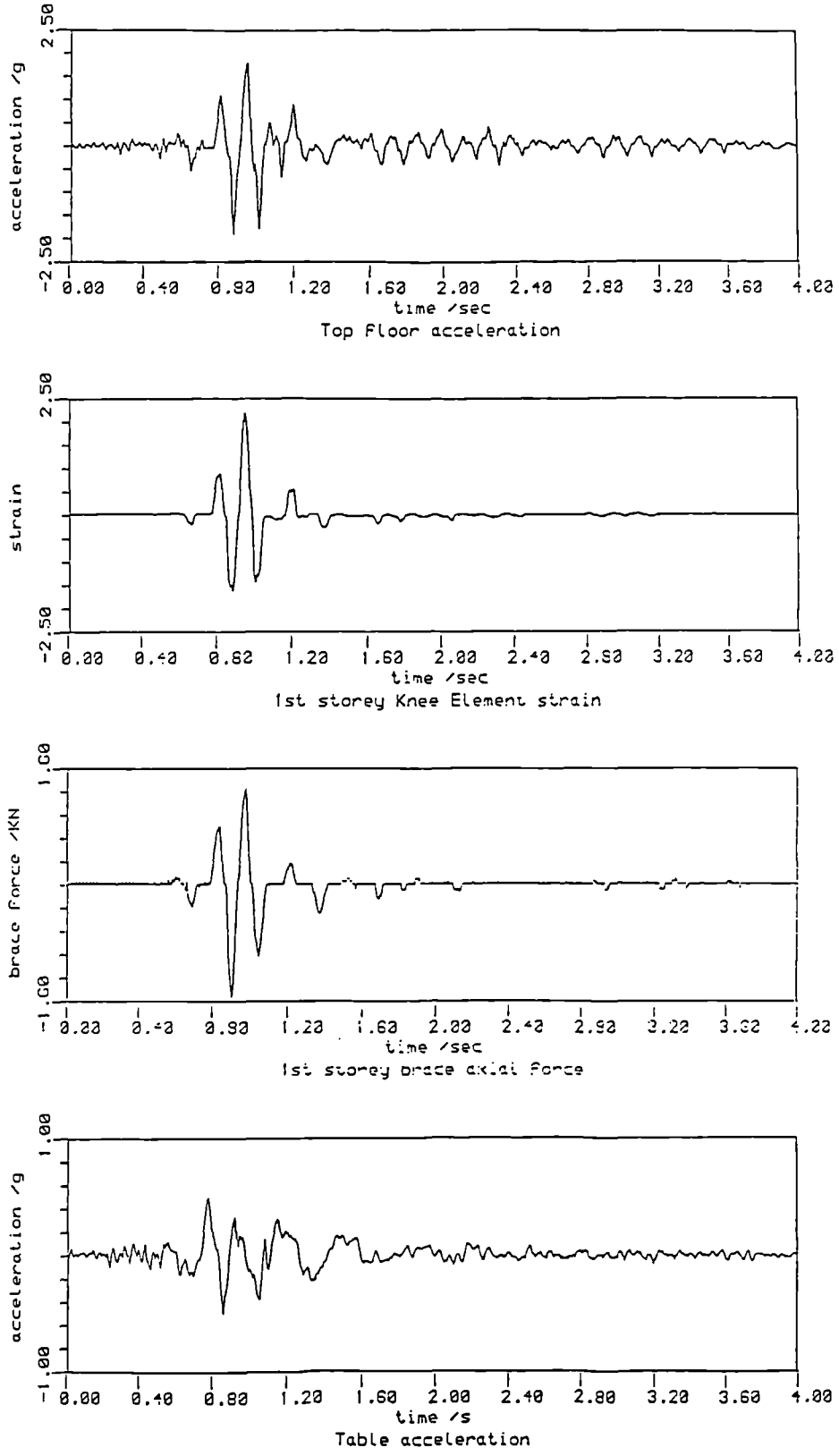

Fig.6.13 Time-history responses of PKSK10 test

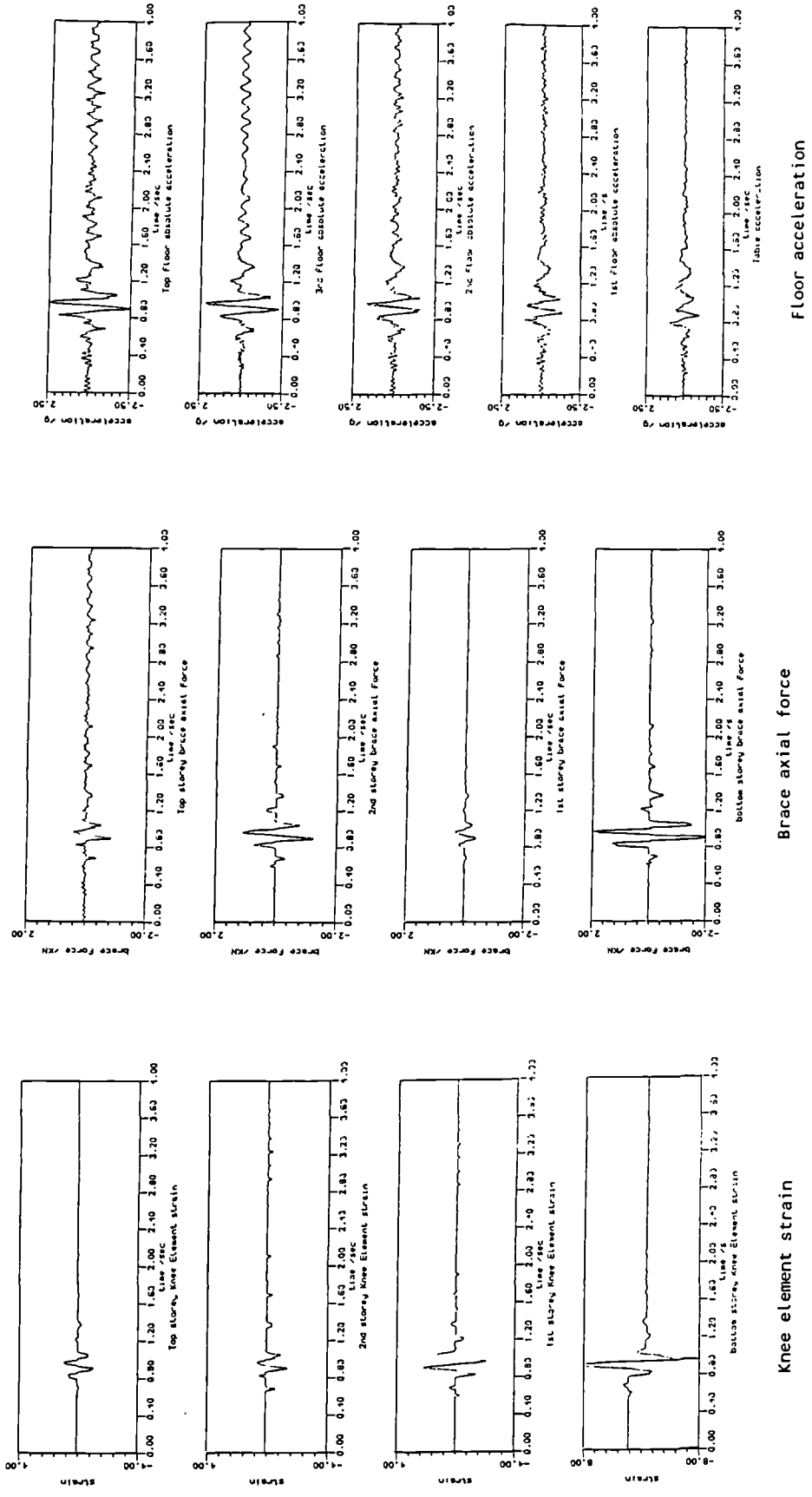

Fig.6.14 Time-history responses of PKWK30 test

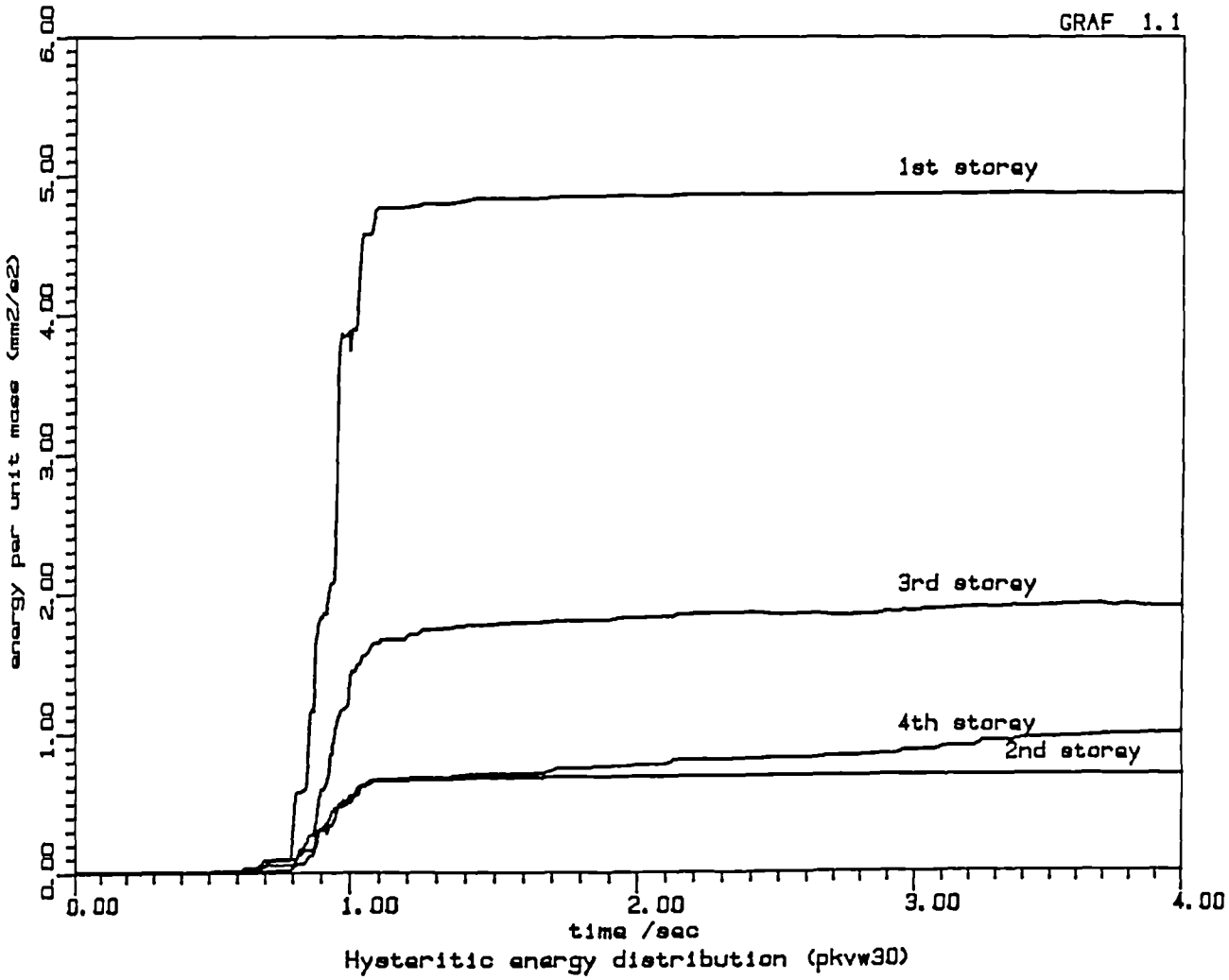

Fig.6.15 Hysteritic energy distribution through the height (PKWK30)

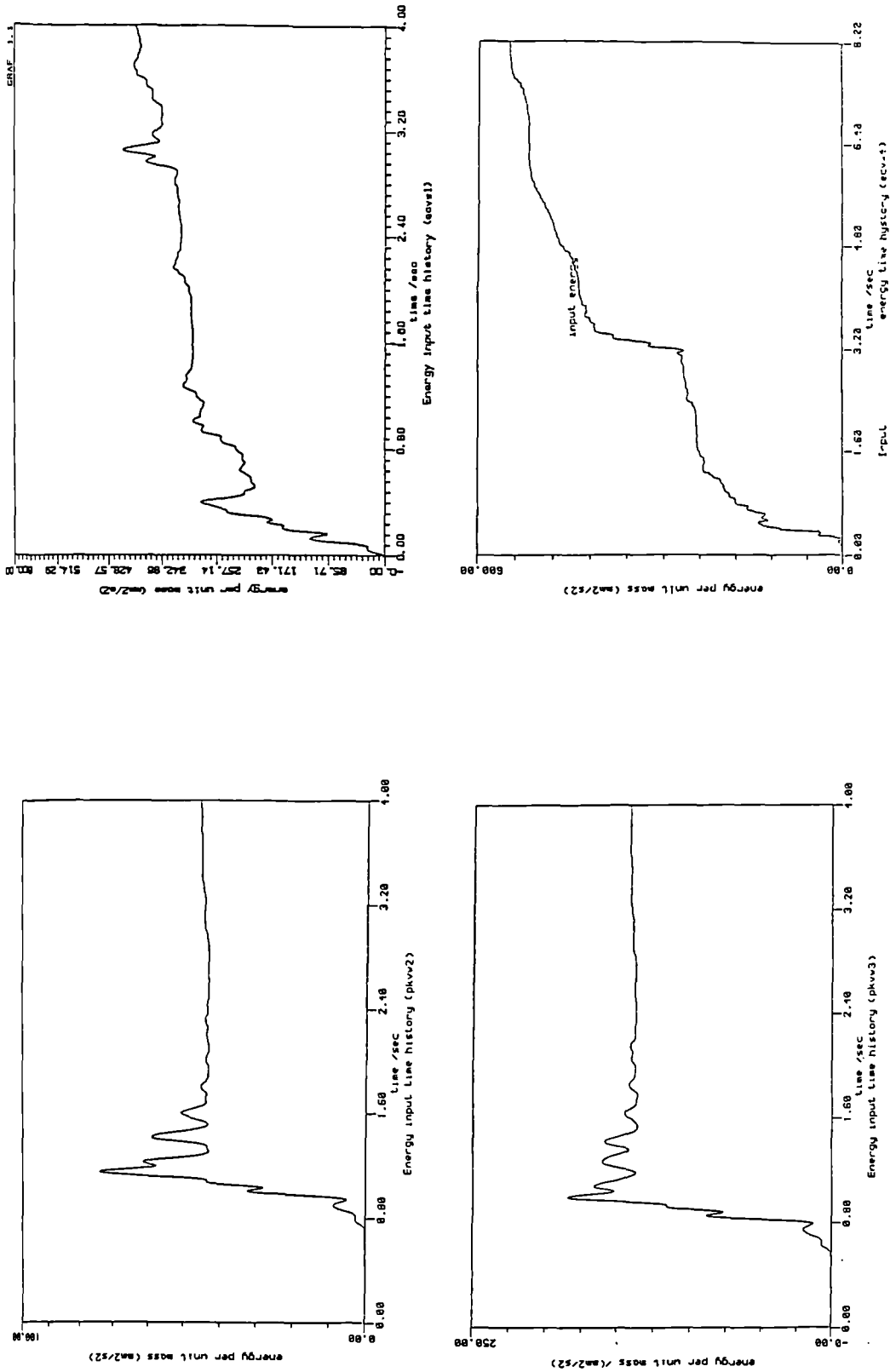

Fig.6.16 Effect of the hysteretic damping on the input energy

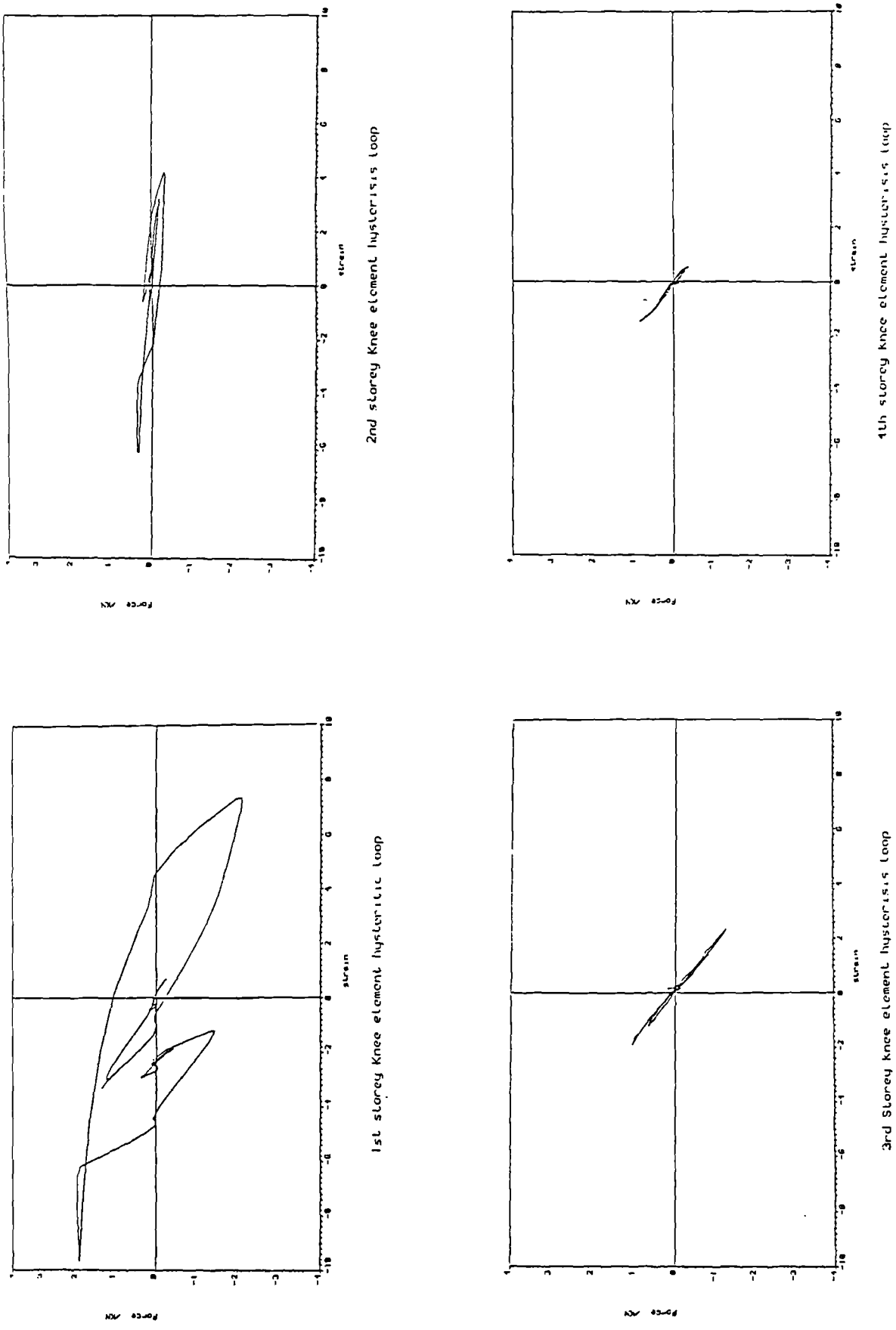

Fig.6.17 Hysterisis loops resulting from PKWK30 test

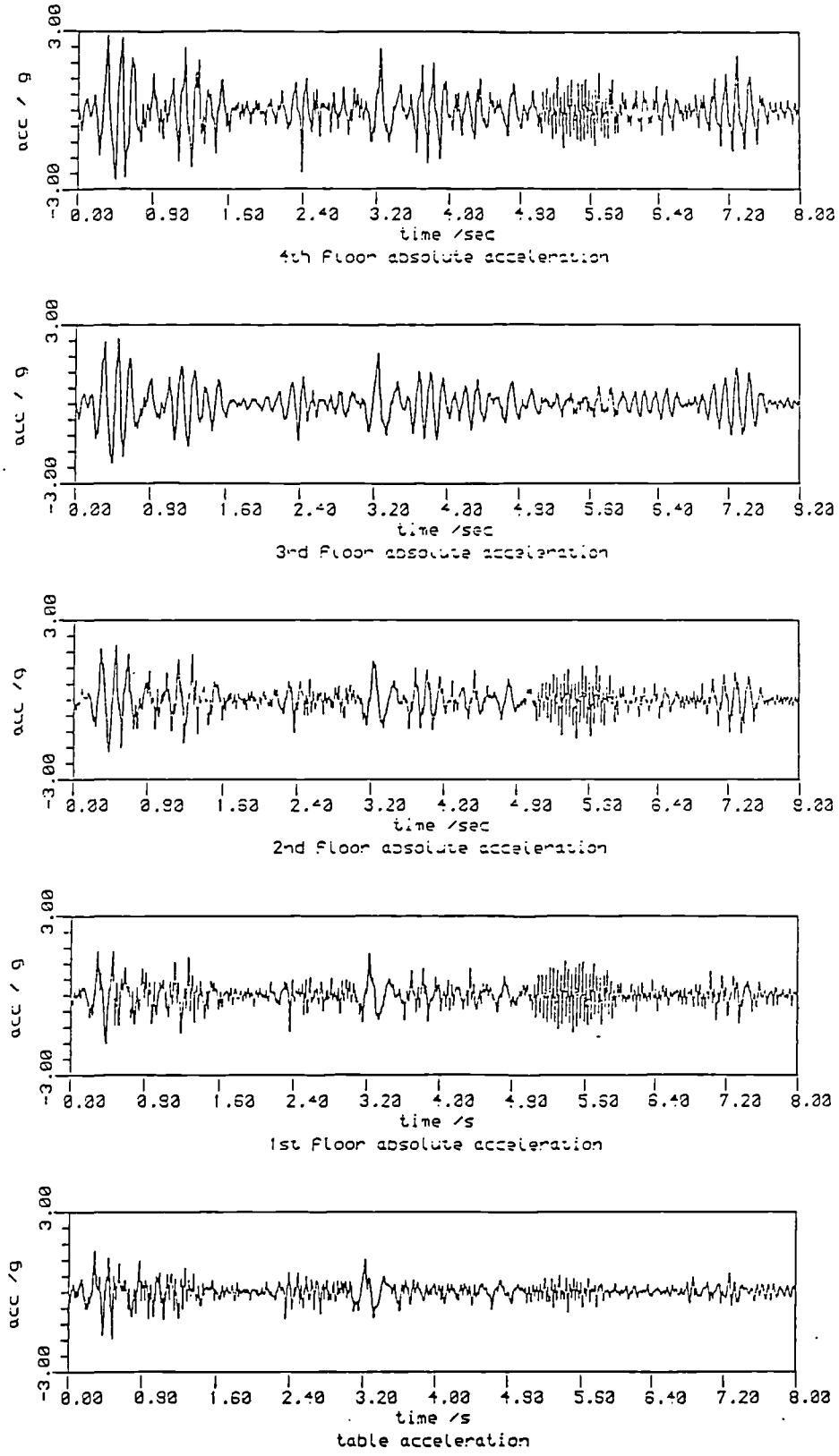

Fig.6.18 Acceleration time-histories of ECVW40 test

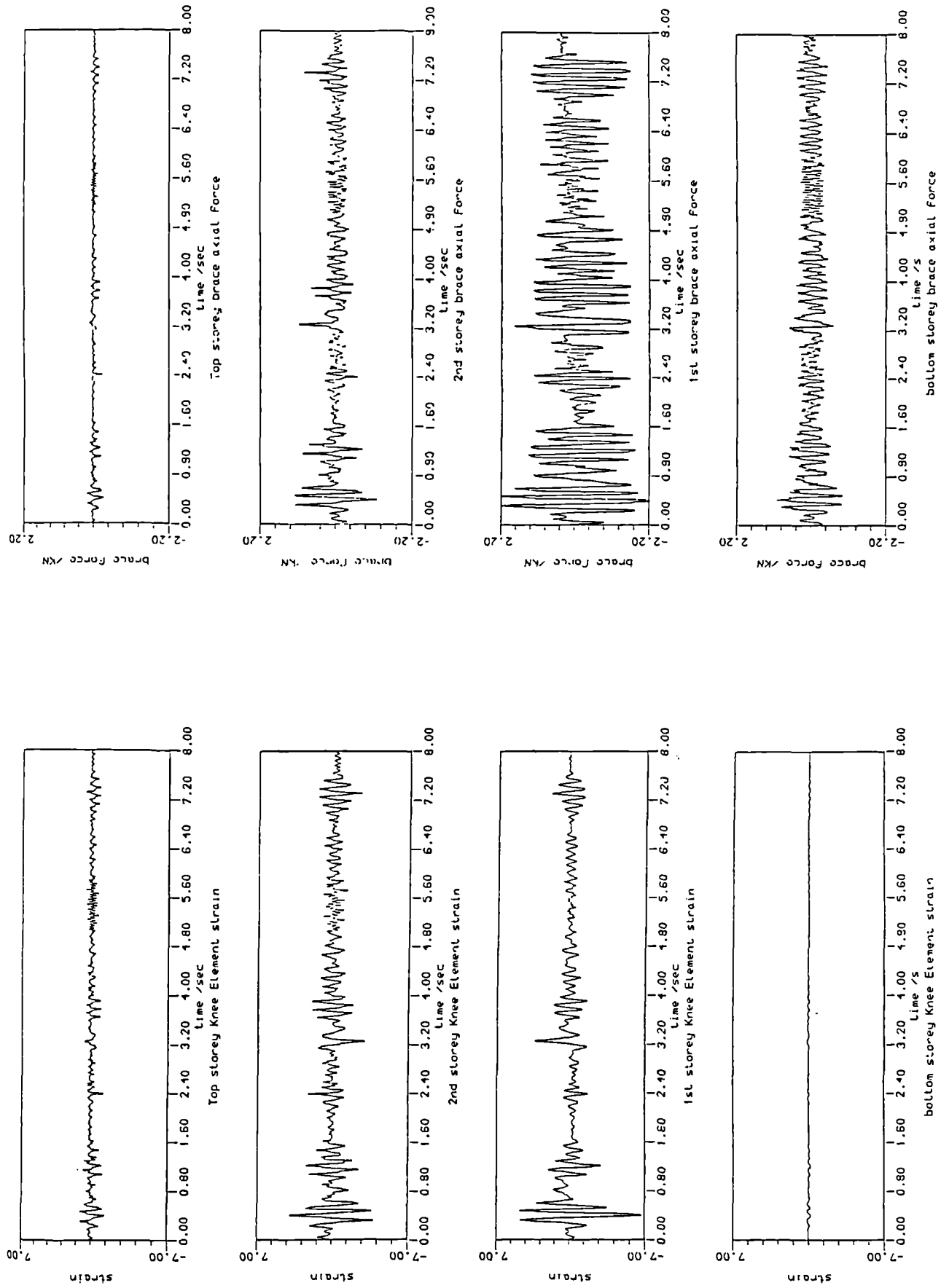

Fig.6.19 Time-histories of the brace force and Knee element strain of ECVW40 test

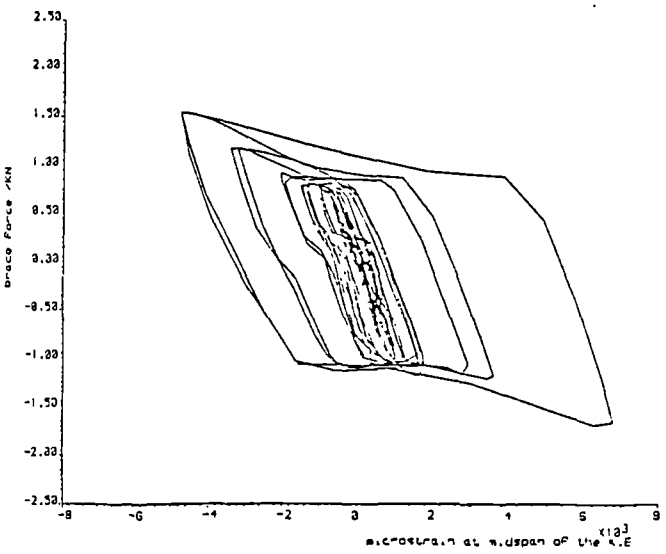

K.E Hysterisis loop of the 2nd storey

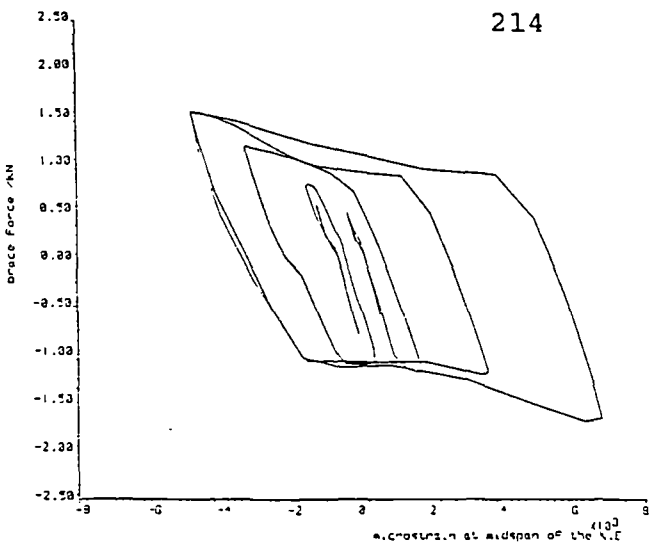

K.E Hysterisis loop of the 2nd storey (0-1sec)

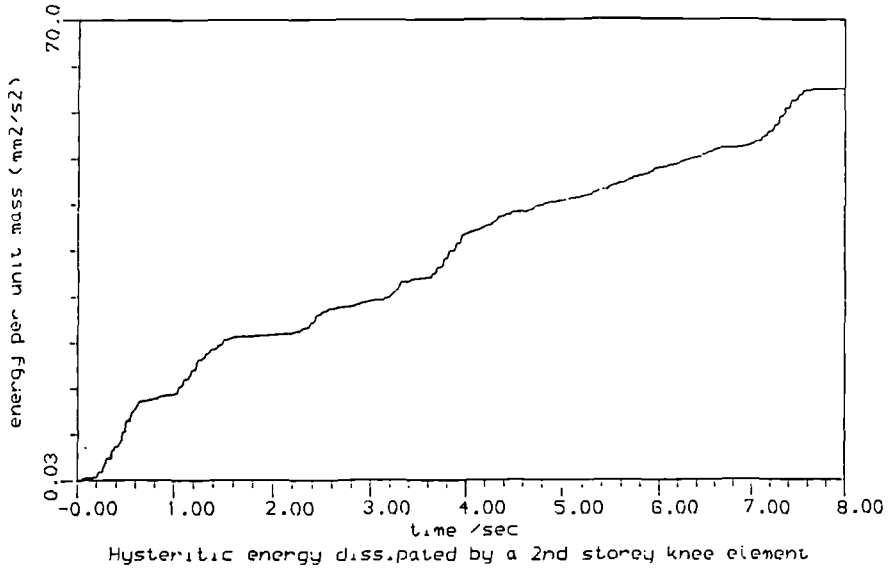

Hysteritic energy dissipated by a 2nd storey knee element

Fig.6.20 Hysterisis loops and time-history of the hysteritic energy of ECVW40 test

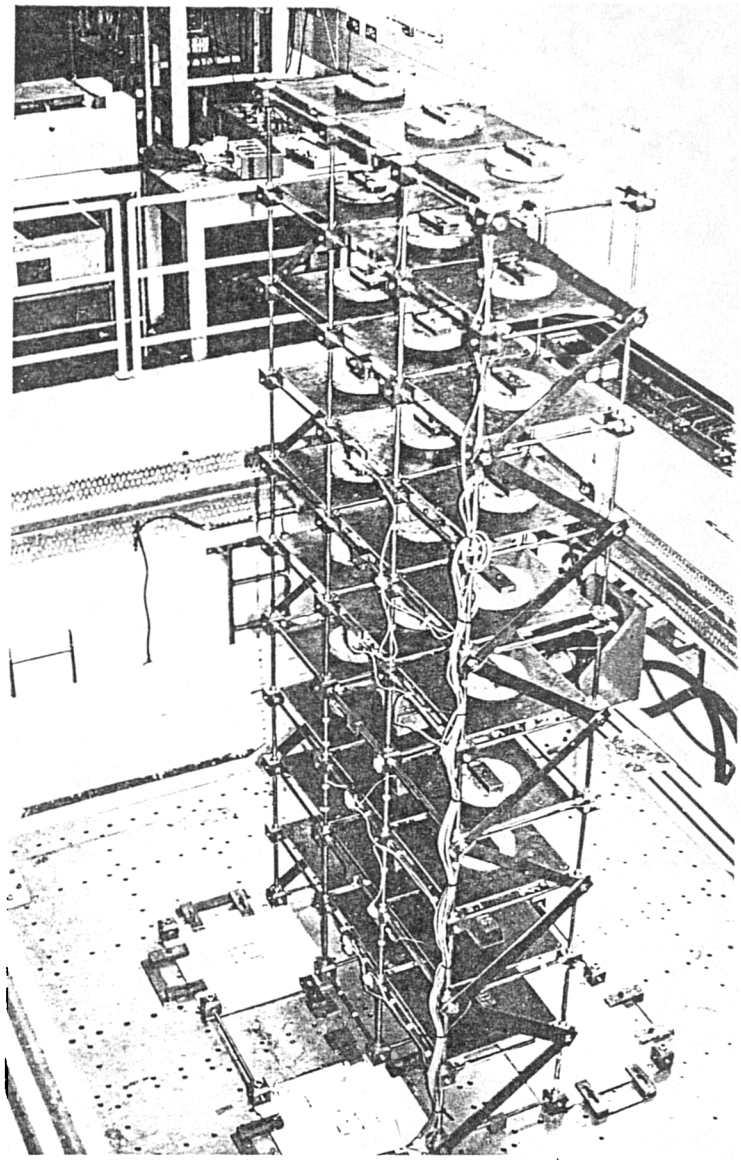

Fig.6.21 Ten-storey frame of test series II

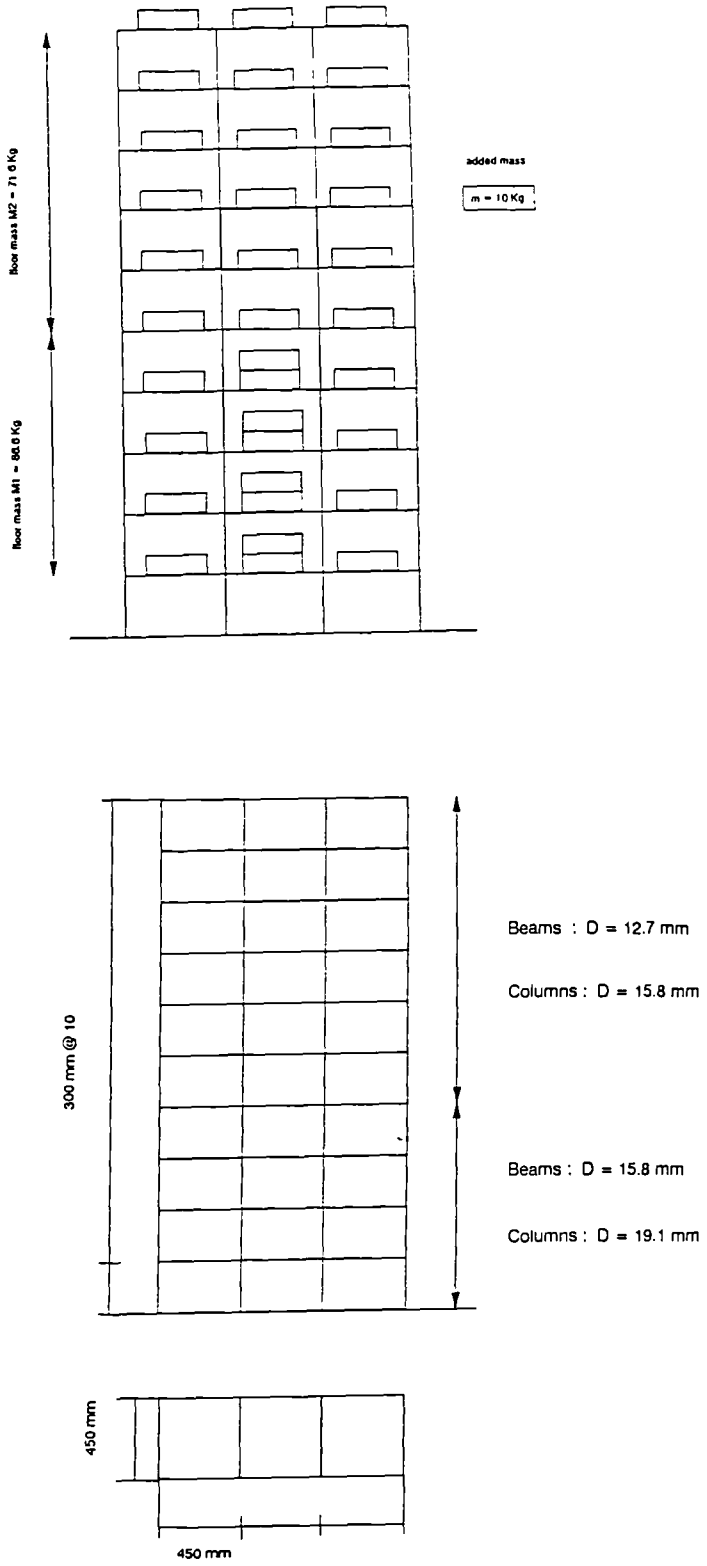

Fig.6.22 Mass distribution of the ten-storey structure

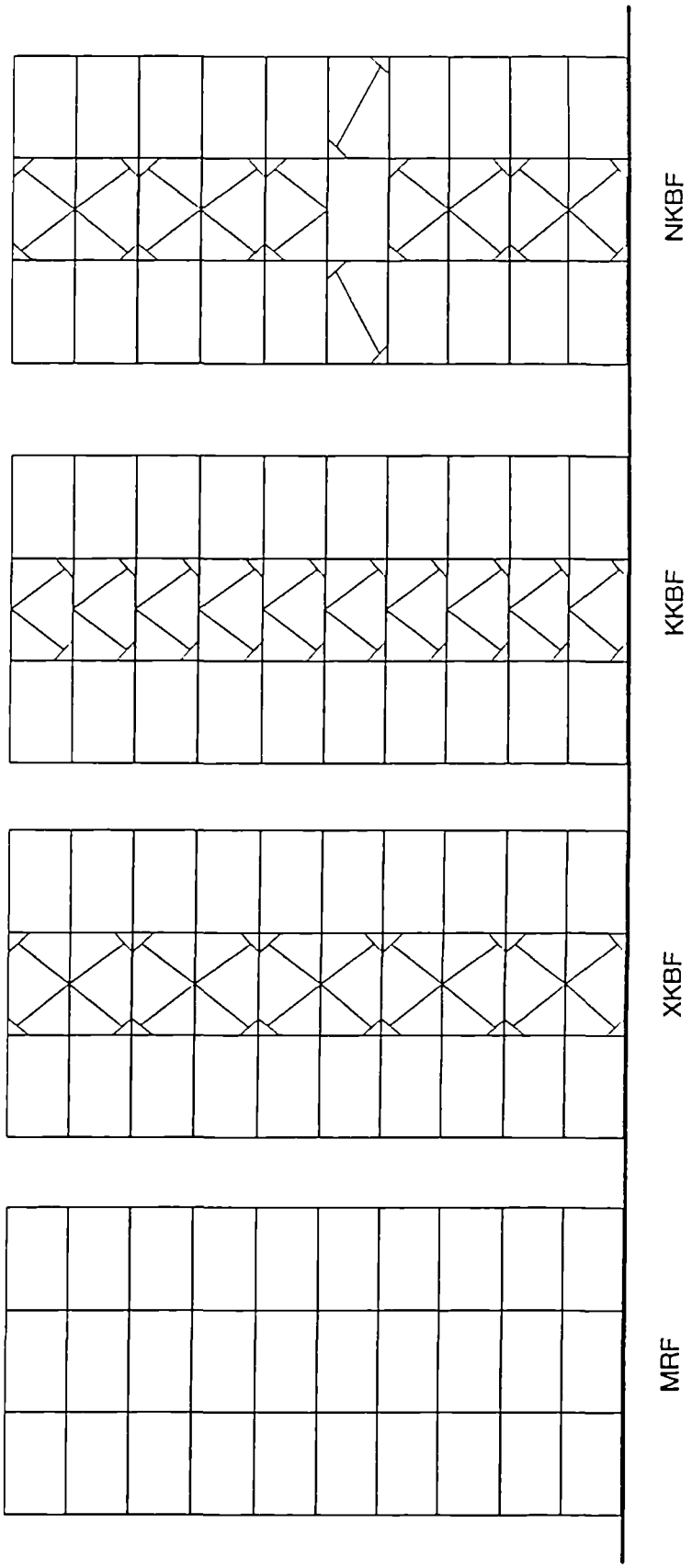

Fig.6.23 Frame configurations of the ten-storey frames

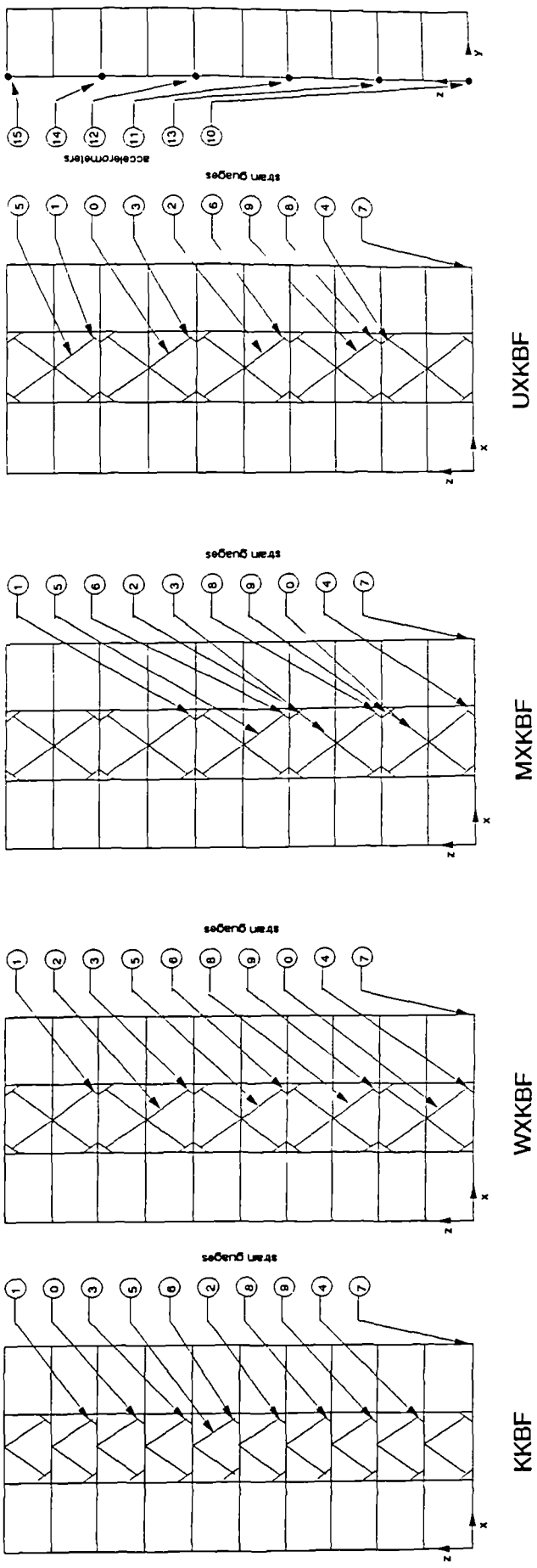

Fig.6.24 Sensors locations on the ten-storey frames

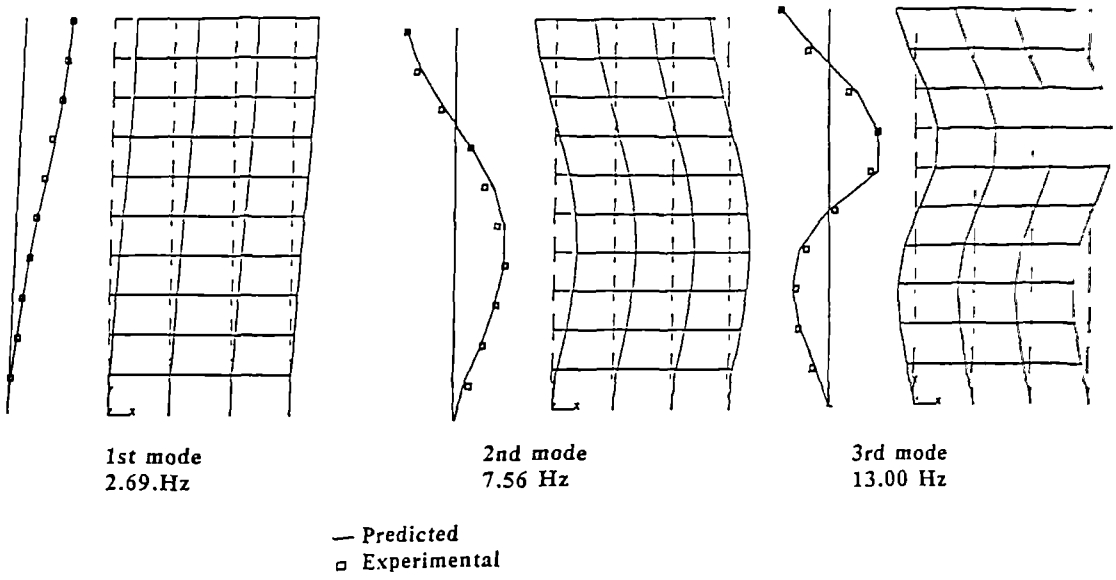

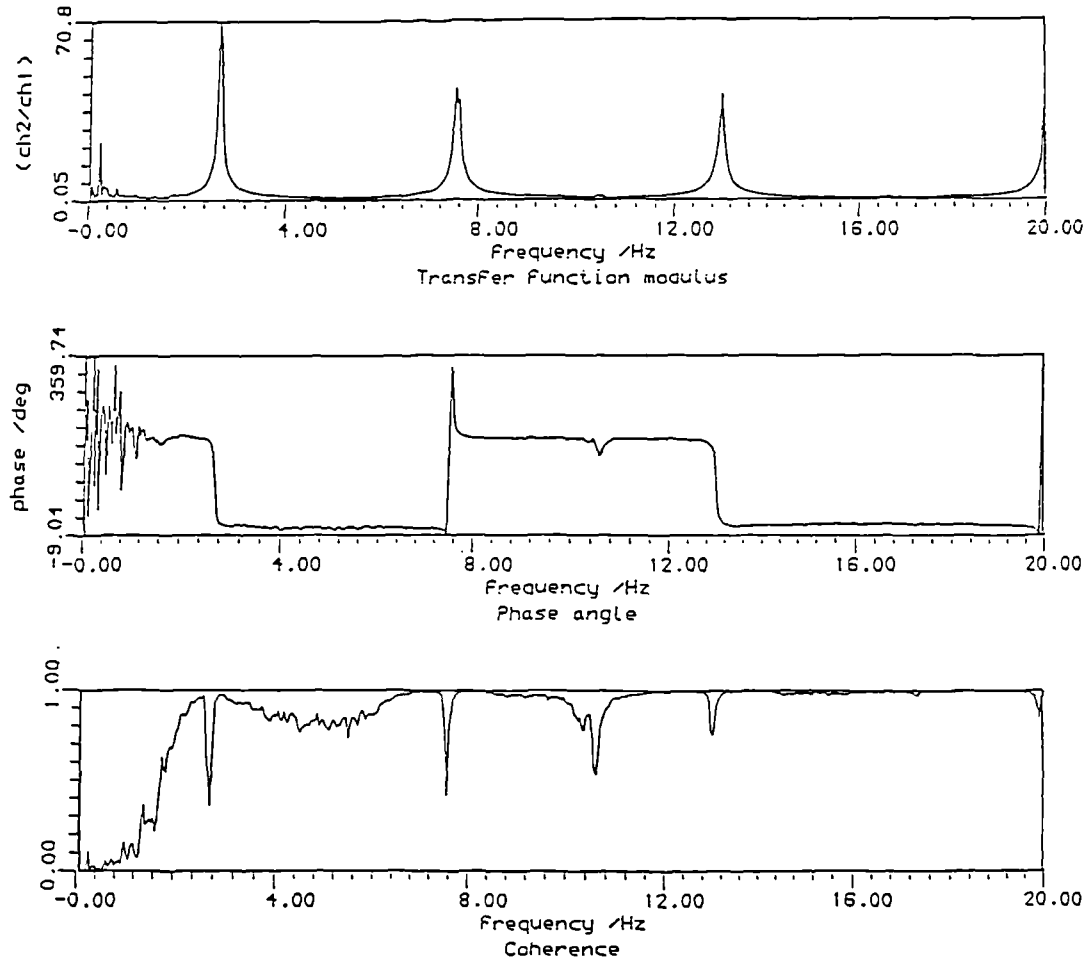

Fig.6.25 Transmissibility function and mode shapes of the MRF

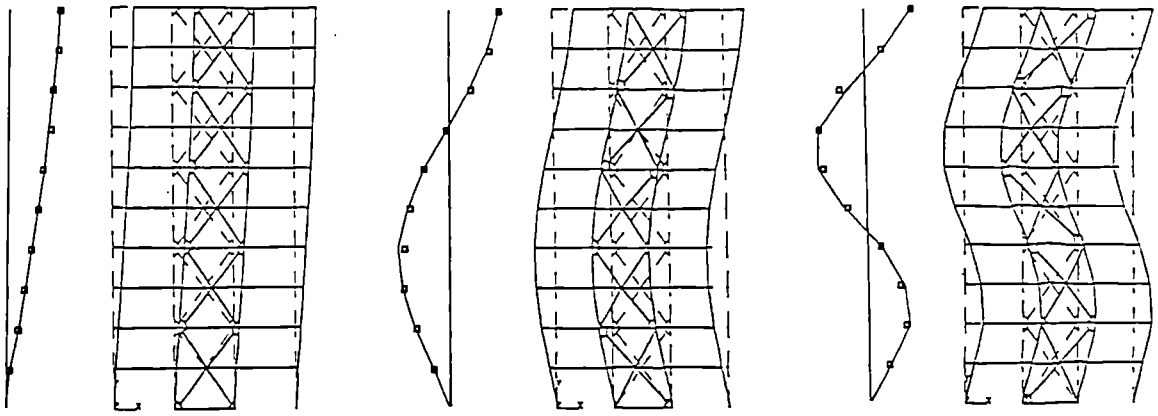

1st mode
5.00Hz

2nd mode
16.75 Hz

3rd mode
30.20 Hz

— Predicted
□ Experimental

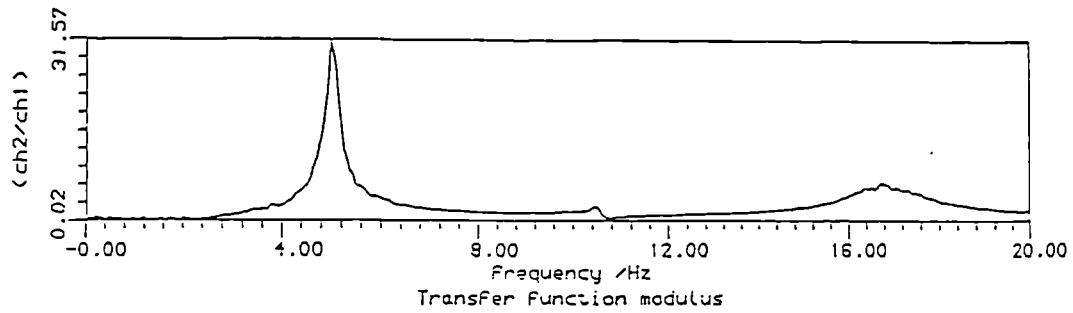

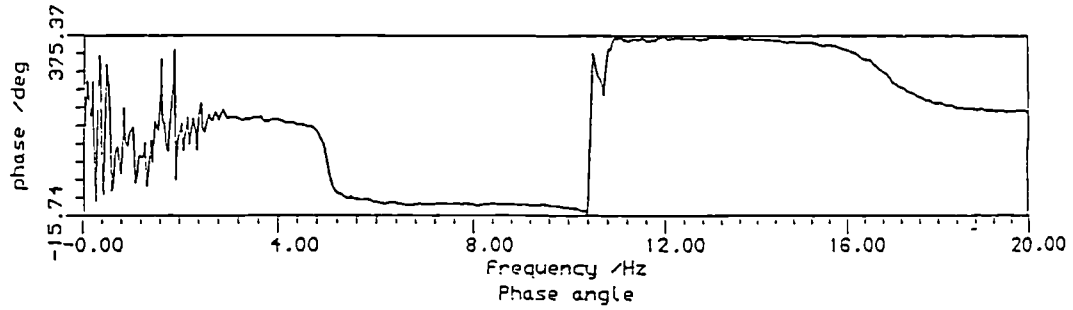

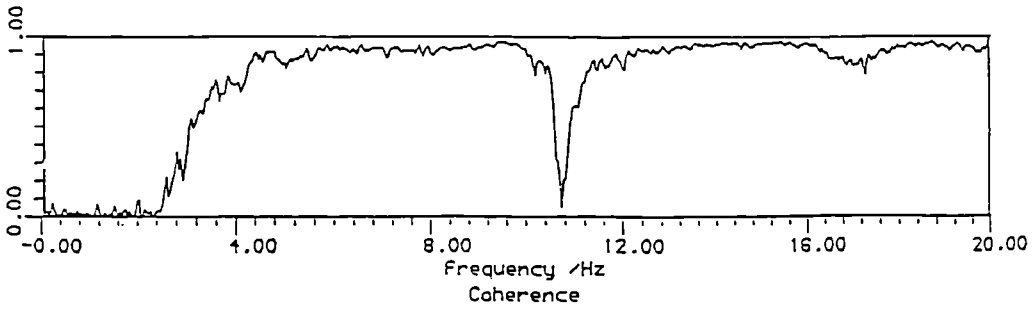

Fig.6.26 Transmissibility function and mode shapes of the XKBF

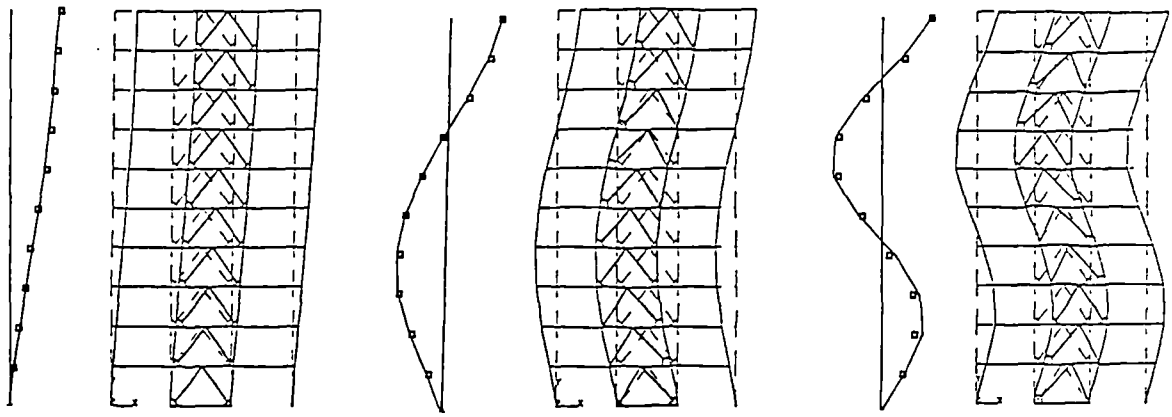

1st mode
5.04Hz

2nd mode
14.45 Hz

3rd mode
28.30 Hz

— Predicted
□ Experimental

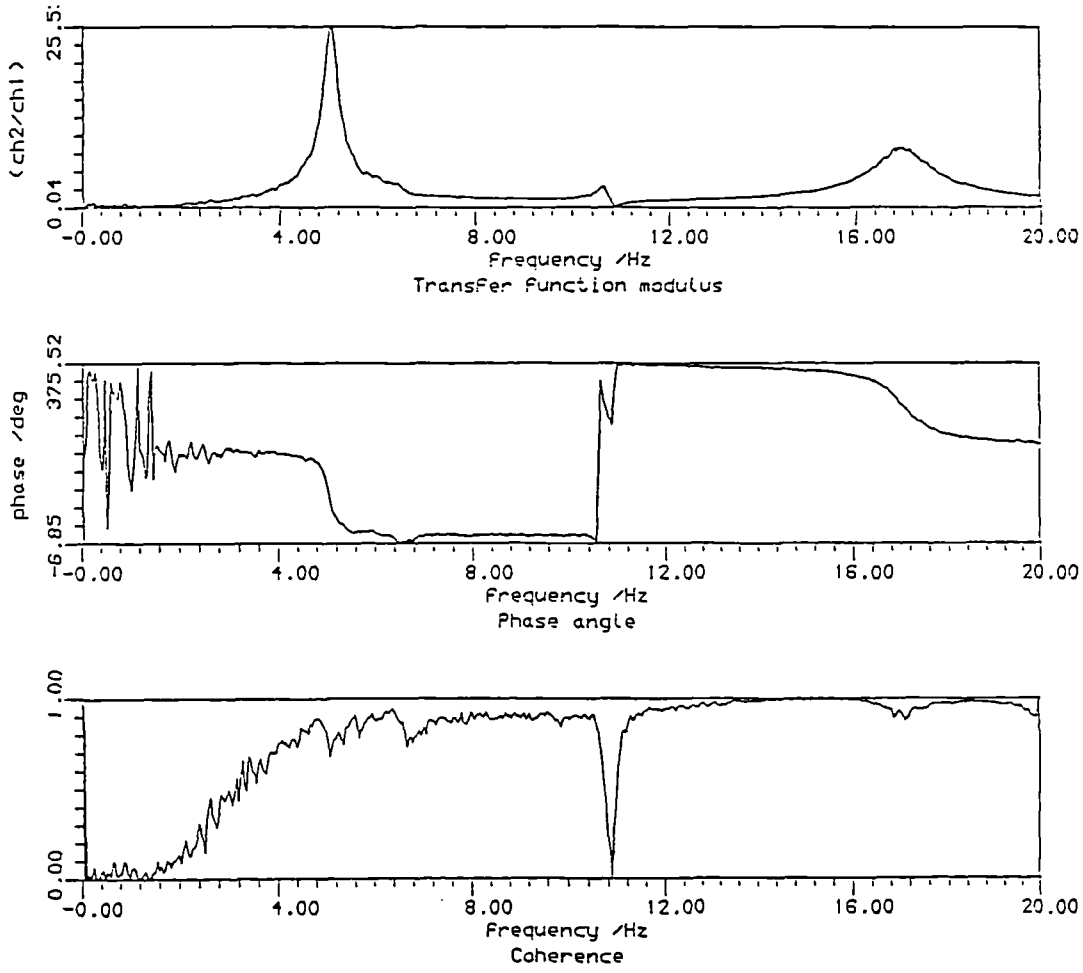

Fig.6.27 Transmissibility function and mode shapes of the KKBF

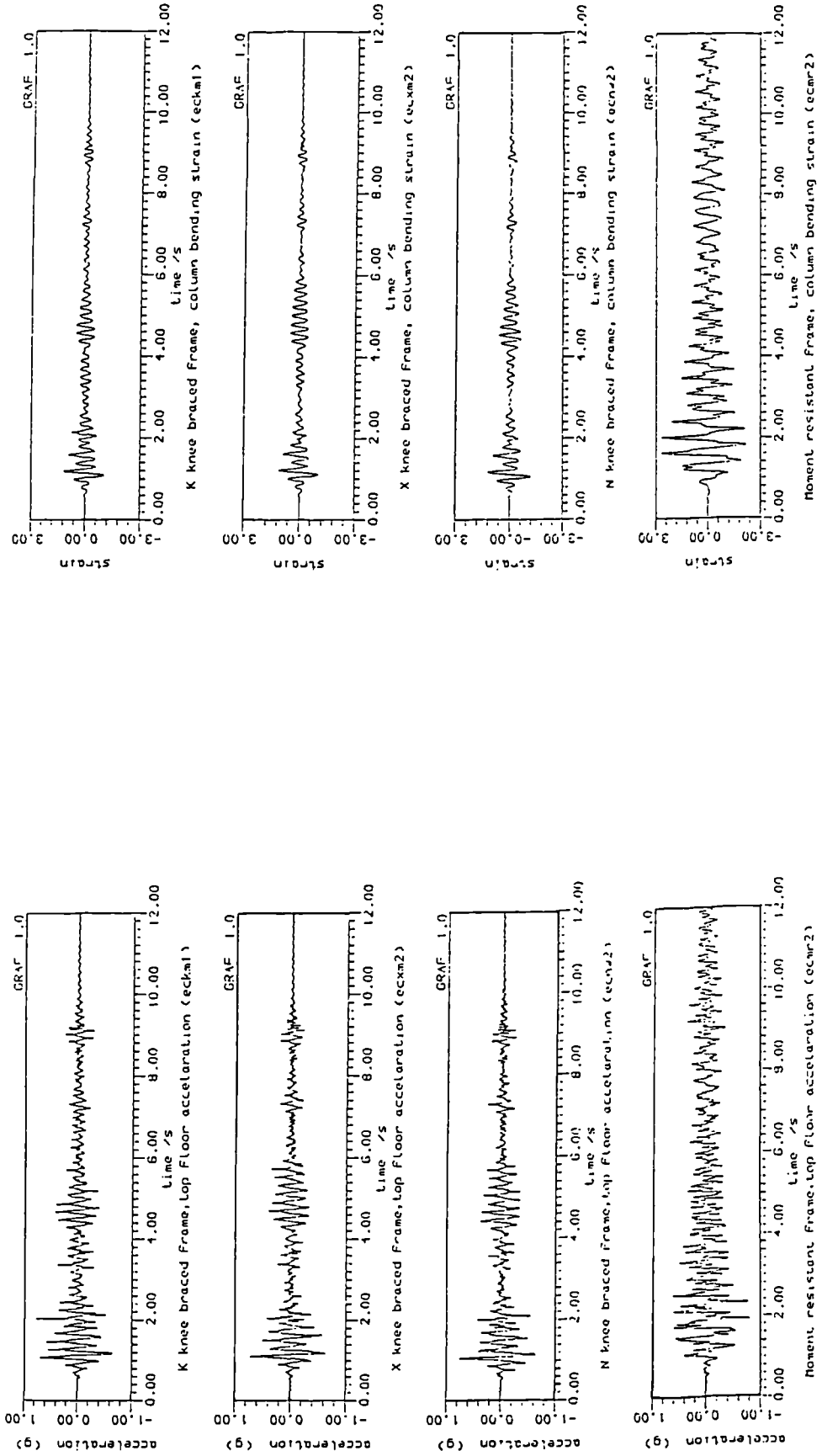

Fig.6.28 Responses of the Different configurations to El-Centro earthquake

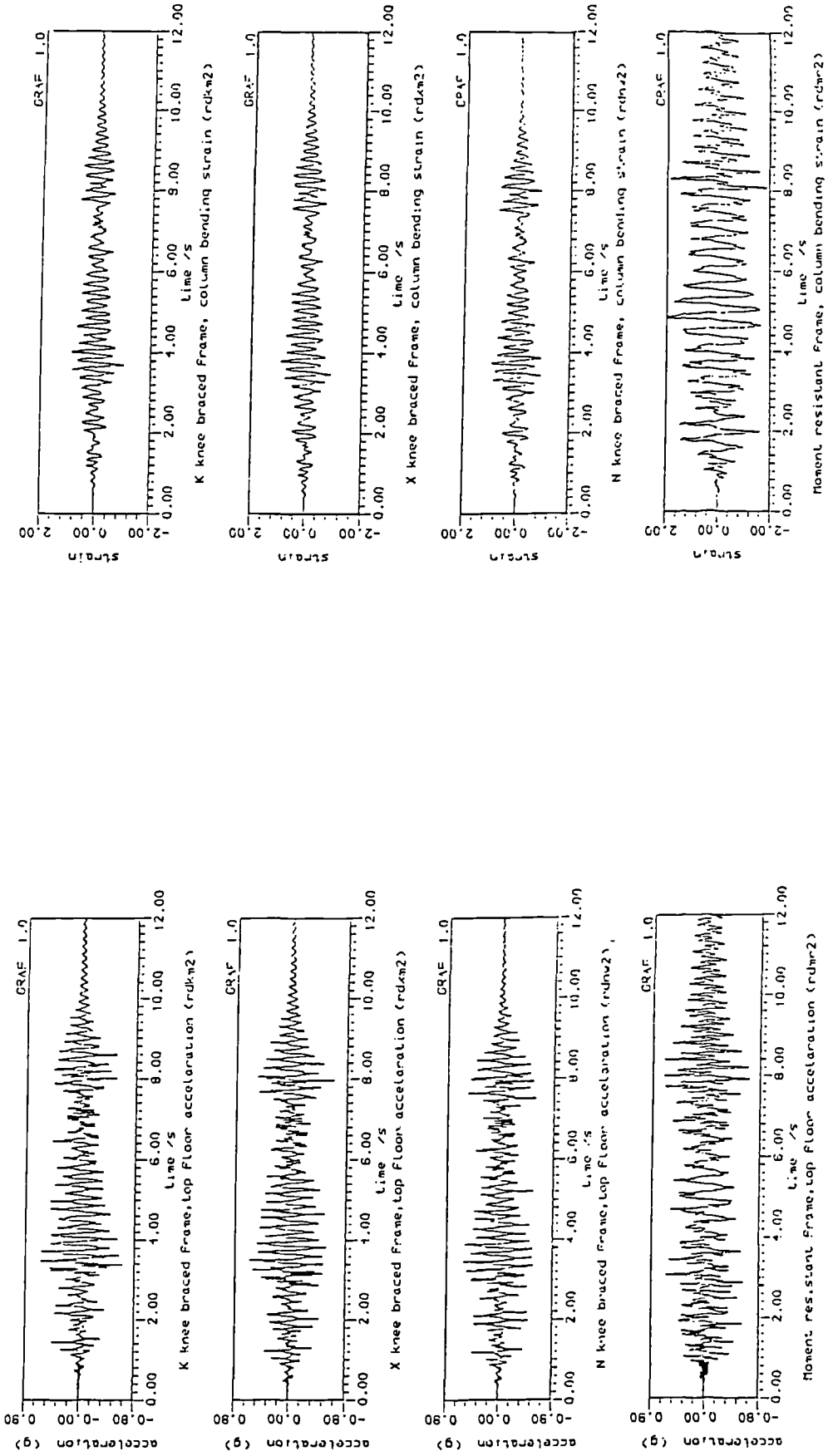

Fig.6.29 Responses of the Different configurations to white noise motion

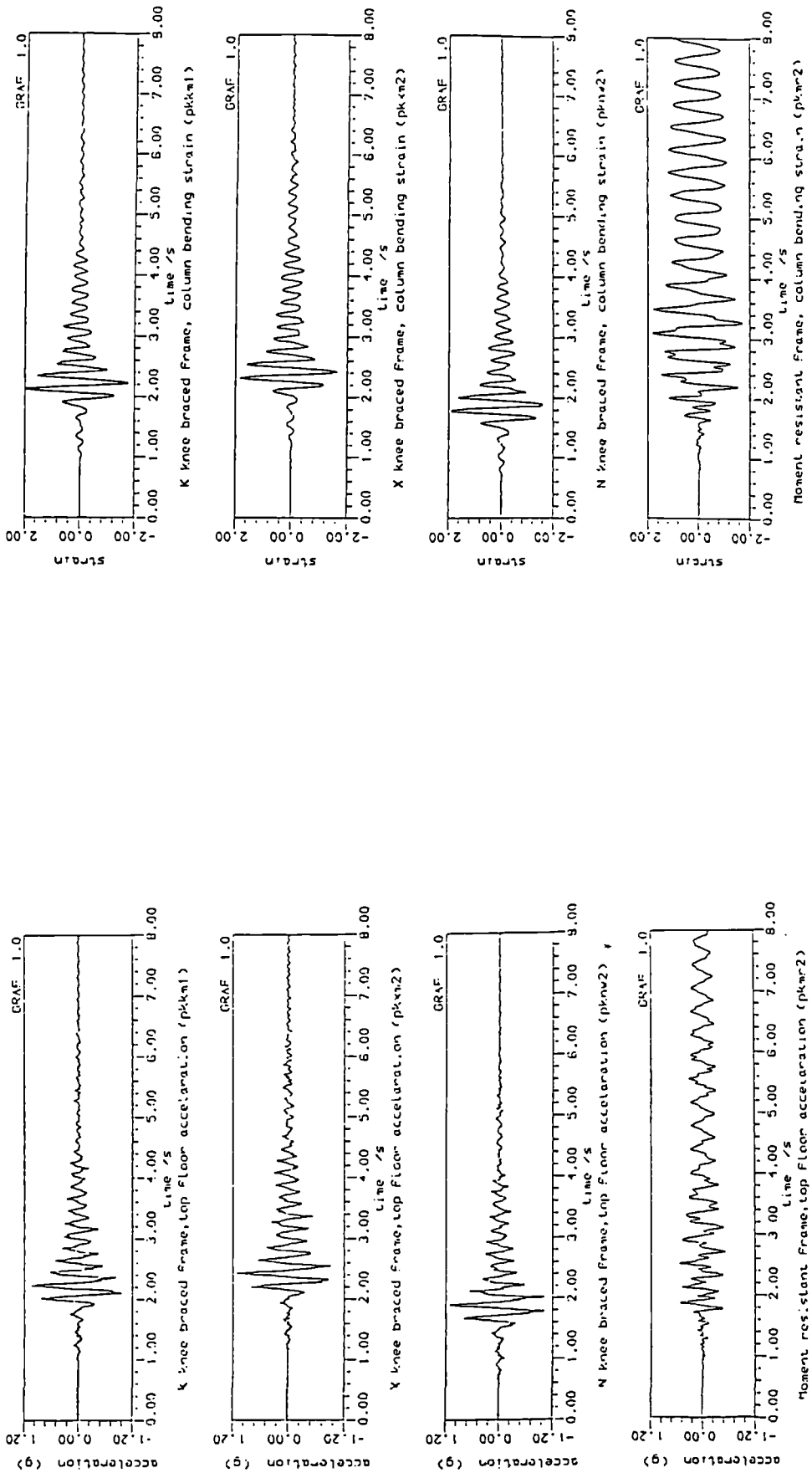

Fig.6.30 Responses of the Different configurations to Parkfield earthquake

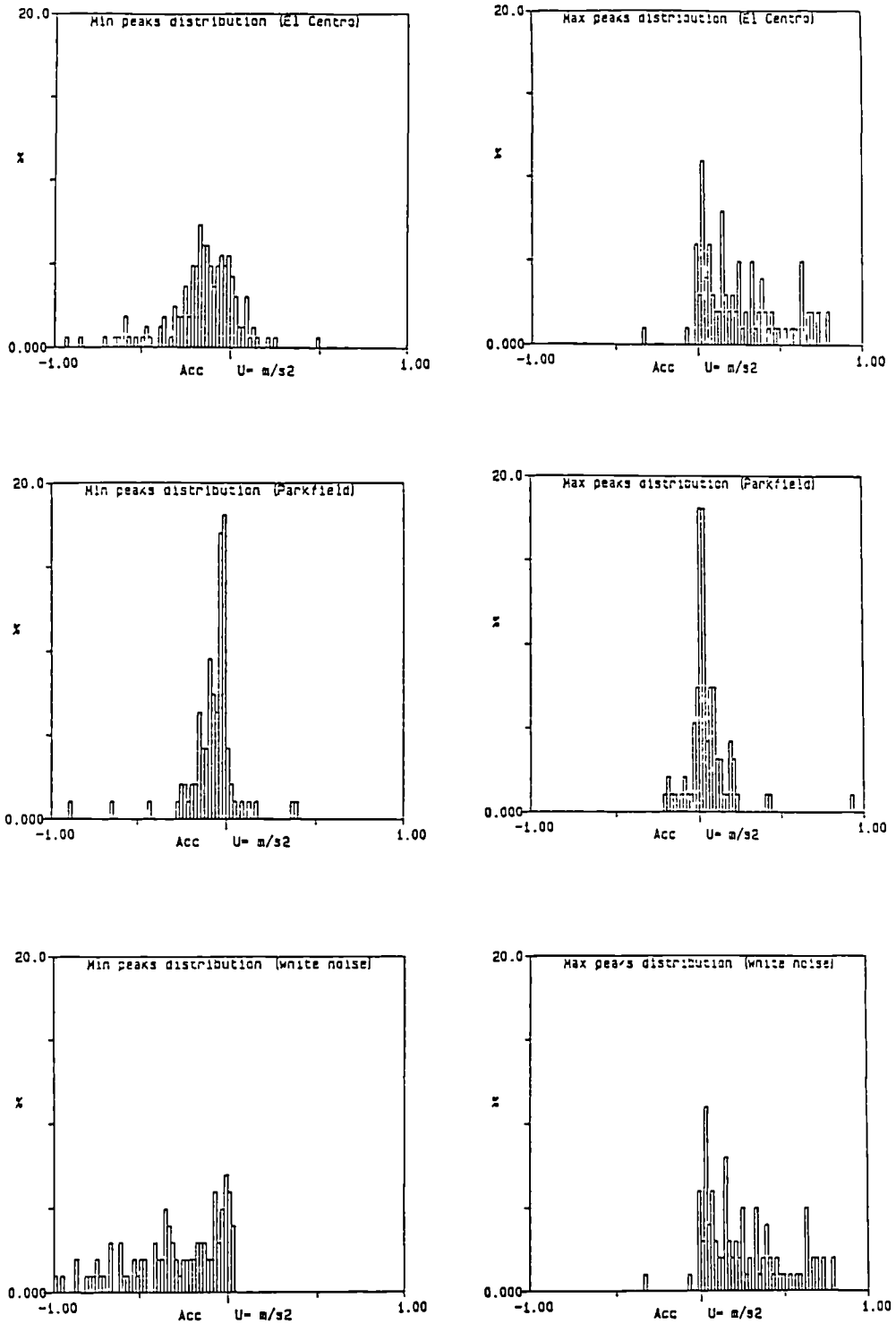

Fig.6.31 Distribution of acceleration peaks of the different input motions

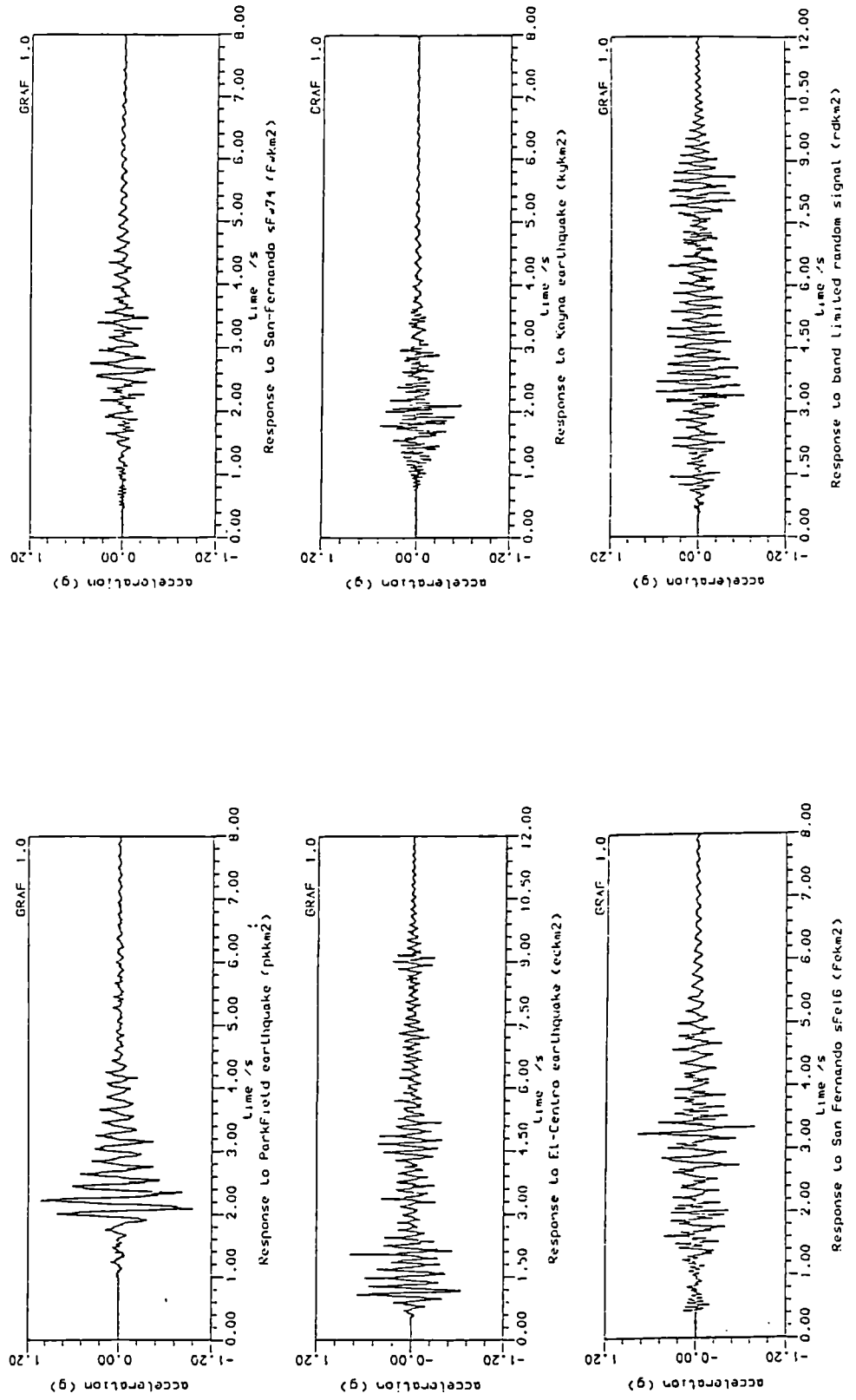

Fig.6.32 Response of the KKBF to the different types of input motions (Acceleration time-histories)

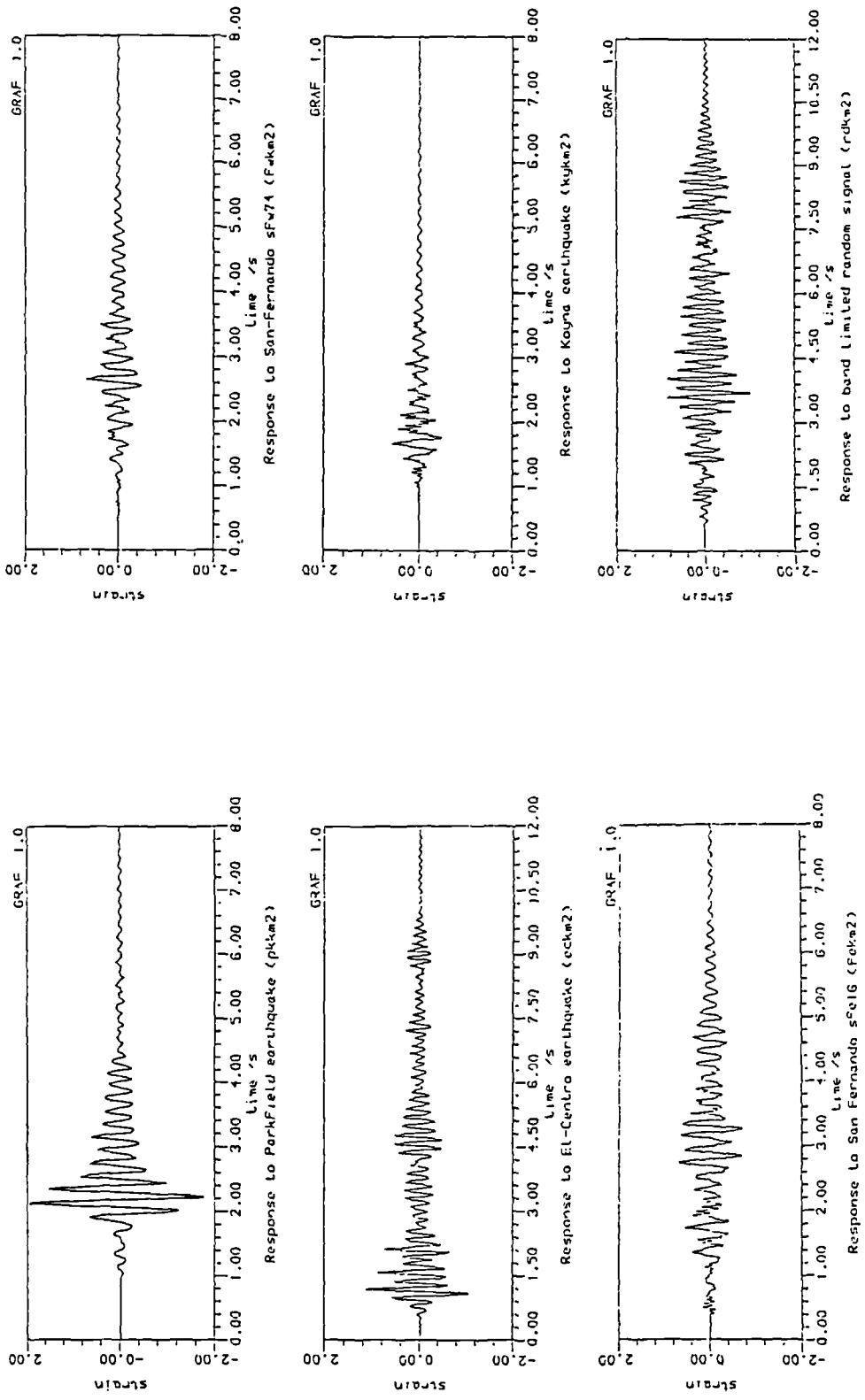

Fig.6.33 Response of the KKBF to the different types of input motions (strain time-histories)

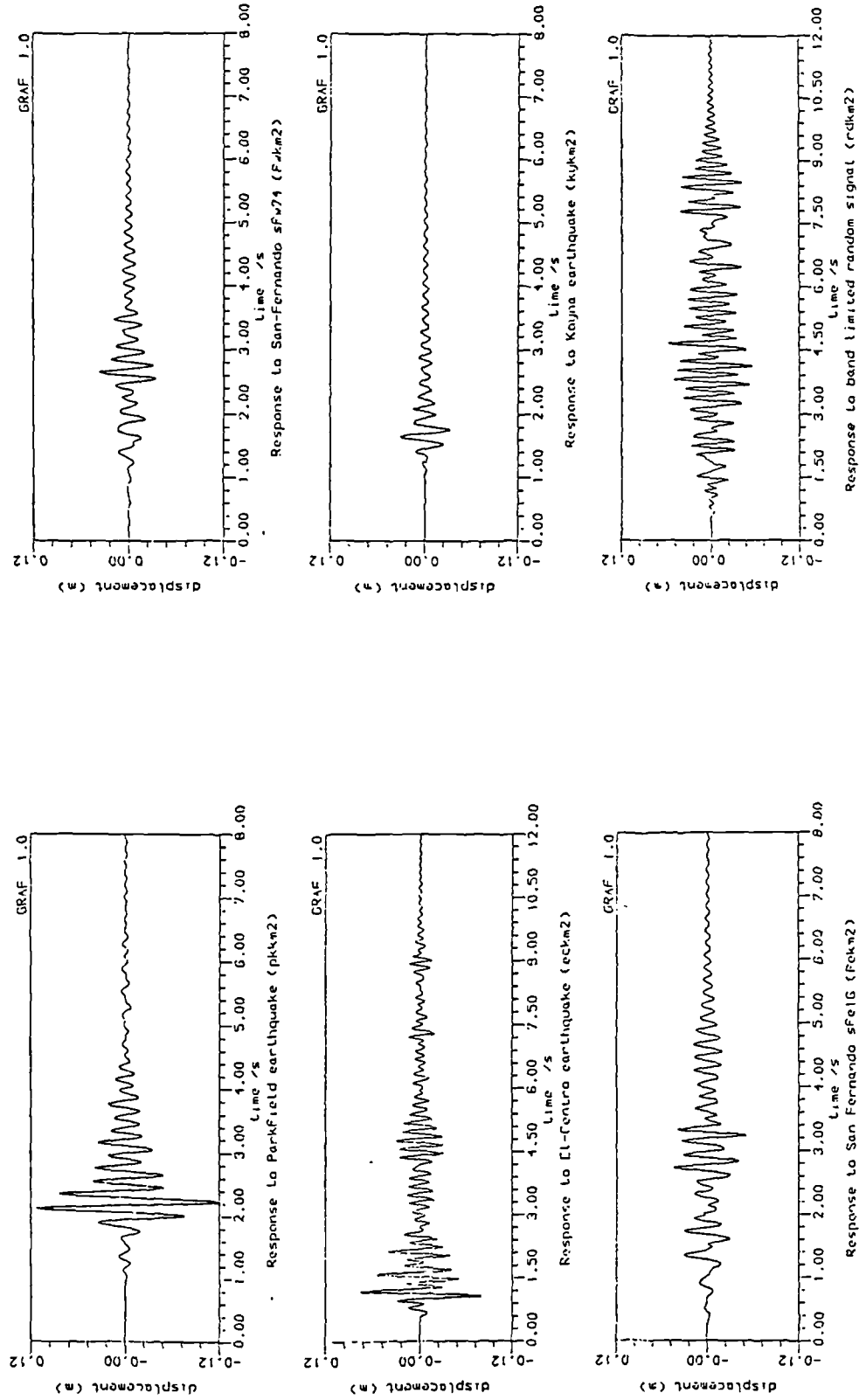

Fig.6.34 Response of the KKBF to the different types of input motions (displacement time-histories)

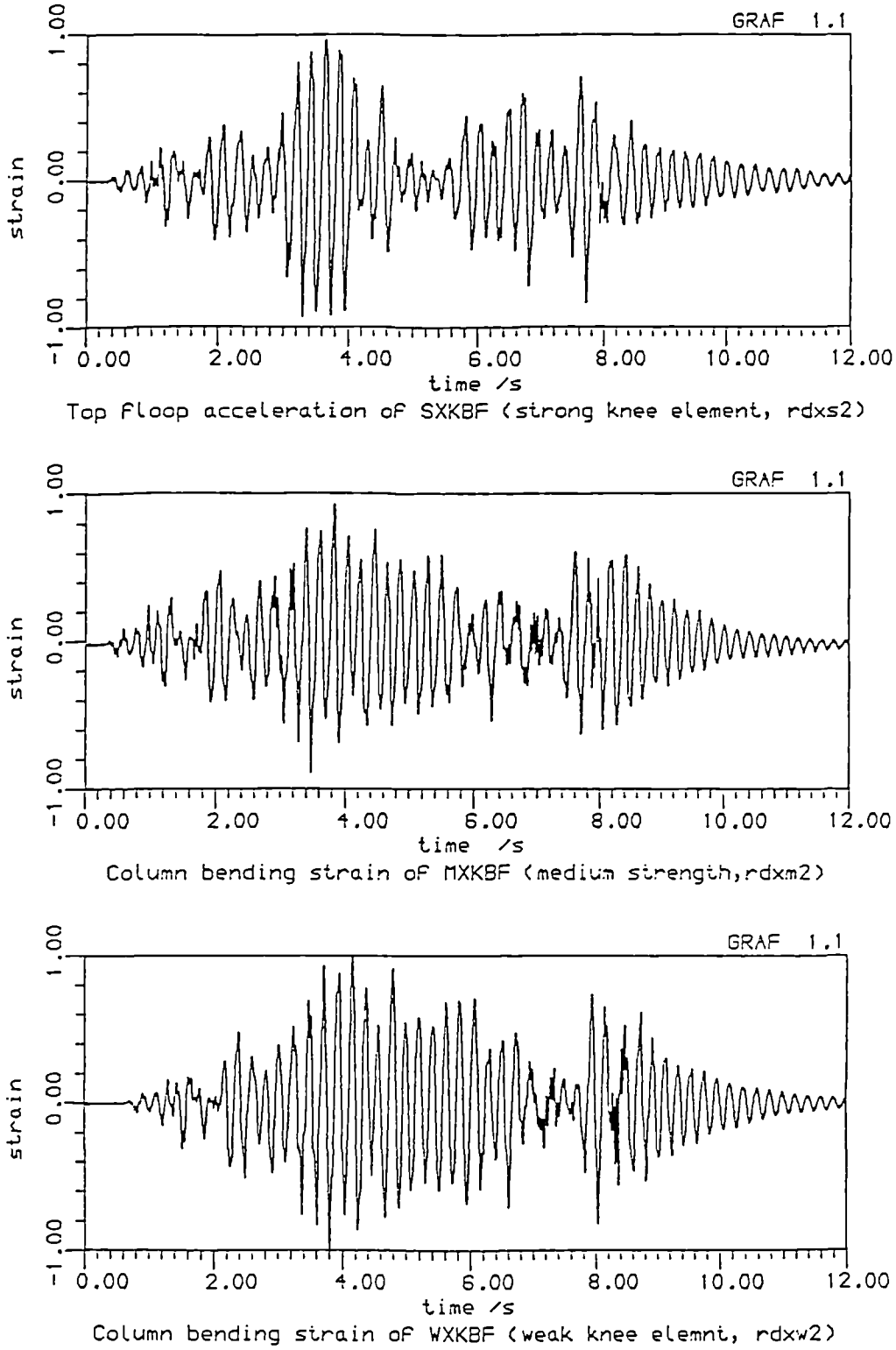

Fig.6.35 Response of XKBF with different knee element strengths to white noise motion

(strain time-histories)

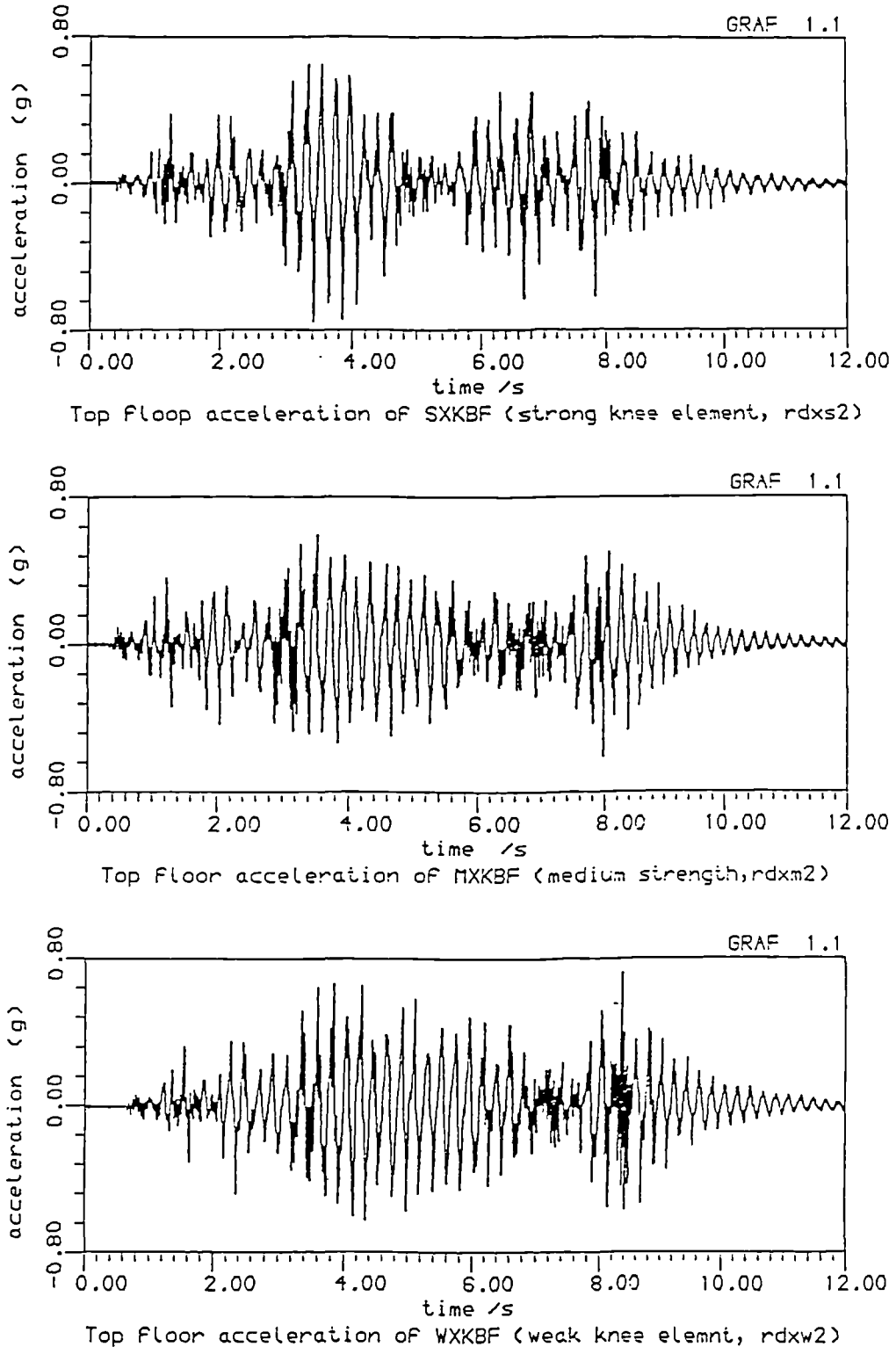

Fig.6.36 Response of XKBF with different knee element strengths to white noise motion (acceleration time-histories)

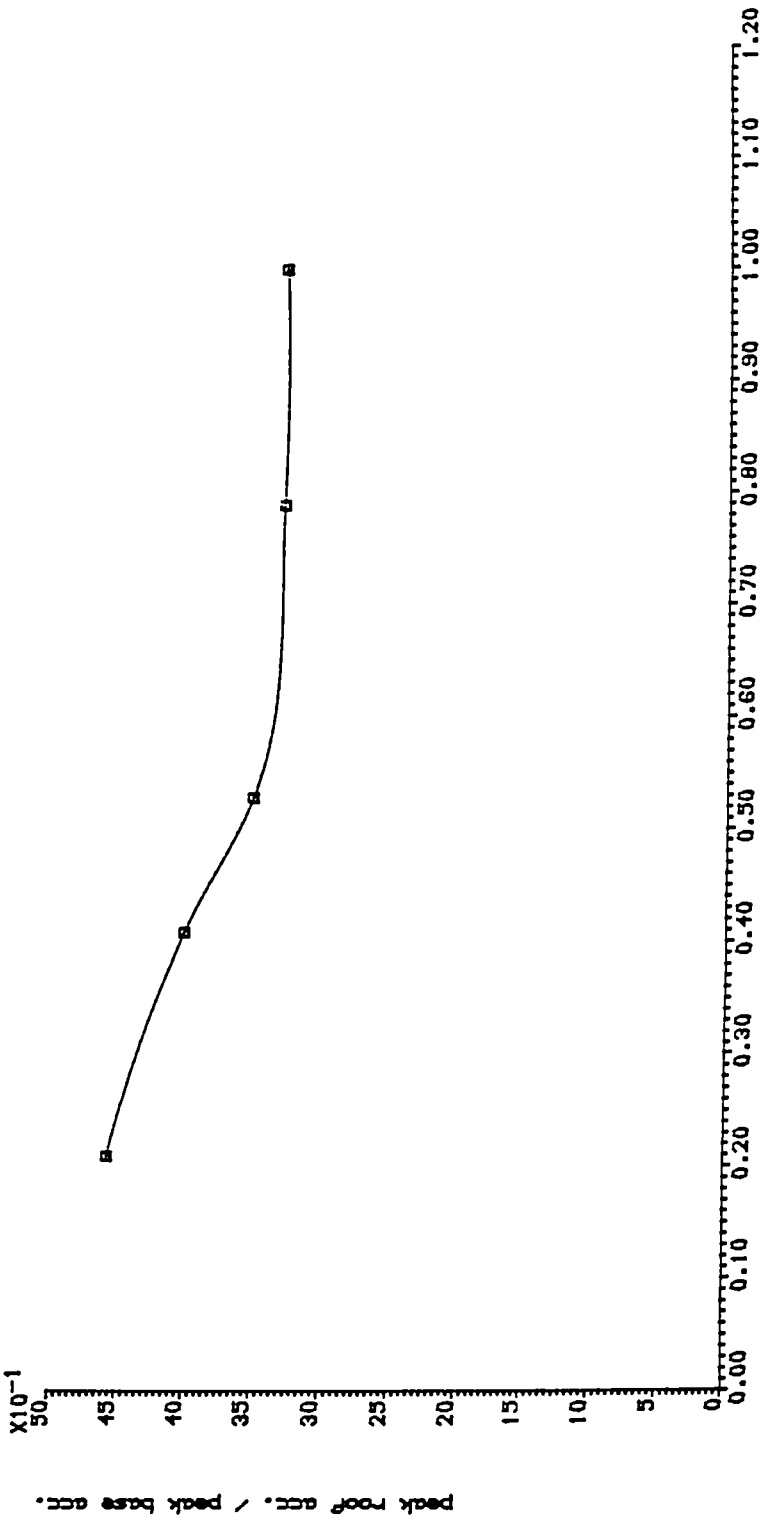

Fig.6.37 Amplification factor of the roof Acceleration vs the intensity of the table acc.

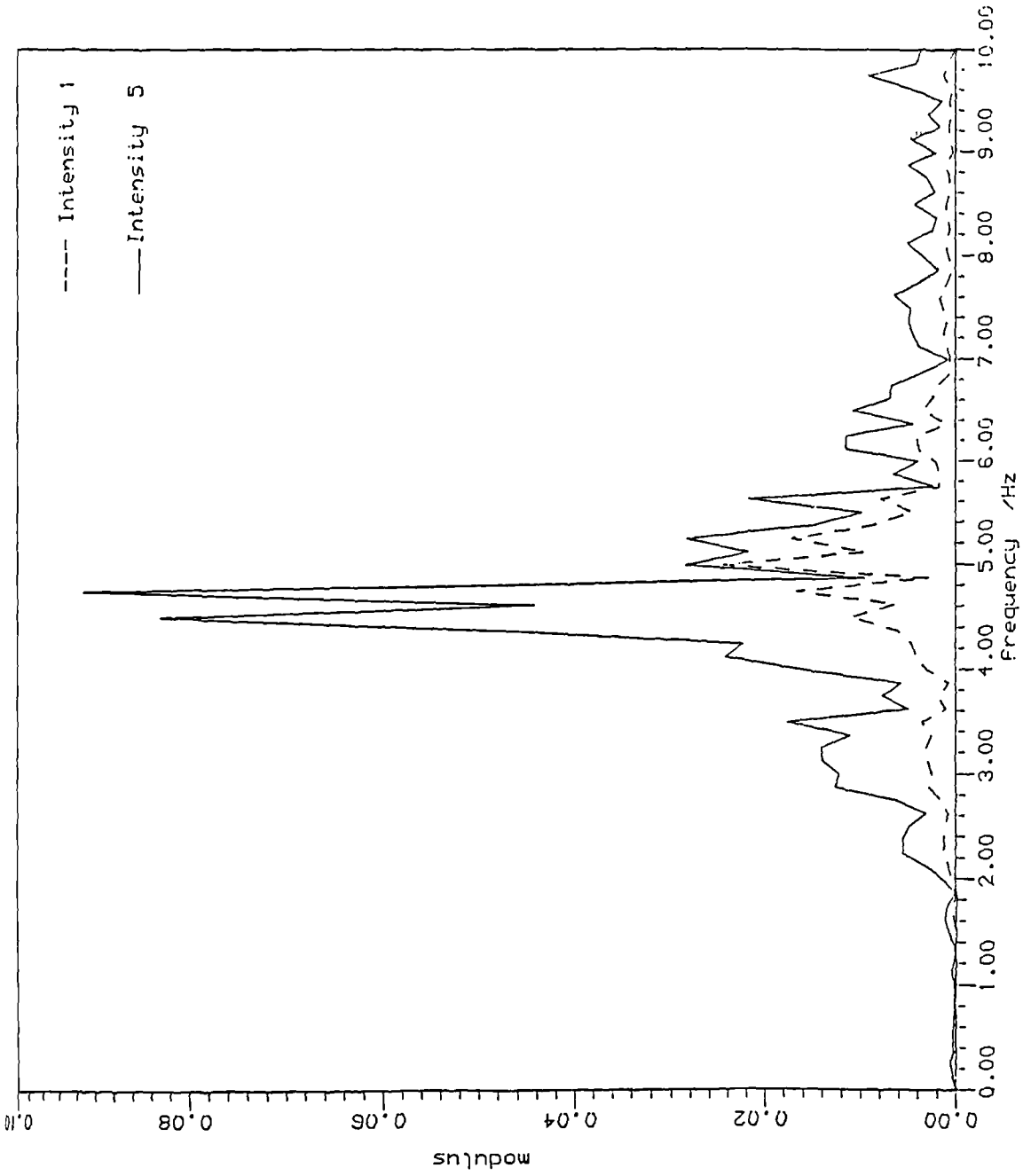

Fig.6.38 Fourier amplitudes of PKXW1 and PKXW5 accelerations (apparent fundamental frequency shift)

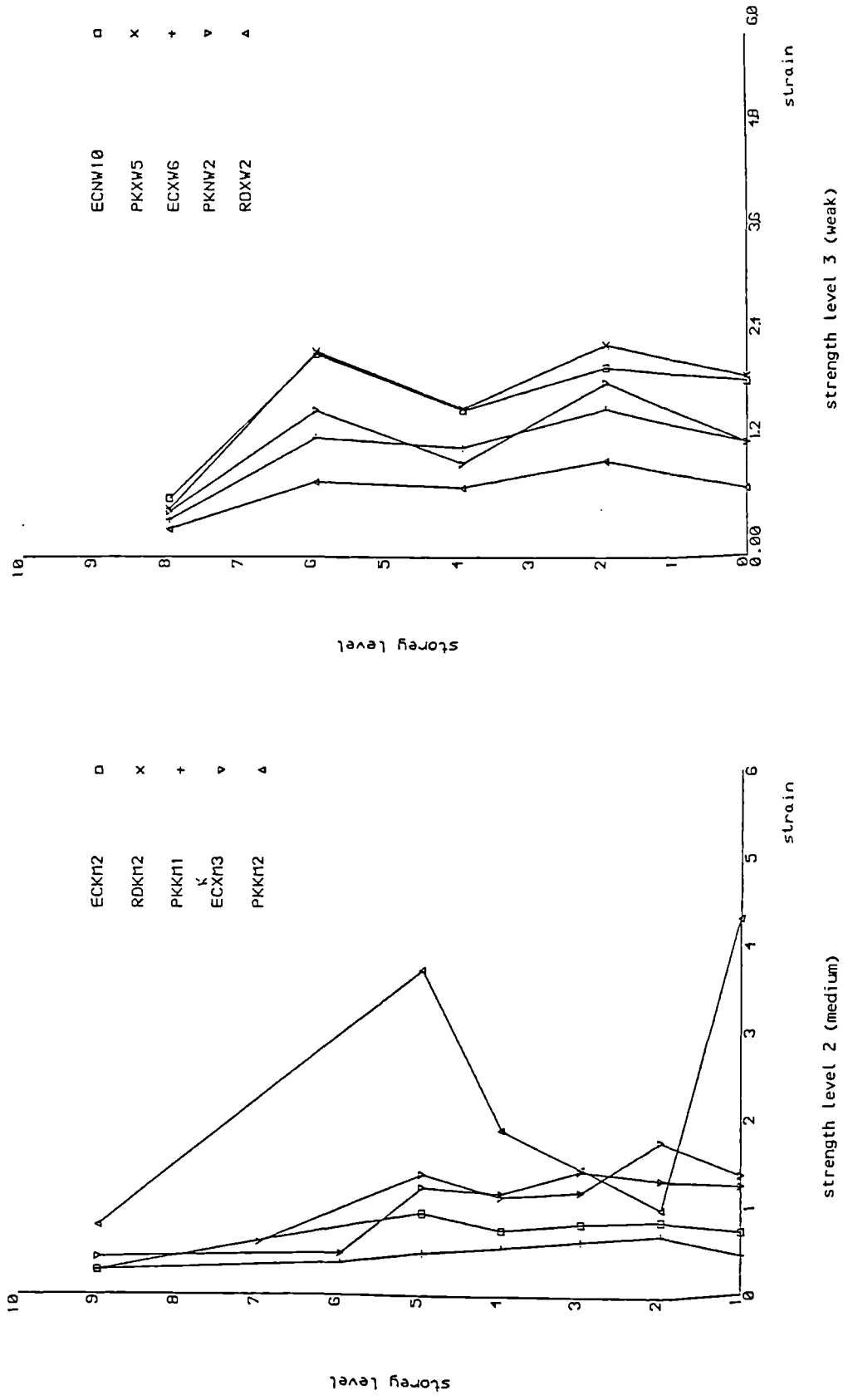

Fig.6.39 Knee element ductility distribution

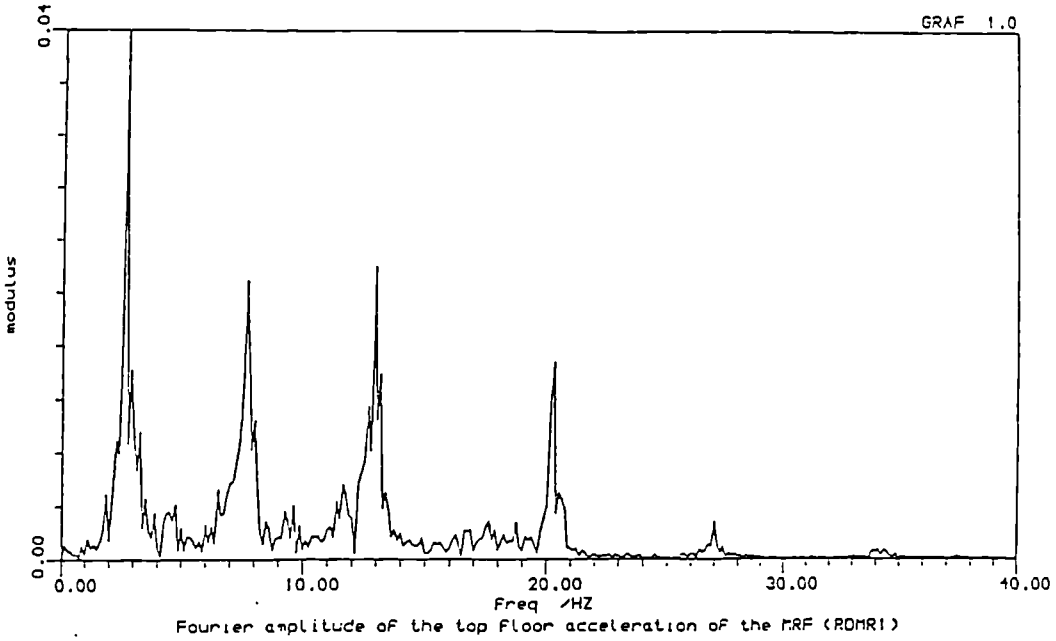

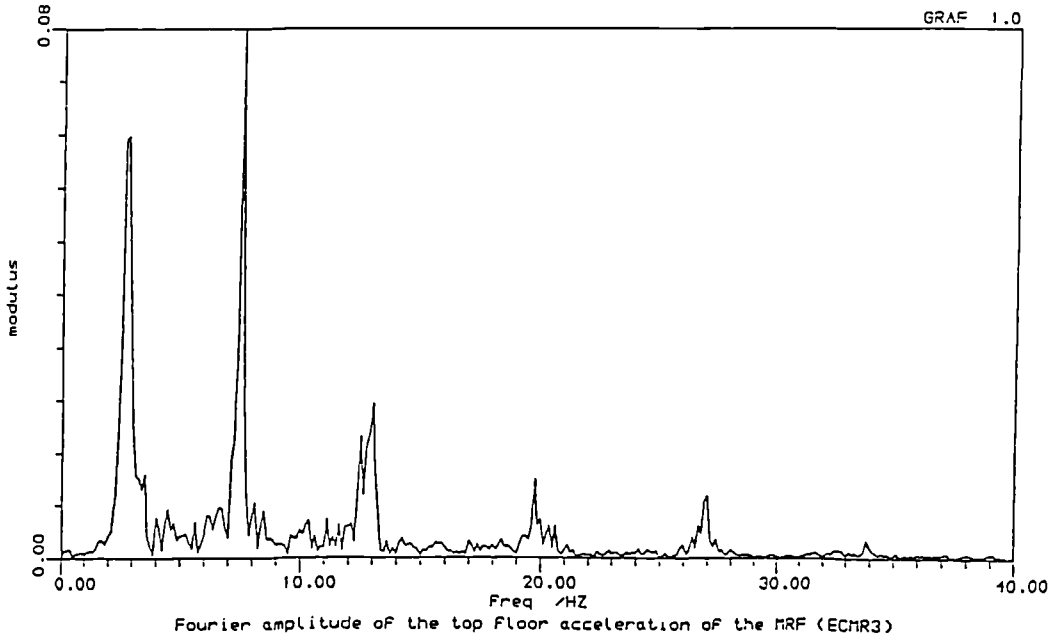

Fig.6.40 Higher mode participation to the response of the MRF

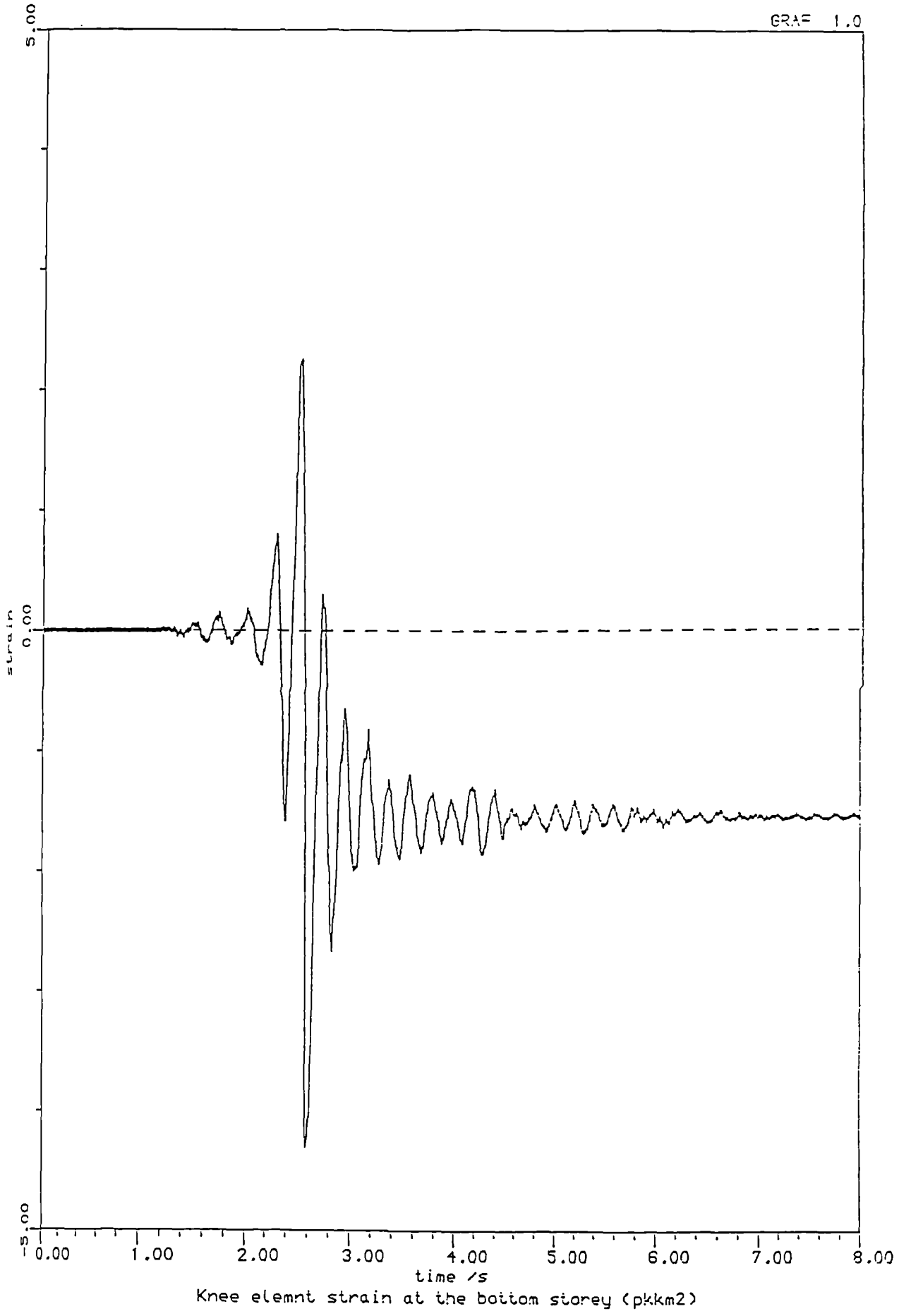

Fig.6.41 Permanent distortion of the knee element of the bottom storey during the PKKM2 test

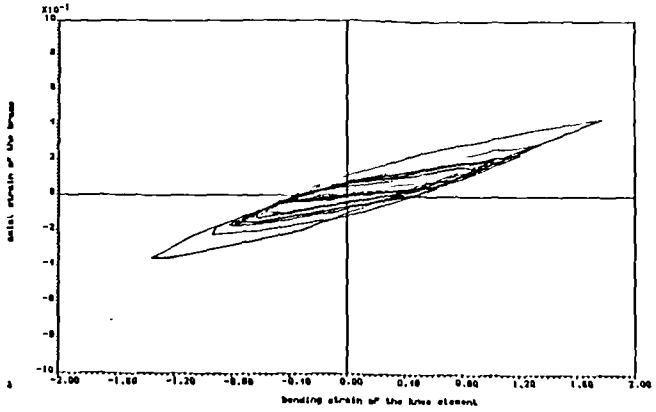

Knee element hysteritic loop 3rd storey ecxw6

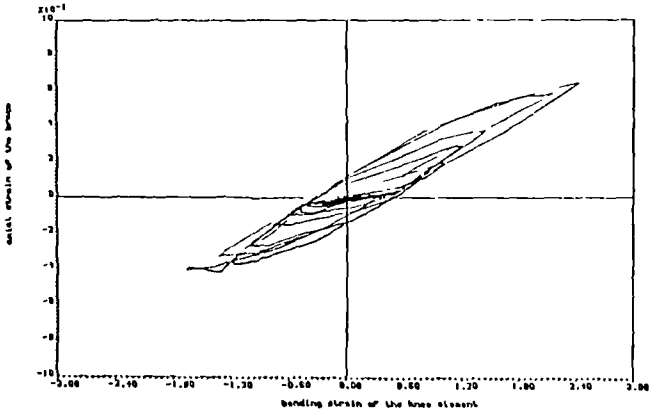

Knee element hysteritic loop 3rd storey phxw5

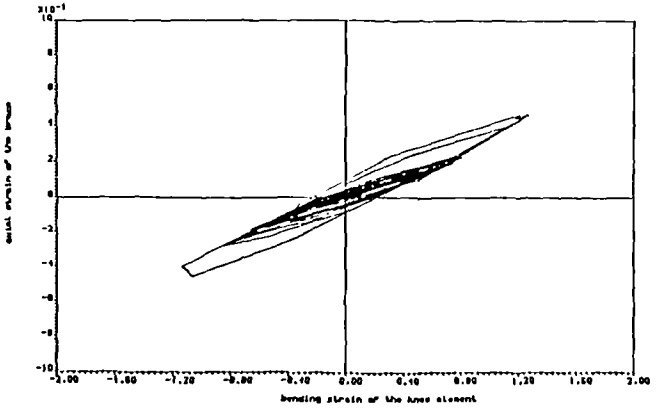

Knee element hysteritic loop 7th storey ecxw6

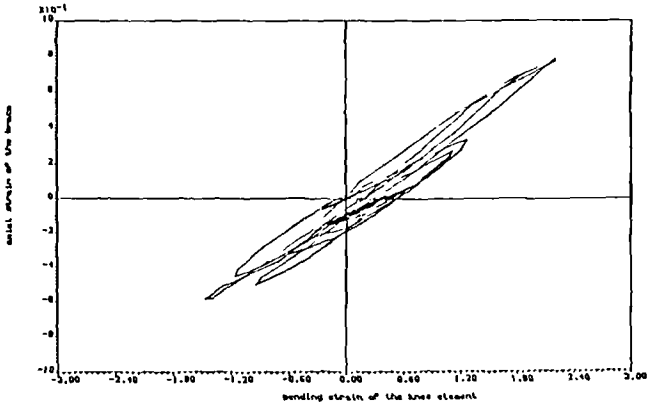

Knee element hysteritic loop 7th storey phxw5

Fig.6.42 Hysteresis loops resulting from PKXW5 and ECXW6 tests

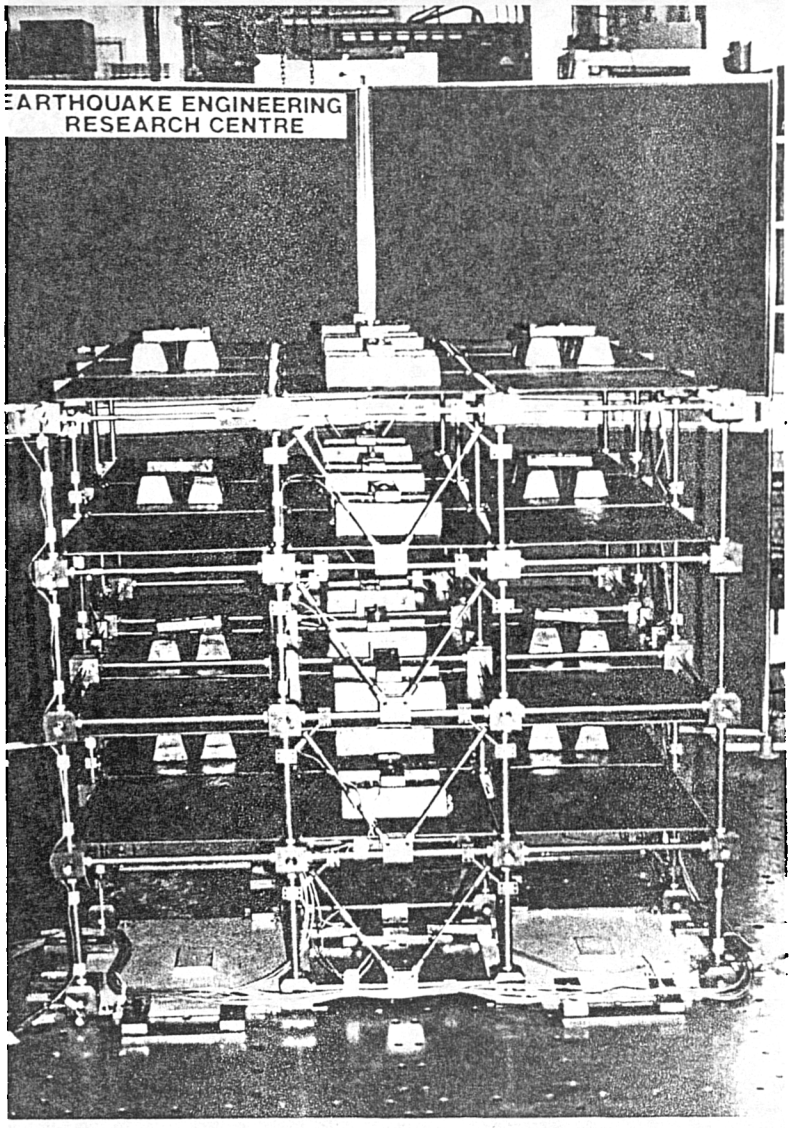

a-OKBF test structure

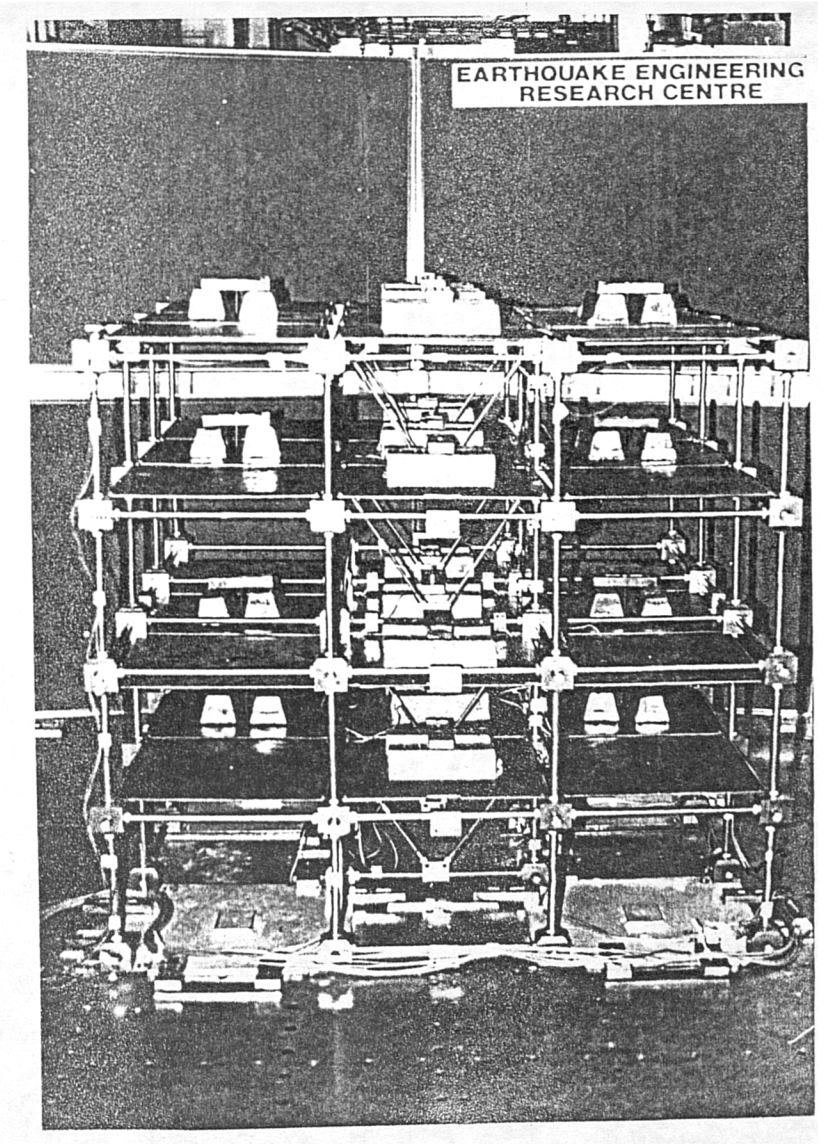

b-IKBF test structure

Fig.6.43 frames of the test series III

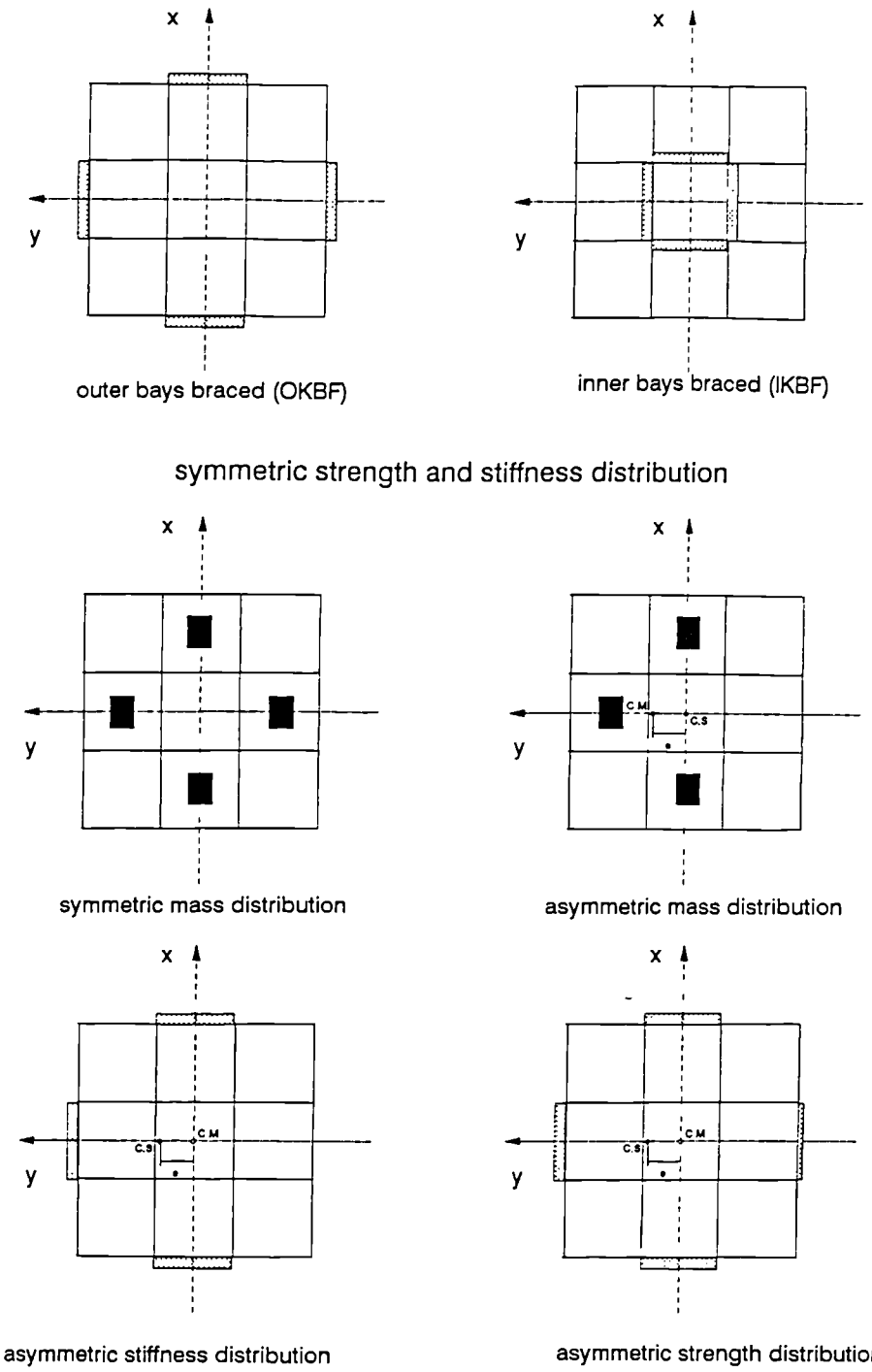

Fig.6.44 Mass, strength and stiffness distribution in a typical floor of the 3-D frames

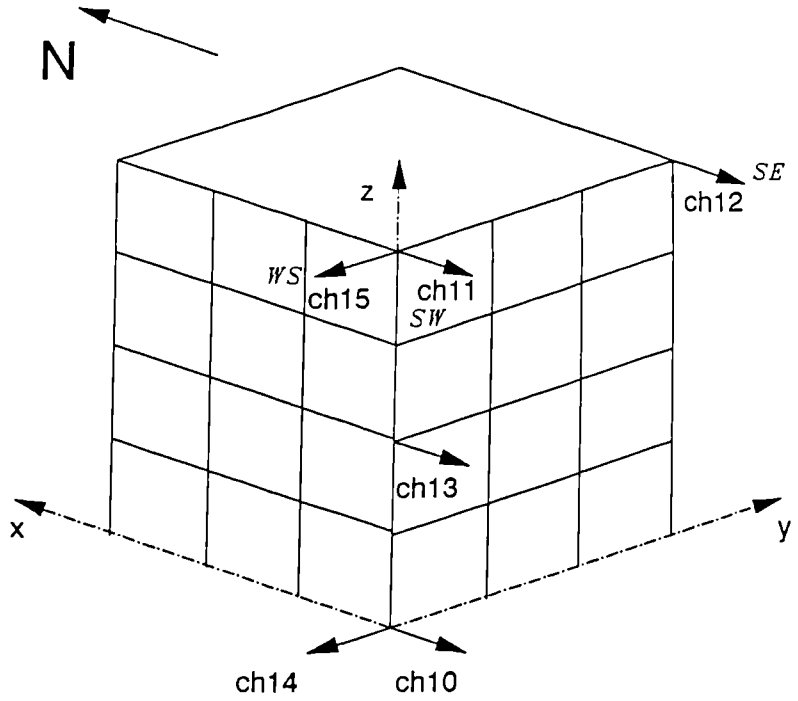

a- Accelerometers

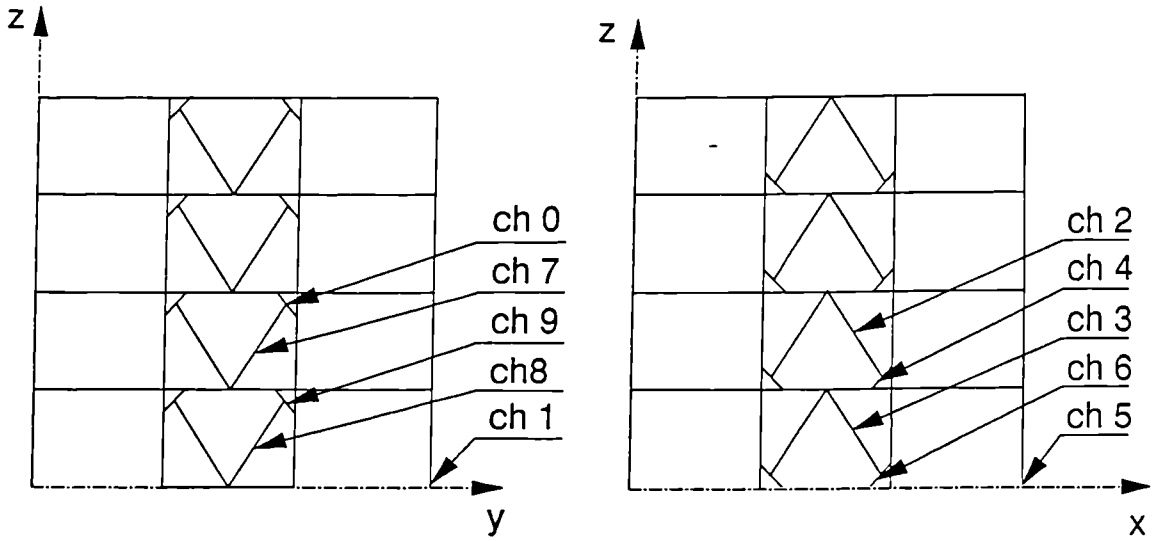

b- strain gauges

Fig.6.45 Sensors locations on the 3-D frames

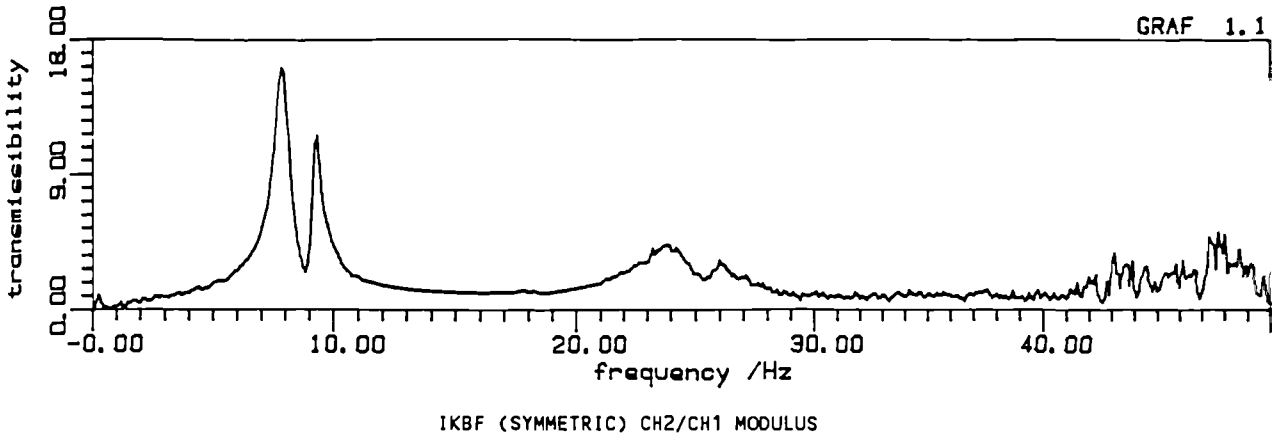

IKBF (SYMMETRIC) CH2/CH1 MODULUS

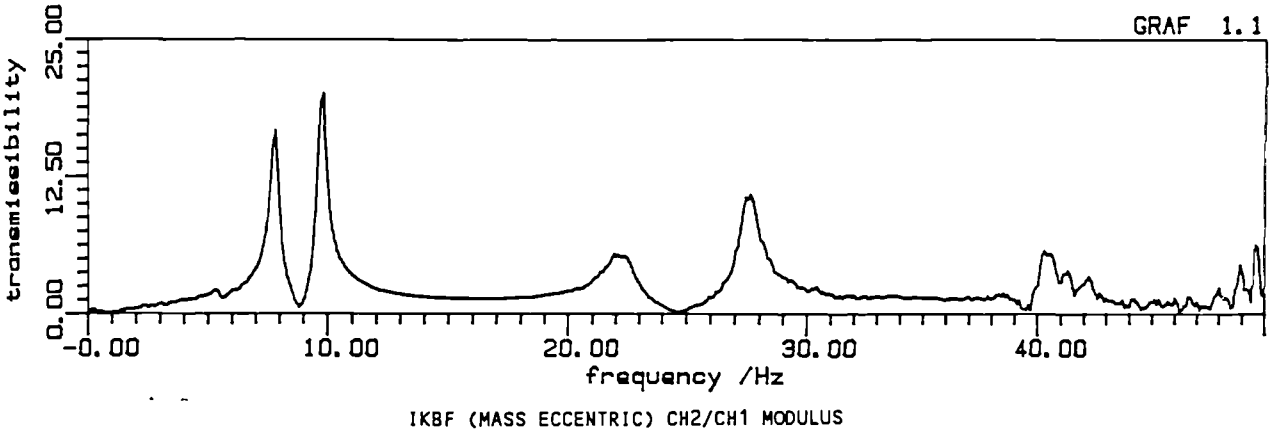

IKBF (MASS ECCENTRIC) CH2/CH1 MODULUS

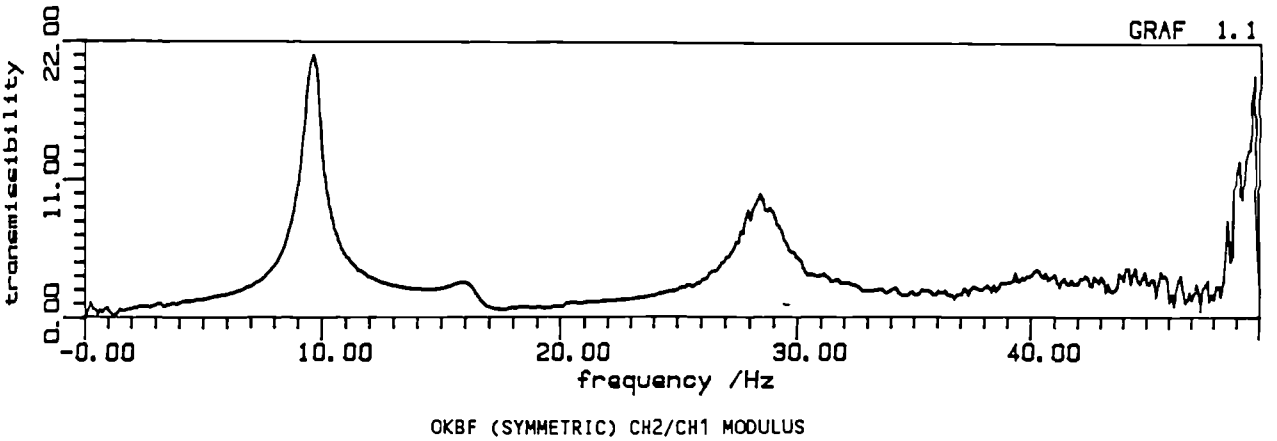

OKBF (SYMMETRIC) CH2/CH1 MODULUS

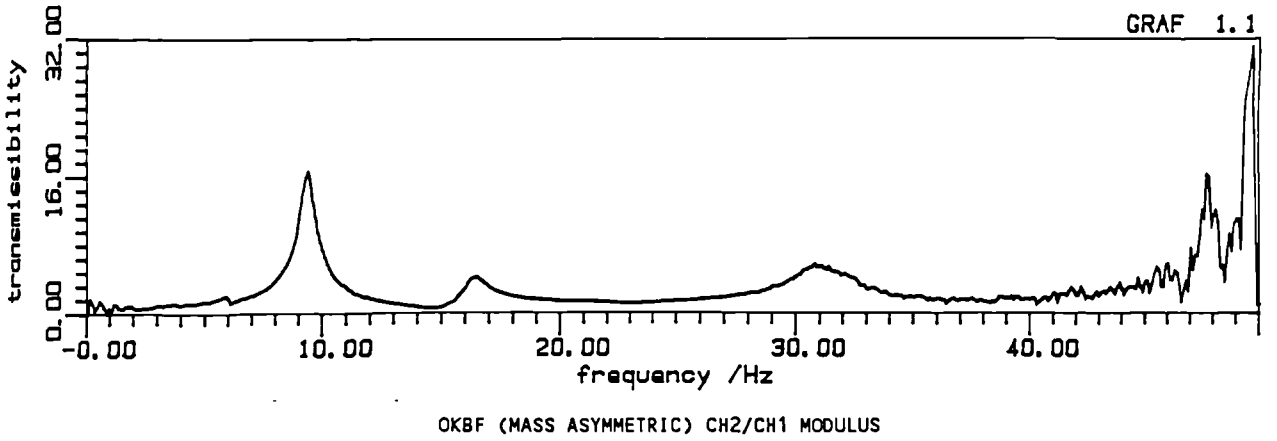

OKBF (MASS ASYMMETRIC) CH2/CH1 MODULUS

Fig.6.46 Typical transfer functions of the 3-D frames

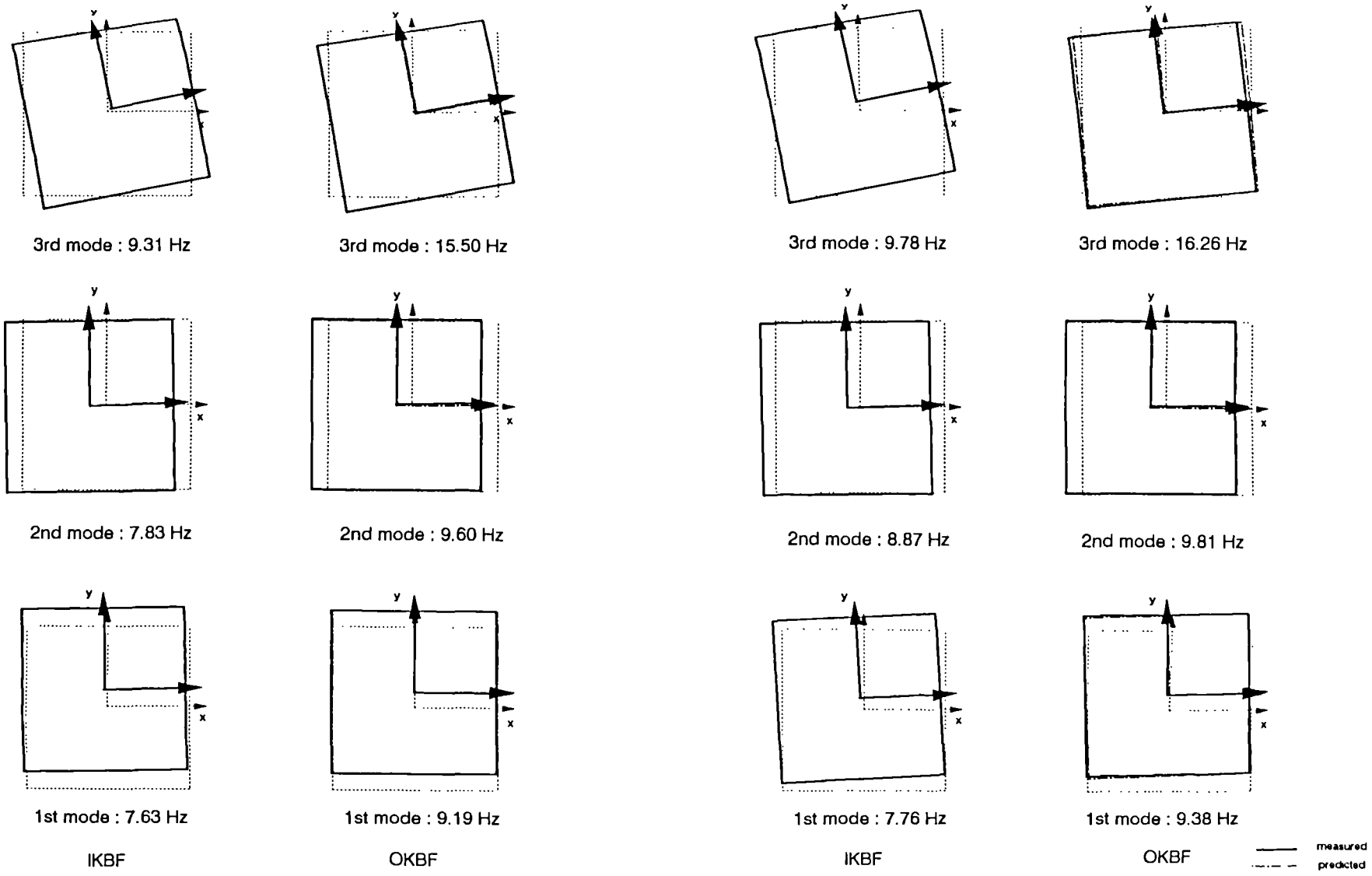

a- Mode shapes of symmetric frames

b- Mode shapes of mass eccentric frames

Fig.6.47 Typical mode shapes of the 3-D frames

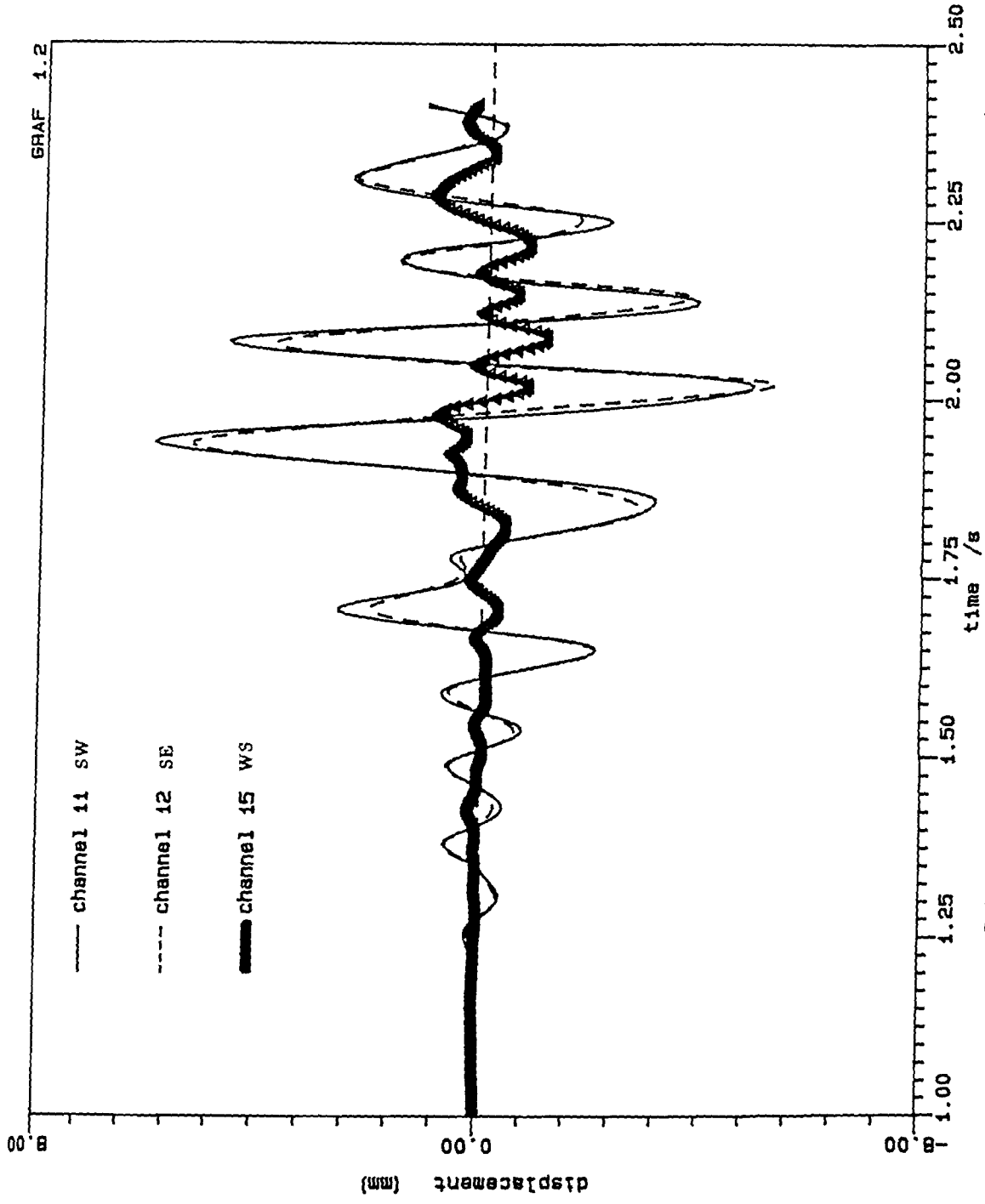

Fig.6.48 Relative displacement time-histories of the OECAS7 test

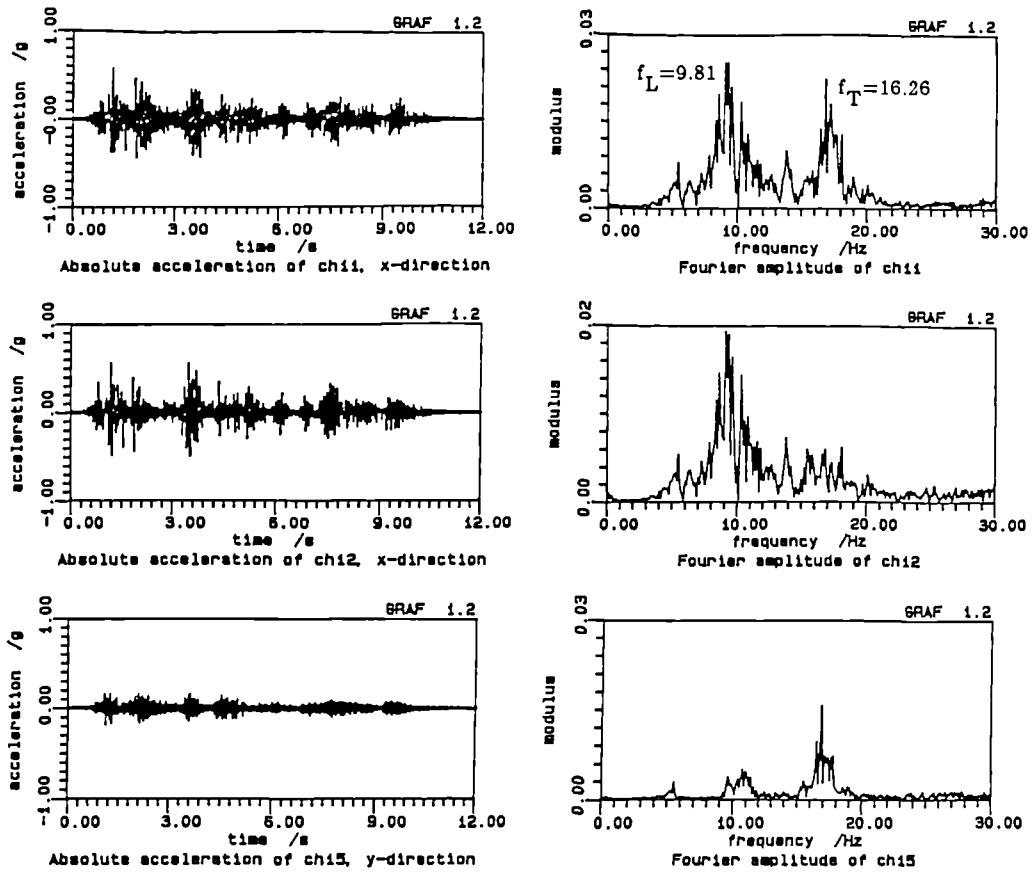

a-OECAM1

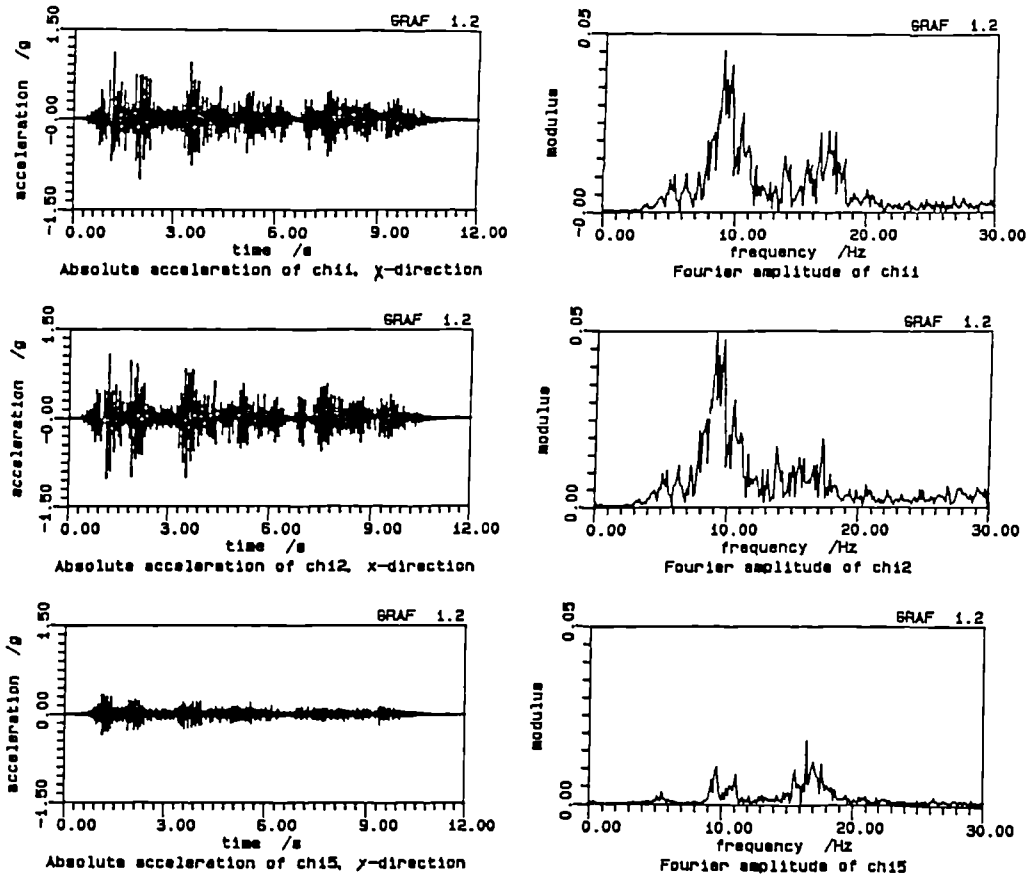

b-OECAM2

Fig.6.49 Acceleration time-histories and FFTs of the OECAM1 and OECAM2 tests

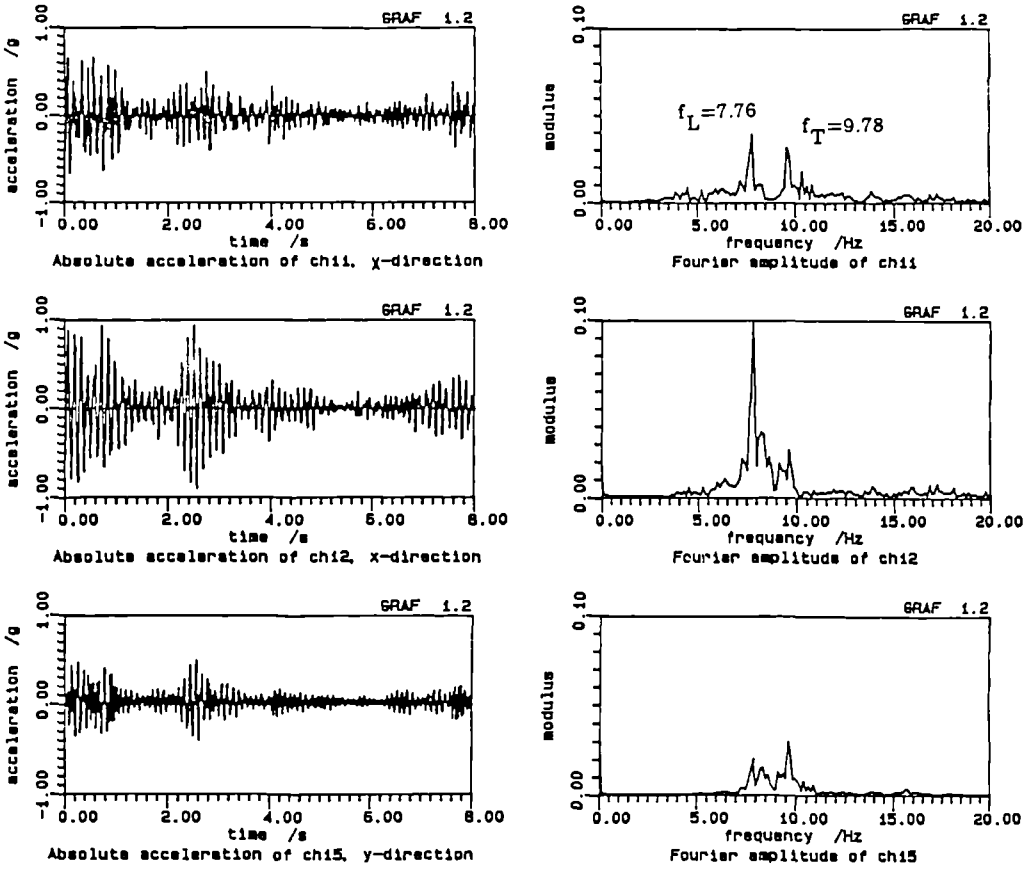

a-IECAM1

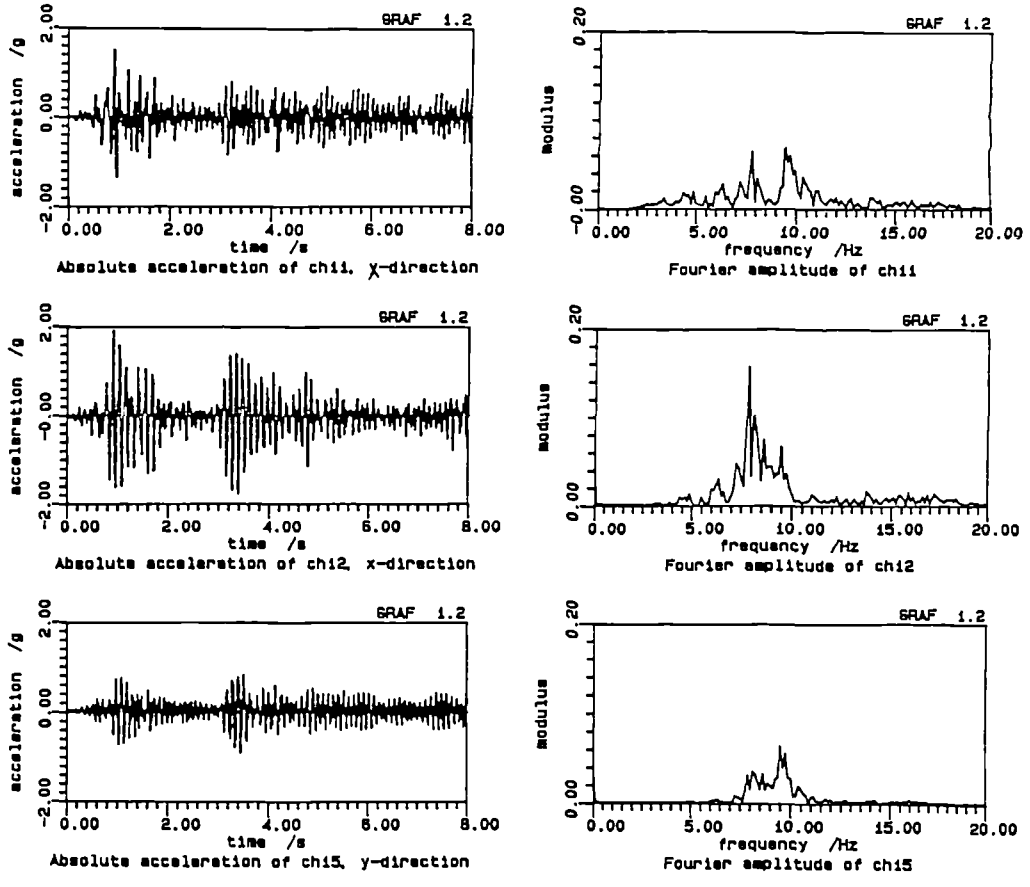

b-IECAM2

Fig.6.50 Acceleration time-histories and FFTs of the IECAM1 and IECAM2 tests

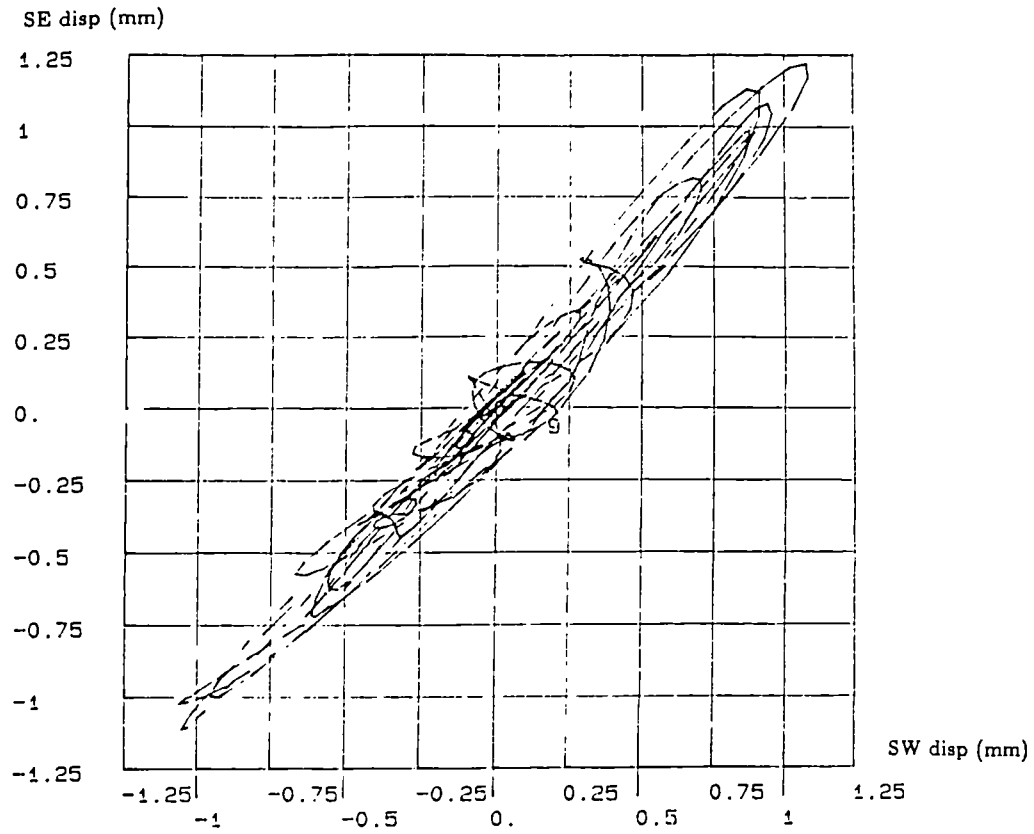

a-OECAM1

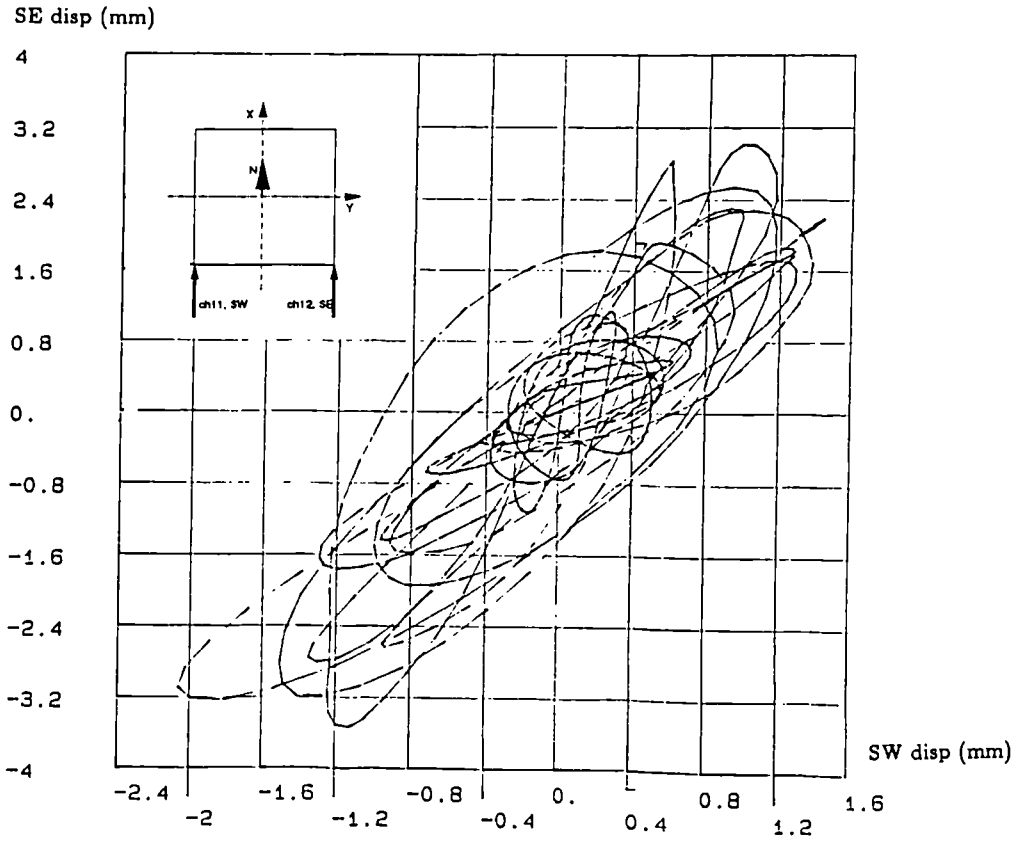

b-IECAM1

Fig.6.51 x and y-displacement relationship (OECAM1, IECAM1)

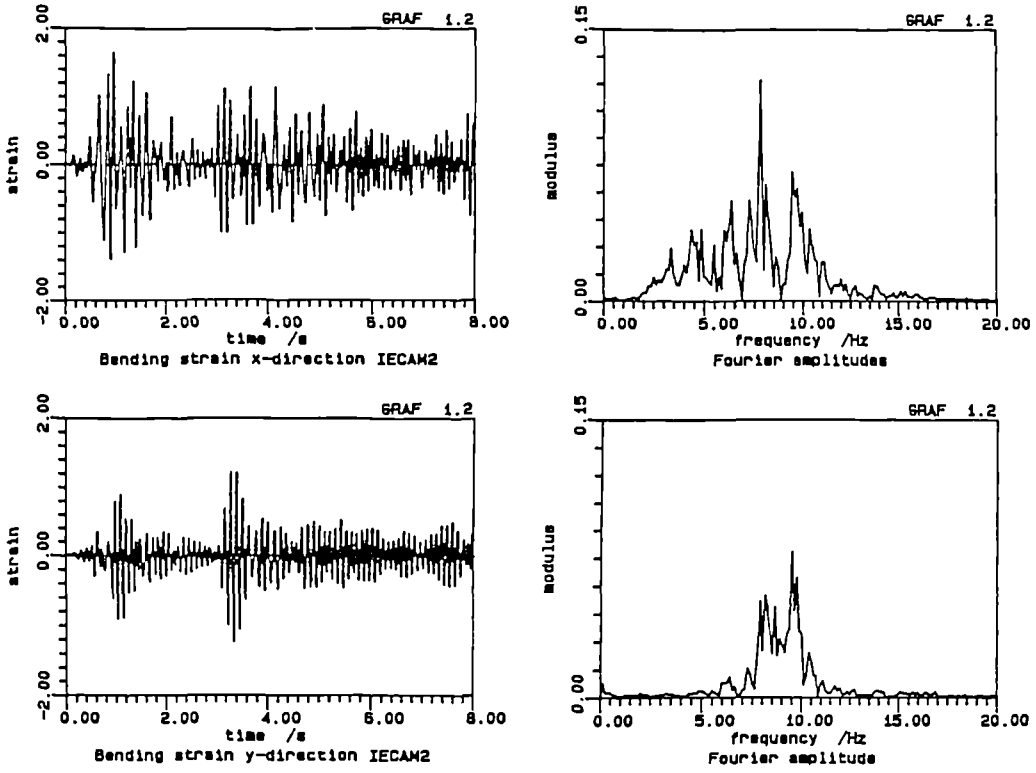

a-IECAM2

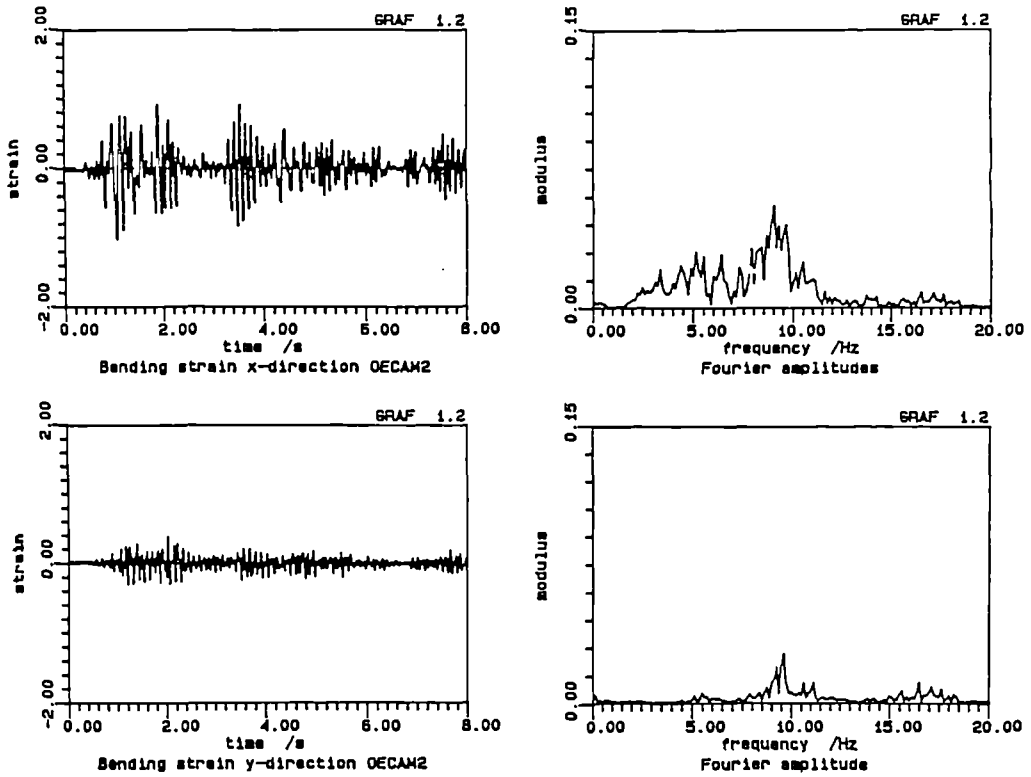

b-OECAM2

Fig.6.52 Bending strain time-histories and FFTs of the IECAM2 and OECAM2 tests

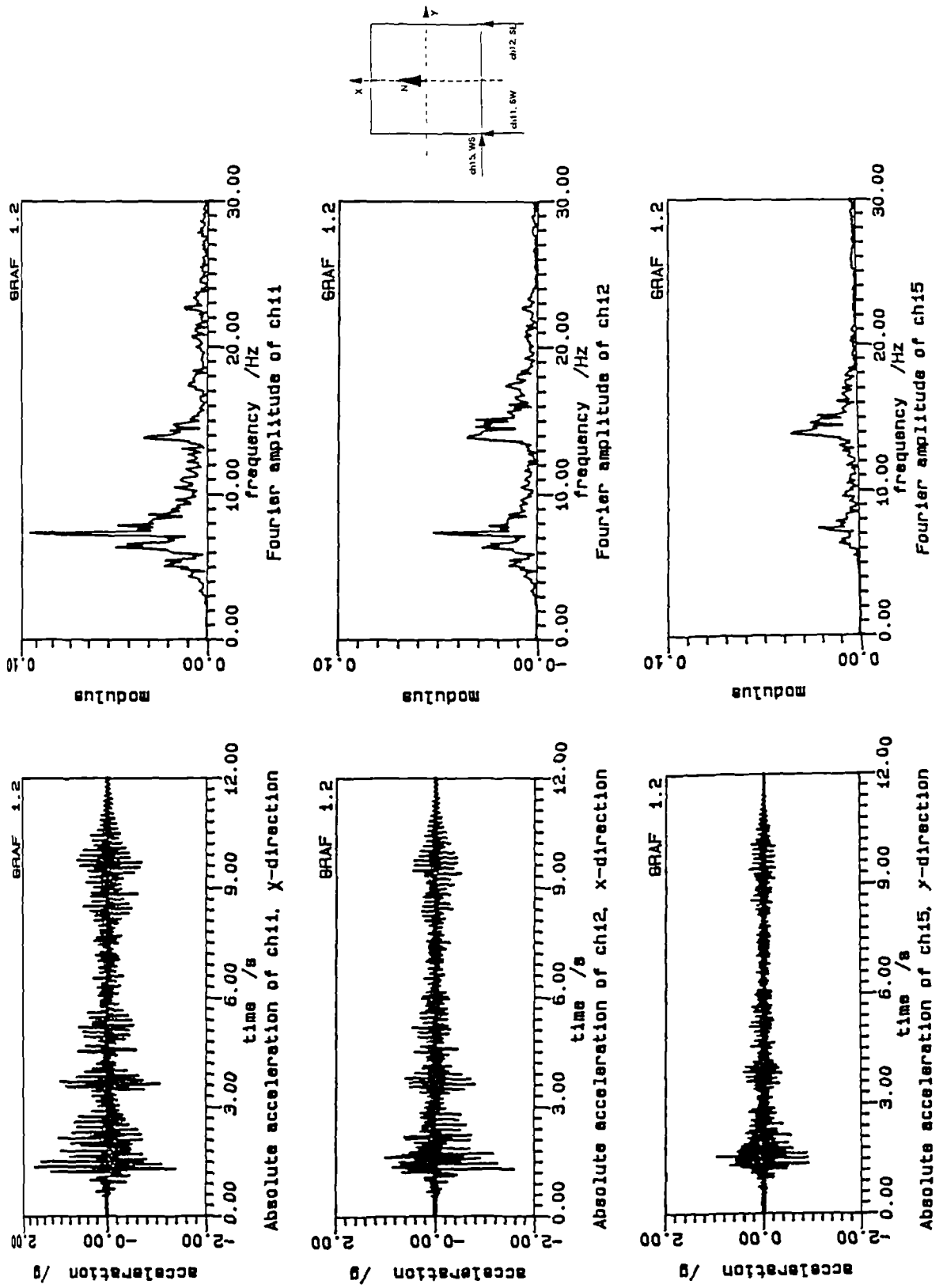

Fig.6.53 Acceleration time-histories and FFTs of the OECAF2 test

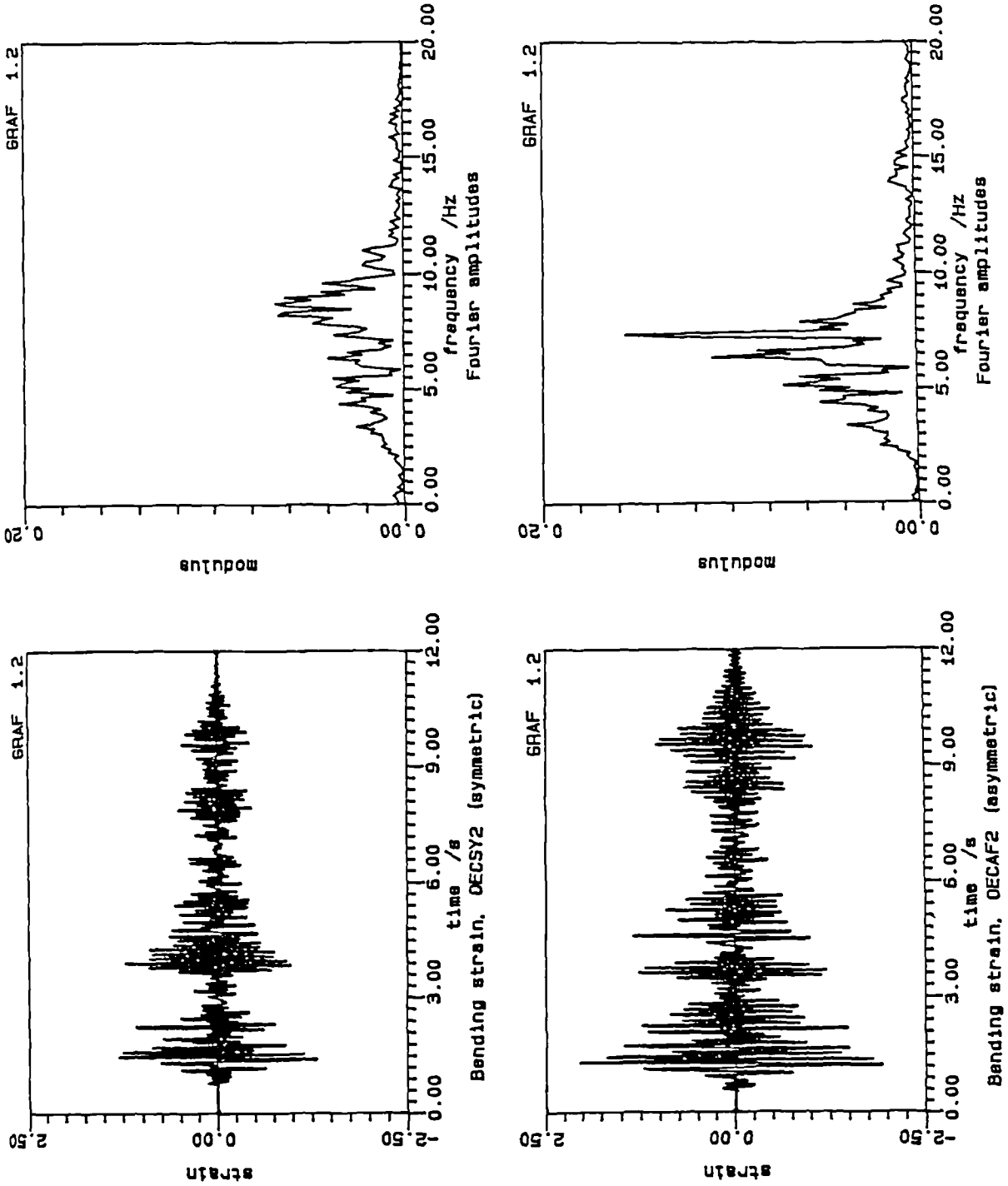

Fig.6.54 Bending strain time-histories and FFTs of the OECSY2 and OECAF2 *tests*

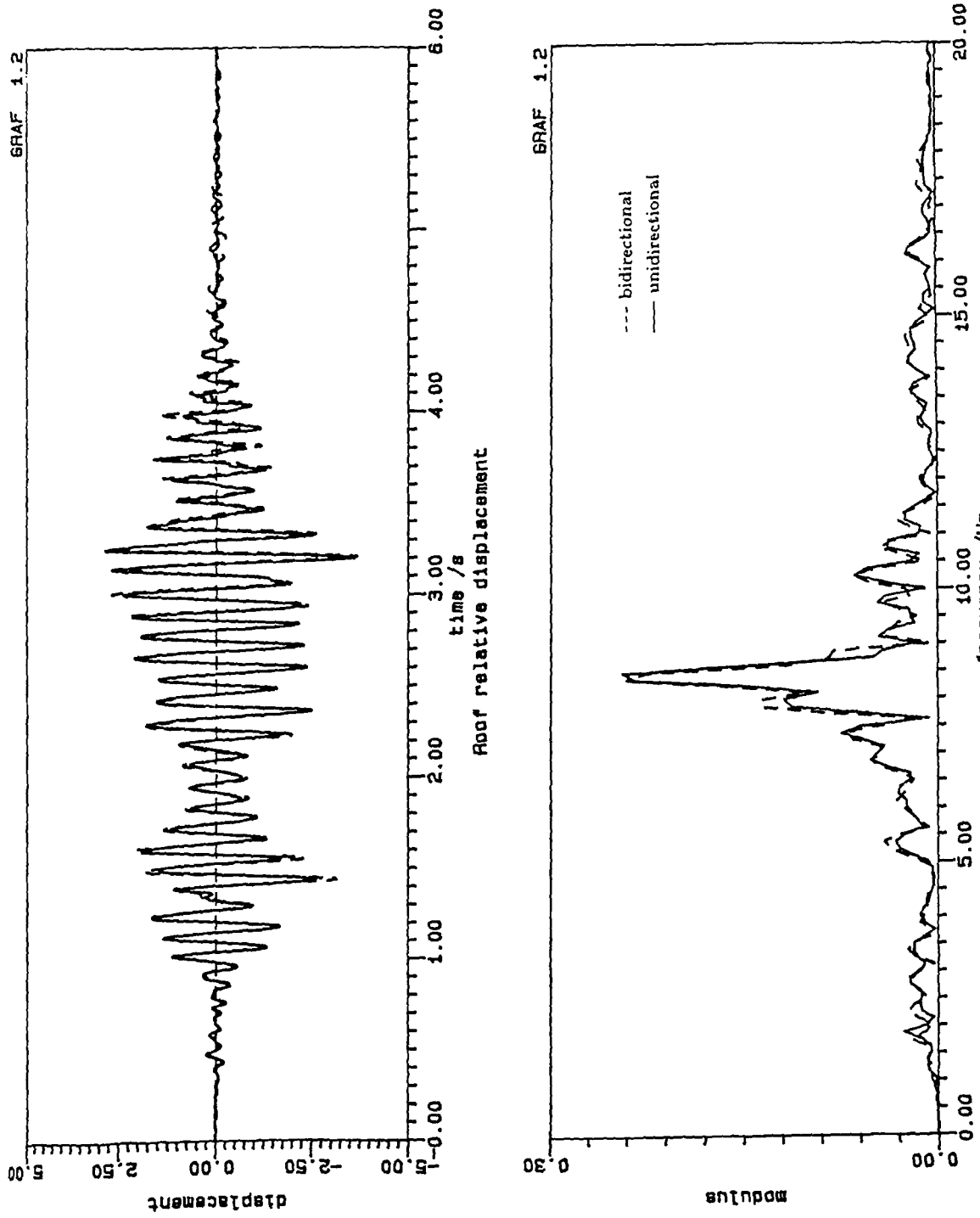

Fig.6.55 Relative displacement time -histories of the OXXSY2, OYYSY2, and OXYSY2 tests

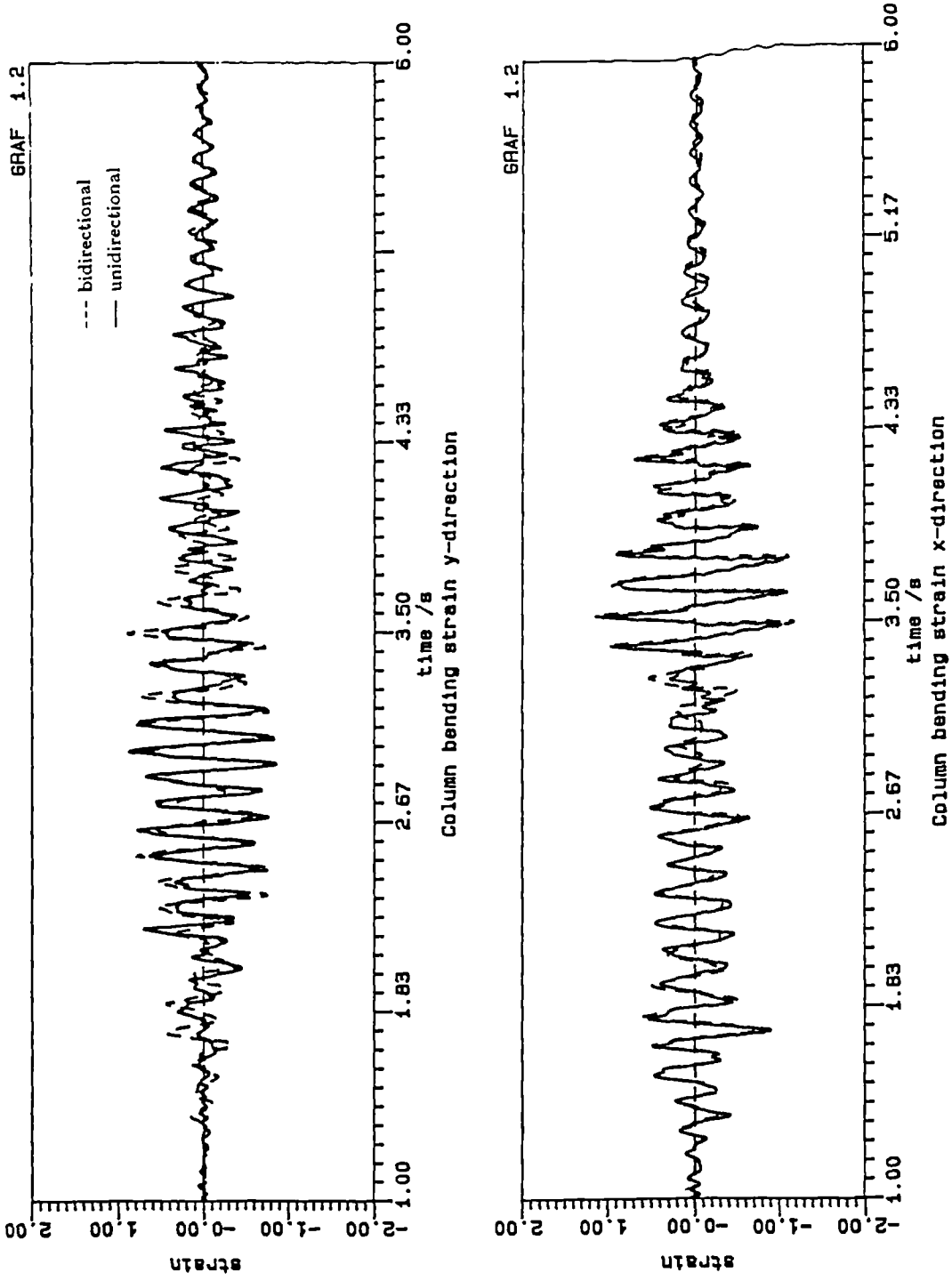

Fig.6.56 Relative displacement time-histories of the OXXAF1, OYYAF1, and OXYAF1 tests

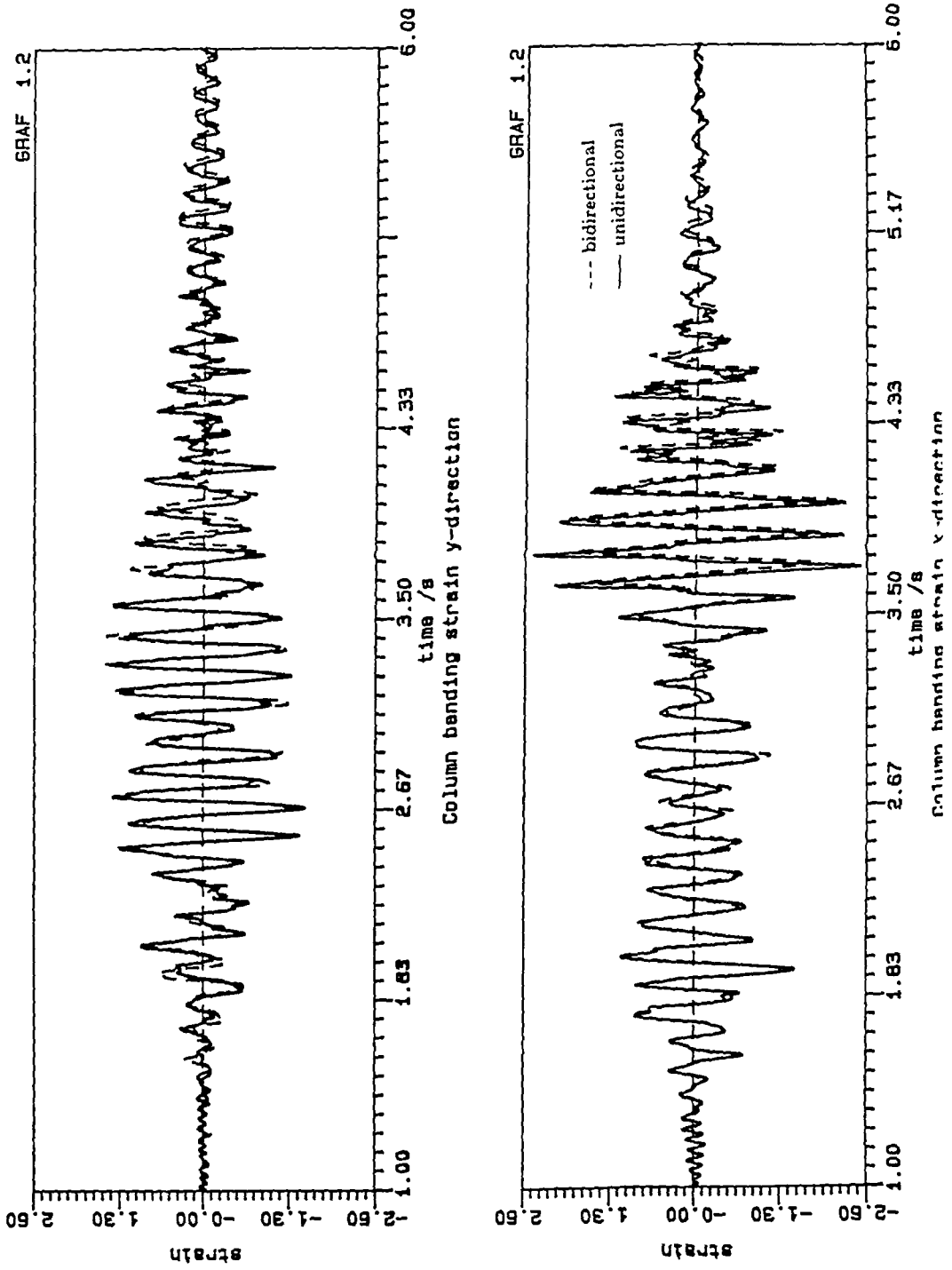

Fig.6.57 Relative displacement time-histories of the OXXAF2, OYYAF2, and OXYAF2 tests

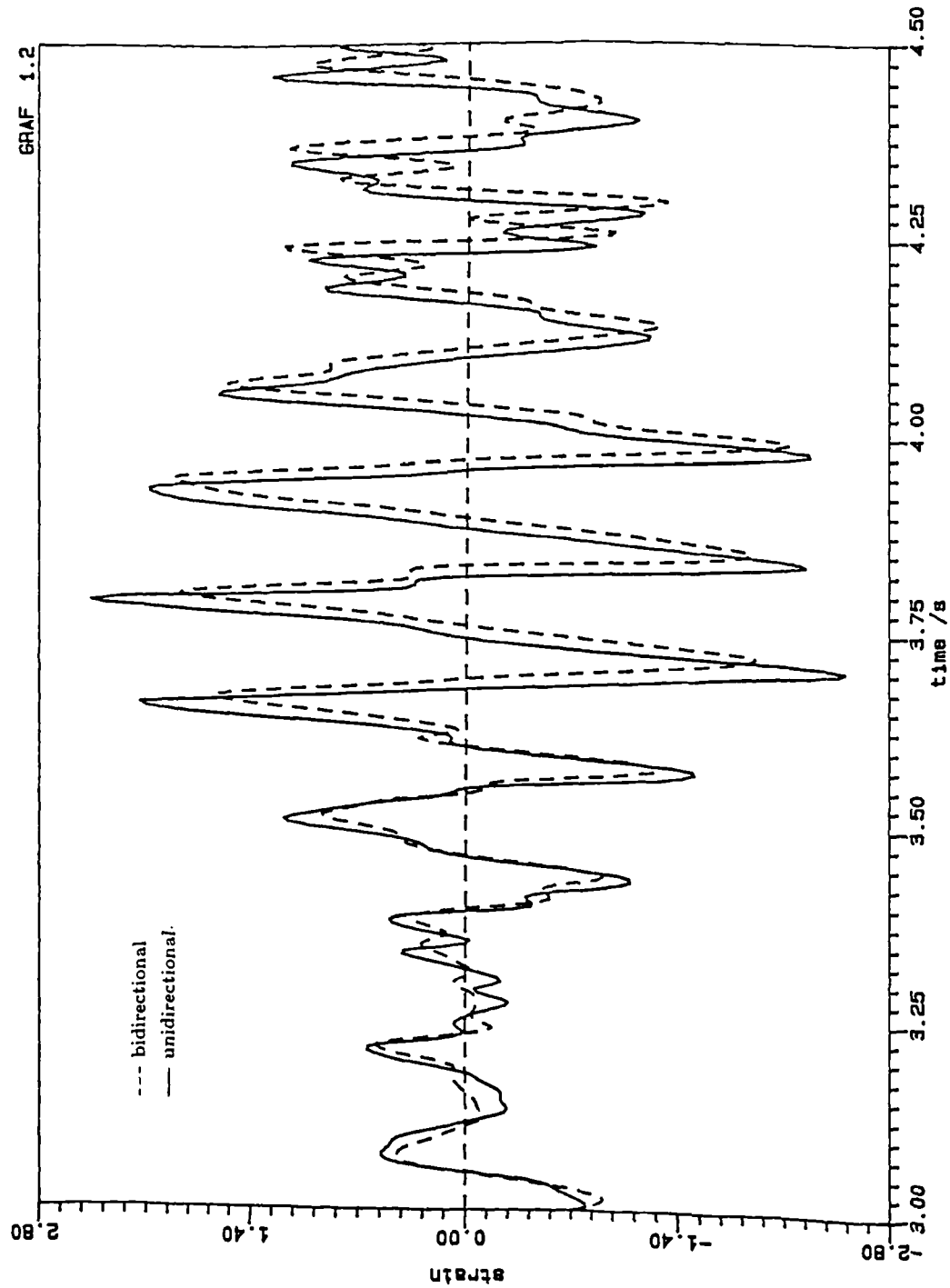

Fig.6.58 Large scale plot of the strongest part of the response of the OXYAF2, OYYAF2, and OXYAF2 tests

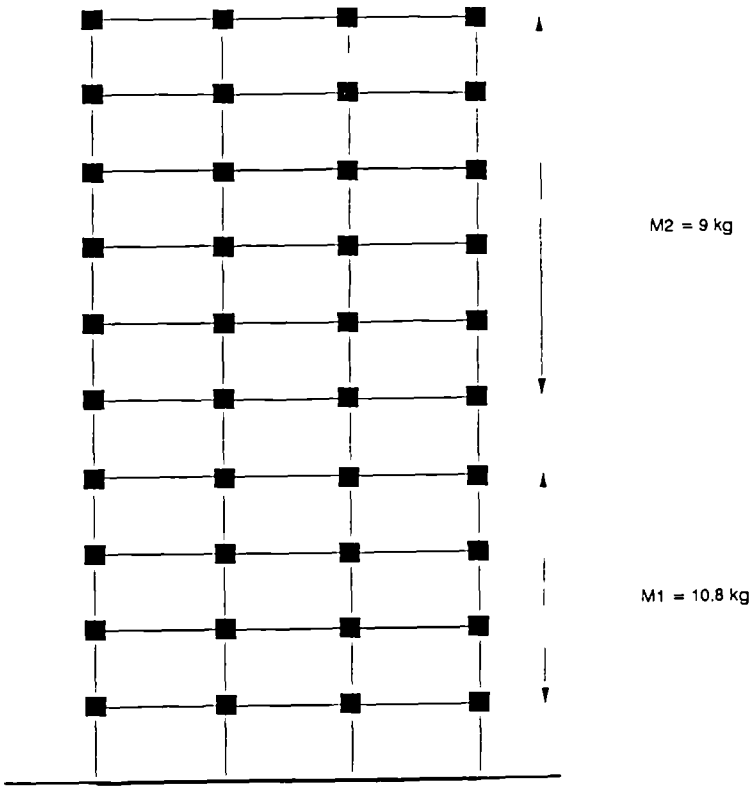

a- Ten storey frame

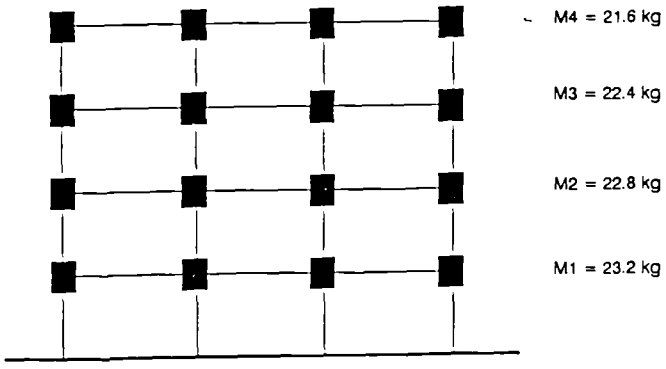

b- Four storey frame

Fig.7.1 Mass distribution in the 2-D models

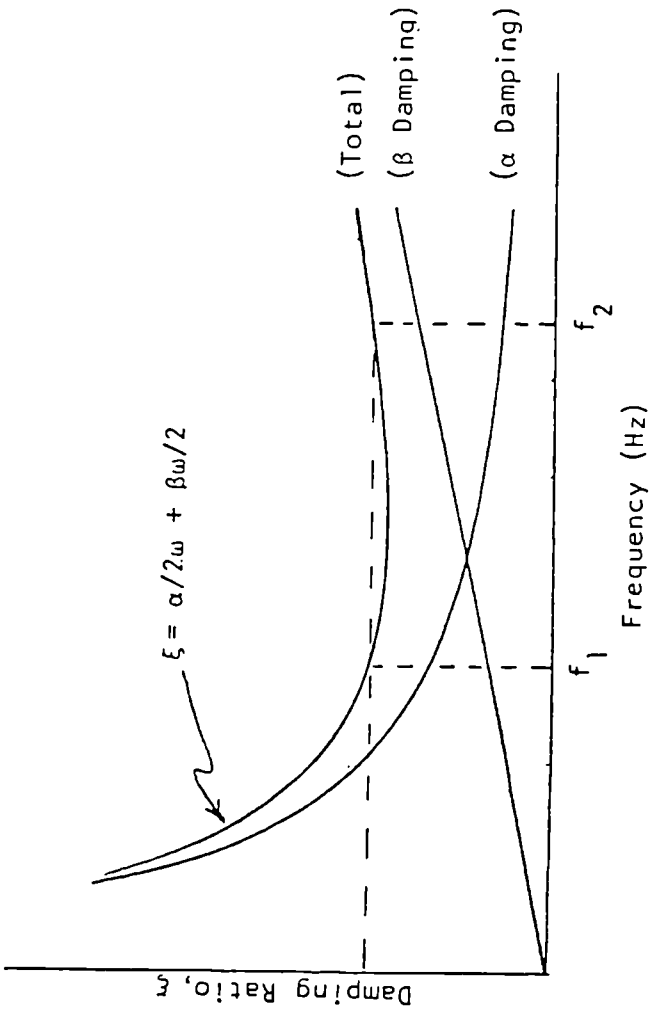

Fig.7.2 Damping coefficient variation with frequency [29]

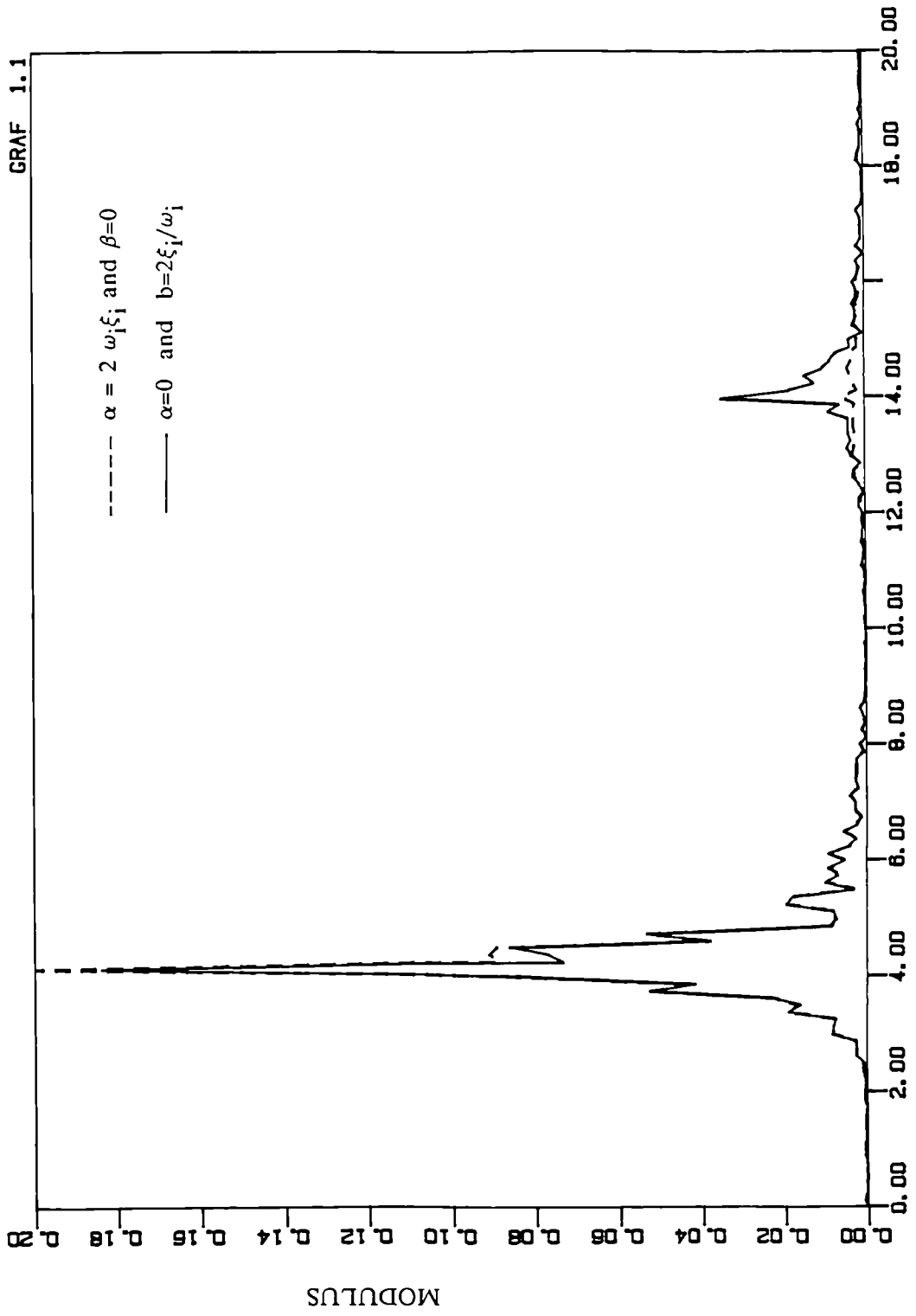

Fig.7.3 Effect of the damping coefficients on the dynamic response

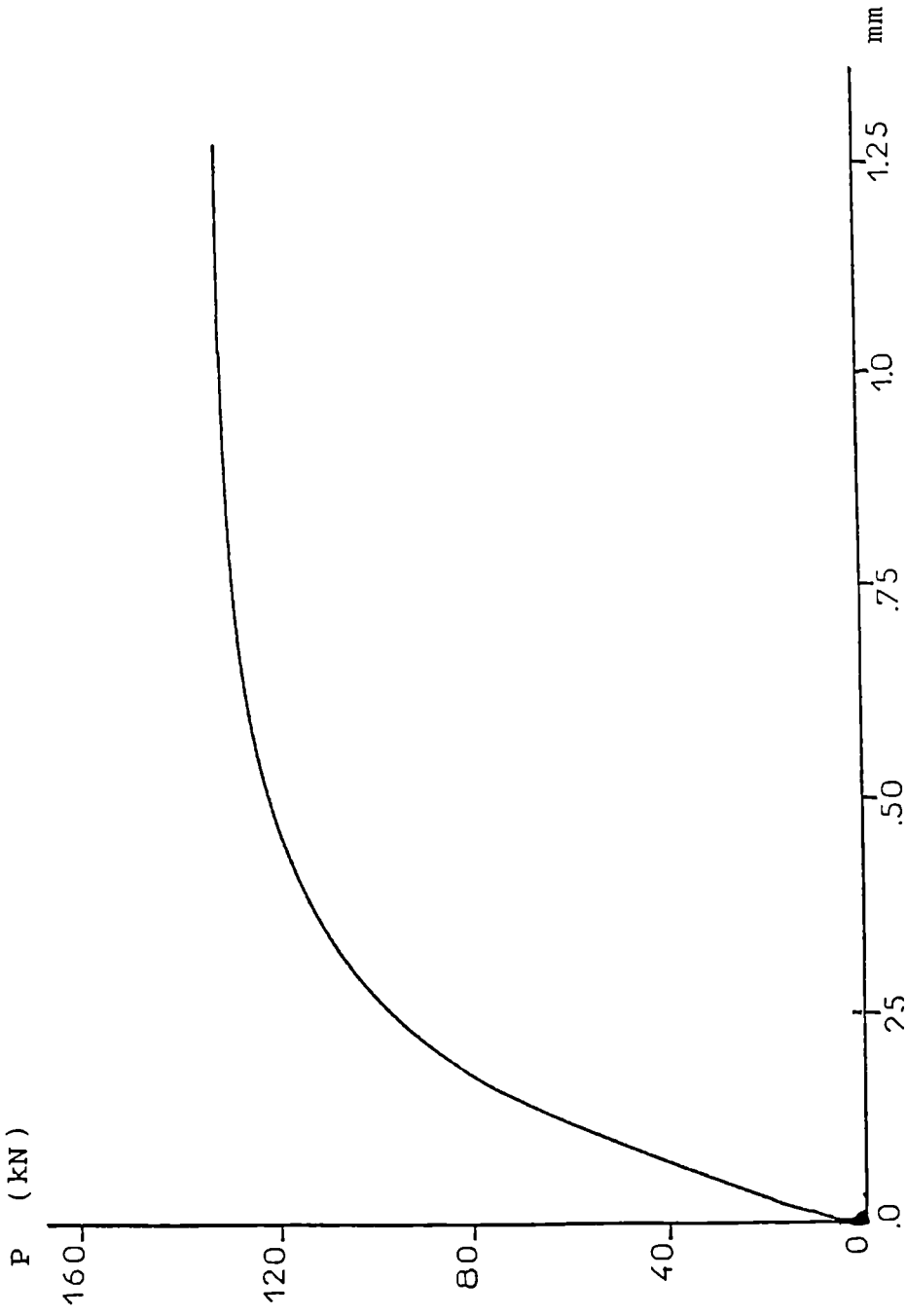

Fig.7.4 Load deformation curve from Uniaxial test on a beam unit

a- Forces and deformations of a 2-D elastic beam element

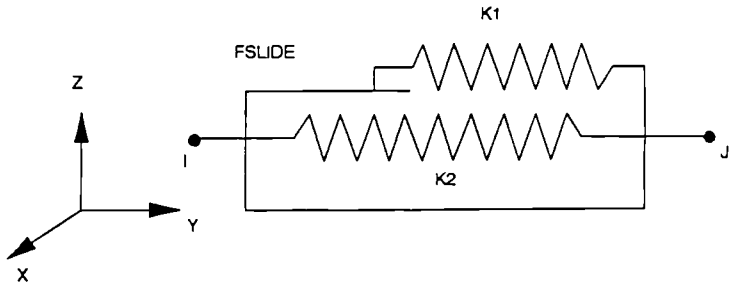

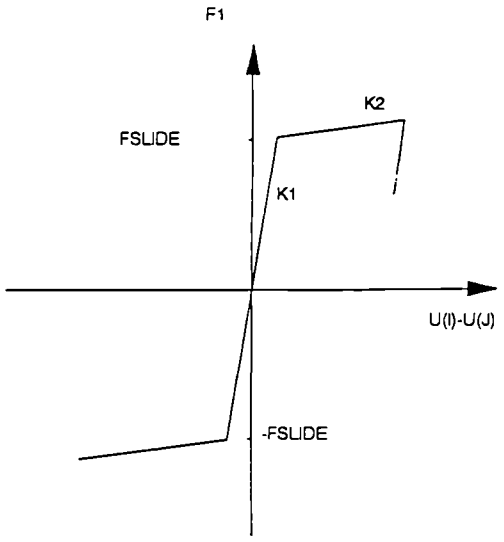

b- Element 40 of ANSYS (gap and dampers removed)

Fig.7.5 Beam and plastic hinge elements

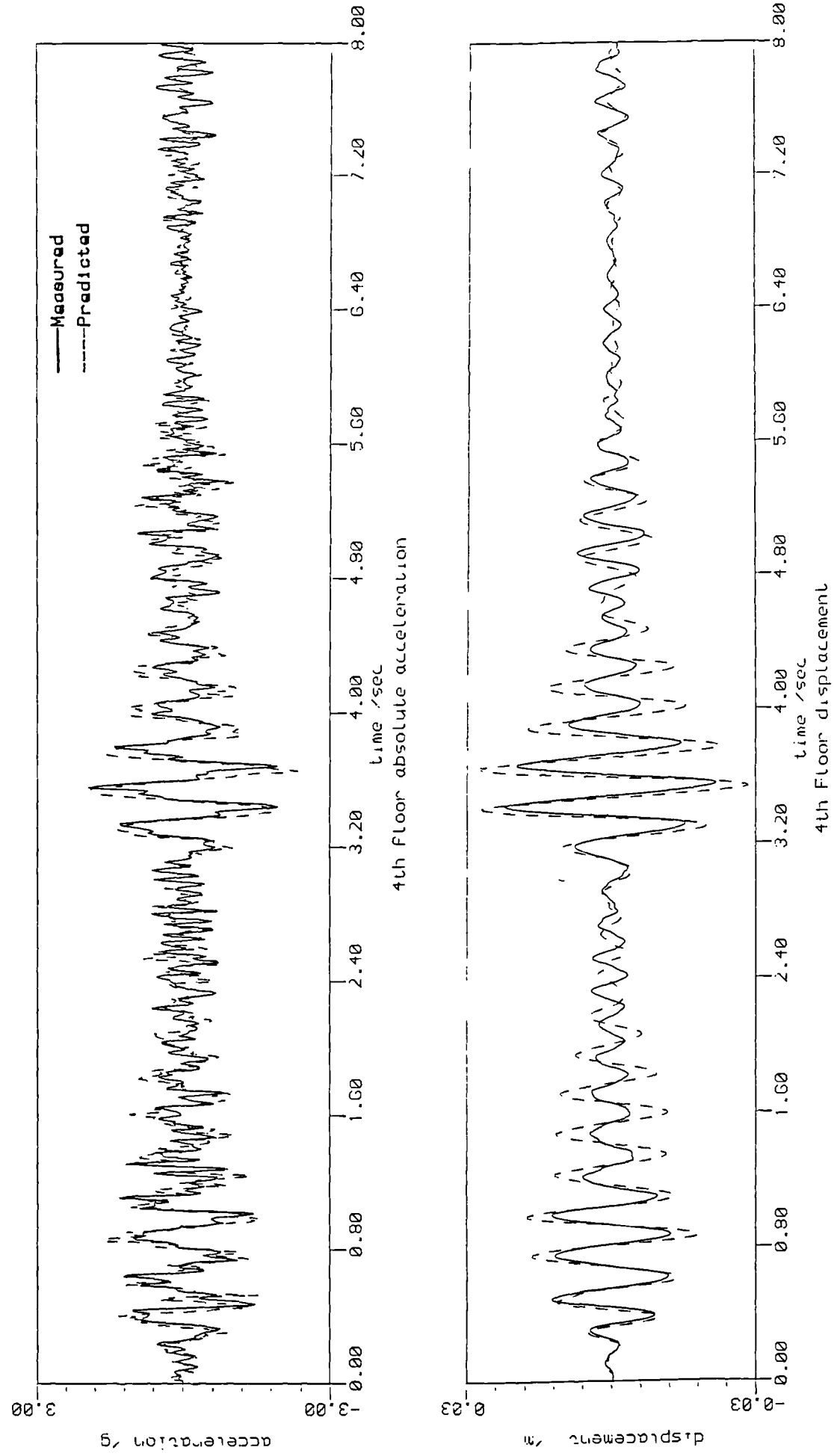

Fig.7.6 Measured and predicted response from ECMR3 test

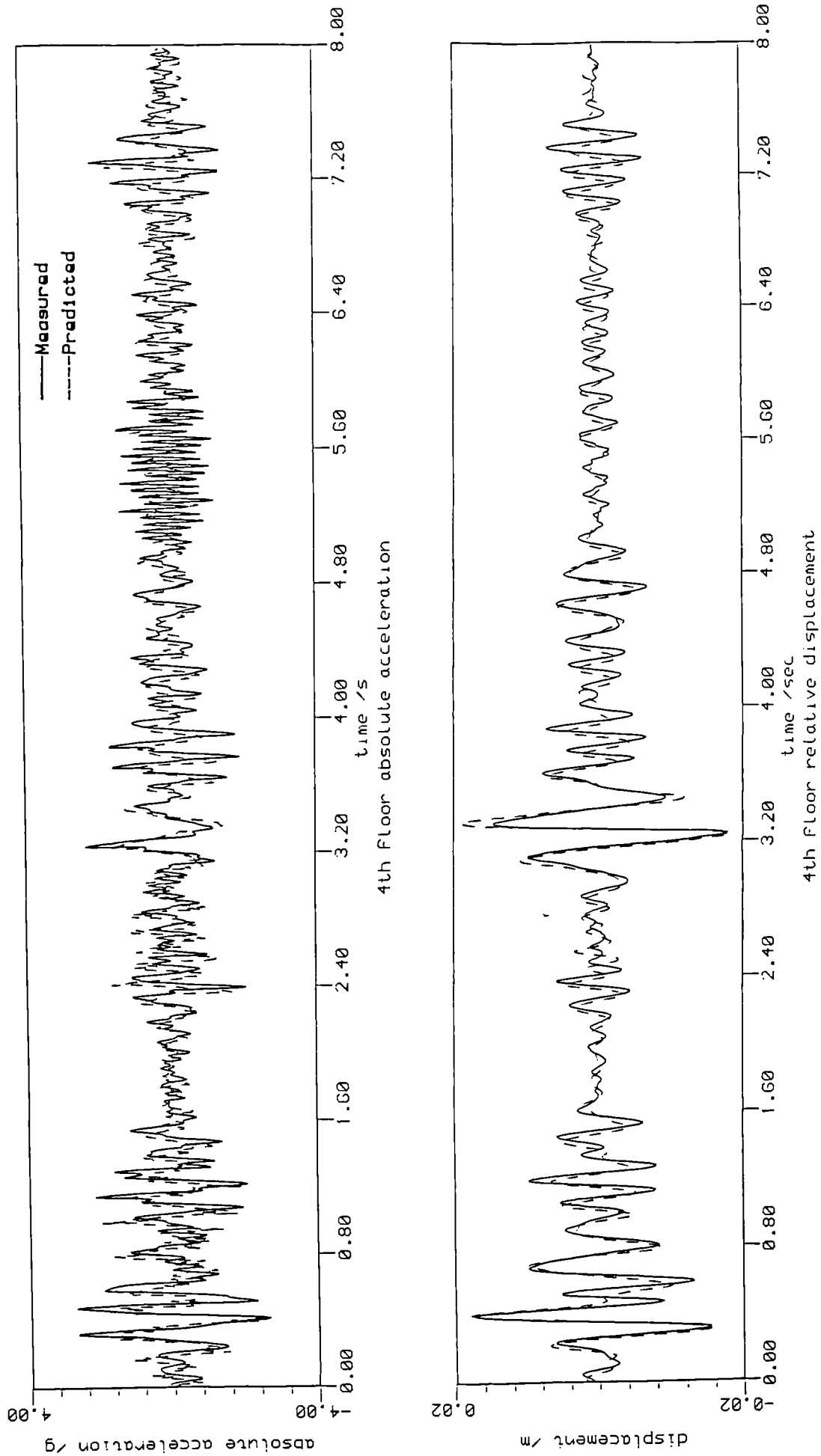

Fig.7.7 Measured and predicted response from ECVW4 test

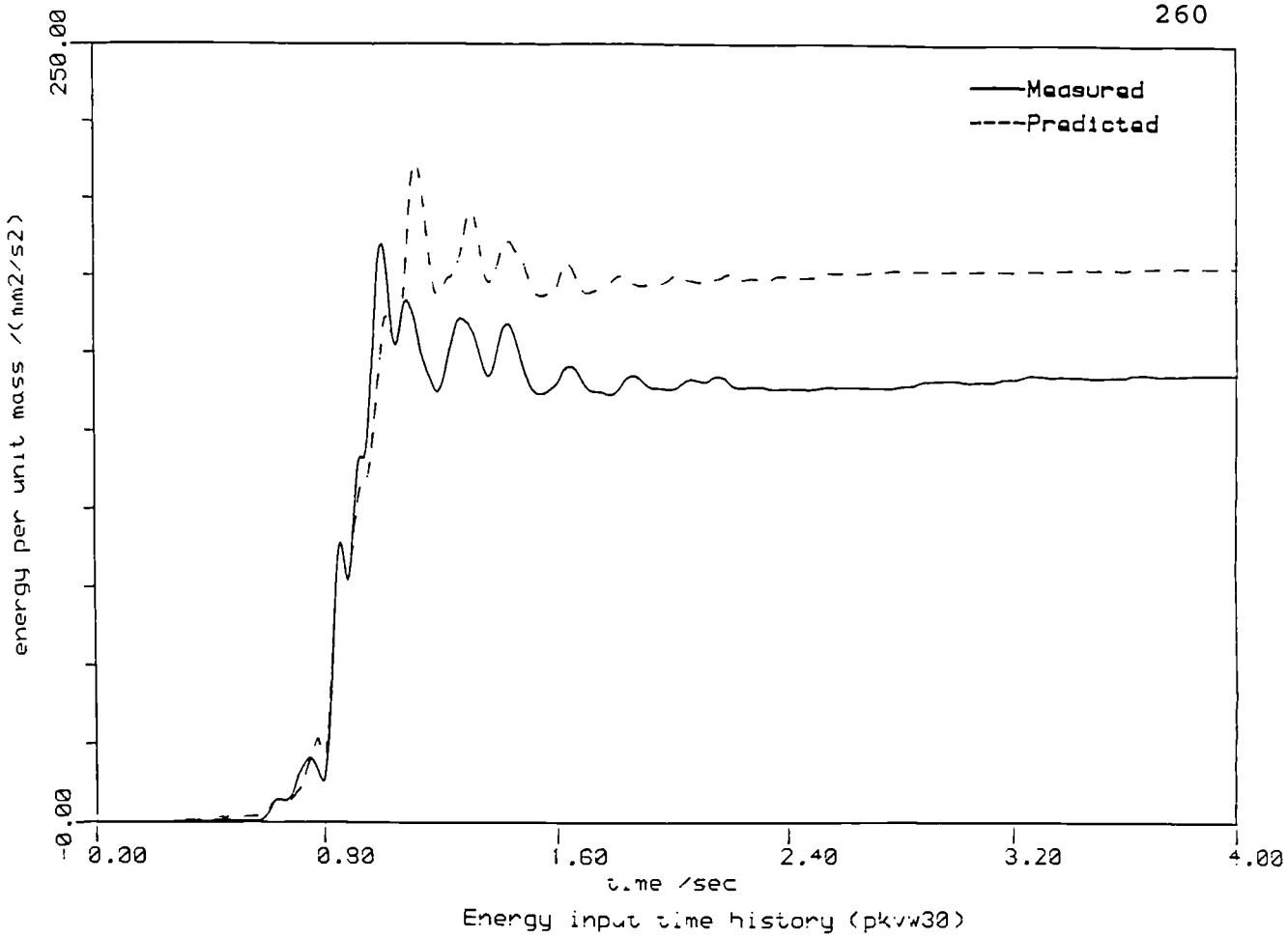

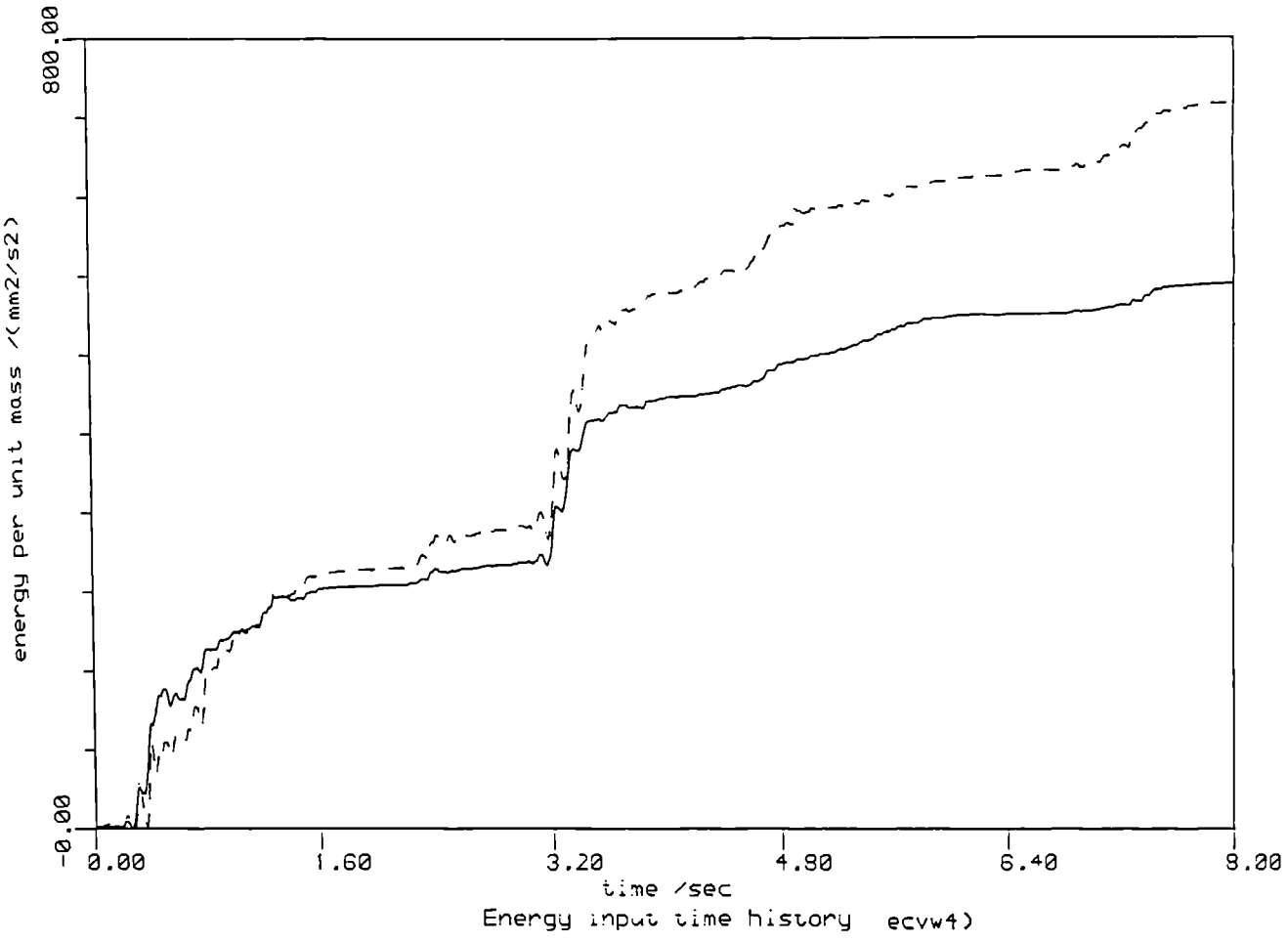

Fig.7.8 Measured and predicted input energy from PKVW3 and ECVW4 test

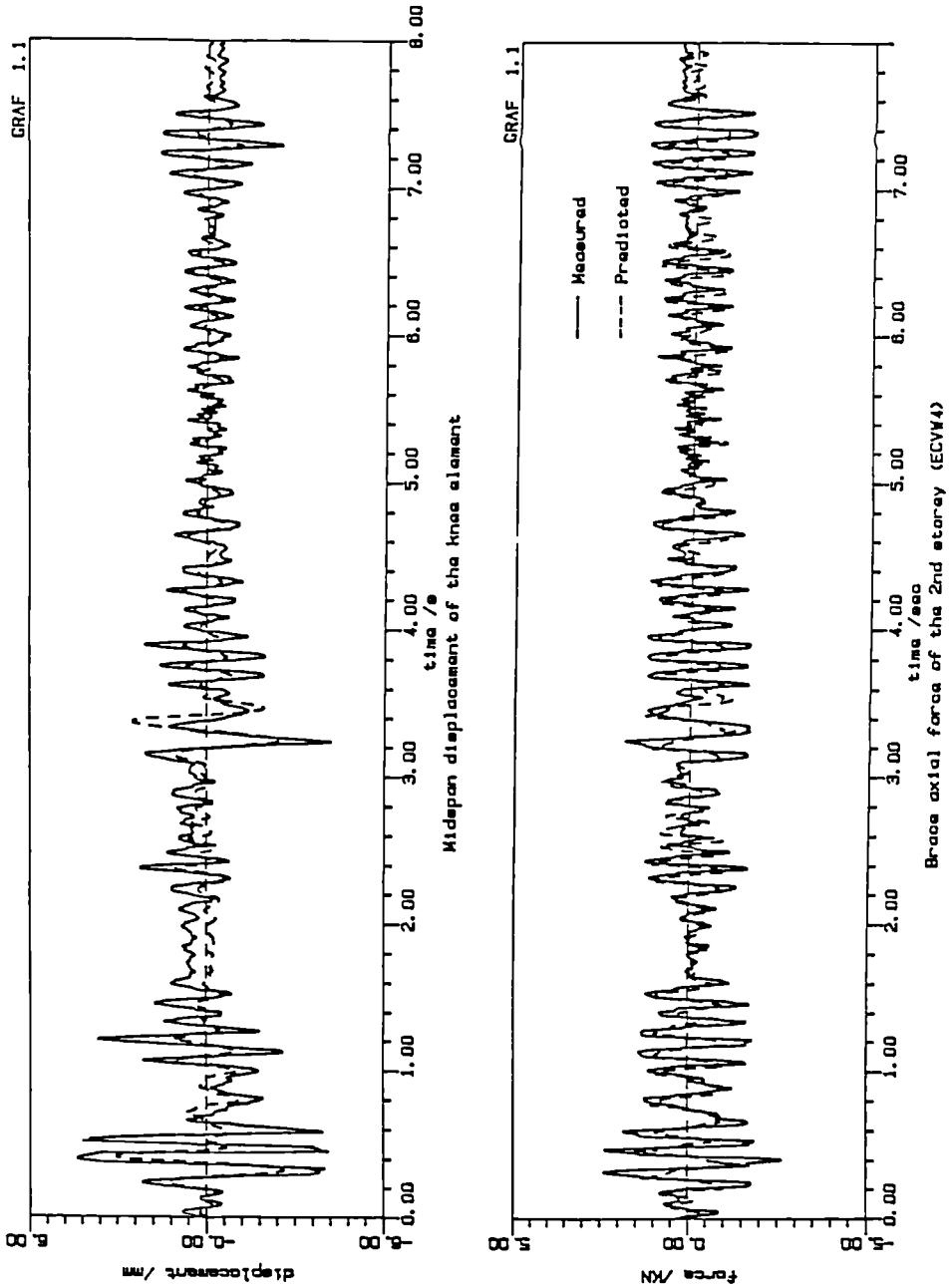

Fig.7.9 Measured and predicted brace force and knee element displacement ECVW4

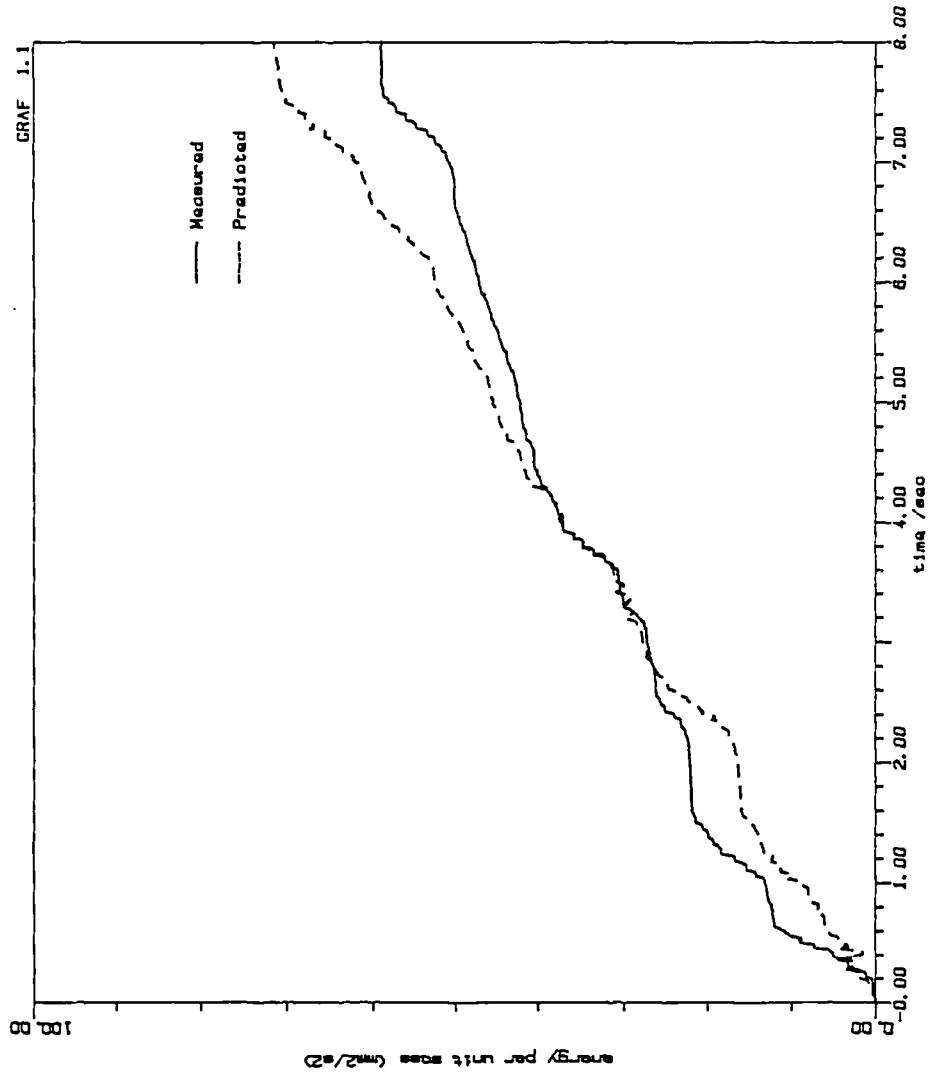

Fig.7.10 Measured and predicted hysteritic energy from ECVW4 test

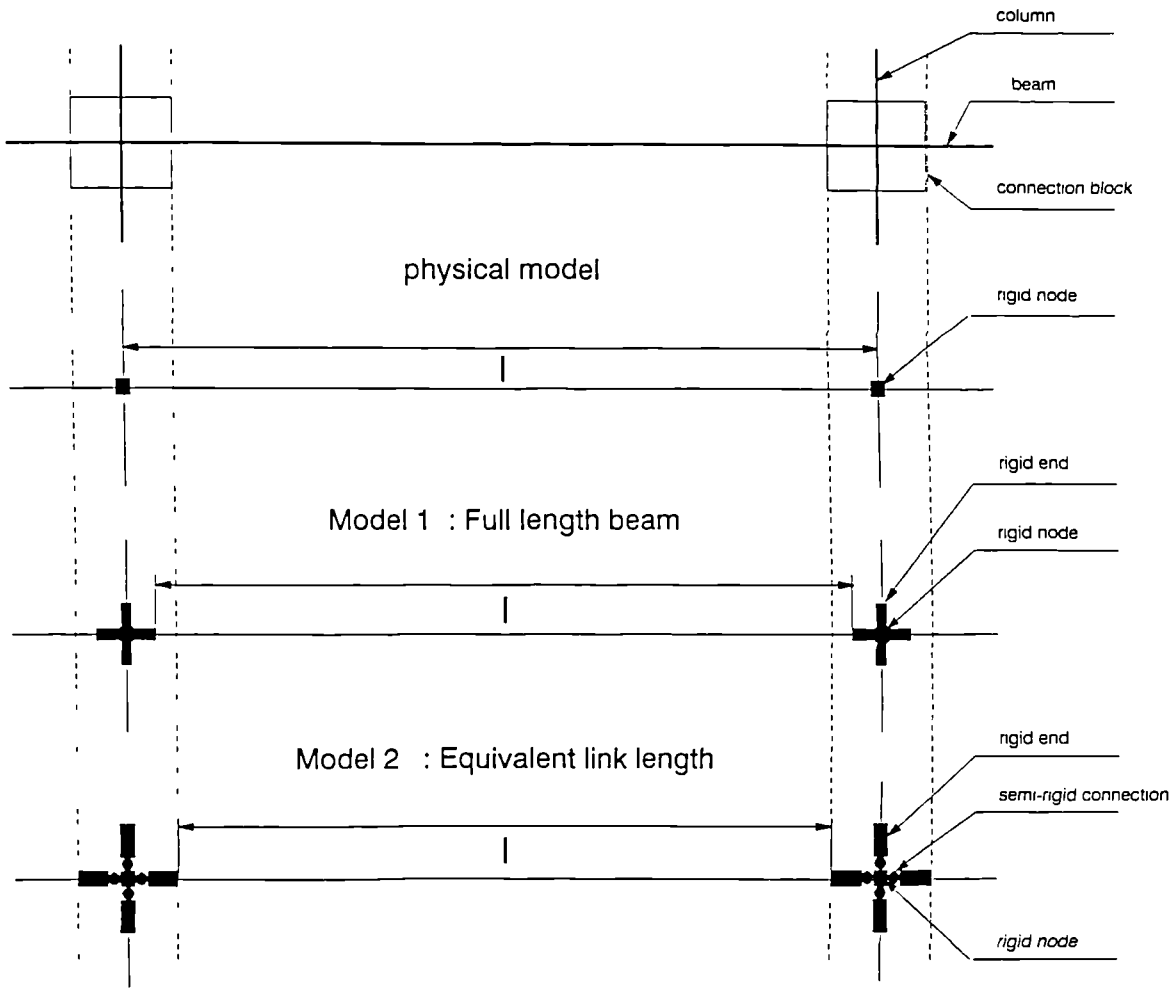

Model 3 : Full link length and semi-rigid connection

l = flexible length

Fig.7.11 Connection models

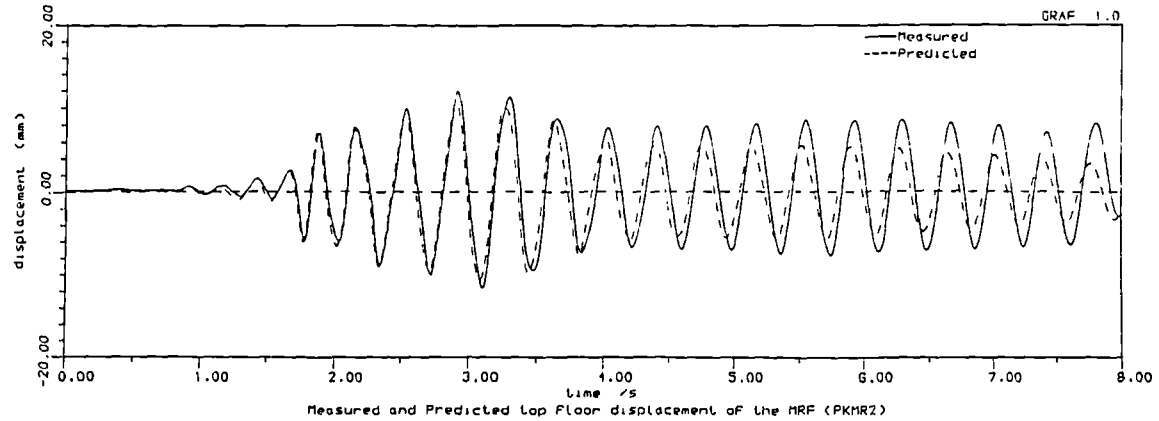

Measured and Predicted top floor displacement of the MRF (PKMR2)

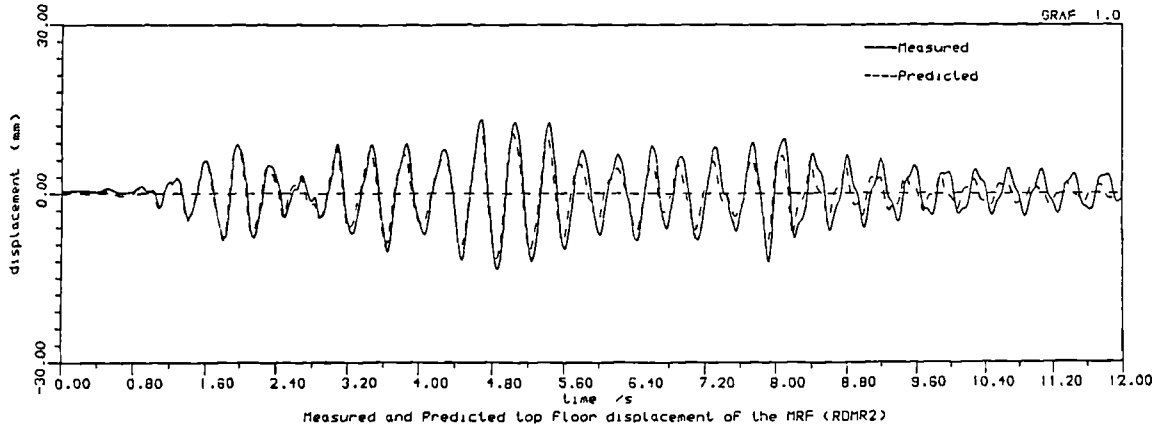

Measured and Predicted top floor displacement of the MRF (RDMR2)

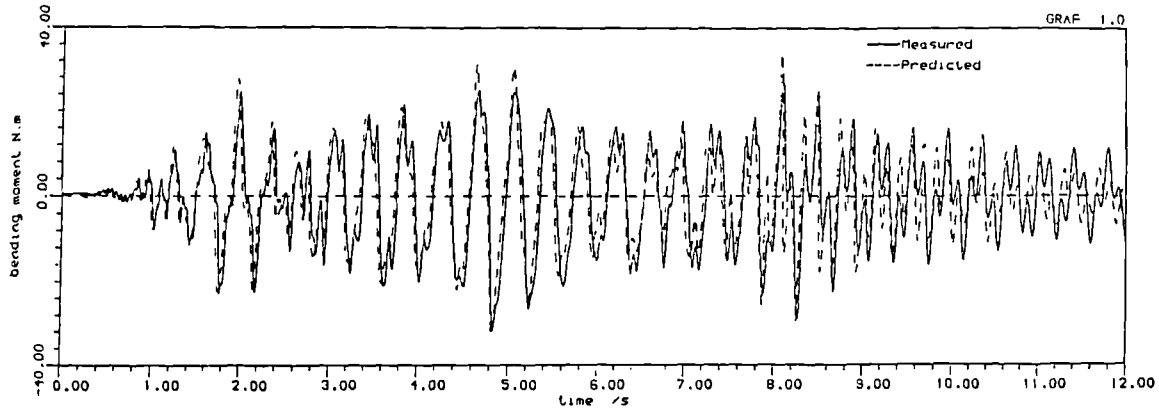

Measured and Predicted top bending moment of the MRF (RDMR2)

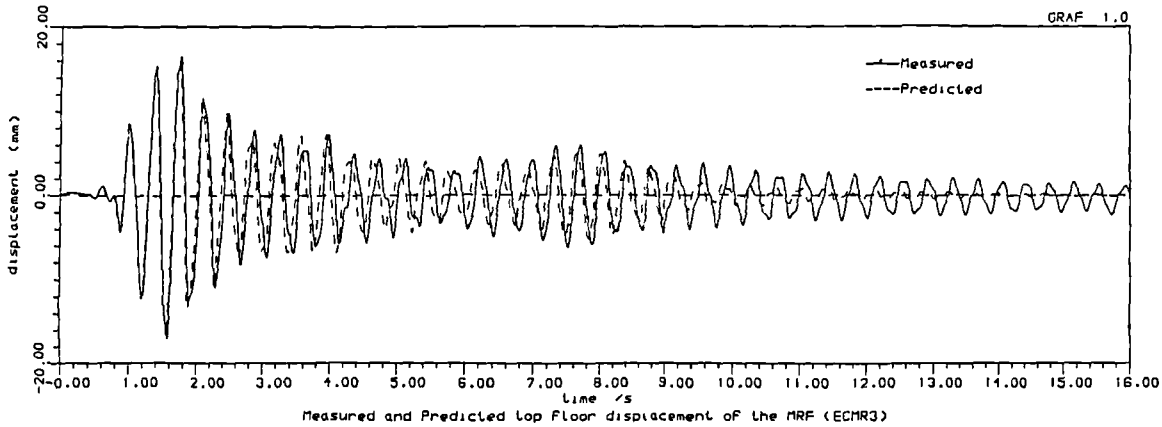

Measured and Predicted top floor displacement of the MRF (ECMR3)

Fig.7.12 Measured and predicted elastic response of the MRF

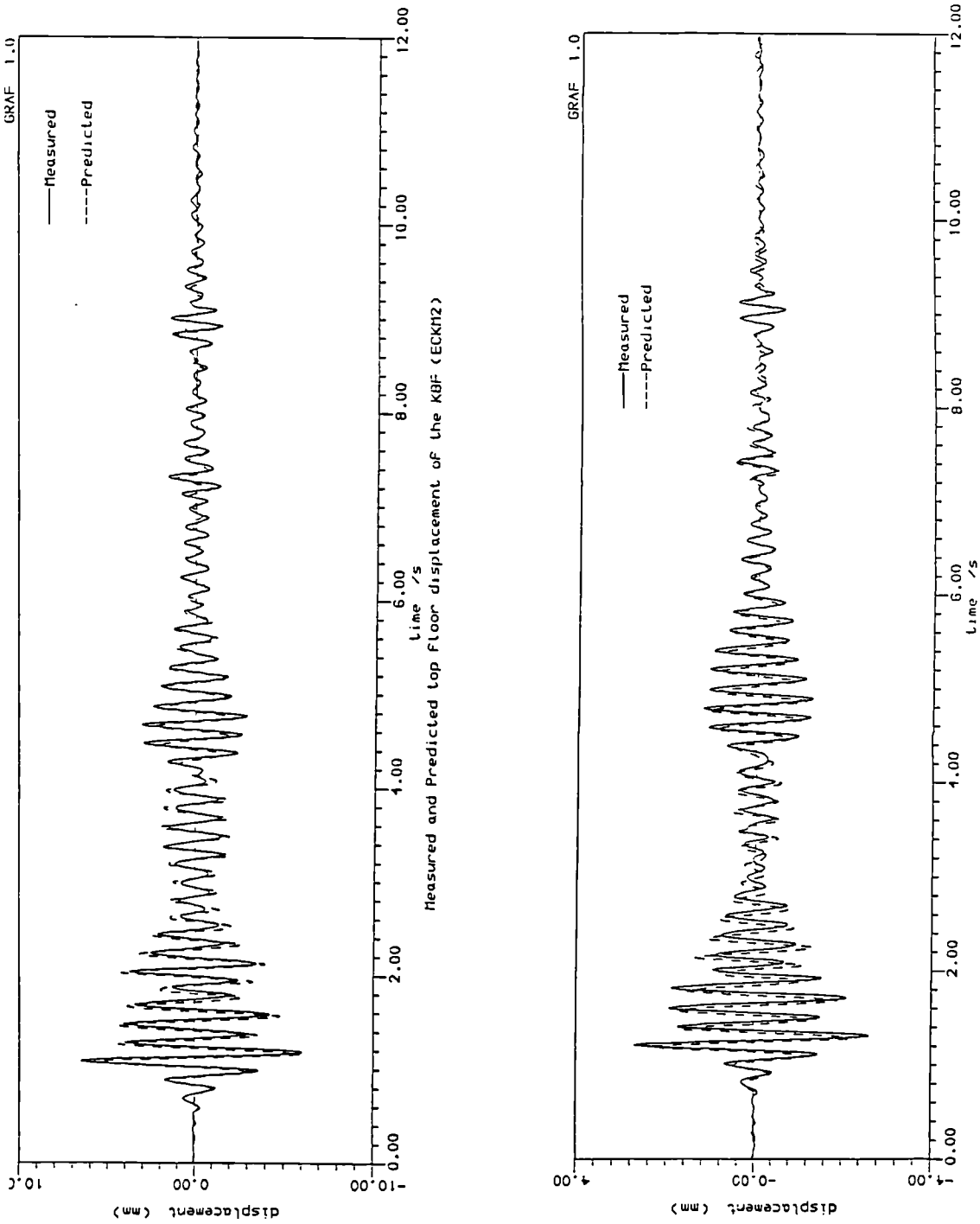

Fig.7.13 Measured and predicted elastic response of the KBF

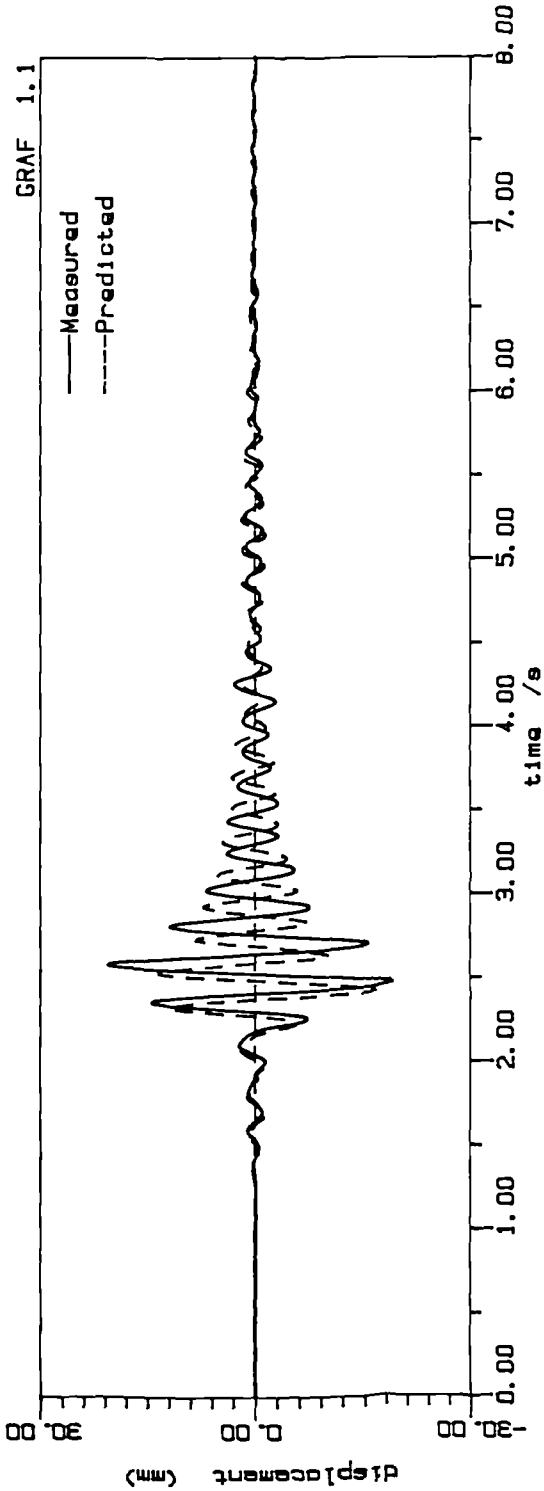

Fig.7.14 Measured and predicted inelastic response of the KBF

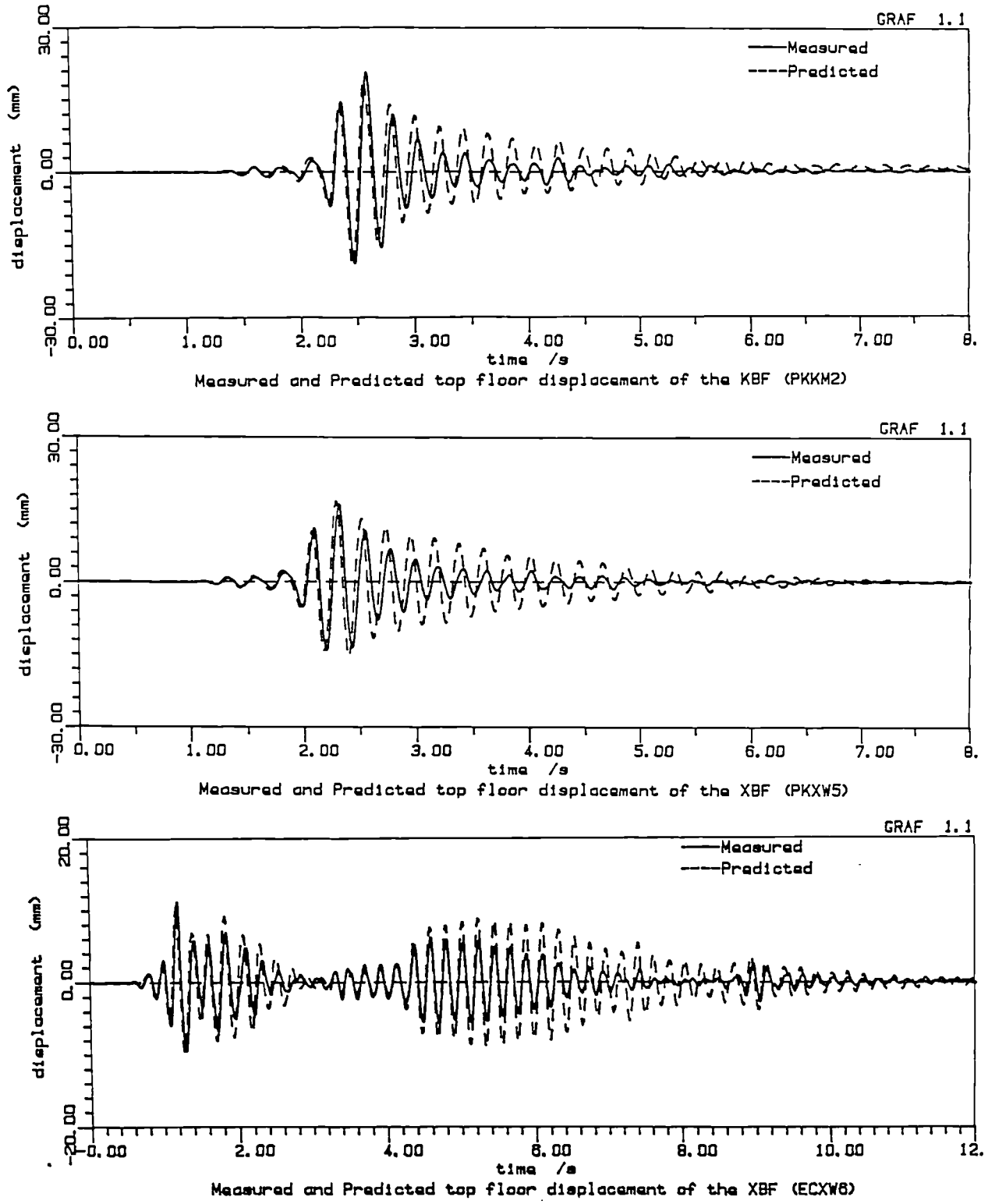

Fig.7.15 Measured and predicted inelastic responses of the KBF (corrected knee element stiffness)

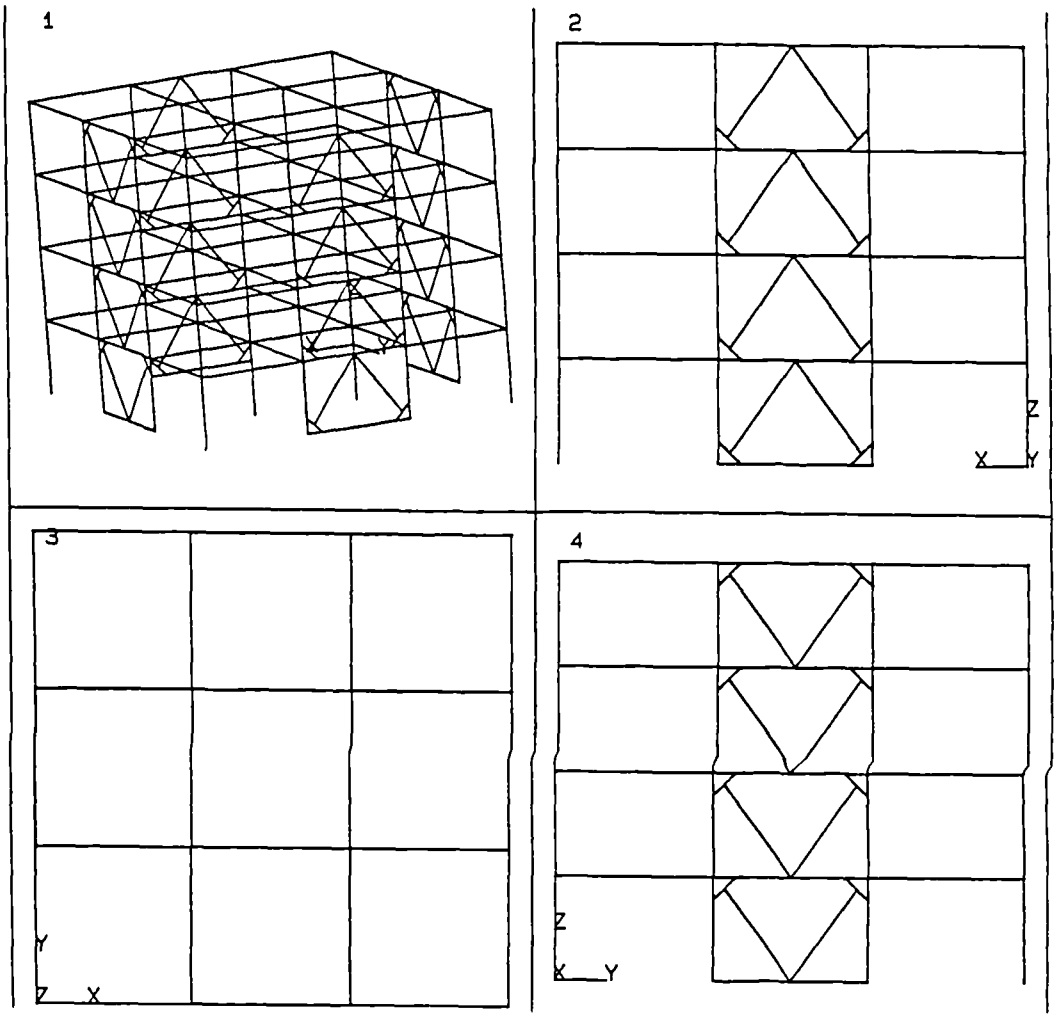

Fig.7.16 Typical 3-D numerical model

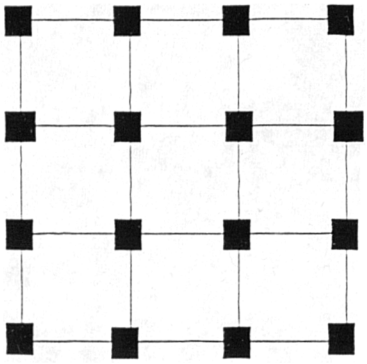

1st and 2nd floor :

m = 12.3 Kg

3rd and 4th floor :

m = 11.7 Kg

a- uniform mass distribution

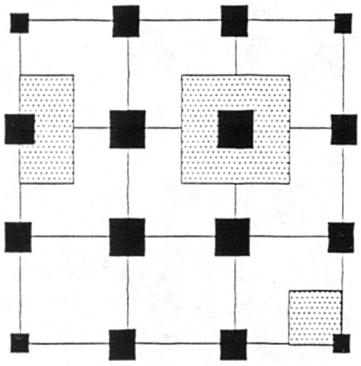

1st and second floor :

m3 = 3.1 Kg

m2 = 11.5 Kg

m3 = 28.1 Kg

3rd and 4th floor :

m1 = 2.9 Kg

m2 = 10.9 Kg

m3 = 26.8 Kg

b- mass distribution 2

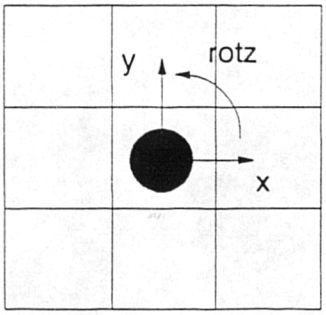

c- Single mass / floor model

Fig.7.17 Mass distribution in a typical floor of the 3-D model

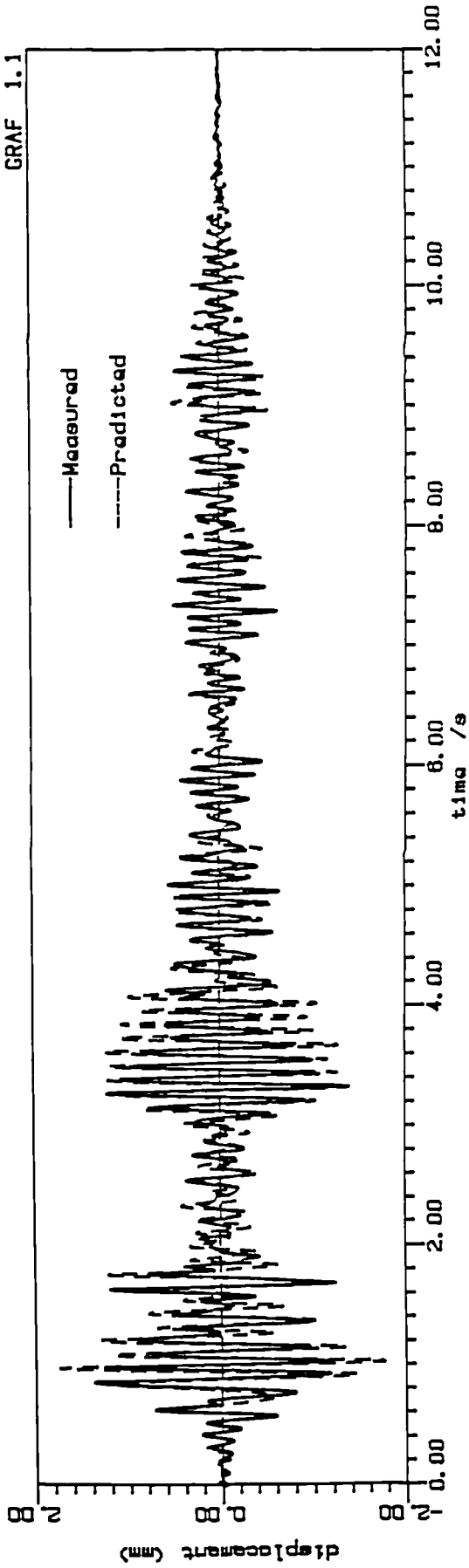

Fig.7.18 Measured and predicted top floor displacement of the OECSY1 test

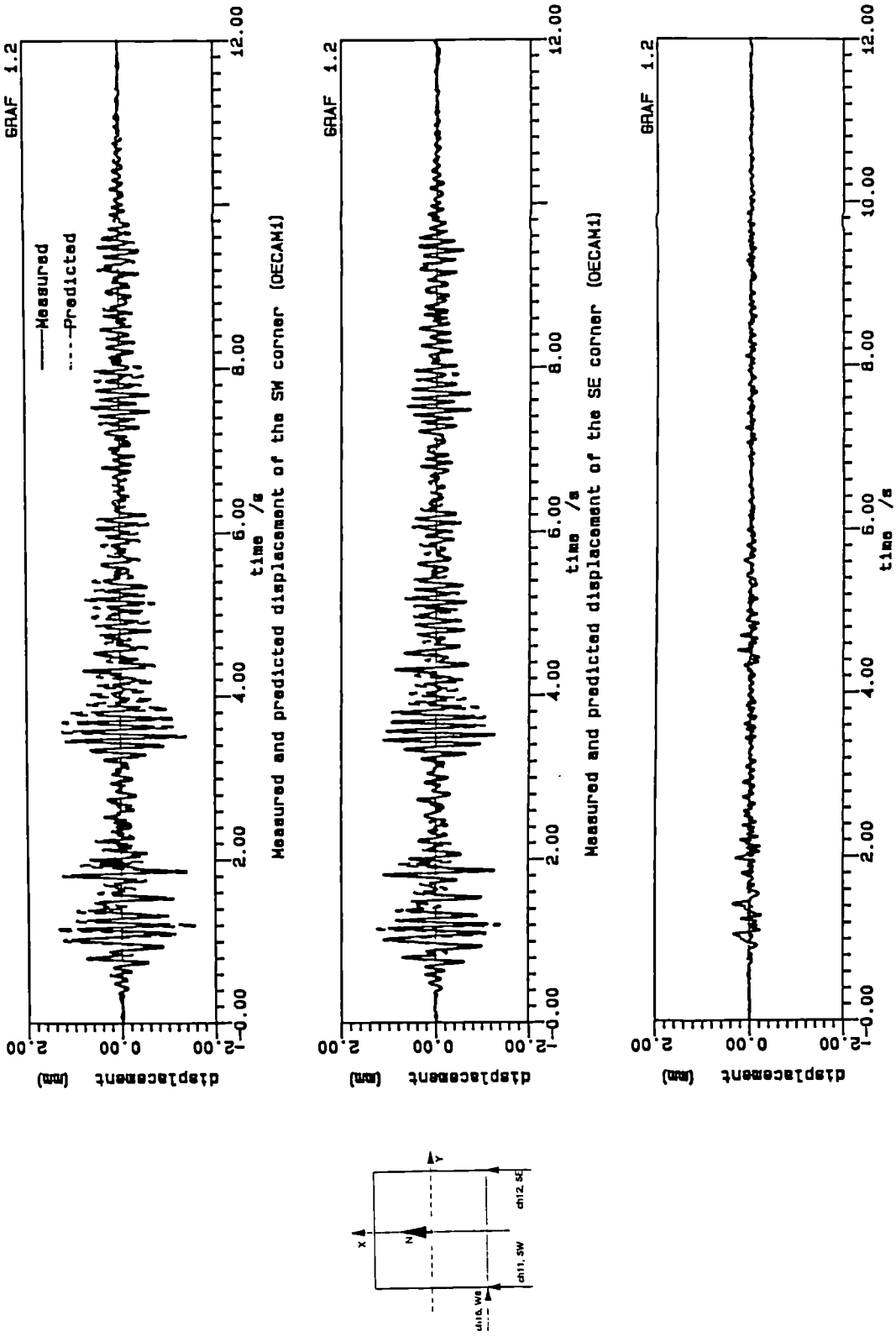

Fig.7.19 Measured and predicted top floor displacements of the OECAM1 test

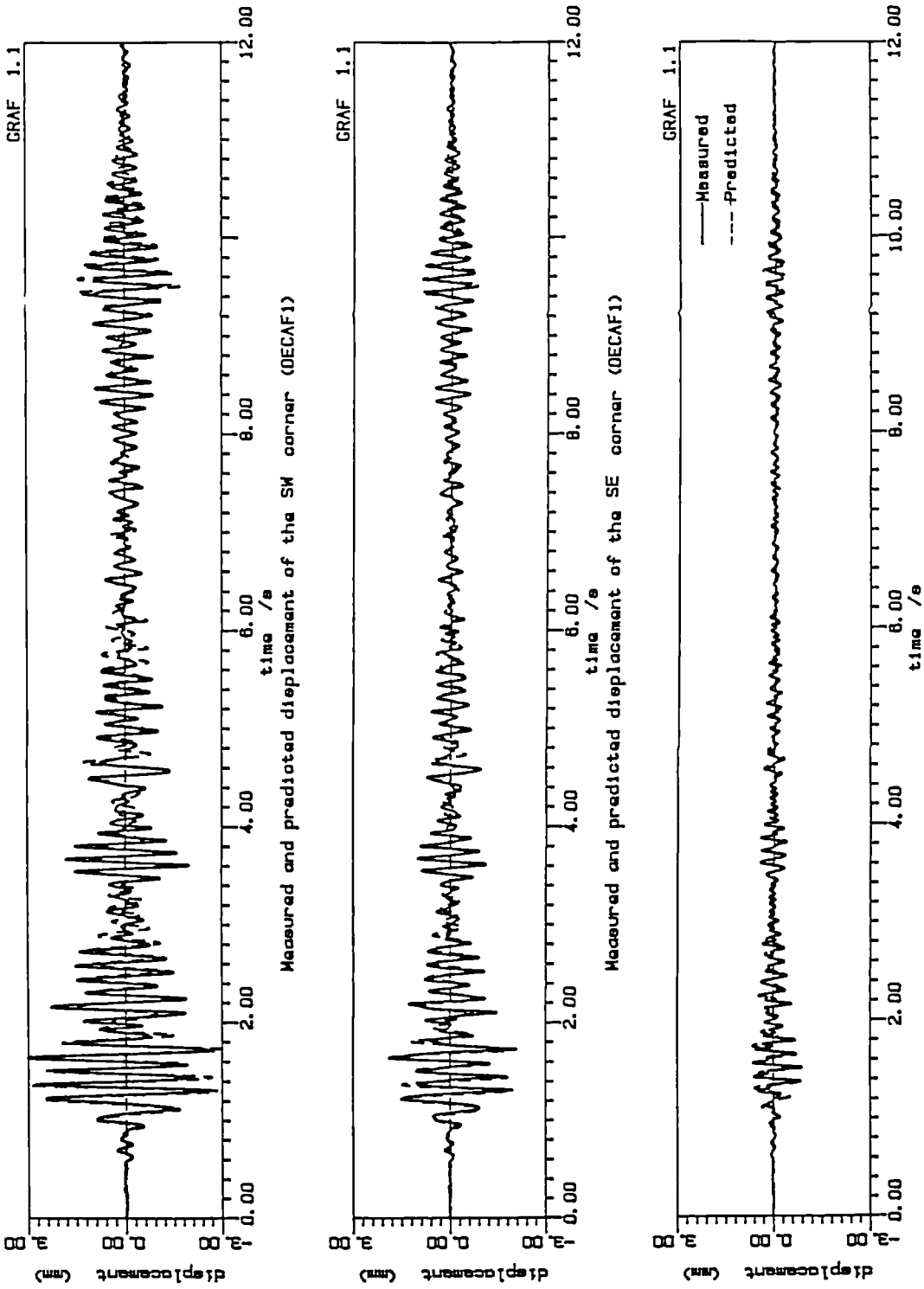

Fig.7.20 Measured and predicted top floor displacements of the OECAF1 test

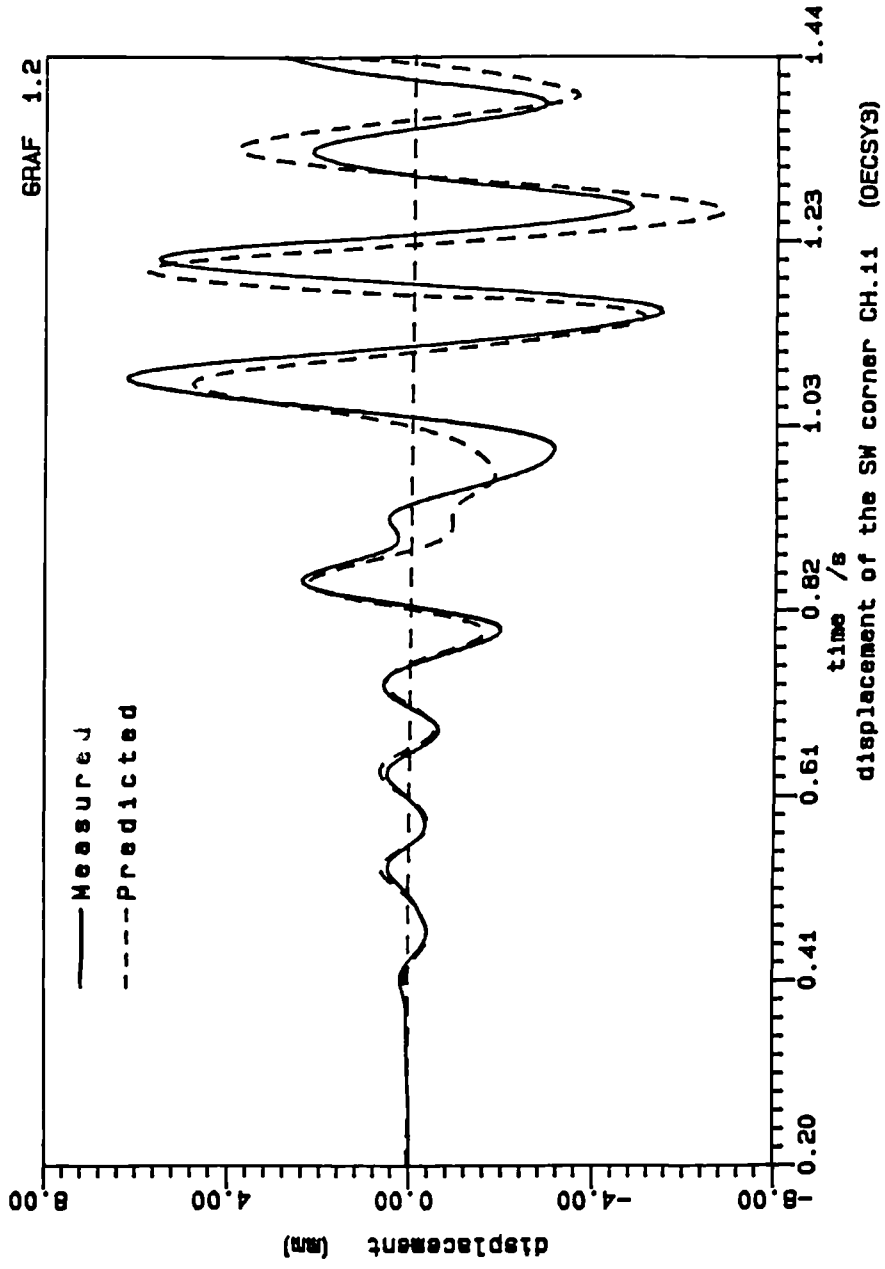

Fig.7.21 Measured and predicted top floor displacements of the OECSY3 test

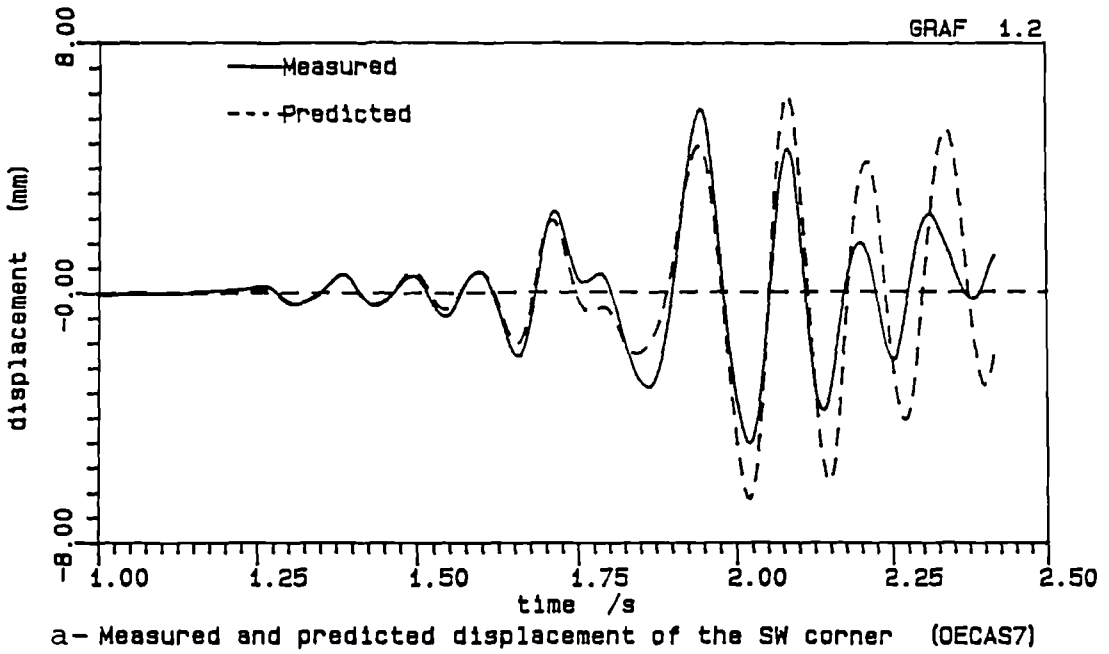

a- Measured and predicted displacement of the SW corner (OECAS7)

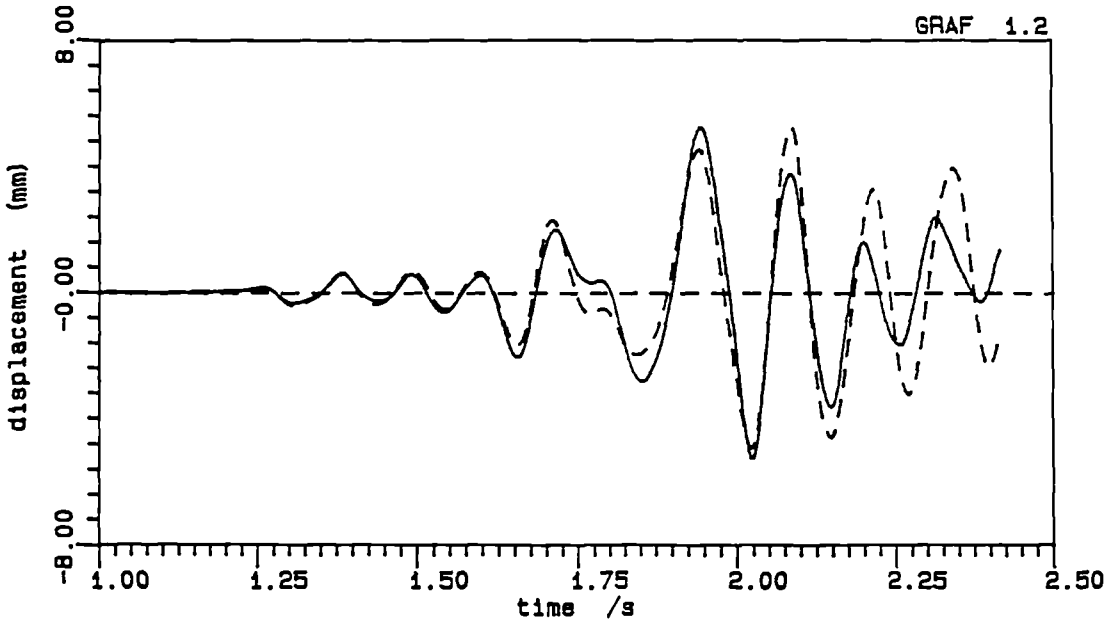

b- Measured and predicted displacement of the SE corner (OECAS7)

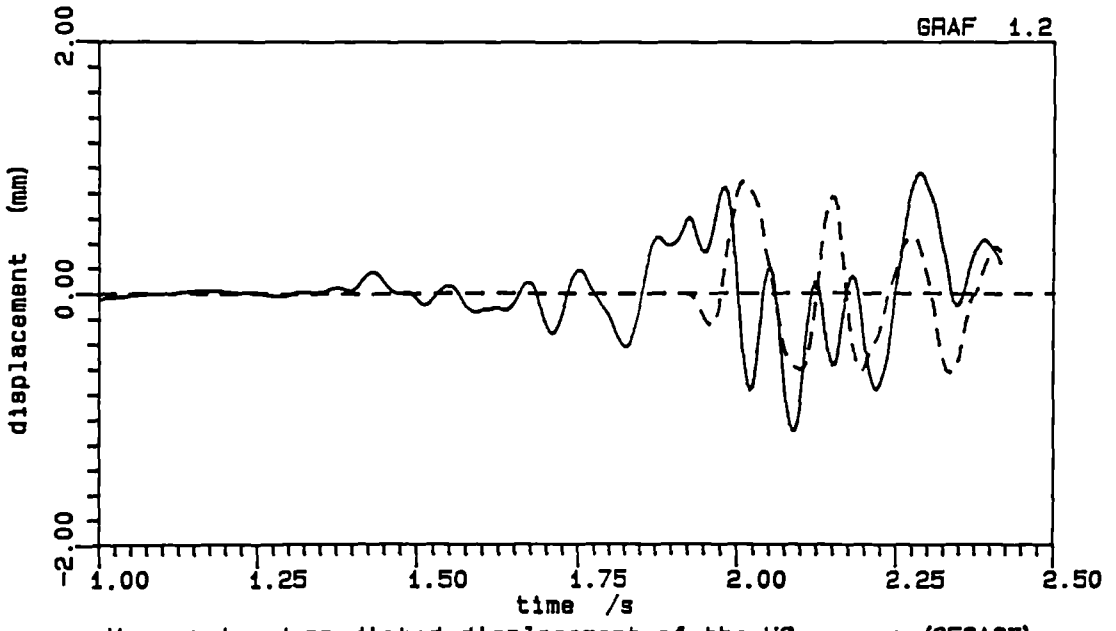

c- Measured and predicted displacement of the WS corner (OECAS7)

Fig.7.22 Measured and predicted top floor displacements of the OECAS7 test

TABLES

(1)	(2)	Dimension (3)	Scale Factors: True Replica Model (4)	Scale Factors: Artificial Mass Simulation (5)	Scale Factors: Gravity Forces Neglected Prototype Material (6)
Loading	Force, Q	F	$S_E S_l^2$	$S_E S_l^2$	S_l^2
	Pressure, q	FL^{-2}	S_E	S_E	1
	Acceleration, a	LT^{-2}	1	1	S_L^{-1}
	Gravitational acceleration, g	LT^{-2}	1	1	Neglected
	Velocity, v	LT^{-1}	$S_l^{1/2}$	$S_l^{1/2}$	1
	Time, t	T	$S_l^{1/2}$	$S_l^{1/2}$	S_l
Geometry	Linear dimension, l	L	S_l	S_l	S_l
	Displacement, δ	L	S_l	S_l	S_l
	Frequency, ω	T^{-1}	$S_l^{-1/2}$	$S_l^{-1/2}$	S_l^{-1}
Material properties	Modulus, E	FL^{-2}	S_E	S_E	1
	Stress, σ	FL^{-2}	S_E	S_E	1
	Strain, ϵ	—	1	1	1
	Poisson's ratio, ν	—	1	1	1
	Mass density, ρ	$FL^{-4}T^2$	S_E/S_l	*	1
	Energy, EN	FL	$S_E S_l^3$	$S_E S_l^3$	S_l^3

*$(g\rho l/E)_m = (g\rho l/E)_p$.

Table 4.1 Similitude scale factors from reference 2

specimen	D-centre (mm)	D-end (mm)	LOADING	COMMENTS
1	4	4	TENSION	Knee element used in dynamic tests
2	3	4	TENSION	
3	"	4	CYCLIC	
4	"	4	TENS/COMP	bad setting up of the shenck
5	"	4	TENSION	
6	"	4	COMP.	knee element bolts loosen
7	"	3	TENSION	
8	"	5	TENSION	
9	"	4	CYCLIC	

Table 4.2 Quasi-static test specimens

	Freq. Hz (prototype time ref.)	
mode	**model**	**prototype**
1	1.32	1.25
2	3.71	3.84
3	6.43	6.73

Table 4.3 Natural frequencies of the prototype and the model

Table 6.1 : Sequence of test series I

No	test name	Date/time	Comment
1	RDMR00	11/08/88 09:34 a	MRF identification test
2	RDSK00	16/08/88 10:20 a	SKBF identification test
3	ECSK10	19/08/88 09:02 a	Unrecorded data (out of range)
4	ECSK11	19/08/88 09:10 a	Lost !
5	ECSK20	19/08/88 09:12 a	
6	ECSK21	19/08/88 09:16 a	
7	ECSK22	19/08/88 09:20 a	
8	PKSK10	19/08/88 10:01 a	
9	PKSK11	19/08/88 10:06 a	
10	PKSK12	19/08/88 10:12 a	
11	PKSK20	19/08/88 10:48 a	
12	ECSK30	19/08/88 11:01 a	
13	PKSK30	19/08/88 11:08 a	Very noisy strain guages channels
14	PKSK31	19/08/88 11:14 a	
15	RDWK00	22/08/88 10:05 a	
16	ECWK10	22/08/88 02:28 p	Pretensionned braces
17	ECWK20	22/08/88 02:53 p	
18	ECWK30	22/08/88 03:14 p	
19	PKWK10	22/08/88 03:38 p	
20	PKWK20	22/08/88 03:41 p	
21	PKWK30	22/08/88 03:45 p	
22	PKWK31	22/08/88 03:54 p	
23	PKWK32	22/08/88 04:08 p	
24	ECWK11	23/08/88 10:36 a	
25	ECWK21	23/08/88 03:39 p	
26	SIWK00	25/08/88 10:56 a	Sinusoidal input
27	PKWK40	25/08/88 11:51 a	
28	ECWK40	25/08/88 12:12 p	mentionned as ECVW4
29	ECWK41	25/08/88 03:37 p	
30	ECWK42	25/08/88 03:42 p	
31	RDMR01	26/08/88 10:14 a	
32	ECMR10	26/08/88 03:24 p	
33	ECMR20	26/08/88 03:28 p	
34	ECMR30	26/08/88 03:30 p	
35	PKMR10	26/08/88 03:32 p	
36	PKMR20	26/08/88 03:36 p	
37	PKMR30	26/08/88 03:38 p	

Table 6.2 : Sequence of test series II

TEST NAME			DATE	TIME	COMMENTS
IDXU1	DAT	34560	4-07-89	9:03a	
ECXU1	DAT	100352	4-07-89	9:30a	
ECXU2	DAT	100352	4-07-89	9:59a	
PKXU1	DAT	67584	4-07-89	10:24a	
ECXU3	DAT	100352	4-07-89	10:29a	
RDXU1	DAT	100352	4-07-89	10:41a	
FEXU1	DAT	67584	4-07-89	10:49a	
FWXU1	DAT	67584	4-07-89	10:56a	
PKXU2	DAT	67584	4-07-89	11:12a	
RDXU2	DAT	100352	4-07-89	11:23a	
FEXU2	DAT	67584	4-07-89	11:27a	
FWXU2	DAT	67584	4-07-89	11:44a	
KYXU1	DAT	34816	4-07-89	2:04p	
KYXU2	DAT	34816	4-07-89	2:06p	
ECKU1	DAT	100352	4-10-89	8:36a	
ECKU2	DAT	100352	4-10-89	8:42a	
PKKU1	DAT	67584	4-10-89	8:44a	
PKKU2	DAT	67584	4-10-89	8:46a	
RDKU1	DAT	100352	4-10-89	8:51a	
RDKU2	DAT	100352	4-10-89	8:52a	
FEKU1	DAT	67584	4-10-89	8:55a	
FEKU2	DAT	67584	4-10-89	8:56a	
FWKU1	DAT	67584	4-10-89	9:00a	
FWKU2	DAT	67584	4-10-89	9:01a	
KYKU1	DAT	67584	4-10-89	9:28a	
KYKU2	DAT	67584	4-10-89	9:32a	
IDKM1	DAT	34688	4-11-89	10:18a	
ECKM1	DAT	100352	4-11-89	11:37a	
ECKM2	DAT	100352	4-11-89	11:43a	
ECKM3	DAT	100352	4-11-89	12:58p	
PKKM1	DAT	67584	4-11-89	1:15p	
PKKM2	DAT	67584	4-11-89	1:19p	
RDMKM1	DAT	100352	4-11-89	1:27p	
RDMKM2	DAT	100352	4-11-89	1:31p	
FEKM1	DAT	67584	4-11-89	1:35p	
FEKM11	DAT	67584	4-11-89	1:37p	
FEKM2	DAT	67584	4-11-89	1:39p	
FWKM1	DAT	67584	4-11-89	1:42p	
FWKM2	DAT	67584	4-11-89	1:46p	
KYKM1	DAT	67584	4-11-89	1:50p	
KYKM2	DAT	67584	4-11-89	1:51p	
PKKM3	DAT	67584	4-11-89	1:52p	
ECXM1	DAT	100352	4-12-89	1:17p	
ECXM2	DAT	100352	4-12-89	1:41p	
PKXM1	DAT	67584	4-12-89	1:46p	
PKXM2	DAT	67584	4-12-89	1:48p	
RDXM1	DAT	100352	4-12-89	1:52p	
RDXM2	DAT	100352	4-12-89	1:58p	
FEXM1	DAT	67584	4-12-89	2:03p	
FEXM2	DAT	67584	4-12-89	2:05p	
FWXM1	DAT	67584	4-12-89	2:13p	

FWXM2	DAT	67584	4-12-89	2:23p
ECXM3	DAT	100352	4-12-89	2:35p
ECXM4	DAT	100352	4-12-89	2:50p
PKXM3	DAT	67584	4-12-89	2:55p
KYXM1	DAT	67584	4-12-89	2:26p
KYXM2	DAT	67584	4-12-89	2:26p
IDXW1	DAT	34560	4-14-89	8:10a
ECXW1	DAT	100352	4-14-89	8:21a
ECXW2	DAT	100352	4-14-89	8:30a
ECXW3	DAT	100352	4-14-89	8:32a
PKXW1	DAT	67584	4-14-89	8:42a
PKXW2	DAT	67584	4-14-89	8:45a
RDXW1	DAT	100352	4-14-89	8:48a
RDXW2	DAT	100352	4-14-89	8:51a
FEXW1	DAT	67584	4-14-89	8:54a
FEXW2	DAT	67584	4-14-89	8:55a
FWXW1	DAT	67584	4-14-89	8:58a
FWXW2	DAT	67584	4-14-89	8:59a
KYXW1	DAT	67584	4-14-89	9:02a
KYXW2	DAT	67584	4-14-89	9:17a
ECXW4	DAT	100352	4-14-89	9:30a
ECXW5	DAT	100352	4-14-89	9:52a
ECXW6	DAT	100352	4-14-89	10:15a
PKXW3	DAT	67584	4-14-89	10:31a
PKXW5	DAT	67584	4-14-89	10:35a
IDNW1	DAT	34560	4-14-89	1:01p
ECNW1	DAT	67584	4-14-89	1:13p
ECNW2	DAT	100352	4-14-89	1:08p
PKNW2	DAT	67584	4-14-89	1:15p
RDNW1	DAT	100352	4-14-89	1:42p
RDNW2	DAT	100352	4-14-89	1:45p
FENW1	DAT	67584	4-14-89	1:47p
RDNW4	DAT	100352	4-14-89	1:57p
FENW2	DAT	67584	4-14-89	2:07p
FWNW2	DAT	67584	4-14-89	2:10p
KYNW1	DAT	67584	4-14-89	2:12p
KYNW2	DAT	67584	4-14-89	2:13p
ECNW7	DAT	100352	4-14-89	2:31p
ECNW10	DAT	100352	4-14-89	2:47p
ECNW11	DAT	100352	4-14-89	3:17p
IDMR1	DAT	34560	4-14-89	4:10p
ECMR1	DAT	100352	4-14-89	4:22p
ECMR2	DAT	100352	4-14-89	4:24p
ECMR3	DAT	133120	4-14-89	4:25p
PKMR1	DAT	67584	4-14-89	4:28p
PKMR2	DAT	67584	4-14-89	4:30p
PKMR3	DAT	100352	4-14-89	4:31p
RDMR1	DAT	100352	4-14-89	4:33p
RDMR2	DAT	100352	4-14-89	4:34p
FEMR1	DAT	67584	4-14-89	4:37p
FEMR2	DAT	100352	4-14-89	4:39p
FWMR1	DAT	100352	4-14-89	4:40p
FWMR2	DAT	100352	4-14-89	4:42p
KYMR1	DAT	100352	4-14-89	4:48p
KYMR2	DAT	100352	4-14-89	4:49p
IDMR2	DAT	34560	4-14-89	5:21p

Table 6.1 : Sequence of test series III

TEST NAME			DATE	TIME	COMMENTS
IBFW3	DAT	34816	3-23-89	3:52p	
IBFYR	DAT	34688	3-27-89	5:08p	
IBFXR	DAT	34688	3-27-89	5:20p	
IECAM1	DAT	67584	3-28-89	10:40a	
IECAM2	DAT	67584	3-28-89	11:01a	
IAMAS1	DAT	34688	3-28-89	11:19a	
IAMAS2	DAT	34688	3-28-89	11:29a	
IAMAS3	DAT	34944	3-28-89	11:43a	
OECAS7	DAT	100352	3-30-89	11:36a	
OECAS1	DAT	67584	3-30-89	11:55a	
OECAF1	DAT	100352	3-30-89	1:49p	
OECAF2	DAT	100352	3-30-89	1:55p	
OXYAF2	DAT	67584	3-30-89	2:00p	
OXYAF1	DAT	67584	3-30-89	2:02p	
OXXAF1	DAT	67584	3-30-89	2:04p	
OYYAF1	DAT	67584	3-30-89	2:05p	
OXXAF2	DAT	67584	3-30-89	2:08p	
OYYAF2	DAT	67584	3-30-89	2:09p	
OECSY1	DAT	100352	3-30-89	3:38p	
OECSY2	DAT	100352	3-30-89	3:43p	
OECSY3	DAT	100352	3-30-89	3:44p	
OXXSY1	DAT	67584	3-30-89	3:51p	
OXXSY2	DAT	67584	3-30-89	3:52p	
OYYSY1	DAT	67584	3-30-89	3:54p	
OYYSY2	DAT	67584	3-30-89	3:55p	
OXYSY1	DAT	100352	3-30-89	3:56p	
OXYSY2	DAT	67584	3-30-89	3:57p	
OECAM1	DAT	100352	3-30-89	4:08p	
OECAM2	DAT	100352	3-30-89	4:10p	
OSYYR	DAT	34560	3-30-89	4:44p	
OSYXR	DAT	34560	3-30-89	4:58p	
OWXL	DAT	34944	3-31-89	9:40a	
OWAM1	DAT	34944	3-31-89	4:37p	
OAMXR	DAT	34560	3-31-89	4:52p	

Appendix A

DYNAMIC RESPONSE OF MDOF SYSTEMS

APPENDIX A : DYNAMIC RESPONSE OF MDOF SYSTEMS

A.1 MODE SUPERPOSITION METHOD [23]

In the dynamic response analysis of a MDOF system the equation of motion can be expressed as

$$M\ddot{U} + CU + KU = P(t) \tag{A-1}$$

where M, C, and K are the mass, stiffness and damping matrices, all of order n; the vectors U and P store the displacements and forces, respectively, and a dot denotes a time derivative.

For undamped, free vibrations, Eq. (A-1) can be reduced to the eigenvalue equation

$$K\Phi = M\Phi\Omega^2 \tag{A-2}$$

from which the vibration mode shape matrix Φ and frequency vector Ω can be determined.

The next step is to write the equation of dynamic equilibrium in the basis of eigenvector by introducing the coordinate transformation:

$$U(t) = \Phi\ Y(t) = \Sigma\ \Phi_n\ Y_n(t) \tag{A-3}$$

where Φ is a vector storing the eigenvectors of the system and $Y_n(t)$ are referred to as normal coordinates. The generalised mass and generalised load for each mode can be computed:

$$M_n = \Phi_n{}^T\ M\ \Phi_n \tag{A-4}$$

$$P_n(t) = \Phi_n{}^T P(t) \tag{A-5}$$

By substituting Eq. (A-3) into Eq. (A-1) and the resulting equation is multiplied by Φ^T the equation of motion for each mode can then be written as

$$M_n\ddot{Y}_n + C_n\dot{Y}_n + K_nY_n = P_n(t) \tag{A-6}$$

or

$$\ddot{Y}_n + 2\xi_n\omega_n\dot{Y}_n + \omega_n{}^2Y_n = P_n(t)/M_n \tag{A-7}$$

where ξ_n is the modal damping ratio and ω_n is the modal frequency. The N uncoupled equations of motion (A-7) can be solved exactly using Duhamel integral or alternatively by numerical integration. The general response expression given by Duhamel integral for each mode as suggested in ref[23]

$$Y_n(t) = \frac{1}{M_n\omega_{Dn}} \int_0^t P_n(\tau)\exp-\xi_n\omega_n(t-\tau)\ \sin\omega_{Dn}(t-\tau)d\tau \tag{A-8}$$

If the initial velocity and displacement are not zero a free vibration response must be added to the Duhamel integral expression for each mode given by

$$Y_n(t) = \exp-\xi_n\omega_n t\ [((Y_n(0)+Y_n(0)\xi_n\omega_n)/\omega_{Dn})\sin\omega_{Dn}t + Y_n(0)\cos\omega_{Dn}t] \tag{A-9}$$

where $Y_n(0)$ and $Y_n(0)$ represent the initial modal displacement and velocity. These can be obtained from the specified initial displacement U(0) and velocity U(0) as follows for each modal component

$$Y_n(0) = \Phi_n{}^TMU(0)/M_n \tag{A-10}$$

$$\dot{Y}_n(0) = \Phi_n{}^TM\dot{U}(0)/M_n \tag{A-11}$$

When the response for each mode $Y_n(t)$ has been determined, the displacements expressed in geometric coordinates are given by the normal coordinate transformation

$$U(t) = \Phi Y(t) \tag{A-12}$$

equation (A-12) may also be written

$$U(t) = \Phi_1 Y_1(t) + \Phi_2 Y_2(t) + \Phi_3 Y_3(t) + \cdots \tag{A-13}$$

that is, merely represents the superposition of the various modal contributions.
The displacement history of the structure may be considered to be the basic measure of its response to dynamic loading. In general other response parameters such as stress or forces developed in various structural components can be evaluated directly from the displacement

A.2 DIRECT INTEGRATION METHOD

The basic operation in the step-by-step solution of simultaneous differential equations of motion in the incremental form, is their conversion to a set of simultaneous algebraic equations. this is accomplished by introducing a simple relationship between displacement, velocity, and acceleration which may be assumed to be valid for a short increment of time[23]. In the Newmark generalised acceleration method (used in the DRAIN2D and the ANSYS program[14]) it is assumed that

$$\dot{u}_{t+\Delta t} = \dot{u}_t + [(1-\delta)\ddot{u}_t + \delta\ddot{u}_{t+\Delta t}]\Delta t \tag{A-14}$$

$$u_{t+\Delta t} = u_t + \dot{u}_{t+\Delta t}\Delta t + [(\tfrac{1}{2}-\alpha)\ddot{u}_t + \alpha\ddot{u}_{t+\Delta t}]\Delta t^2 \tag{A-15}$$

where δ and α are the integration parameters based on the value of the amplitude decay factor γ

$$\alpha = .25(1+\gamma)^2 \tag{A-16}$$

$$\delta = .5(1+2\gamma)^2 \tag{A-17}$$

Newmark proposed as an unconditionally stable scheme the constant average acceleration method, in which case $\delta=\frac{1}{2}$ and $\alpha=\frac{1}{4}$ [9]. Combining equations (A-14), (A-15) with (A-1) results in the integration equation as given in ref.[9]

$$(a_0[M] + a_1[C] + [K])\{u_t\} = \{P(t)\} + [M](a_0\{u_{t-\Delta t}\}+a_2\{u_{t-\Delta t}\}+a_3\{\ddot{u}_{t-\Delta t}\})$$
$$+ [C](a_1\{u_{t-\Delta t}\}+a_4\{u_{t-\Delta t}\}+a_5\{\ddot{u}_{t-\Delta t}\}) \tag{A-18}$$

The terms on the left side of the above equation do not necessarily remain constant, due to changing in the damping and stiffness matrices in nonlinear problems. A number of iterations may be solved at a time point in order to converge any nonlinearities.
At any particular time, equation (A-1) may be written as:

$$[K_{eff}]\{u_t\} = \{P_{eq}(t)\} \tag{A-19}$$

The mass, damping and stiffness matrices are used to calculate an effective dynamic stiffness matrix at each time point from:

$$[K_{eff}] = [K] + a_0[M] + a_1[C] \tag{A-20}$$

Also, at each time point, an equivalent load vector is formed from:

$$\{P_{eq}(t)\} = \{P(t)\} + [M](a_0\{u_{t-\Delta t}\} + a_2[u_{t-\Delta t}] + a_3[\ddot{u}_{t-\Delta t}])$$
$$+ [C](a_1\{u_{t-\Delta t}\}+a_4\{u_{t-\Delta t}\}+a_5\{\ddot{u}_{t-\Delta t}\}) \tag{A-21}$$

After convergence the velocities and accelerations are calculated using results from the current and previous time step according to the assumptions in equations (A-14) and (A-15)

$$\{\ddot{u}_t\} = a_0(\{u_t\}-\{u_{t-\Delta t}\}) - a_2\{u_{t-\Delta t}\} - a_3\{\ddot{u}_{t-\Delta t}\} \quad \text{(A-22)}$$

$$\{u_t\} = \{u_{t-\Delta t}\} + a_6\{\ddot{u}_{t-\Delta t}\} + a_7\{\ddot{u}_t\} \quad \text{(A-23)}$$

these velocities and accelerations will then be used in the next load step to calculate an equivalent load vector as well as the new velocities and accelerations[14].

The coefficients a_0 to a_7 are

$a_0 = 1/\alpha\Delta t^2$ $\qquad$ $a_4 = (\delta/\alpha) - 1$

$a_1 = \delta/\alpha\Delta t$ $\qquad$ $a_5 = \Delta t(\delta/\alpha - 2)/2$

$a_2 = 1/\alpha\Delta t$ $\qquad$ $a_6 = \Delta t(1 - \delta)$

$a_3 = (1/2\alpha) - 1$ $\qquad$ $a_7 = \delta\Delta t$